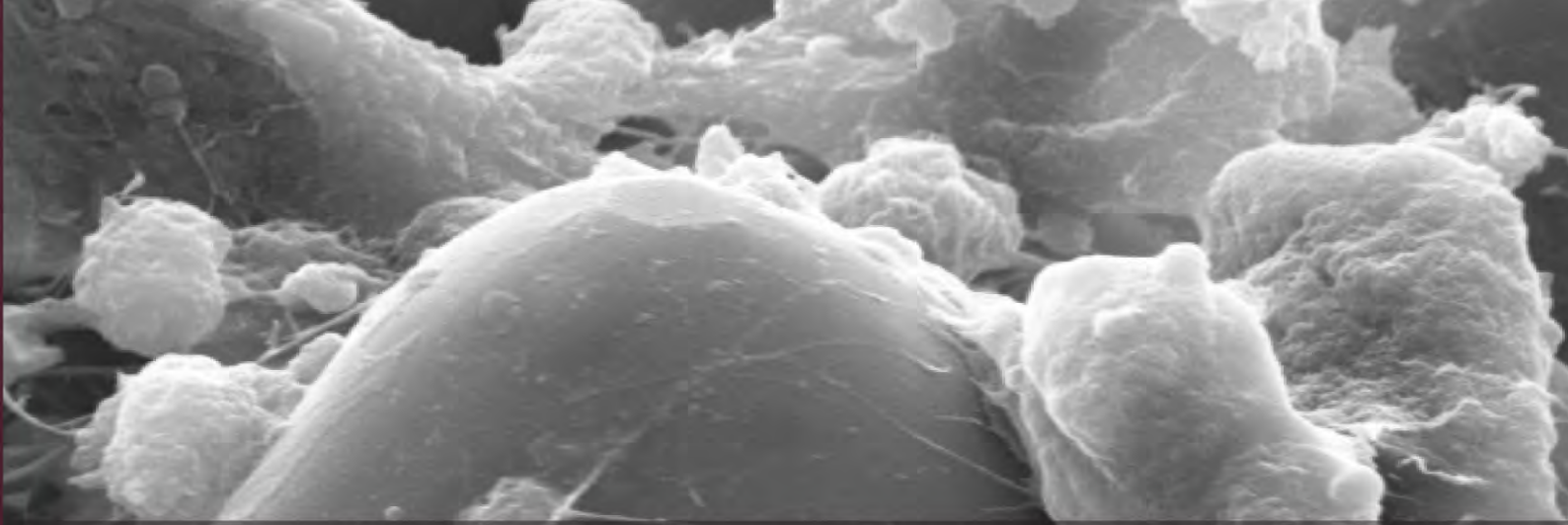

Aus der Klinik mit Schwerpunkt Rheumatologie und Klinische Immunologie
der Medizinischen Fakultät Charité – Universitätsmedizin Berlin

Development of joint components for *in vitro* modeling of arthritis

Inaugural-Dissertation

zur Erlangung des akademischen Grades des
Doktors der Naturwissenschaft (Dr. rer. nat.)

eingereicht im Fachbereich Biologie, Chemie, Pharmazie
der Freien Universität Berlin

vorgelegt von
Alexandra Damerau
aus Berlin

2022

mbvberlin | mensch und buch verlag

From the Department of
Rheumatology and Clinical Immunology
Charité – Universitätsmedizin Berlin

Development of joint components for *in vitro* modeling of arthritis

Inaugural-Dissertation
to obtain the academic degree
Doctor rerum naturalium (Dr. rer. nat.)

submitted to the Department of Biology, Chemistry, Pharmacy
of Freie Universität Berlin

by
Alexandra Damerau
from Berlin

2022

Gedruckt mit Unterstützung der Ernst-Reuter-Gesellschaft der Freunde, Förderer und Ehemaligen der Freien Universität Berlin e.V..

This thesis and all associated experiments were prepared and performed from March 2018 to September 2022 under the supervision of Prof. Dr. Frank Buttgereit at the Department of Rheumatology and Clinical Immunology, Charité – Universitätsmedizin Berlin, Germany.

1st reviewer: Prof. Dr. Frank Buttgereit
Current address: Charité – Universitätsmedizin Berlin
Department of Rheumatology and Clinical Immunology
Charitéplatz 1
10117 Berlin, Germany

2nd reviewer: Prof. Dr. Sigmar Stricker
Current address: Freie Universität Berlin
Institute of Chemistry and Biochemistry - Biochemistry and Genetics
Thielallee 63
14195 Berlin, Germany

Date of defense: 13.01.2023

Bibliografische Information der *Deutschen Nationalbibliothek*
Die Deutsche Nationalbibliothek verzeichnet diese Publikation in der Deutschen Nationalbibliografie; detaillierte bibliografische Daten sind im Internet über <https://dnb.de> abrufbar.

ISBN: 978-3-96729-202-2
Zugl.: Berlin, Freie Univ., Diss., 2022
Dissertation, Freie Universität Berlin
D 188

 Choriner Str. 85 - 10119 Berlin
verlag@menschundbuch.de – www.menschundbuch.de

ART IS I; SCIENCE IS WE.

Claude Bernard (1813-1878)

Gewidmet Familie & Freunden

DANKSAGUNG

An dieser Stelle möchte ich allen beteiligten Personen meinen großen Dank aussprechen, die mich in den letzten Jahren unterstützt und es mir ermöglicht haben meine Doktorarbeit zu bearbeiten. Ohne diese Unterstützung hätte sie in dieser Form nicht realisiert werden können.

Mein besonderer Dank gilt meinem Doktorvater Prof. Dr. Frank Buttgereit für die enorme Unterstützung bei der Umsetzung meiner Forschungsvorhaben, die konstruktiven Anregungen und das Vertrauen, das Sie in mich gesetzt haben. Außerdem möchte ich Ihnen dafür danken, dass Sie es mir stets ermöglichen an Kongressen und Veranstaltungen teilzunehmen und meine wissenschaftliche Karriere fördern.

Des Weiteren möchte ich mich herzlichst bei Prof. Dr. Sigmar Stricker bedanken, der meine Doktorarbeit als zweiter Gutachter so kurzfristig übernommen, bereitwillig betreut und mich bei der Umsetzung der Arbeit unterstützt hat.

Besonders danken möchte ich meinem Mentor Dr. Timo Gaber. Ich danke dir für deine herausragende wissenschaftliche Expertise, die du mit mir geteilt hast. Aber vor allem danke ich dir für deine hervorragende Betreuung, die produktiven Gesprächen, deine motivierenden Worte, deine Geduld und dass du das wissenschaftlich Beste aus mir herausgeholt hast.

Ich möchte mich hiermit auch bei der gesamten Arbeitsgruppe für die unterstützende, angenehme und motivierende Atmosphäre bedanken. Es war schön, diese Zeit mit all ihren Höhen und Tiefen gemeinsam mit Euch zu erleben. Ein besonderer Dank geht an Annemarie Lang für die Motivation, produktiven Gespräche und die gemeinsame Leidenschaft zur Histologie, die uns schöne Momente bereitet hat. Auch möchte ich besonders Lisa Ehlers, Manuela Jakstadt und Gabriele May nennen, die immer ein offenes Ohr für mich hatten und mir wunderschöne Momente bereitet haben.

Bei dieser Gelegenheit möchte ich Moritz Pfeiffenberger einen besonderen Dank aussprechen. Lieber Moritz, mit dir habe ich alle Freuden und Sorgen geteilt und du bist in dieser Zeit ein sehr wichtiger Freund geworden. Ich danke dir für deine fachliche Expertise und vor allem für deine persönliche Unterstützung in allen Lebenslagen.

Danken möchte ich außerdem der Studienstiftung des deutschen Volkes für die finanzielle Unterstützung während meiner Doktorarbeit und das vielfältige interdisziplinäre Angebot. Mein Dank geht auch an die Dahlem Research School (DRS) und Berlin-Brandenburger Forschungsplattform BB3R, für interdisziplinäre Workshops und Symposien.

An dieser Stelle möchte ich mich besonders bei Sven Flatow, Sarah Altekrüger und Francis Rätsch bedanken. Ihr habt mich in jeder Lebenslage und auf meinem gesamten Weg unterstützt, motiviert und wart immer an meiner Seite. Ein besonderer Dank geht an dich, liebe Sarah für deine Geduld, deine Ratschläge und deine anhaltende Unterstützung.

Abschließend geht mein ganz besonderer Dank an meine Eltern. Mama und Papa, ohne euch hätte ich diesen Weg nie einschlagen können und für dieses Vertrauen und die Unterstützung danke ich euch von Herzen.

SELBSTSTÄNDIGKEITSERKLÄRUNG

Hierdurch versichere ich, dass ich meine Dissertation selbstständig verfasst und keine anderen als die von mir angegeben Quellen und Hilfsmittel verwendet habe.

Die Dissertation ist in keinem früheren Promotionsverfahren angenommen oder abgelehnt worden.

Berlin, den 16.09.2022

_____

Alexandra Damerau

TABLE OF CONTENT

LIST OF FIGURES

LIST OF TABLES

LIST OF ABBREVIATIONS

µCT	Micro-computed tomography
ACAN	Aggrecan
ACPA	Anti-citrullinated protein antibody
ADAMT	A disintegrin and metalloproteinase with thrombospondin motifs
ALP	Alkaline phosphatase
APC	Antigen-presenting cells
BAX	Bcl-2 associated X-protein
BCP	Biphasic calcium phosphate
BMP	Bone morphogenic protein
CD	Cluster of differentiation
COL	Collagen
COMP	Cartilage oligomeric matrix protein
CTGF	Connective tissue growth factor
DFO	Deferoxamine
DMARD	Disease-modifying anti-rheumatic drug
ECM	Extracellular matrix
EU	European Union
FCS	Fetal calf serum
FGF	Fibroblast growth factor
FLS	Fibroblast-like synoviocytes
FN1	Fibronectin 1
GAG	Glycosaminoglycan
GC	Glucocorticoid
GM-CSF	Granulocyte-macrophage colony-stimulating factor
HA	Hydroxyapatite
HIF	Hypoxia-inducible factor
HLA	Human leukocyte antigen
HUVEC	Human umbilical vein endothelial cells
IFN-γ	Interferon gamma
IL	Interleukin
iMPC	iPSCs-derived MSCs

iPSC	Induced pluripotent stem cell
JAK	Janus kinase
LDH	Lactate dehydrogenase
macroSFCC	Macroscale scaffold-free chondrogenic component
MHC	Major histocompatibility complex
MIF	Macrophage migration inhibitory factor
miniSFCC	Microscale scaffold-free chondrogenic component
MMP	Matrix metalloproteinase
MSC	Mesenchymal stromal cell
MTX	Methotrexate
NO	Nitric oxide
NSAID	Non-steroidal anti-inflammatory drug
OA	Osteoarthritis
OECD	Organization for Economic Co-operation and Development
ON	Osteonectin
OPG	Osteoprotegerin
OPN	Osteopontin (Gen: *SPP1*)
OSX	Osterix
PLA	Poly-$_{D,L}$-lactic acid
RA	Rheumatoid arthritis
RANK	Receptor activator of nuclear factor kappa (NF-κ) B
RANKL	Receptor activator of NF-κB ligand
REACH	Registration, Evaluation, Authorization of Chemicals
RF	Rheumatoid factor
RUNX2	Runt-related transcription factor 2
SPP1	Secreted phosphoprotein 1
TCP	Tricalcium phosphate
Tfh	T follicular helper cells
TGF	Transforming growth factor
Th	T helper cell
TNF	Tumor necrosis factor
VEGF	Vascular endothelial growth factor

SUMMARY

Rheumatoid arthritis (RA) is one of the most common autoimmune diseases (prevalence 0.5-1.0%), which can lead to pain and a considerable loss of life quality in affected patients. Many details of underlying causes and mechanisms are still elusive. The persistent autoimmune-mediated inflammation of the joint is one of the key features of this systemic, chronic-inflammatory disease accounting for progressive cartilage destruction. Despite major progress in the treatment of RA, a strong unmet medical need remains. Therefore, a better understanding of the underlying pathomechanisms driving RA progression is required to develop new therapeutic strategies to effectively treat patients at every stage of disease progression.

Although various RA models already exist, they either employ phylogenetically distant species or rely on human cells cultured in an oversimplified environment. To date, none of these models allows sufficient or complete extrapolation to the human patient. Therefore, the use of human-based *in vitro* 3D tissue equivalents of an artificial joint is a promising alternative approach to investigate pathomechanisms and test new therapeutic approaches. Hence, the aim of this thesis was to develop and characterize human *in vitro* 3D tissue equivalents of the joint, namely (i) cancellous bone, (ii) articular cartilage, and (iii) synovial membrane using bone marrow-derived mesenchymal stromal cells (MSCs). Here, MSCs provide the possibility of producing a complete joint model from single donor material thus offering the opportunity of a personalized testing platform.

The results described in this thesis show the potential of mimicking key features of arthritis in three different tissues of a joint. Firstly, to simulate the bone component, β-tricalcium phosphate (TCP) – mimicking the mineral bony part – was populated with MSCs. Cell seeding was optimized using cell sheet technology. In contrast, the cartilage component was produced by cellular self-assembly without any supporting materials. Both models exhibit phenotypic features of native tissue, including expression of bone- or cartilage-related markers, mineralization of bone that was absent in cartilage, and development of distinct zones in the glycosaminoglycan-rich cartilage model. Co-cultivation of both tissue models generated the osteochondral unit characterized by inter-tissue connectivity, cell colonization, and initial calcification implying a functional transitional bridging area. Finally, the synovial membrane model was generated based on a xeno-free synthetic hydrogel populated with MSCs indistinguishable from synovial fibroblasts with regard to classical markers. Similar to the human synovial membrane, a confluent layer of up to four cell layers was detectable within the hydrogel allowing immune cell migration.

To simulate inflammation, the individual tissue components were treated with cytokines relevant for RA, such as interleukin-6, tumor necrosis factor-α, and macrophage migration inhibitory factor. This resulted in cytokine-driven cell- and matrix-related changes in accordance with those observed during RA, while treatment using biologics prevented the induction of arthritis in the osteochondral model. These results confirm the pathophysiological mutability, architecture, integrity, and viability of the distinct *in vitro* 3D joint components.

Prospectively, the complete *in vitro* 3D joint model will serve as a preclinical test platform in basic and applied biomedical research to (i) study pathophysiological processes of musculoskeletal diseases, (ii) identify new potential targets, (iii) test novel therapeutic strategies, including biologic therapies, and (iv) reduce the number of animal experiments.

ZUSAMMENFASSUNG

Rheumatoide Arthritis (RA) ist eine der häufigsten Autoimmunerkrankungen (Prävalenz 0,5-1,0 %), die bei den betroffenen Patienten zu Schmerzen und einem erheblichen Verlust an Lebensqualität führen kann. Zugrundeliegende Ursachen und Mechanismen sind nach wie vor ungeklärt. Die anhaltende autoimmunvermittelte Entzündung des Gelenks ist eines der Hauptmerkmale dieser systemisch, chronisch-entzündlichen Gelenkerkrankung. Trotz erheblicher Fortschritte bei der Behandlung der Betroffenen besteht nach wie vor eine große medizinische Versorgungslücke. Ein besseres Verständnis der zugrundeliegenden Pathomechanismen ist daher die Grundvoraussetzung für die Entwicklung neuer Therapieansätze.

Bisher wurden zahlreiche RA-Modelle entwickelt, jedoch basieren diese entweder auf phylogenetisch unterschiedlichen Spezies oder auf stark vereinfachten humanen *in vitro* Kulturen. Bis heute lassen sich die Ergebnisse aus diesen Modellen nicht ausreichend oder vollständig auf den Patienten extrapolieren. Die Verwendung von humanen *in vitro* 3D Gewebeäquivalenten des Gelenks ist daher ein vielversprechender präklinischer Ansatz zur Untersuchung von Pathomechanismen und zur Prüfung neuer Therapien. Ziel dieser Arbeit war es, basierend auf humanen mesenchymalen Stromazellen (MSCs), *in vitro* 3D Gewebeäquivalente des Gelenks zu entwickeln. Diese Gewebeäquivalente umfassen (i) spongiösen Knochen, (ii) Gelenkknorpel und (iii) Synovialmembran. MSCs bieten hierbei die Möglichkeit, ein Gelenkmodell ausgehend vom Material eines einzelnen Spenders zu entwickeln.

Das 3D Knochenmodell basiert auf dem Trägermaterial β-Trikalziumphosphat (TCP), das den mineralischen Knochenanteil des Gelenkes simuliert. Die Aussaat von Zellen auf das Trägermaterial TCP wurde mittels ‚sheet technology' optimiert. Im Gegensatz dazu wurde das 3D Knorpelmodell durch zelluläre Selbstorganisation, frei von zusätzlichen Trägermaterialen erzeugt. Beide Modelle weisen dem nativen Gewebe ähnelnde phänotypische Merkmale auf, wie z.B. die Expression von Knochen- oder Knorpel-spezifischen Markern, die Mineralisierung des Knochens, die im Knorpel fehlte, und die Entwicklung charakteristischer Zonen des Glykosaminoglykan-reichen Knorpelmodells. Zudem generierte die Co-Kultivierung beider Modelle eine osteochondrale Einheit, die durch Kolonisierung, Konnektivität und initiale Kalzifizierung gekennzeichnet war. Diese Eigenschaften deuten auf einen funktionellen Übergangsbereich beider Gewebeäquivalente hin.

Schließlich wurde das xeno-freie Synovialmembranmodell basierend auf einem synthetischen Hydrogel entwickelt. Da sowohl MSCs als auch synovialen Fibroblasten anhand klassischer Marker nicht unterscheidbar sind, wurden MSCs in das Hydrogel eingebracht. Das

Synovialmembranmodell wies eine konfluente Schicht von bis zu vier Zellschichten auf, was der physiologischen Struktur der humanen Synovialmembran entspricht. Das Hydrogel ermöglicht zudem die Migration von Immunzellen; die Voraussetzung für die Simulation des inflammatorischen Zustandes.

Final wurden RA-relevante Zytokine wie Interleukin-6, Tumornekrosefaktor-α und Makrophagen-Migrationshemmungsfaktor appliziert, um Entzündungsprozesse in den Gewebeäquivalenten zu simulieren. Die Zytokin-vermittelte Stimulation resultierte in Zell- und Matrix-Veränderungen, wie sie auch bei RA beobachtet werden können. Die therapeutische Intervention hingegen führte zur Reduktion der Ausprägung der Arthritis im osteochondralen Modell. Diese Ergebnisse bestätigen die pathophysiologische Variabilität, Architektur, Integrität und Lebensfähigkeit der verschiedenen *in vitro* 3D Gelenkkomponenten.

Perspektivisch soll das kombinierte *in vitro* 3D Gelenkmodell als präklinische Testplattform in der Grundlagenforschung und angewandten biomedizinischen Forschung dienen, um schlussendlich (i) pathophysiologische Prozesse muskuloskelettaler Erkrankungen studieren zu können, (ii) neue potenzielle Zielmoleküle zu identifizieren, (iii) neue therapeutische Strategien einschließlich Therapien mit Biologika zu testen und (iv) Tierversuche zu reduzieren.

1. CHAPTER: INTRODUCTION

Chapters 1.2, 1.3, and **1.5** were published as original peer-reviewed review article (Damerau A, Gaber T. Modeling Rheumatoid Arthritis In Vitro: From Experimental Feasibility to Physiological Proximity. Int J Mol Sci. 2020 Oct 25;21(21):7916. http://doi.org/10.3390/ijms21217916) (Damerau and Gaber 2020).

The original text was slightly modified to improve readability.

1.1. Arthritis

Joint inflammation or 'arthritis' occurs in the context of more than 100 different types of joint diseases. Osteoarthritis (OA) and rheumatoid arthritis (RA) are the most prevalent forms of arthritis with different etiologies (OA prevalence: 5% / RA prevalence: 0.5–1.0%) (Firestein and McInnes 2017, Sanchez-Lopez, Coras et al. 2022). Although arthritis has been studied for more than 140 years, it is still the leading cause of years lived with disability for millions of people worldwide (Cieza, Causey et al. 2021). Other inflammatory joint diseases include psoriatic arthritis, axial spondyloarthritis, and arthritides in the context of systemic rheumatic diseases like systemic lupus erythematosus and vasculitis affecting >1.0% of adults in industrialized countries (Roelsgaard, Esbensen et al. 2019, Rech, Sticherling et al. 2020, Barber, Drenkard et al. 2021, Ritchlin and Adamopoulos 2021, Saadoun, Vautier et al. 2021). The primary target of inflammatory processes in arthritis is the entire synovial joint, comprising the (i) synovium, (ii) articular cartilage, and (iii) subchondral bone and the extra synovial tissue including infrapatellar fat pad, bursae, and tendons (Macchi, Stocco et al. 2018, Senthelal, Li et al. 2021). Along with the joints, several rheumatic diseases can affect many other organs, including the heart, eyes, skin, intestine, kidney, lung, brain, and skeleton (Burmester and Pope 2017, Cassotta, Pistollato et al. 2020). Although rheumatic diseases differ regarding etiology, pathogenesis, clinical symptoms, patient characteristics, and disease subtypes, they all share the need for patient-related biomarkers and optimized therapeutic management.

OA is the most prevalent form of arthritis. It is defined as a chronic and progressive degenerative joint disease that is the leading cause of age-related disability due to increasing

life expectancy and an active, aging population (Glyn-Jones, Palmer et al. 2015). It is characterized by structural damage to one or more joints, often detected late on X-rays when irreparable damage has already occurred (Sanchez-Lopez, Coras et al. 2022). Given that OA is expected to affect more than 10% of the population over 60 years of age worldwide, the impact of this health problem is still underestimated (Nelson 2018). Current therapeutic approaches only relieve symptomatic pain and inhibit inflammation (Hunter and Bierma-Zeinstra 2019). In contrast, RA is an autoimmune-mediated, chronic, systemic inflammatory disease that primarily affects the joints. It can be predicted very early before the onset of clinical symptoms by serum parameters such as autoantibodies (Smolen, Aletaha et al. 2018). However, significant efforts have been made over the past decades to better understand the underlying pathomechanisms of both disorders (Burmester and Pope 2017, Deng, Zhang et al. 2021, Stolberg-Stolberg, Boettcher et al. 2022).

Cells from the distinct parts of the joint possess different abilities to initiate and respond to an inflammatory environment. These processes are initiated by, e.g., activated immune cells or immune complexes, ultimately resulting in articular cartilage degeneration (Pap and Korb-Pap 2015). Insights gained through *in vitro* and *in vivo* studies have contributed to the development of effective therapeutic drugs that specifically disrupt critical signaling pathways in the inflammatory cascade, minimizing cytokine-driven cell activation and, finally, cartilage degradation (Klareskog, van der Heijde et al. 2004, Burmester and Pope 2017, Liu, Ma et al. 2021). Although there has been considerable progress in the treatment of RA, a substantial therapeutic need remains, i.e., not all patients achieve durable clinical remission, and a substantial number of patients still suffer from moderate or even high disease activity (Haugeberg, Hansen et al. 2015, Ajeganova and Huizinga 2017, Burmester and Pope 2017). Even in the current era of biological targeted therapies, the combination of glucocorticoids (GCs) and methotrexate (MTX) remain the initial preferred basic anti-rheumatic therapy and is the gold standard for treatment of RA (Smolen, Landewe et al. 2014). Given the high rate of disability in patients with OA and RA, there is an urgent need for new therapeutic approaches and early-onset biomarkers.

In recent years, we have observed the failure of new therapies in clinical trials, even though their development was based on promising preclinical data from either *in vitro* or animal experiments (Firestein 2009, Koenders and van den Berg 2016). Therefore, considering the underlying mechanisms already known, complex human *in vitro* systems will help to (i) improve transferability of results, (ii) understand specific pathomechanisms, (iii) identify new targets for diagnosis or treatment, and (iv) serve as preclinical tools for drug testing, thereby reducing the number of animal experiments.

1.2. Rheumatoid arthritis

Rheumatoid arthritis is a progressive systemic, chronic, and inflammatory autoimmune disease with an average prevalence of 0.5–1.0% worldwide, demonstrating ethnic and geographic differences (Smolen, Aletaha et al. 2018). Its pathogenesis is characterized by immune cell infiltration into the synovial membrane and the joint cavity and hyperplastic and invasive synovium formation, resulting in progressive cartilage destruction and subchondral bone erosion in the late stages of the disease if not treated (Figure 1). RA, a disease most likely recognized more than 20 centuries ago, painfully affects the body's joints (Parish 1963). It is the most common inflammatory joint disease impacting both individuals and society. These patients suffer a considerable loss of quality of life and a decline in productivity. Subsequent effort and costs of health care increase, ultimately resulting in a significant economic and social burden (Scott, Wolfe et al. 2010). The most common symptoms of RA include pain, swelling, and morning stiffness in the affected joints. It is a multifactorial disorder, and recent studies have identified multiple genetic and environmental factors associated with an increased risk of RA, e.g., female sex, smoking, and major histocompatibility complex (c) regions encoding human leukocyte antigen (HLA) proteins (amino acids at positions 70 and 71) (Burmester and Pope 2017, Deane, Demoruelle et al. 2017). Years before the first clinical symptoms of RA occur, autoimmunity against modified self-proteins is initiated, which results in the onset of the disease (Smolen, Aletaha et al. 2018, Damerau and Gaber 2020).

As the course of RA within the individual patients may differ regarding pathogenesis, clinical symptoms, and disease subtypes, personalized precision medicine must be the ultimate goal to achieve disease remission. We are far from curing RA due to the need for (i) objective patient-related biomarkers to identify disease subtypes and treatment responses and (ii) the management of patients who are refractory or resistant to available treatments. Both will enable us to understand the disease and its pathogenic processes to optimize and introduce personalized precision health care (Damerau and Gaber 2020).

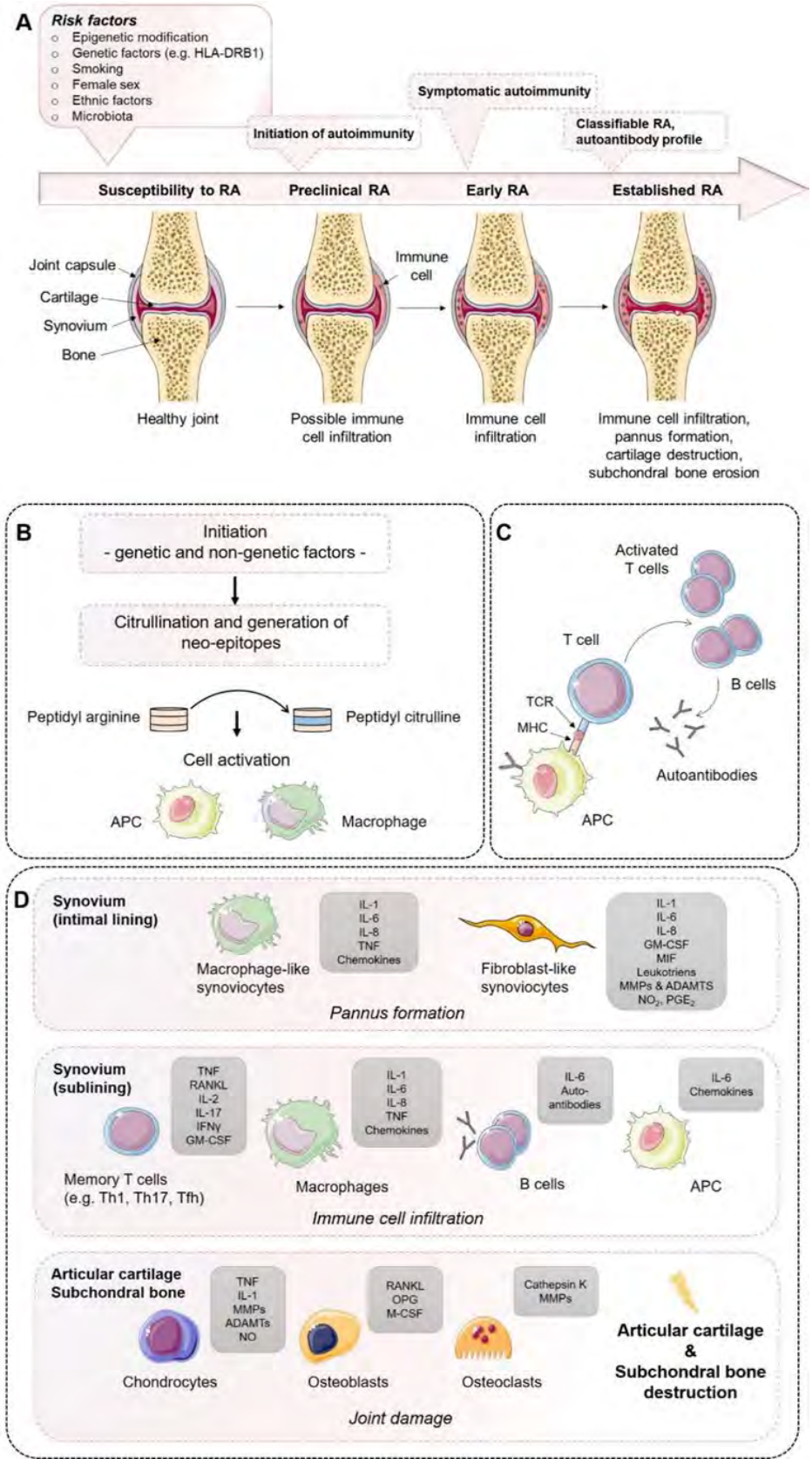

Figure 1: Establishment of rheumatoid arthritis (RA): Mechanisms of disease initiation, development, and progression (Damerau and Gaber 2020). (A) Multiple risk factors, both genetic and non-genetic, are required to induce the development of RA in susceptible individuals. Years before the first clinical symptoms of RA occur, autoimmunity against modified self-proteins is initiated, which results in the onset of subclinical inflamed synovium (symptomatic autoimmunity) propagated by

immune cell infiltration and pannus formation. Once established, RA can be classified according to clinical symptoms. (B) The onset of autoimmunity occurs in the mucosa (e.g., mouth, lung, and gut) where neo-epitopes are created because of post-translational modifications, e.g., by citrullination. These neo-epitopes can be recognized by antigen-presenting cells (APCs) of the adaptive immune system, and (C) are presented to adaptive immune cells in lymphoid tissues, activate an immune response, and induce autoantibody formation (e.g., ACPA and RF). (D) Activated immune cells and immune complexes can activate synovial cells, such as fibroblast-like synoviocytes (FLS) and macrophage-like synoviocytes of the intimal lining and APCs in the sublining area, to produce a range of inflammatory factors and expand and form the cartilage- and bone-invasive pannus. Autoimmune activation and immune cell infiltration (T cells, B cells, macrophages) of the sublining area further contribute to the excessive production of inflammatory factors, autoantibodies, and synovial vascular leakage, ultimately leading to articular cartilage and subchondral bone destruction as a result of matrix-degrading enzymes and de-balanced bone homeostasis characterized by an imbalanced RANKL/RANK/OPG system and activated osteoclasts. ADAMTS, a disintegrin and metalloproteinase with thrombospondin motifs; APCAs, anti-citrullinated protein antibodies; RF, rheumatoid factor; GM-CSF, granulocyte-macrophage colony-stimulating factor; M-CSF, macrophage colony-stimulating factor; MHC, major histocompatibility complex; MMP, matrix metalloproteinase; NO, nitric oxide; OPG, osteoprotegerin; RANKL, receptor activator of nuclear factor-κB ligand; RANK, receptor activator of nuclear factor-κB; TCR, T cell receptor; TNF, tumor necrosis factor. The figure contains graphics from Servier Medical Art, licensed under a Creative Common Attribution 3.0 Generic License. http://smart.servier.com/ (Damerau and Gaber 2020).

1.2.1. The course of RA pathogenesis

The course of RA pathogenesis involves several stages. Before clinical symptoms are established, a certain level of RA susceptibility (e.g., genetic factors) coupled with the accumulation of risk factors proceed through the pre-clinical stage of the disease, leading to synovial inflammation, which, if not resolved, ultimately leads to the development of RA. During the early development of RA, post-translational modifications of a wide range of cellular (e.g., collagen) and nuclear proteins (e.g., histones) occur, including the conversion of the amino acid arginine to citrulline, a process called citrullination. Citrullination may result from smoking, induced by microbiota (e.g., *Porphyromonas gingivalis*) or by an uncontrolled neutrophil reaction. Altered modified self-proteins engage professional antigen-presenting cells (APCs) such as macrophages and trigger a normal immune response via the help of T cells. This stimulates B cells to produce a wide range of (auto)antibodies recognizing self-proteins, such as rheumatoid factor (RF) and anti-citrullinated protein antibodies (ACPAs). Autoantibodies are often found before the onset of clinical synovitis, suggesting that a second not-fully-understood mechanism is necessary for the transition of autoimmunity to local synovial inflammation (Burmester and Pope 2017, Deane, Demoruelle et al. 2017, Smolen, Aletaha et al. 2018, Damerau and Gaber 2020).

However, during the progression of RA, an increase in vascular permeability, a disrupted extracellular matrix (ECM), and synovial immune cell infiltration transforms the paucicellular synovium into chronically inflamed tissue. This process includes the expansion of the intimal lining and activation of macrophage- and stromal fibroblast-like synoviocytes (FLSs). These

cells produce a variety of pro-inflammatory humoral mediators, such as cytokines and chemokines, including interleukin (IL)-6, IL-1β, IL-8, tumor necrosis factor (TNF)-α, granulocyte-macrophage colony-stimulating factor (GM-CSF), macrophage migration inhibitory factor (MIF), and matrix-degrading enzymes, e.g., matrix metalloproteinases (MMPs) as well as a disintegrin and metalloproteinase with thrombospondin motifs (ADAMTs), prostaglandins, leukotrienes, and reactive nitric oxide (NO). The aggressive and invasive phenotype of expanding FLSs, forming the hyperplastic pannus tissue, contributes to cartilage damage but may also be responsible for the propagation and systemic spreading of inflammation by migrating from joint to joint and other organs (Kiener, Niederreiter et al. 2009, Pretzel, Pohlers et al. 2009, Bustamante, Garcia-Carbonell et al. 2017, Damerau and Gaber 2020).

The inflammation-induced expansion of FLSs and the infiltration of inflammatory cells into the usually paucicellular synovium lead to an enhanced metabolic need and, therefore, to an undersupply of both nutrients and oxygen to the synovial tissue. Due to the resulting local hypoxia, new vessels are formed that further facilitate the inflammatory process by increasing the amount of adaptive immune cells, in particular CD4+ memory T helper (Th) cells infiltrating the synovial sublining. Lymphocyte infiltrates accumulate and form aggregates ranging from small and loosely arranged lymphocyte clusters to large and organized ectopic lymphoid structures which, in some cases, develop germinal centers that facilitate local T cell - B cell interactions. In these ectopic germinal structures, specific pathologic follicular helper T cells (Tfh) promote B cell responses and (auto)antibody production within pathologically inflamed non-lymphoid tissues. Apart from pathogenic Tfh cells, Th1 and Th17 cells have been identified in the pathogenesis of RA. Although the evidence of the pathogenic function of Th1 cells in RA is controversial due to the lack of therapeutic efficiency of interferon (IFN)-γ targeting treatments (Feldmann 2002, Pollard, Cauvi et al. 2013), it should be noted that biologic targeting of the Th1 cytokine TNF-α, is successful in treating RA (Feldmann 2002, Damerau and Gaber 2020).

IL-17-producing CD4+ T cells have been identified in synovial tissues from patients with RA, including their inducing cytokines IL-6, IL-1β, IL-21, transforming growth factor (TGF)-β, and IL-23 (Manel, Unutmaz et al. 2008, Pene, Chevalier et al. 2008, Volpe, Servant et al. 2008, Cascao, Moura et al. 2010, Gaffen, Jain et al. 2014), and have been demonstrated to be increased/maintained in the peripheral blood of RA patients (Shahrara, Huang et al. 2008, Yamada, Nakashima et al. 2008, Leipe, Grunke et al. 2010, van Hamburg, Asmawidjaja et al. 2011). However, IL-17 was shown to induce bone resorption and contribute to neutrophil recruitment, particularly into the synovial fluid, a hallmark of RA (Kotake, Udagawa et al. 1999, Kaplan 2013). Besides effector T helper cells, antigen-presenting follicular dendritic cells,

macrophages, and mast cells are present in the synovial sublining and contribute to chronic inflammation by many inflammatory mediators, such as cytokines, chemokines, and reactive oxygen and nitrogen species, as well as matrix-degrading enzymes. Recent studies proposed that distinct subtypes of synovial histology displaying inflammatory versus non-inflammatory patterns are associated with different clinical phenotypes and a concurring response to novel targeted therapeutic interventions (Dennis, Holweg et al. 2014, Orr, Vieira-Sousa et al. 2017). Technical progress and the development and combination of state-of-the-art methods from single-cell genomics to mass cytometry have provided new insights into the complex interplay of cells and soluble immune mediators, particularly cytokines and chemokines (Burmester and Pope 2017). Thus, specific pathogenic infiltrating immune cell subsets ─ pro-inflammatory monocytes, autoimmune-associated B cells, peripheral Th cells, distinct subsets of CD8+ T cells, and mast cells ─ contribute to the inflammatory pattern of the RA synovial lining and sublining layer (Schubert, Dudeck et al. 2015, Rao, Gurish et al. 2017, Rivellese, Mauro et al. 2018, O'Neil and Kaplan 2019, Zhang, Wei et al. 2019, Damerau and Gaber 2020, Smolen, Landewe et al. 2020).

Invading immune cells and FLSs of the synovial lining produce large amounts of pro-inflammatory cytokines and express high levels of MMPs. At the same time, the expression of endogenous MMP inhibitors remains insufficiently low. Finally, the invasive and destructive FLS-front of synovial tissue, called the pannus, attaches to the articular surface and contributes to local matrix destruction and cartilage degradation. The chondrocytes of the damaged articular cartilage contribute to the vicious cycle of cartilage degeneration by inducing inflammatory cytokines, such as IL-1β and TNF-α, and MMPs and NO. Additionally, FLSs negatively affect the subchondral bone by activation and maturation of bone-resorbing osteoclasts. Osteoclasts are highly responsive to autoantibodies; pro-inflammatory cytokines, in particular TNF-α, IL-1β, and IL-6; and more importantly, receptor activator of nuclear factor kappa B ligand (RANKL) which is the key regulator of osteoclastogenesis. RANKL binds to its receptor, the receptor activator of nuclear factor-κB (RANK), and activates osteoclasts, enhancing bone resorption (Damerau and Gaber 2020).

Conversely, osteoblasts that play a key role in regulating anabolic bone metabolism produce bone matrix constituents, induce bone matrix mineralization, and modulate osteoclasts through the production of osteoprotegerin (OPG) (Corrado, Maruotti et al. 2017). Although osteoblasts protect themselves from bone destruction by osteoclasts by producing OPG, a decoy receptor for RANKL, they also generate RANKL and M-CSF, both of which contribute to osteoclastogenesis. Imbalanced bone remodeling in the subchondral and periarticular bone of joints leads to erosions and periarticular osteopenia; generalized bone loss is a general feature of established RA (Damerau and Gaber 2020).

1.3. Lessons from animal models of arthritis

Animal models represent an integral part of the preclinical drug discovery process and are used to study the pathophysiological mechanisms of RA. Despite their extreme usefulness for testing new interventions in many cases, concerns about low clinical development success rates for investigational drugs have been raised (Firestein 2009), “Dozens of preclinical arthritis models have been developed...none of these, however, is truly RA, and none consistently predicts the effect of a therapeutic agent in patients” (Firestein 2009, Damerau and Gaber 2020).

Importantly, animals do not naturally develop autoimmune disorders, such as RA, which is an inherent limitation of these arthritis models (Table 1). Instead, animal models can be used to study certain specific pathophysiological aspects of human diseases, such as destructive pathways involved in the erosion of articular cartilage and bone. To this end, arthritis can be chemically induced in these animals by soluble agents (e.g., type II collagen (COL)-induced arthritis model) or develop spontaneously after genetic manipulation (e.g., human TNF transgene model) (Table 1) (Asquith, Miller et al. 2009, Bevaart, Vervoordeldonk et al. 2010, Choudhary, Bhatt et al. 2018). Most of these models display features of human RA, such as inflammatory cell infiltration, synovial hyperplasia, pannus formation, cartilage destruction, and bone erosions. However, they also demonstrate specific limitations, such as the development of self-limiting arthritis, the development of arthritis only in susceptible strains of rodents, and a pathophysiology that does not recapitulate the endogenous breach of tolerance and excludes systemic components of disease (Asquith, Miller et al. 2009, Bevaart, Vervoordeldonk et al. 2010, Choudhary, Bhatt et al. 2018). The mutations used in genetically engineered arthritis models have not been identified in human RA (Asquith, Miller et al. 2009). When comparing transcriptional programs of mice and humans overlapping but notably different gene expression patterns have been observed (Breschi, Gingeras et al. 2017). Therefore, therapeutic approaches, such as biologics highly specific to human target proteins, cannot be proven using non-humanized rodent models (Schinnerling, Rosas et al. 2019). Finally, mice and humans differ in their locomotion, life span, evolutionary pressures, ecological niches, circadian rhythms, weight-bearing, and blood leukocyte population ratios. Thus, none of the animal models can fully replicate the human pathogenesis of RA, which explains the observed challenges in clinical translation (Firestein 2009, Damerau and Gaber 2020).

Current management guidelines recommend early and rigorous treatment to achieve low disease activity or remission targets as rapidly as possible. Thus, RA is currently treated with a wide variety of therapeutic drugs ranging from non-steroidal anti-inflammatory drugs (NSAID) and GCs to disease-modifying anti-rheumatic drugs (DMARDs) of synthetic origin. The latter

includes conventional synthetic DMARDs (e.g., MTX), biological and biosimilar DMARDs (e.g., TNF inhibitors or IL-6 inhibitors), and targeted synthetic DMARDs (the Janus kinase (JAK) inhibitors) targeting specific immune cells, cytokines, or pro-inflammatory pathways (Burmester and Pope 2017, Chatzidionysiou, Emamikia et al. 2017, Smolen, Landewe et al. 2020). Today's therapeutic approaches using state-of-the-art biologicals or JAK inhibitors have been proven to be highly successful and effective in most patients with RA, including those with severe disease progression. As already mentioned, despite major progress in the treatment of RA, a strong unmet medical need remains (Burmester and Pope 2017, Winthrop, Weinblatt et al. 2020). Therefore, it is necessary in RA to (i) define patients who are refractory to available treatments among those who are undertreated or non-adherent to treatment, (ii) identify objective biomarkers of disease states (e.g., early versus established RA), (iii) define 'refractory' states, and finally (iv) determine treatment response (Winthrop, Weinblatt et al. 2020). The lack of therapeutic efficacy in true refractory patients may be due to the nature of the "one-fits-it-all" approach of standardized therapeutic regimes. Thus, clinical management of patients often neglects their heterogeneity regarding the endogenous circadian rhythms, disease states, subtypes and duration, as well as autoantibody, cytokine, and infiltrating immune cell pattern. Identifying objective biomarkers to delineate disease subtypes and treatment response will be necessary to provide a 'precise' customized strategy for each individual patient enhancing our repertoire in the battle against this potentially devastating disease (Damerau and Gaber 2020).

Therefore, preclinical models are essential to improve our understanding of pathological mechanisms and to develop and verify new therapeutic approaches with the aim of addressing this unmet medical need. This includes the investigation of human-specific alternatives to identify objective biomarkers to delineate disease subtypes and treatment responses, and novel targets to manipulate the function of immune cells involved in the pathogenesis of RA (Damerau and Gaber 2020).

Table 1: Selected rodent models for rheumatoid arthritis (Asquith, Miller et al. 2009, Bevaart, Vervoordeldonk et al. 2010, Choudhary, Bhatt et al. 2018, Damerau and Gaber 2020)

Animal Models	Species	Induction/Genetic Alteration	Limitations	References
		Induced Arthritis Models		
Collagen-induced arthritis (CIA)	Mouse, rat	Inoculation with type II heterologous or homologous collagen in complete Freund's adjuvant in strains expressing major histocompatibility complex (MHC) Class II I-Aq haplotypes	▪ General variable incidence, severity, and inter-group inconsistency ▪ Only inducible in susceptible strains of rodents ▪ Low incidence and variability of arthritis severity in c57bl/6 mice ▪ Acute and self-limiting polyarthritis in contrast to human RA ▪ Greater incidence in males in contrast to human RA	(Trentham, Townes et al. 1977, Courtenay, Dallman et al. 1980, Holmdahl, Jansson et al. 1986, Asquith, Miller et al. 2009)
Collagen-antibody-induced arthritis (CAIA)	Mouse	Anti-collagen antibodies have been demonstrated to induce arthritis	▪ Pathogenesis is not mediated via T and B cell response in contrast to human RA ▪ Pathogenesis is inducible irrespective of the presence of MHC class II haplotype in contrast to human RA	(Holmdahl, Rubin et al. 1986, Nandakumar and Holmdahl 2005)
Adjuvant-induced arthritis (AA)	Mouse, rat	Mixture of mineral oils, heat-killed mycobacteria, and emulsifying agent, which was termed complete Freund's adjuvant (CFA); when omitting mycobacteria, also known as incomplete Freund's adjuvant (IFA); see also pristane-induced arthritis (PIA)	▪ Acute and self-limiting polyarthritis in contrast to human RA ▪ Not antigenic but displays an autoimmune pathophysiology	(Holmdahl, Lorentzen et al. 2001, Kim and Moudgil 2009, Bevaart, Vervoordeldonk et al. 2010, Choudhary, Bhatt et al. 2018)
Zymosan-induced arthritis	Mouse, rat	Intra-articular injection of zymosan, a polysaccharide from the cell wall of *Saccharomyces cerevisiae*, into the knee joints of mice causes proliferative arthritis, including immune cell infiltration, synovial hypertrophy, and pannus formation	▪ Technical skill required for an intra-articular injection in mice ▪ Monoarthritis in contrast to human RA	(Keystone, Schorlemmer et al. 1977, Frasnelli, Tarussio et al. 2005)
Streptococcal cell-wall-induced arthritis (SCWIA)	Mouse, rat	*Streptococcus pyogenes* synthesize a peptidoglycan-polysaccharide (PG-PS) polymer	▪ Pathogenesis is inducible in selected susceptible strains of rodents ▪ Germ-free conditions are necessary to reach susceptibility in rats ▪ Multiple injections are needed; otherwise, acute and self-limiting arthritis develops, in contrast to human RA ▪ Tumor necrosis factor (TNF)-α is less important in SCW-induced arthritis but not in human RA ▪ Rheumatoid factor is missing in polyarticular arthritis in rats	(Wilder 2001, Joosten, Abdollahi-Roodsaz et al. 2008, Bevaart, Vervoordeldonk et al. 2010)

Animal Models	Species	Induction/Genetic Alteration	Limitations	References
Cartilage oligomeric matrix protein (COMP)-induced arthritis	Mouse, rat	Immunization with IFA combined with native and denatured COMP, which is a large protein that is synthesized by chondrocytes (see also adjuvant-induced arthritis)	▪ Acute and self-limiting polyarthritis in contrast to human RA ▪ Not antigenic but displays an autoimmune pathophysiology	(Carlsen, Hansson et al. 1998, Carlsen, Nandakumar et al. 2008)
Pristane-induced arthritis (PIA)	Mouse, rat	Injection of the hydrocarbon pristane intraperitoneally into mice	▪ No evidence of autoimmune reactions ▪ Inflammation is restricted to the joints but systemic abnormalities are absent in rats	(Wooley, Seibold et al. 1989, Vingsbo, Sahlstrand et al. 1996, Holmdahl, Lorentzen et al. 2001)
Antigen-induced arthritis (AIA)	Mouse	Inoculation with antigen by intra-articular injection	▪ Intra-articular injection in mice requires advanced technical skills ▪ Does not recapitulate the endogenous breach of tolerance in contrast to human RA ▪ Excludes systemic component of disease	(Brackertz, Mitchell et al. 1977, Brackertz, Mitchell et al. 1977, Asquith, Miller et al. 2009)
Proteoglycan-induced arthritis	Mouse	Intraperitoneal injection of proteoglycan that is emulsified with an adjuvant	▪ Only inducible in susceptible strains of mice ▪ Incidence of ankylosing spondylitis without any exacerbations and remissions in contrast to human RA	(Asquith, Miller et al. 2009, Bevaart, Vervoordeldonk et al. 2010, Choudhary, Bhatt et al. 2018)
Glucose-6-phosphate isomerase (G6PI)-induced arthritis	Mouse	Immunization using the ubiquinone containing glycolytic enzyme G6PI with CFA for induction of RA	▪ Only inducible in susceptible strains of mice ▪ Low prevalence of antibodies against G6PI in patients with RA	(Matsumoto, Lee et al. 2003, Asquith, Miller et al. 2009, Bevaart, Vervoordeldonk et al. 2010, Choudhary, Bhatt et al. 2018)
Genetically manipulated spontaneous arthritis models				
K/BxN model	Mouse	K/B×N mice were generated by crossing mice expressing the MHC class II molecule A^{g7} with the T cell receptor (TCR) transgenic KRN line expressing a TCR specific for a G6PI-peptide	▪ Mutations have only been identified in mice ▪ Low prevalence of antibodies to g6pi in patients with RA ▪ Without systemic manifestations or production of rheumatoid factor in contrast to human RA	(Kouskoff, Korganow et al. 1996, Matsumoto, Lee et al. 2003, van Gaalen, Toes et al. 2004)

Animal Models	Species	Induction/Genetic Alteration	Limitations	References
SKG model	Mouse	Induction of arthritis due to point mutation in ZAP-70	▪Mutations have only been identified in mice ▪Disease manifestations in germ-free mice only upon induction	(Sakaguchi, Takahashi et al. 2003, Asquith, Miller et al. 2009, Bevaart, Vervoordeldonk et al. 2010, Choudhary, Bhatt et al. 2018)
Human TNF transgene model	Mouse	Transgene for human TNF-α	▪Mutations have only been identified in mice ▪No production of rheumatoid factor in contrast to human RA	(Keffer, Probert et al. 1991, Butler, Malfait et al. 1997, Asquith, Miller et al. 2009, Bevaart, Vervoordeldonk et al. 2010, Choudhary, Bhatt et al. 2018)

1.4. Building blocks for the development of a human *in vitro* joint

To mimic a preclinical model of joint diseases including arthritis the structural and cellular anatomy of a healthy joint ─ a flexible connection of two or more bones ─ needs to be fully established *in vitro*. Although joints can be subdivided into “true” (discontinuous) and “false” (continuous), only discontinuous joints, such as the joints of the ankle, knee, shoulder, and hip, have a cavity filled with synovial fluid and are affected by arthritis, in contrast to continuous joints (e.g., synchondrosis, syndesmosis) (Guyton 1985, Bhat and Janarthanan 2017). Despite different functions, the structure of the joints is basically comparable (Figure 2).

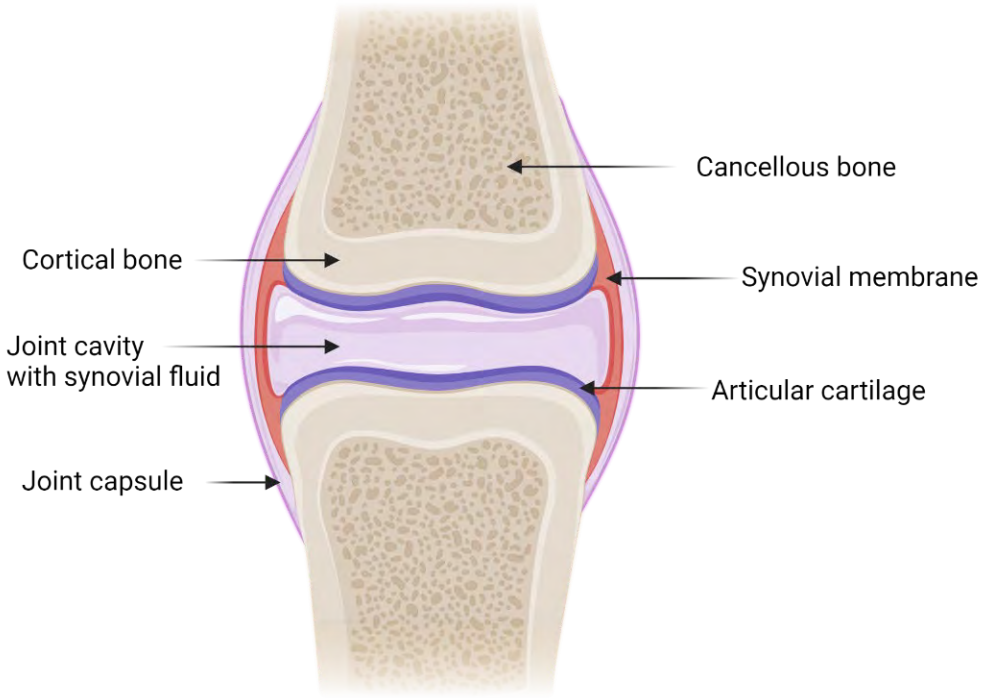

Figure 2: Basic structure of a synovial joint. Created with BioRender.com.

The joint space, a cavity filled with synovial fluid, separates the bone ends covered with hyaline cartilage (Barbe, Driban et al. 2009, Bhat and Janarthanan 2017). Synovial fluid is a clear, viscous fluid containing numerous plasma proteins. Mucins, such as hyaluronic acid, are secreted by the cells of the *membrana synovialis* and are responsible for the viscosity of the synovial fluid (Tamer 2013). The synovium acts as a natural lubricant that enables smooth movement (Barbe, Driban et al. 2009). In addition to its function as an elastic shock absorber, it also serves to nourish the bradytrophic articular cartilage as cartilage is not supplied by blood vessels (Bhat and Janarthanan 2017). Furthermore, the joint is enclosed externally by a joint capsule connecting the adherent bones and consisting of an outer membrane (*membrana fibrosa*) and an inner membrane (*membrana synovialis*) (Ralphs and Benjamin 1994, Bhat and Janarthanan 2017). The *membrana fibrosa* consists of firm collagenous connective tissue (collagen type I), whereas the *membrana synovialis* is composed of loose connective tissue

rich in vessels and nerves. Joints are formed during embryonic development, with the mesenchyme giving rise to bones, cartilage, and connective tissues of the body (Ralphs and Benjamin 1994, Barbe, Driban et al. 2009, Bhat and Janarthanan 2017).

1.4.1. Bone morphology

The subchondral bone is covered with hyaline cartilage. In general, bone is a highly vascularized, supportive connective tissue that undergoes constant, dynamic (re)modeling processes. The ECM comprises 50-70% inorganic components and 20-40% organic matrix. The remaining components are water deposits (5-10%) and lipids (<3%) (Florencio-Silva, Sasso et al. 2015). Hydroxyapatite (HA) ─ the main inorganic component ─ consists of calcium and phosphorus and is responsible for the high mechanical stability. The organic matrix with its main component collagen type I is responsible for elasticity and flexibility (Florencio-Silva, Sasso et al. 2015, Lopes, Martins-Cruz et al. 2018). Due to the diverse functional requirements for bone, the bone matrix composition consists of two characteristic features. The outer shell consists of dense, compact, and structured cortical bone externally covered by the periosteum, while the inner cavity consists of cancellous bone structures (Figure 3) (Clarke 2008, Tzelepi, Tsamandas et al. 2009). Cancellous bone cavities are filled with bone marrow, habituating the hematopoietic stem cell niche that comprises immune cells, osteoprogenitor cells such as mesenchymal stromal cells (MSCs), and osteoblasts (Shiozawa, Havens et al. 2008, Morrison and Scadden 2014).

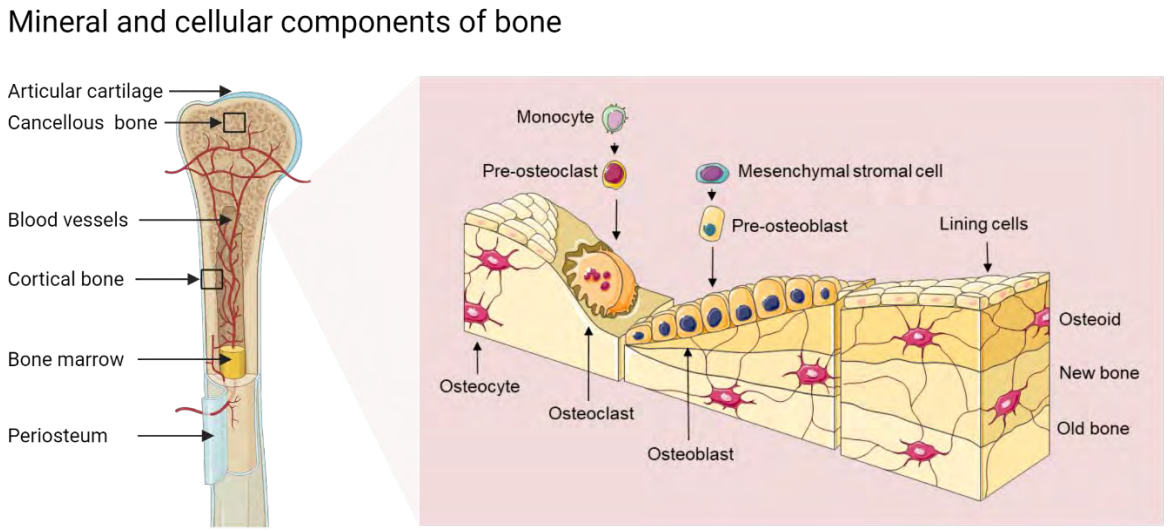

Figure 3: Representation of the mineral and cellular bone architecture. The mineral bone is composed of cancellous and cortical bone. Osteoblasts, derived from mesenchymal stem cells, are responsible for the mineralization of bone during both initial bone formation and bone remodeling. Osteoclasts derive from hematopoietic stem cells and resorb bone. The figure contains graphics from Servier Medical Art, licensed under a Creative Common Attribution 3.0 Generic License. http://smart.servier.com/. Created with BioRender.com.

In general, four types of highly specialized cells embedded in the ECM are characteristic for bone (Figure 3) (Lin, Patil et al. 2020). Osteoprogenitor stem cells from e.g., bone marrow and canals, have the ability to differentiate into osteoblasts. Bone-forming osteoblasts are of mesenchymal origin and synthesize bone osteoid by secretion of COL1, osteopontin (OPN), and osteocalcin (El Sayed, Nezwek et al. 2022). They display a cuboidal morphology with a round, basally located nucleus. In the final phase of bone formation, osteoblasts are enclosed by the ECM and enter a quiescent, mature state, to form non-proliferating, mechanosensing osteocytes (Clarke 2008). Osteocytes account for more than 90% of bone-specific cells. They exhibit a star-shaped morphology, are interconnected by canaliculi, gap junctions, and dendritic extensions, and are responsible for mechanosensing and mechanotransduction (Bonewald and Johnson 2008, Clarke 2008). In contrast, multinucleated osteoclasts are derived from hematopoietic mononuclear progenitor cells and are responsible for bone resorption (Lopes, Martins-Cruz et al. 2018, El Sayed, Nezwek et al. 2022).

1.4.2. Articular cartilage

Articular cartilage that covers the bony ends is an avascular, aneural, and alymphatic tissue. Nutrients are supplied by diffusion either through a vascular cartilage membrane or directly through the synovial fluid (Poole, Kojima et al. 2001). In cartilage, matrix-building and matrix-degrading processes are in equilibrium. Anabolic factors include TGF-β and bone morphogenetic proteins (BMPs) such as BMP 2 and BMP-7, whereas IL-1β and MMPs are catabolic factors. Chondrocytes, the cells mainly resident in the cartilage, respond to various stimuli, with static loading of cartilage suppressing matrix synthesis and cyclic, intermittent loading stimulating chondrocyte metabolism (Knobloch, Madhavan et al. 2008). Articular cartilage is composed of ECM containing cartilage-specific cells ─ chondroblasts and chondrocytes. The ECM, a three-dimensional network, consists of specialized collagen matrix such as collagen type 2, proteoglycans, non-collagenous glycoproteins, and 65-80% water (Poole, Kojima et al. 2001, Prein and Beier 2019, Eschweiler, Horn et al. 2021). The latter bind to the hydrophilic, negatively charged proteoglycans. Aggrecan (ACAN) is the most abundant and largest proteoglycan in cartilage. The complex of ACAN molecules consists of more than 100 glycosaminoglycan (GAG) chains. These molecules link with hyaluronic acid and can reversibly bind large amounts of water (Kiani, Chen et al. 2002). The binding of water is an important ability, which contributes to the maintenance of cartilage function.

Starting from MSCs, chondrocytes develop from chondroblasts. Chondroblasts are the active form of chondrocytes that synthesize the cartilage matrix components and subsequently differentiate into chondrocytes. The smaller, spherical chondrocytes have a round nucleus and are present in cartilage cavities. The chondron is the functional cartilage unit, bounded by a

cartilage capsule and enclosed by a cartilage vestibule containing chondrocytes. Two phases characterize cartilage growth. First, the cartilage matrix production supports to the proliferation of chondroblasts, resulting in cartilage growth, which is called interstitial growth. Subsequently, chondrocytes are produced by cell division and assemble in groups. In appositional growth, the chondroblasts form new cartilage matrix in the inner layer of the cartilage skin, which leads to cartilage growth from the exterior (Sophia Fox, Bedi et al. 2009, Purcell and Trainor 2015). Articular cartilage is divided into different zones (Figure 4).

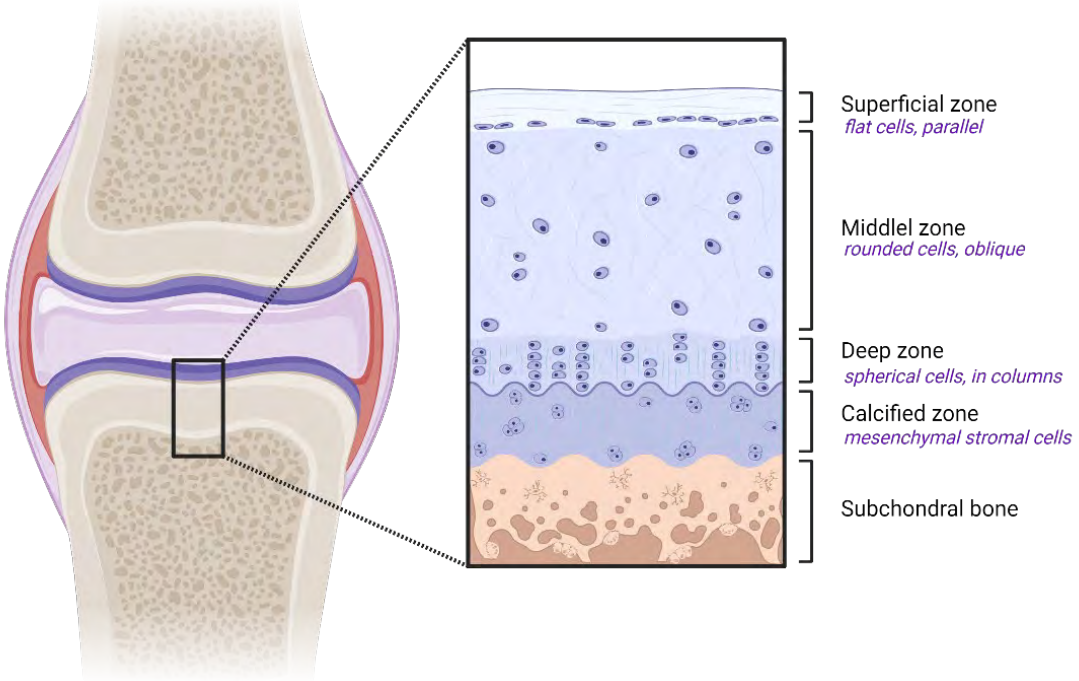

Figure 4: Structure of hyaline articular cartilage. Articular cartilage is divided into distinct zones – superficial zone, middle zone, deep zone, and calcified zone. The 3D orientation of the cells and their morphology vary with cartilage depth such that they are flat and parallel to the surface in the superficial zone, rounded cells randomly orientated in the middle zone, spherical cells perpendicular orientated to the surface in the deep zone next to the calcified zone. Created with BioRender.com.

The superficial zone forms the articular surface and is the thinnest, most cell-rich cartilage zone. Chondrocytes are present as inactive, flattened cells. The middle zone (tangential zone) accounts for 40% to 60% of the cartilage volume. Chondrocytes are marked by a spherical morphology and lower cell density. The deep zone accounts for 30% of the cartilage volume, has the lowest water content and the highest proportion of proteoglycans (Sophia Fox, Bedi et al. 2009, Eschweiler, Horn et al. 2021). Here, the chondrocytes are columnar and aligned parallel to the collagen fibers. The deep zone is adjacent to the calcified zone, which is the transition to the subchondral bone. This transition zone ensures cohesion between cartilage and bone because the collagen fibrils of the deep zone are anchored in the subchondral bone. Here, cell density is low, and chondrocytes are hypertrophic (Cova and Toffanin 2002, Goldring and Marcu 2009, Sophia Fox, Bedi et al. 2009).

1.4.3. Synovial membrane

The stroma forms the structural framework and covers tissue or lines cavities. The term synovium or synovial membrane refers to the connective tissue characterized by the absence of an epithelial cell layer. The synovium encapsulates the joints and lines the inner surface of the joint capsule and the joint cavity (Rhee, Marcelino et al. 2005, Smith 2011). It provides structural support, lubricates the surfaces, and supplies nutrients to the cartilage. The synovium consists of two anatomical and functional layers: the intimal lining (intima) and sublining (subintima) layer. Two types of synoviocytes with relatively similar proportions form the intima: macrophage-like cells (type A cells) and fibroblast-like cells (type B cells) (Scanzello and Goldring 2012). The synovial lining lacks a basement membrane and tight junctions. Hence, it is a loose composite of cells embedded in an amorphous matrix composed of collagens such as types I, III, IV, V, and VI (Orr, Vieira-Sousa et al. 2017). In addition, the intima is in contact with the intraarticular cavity and produces synovial fluid. Usually, it is one to four cell layers thick. In contrast, the subintima, consists of fibroblast-like synoviocytes with few macrophage type A cells and is composed of fibrous and fatty tissue, blood, and lymphatic vessels. The subintima is up to 5 mm in thickness (Figure 5) (Smith 2011).

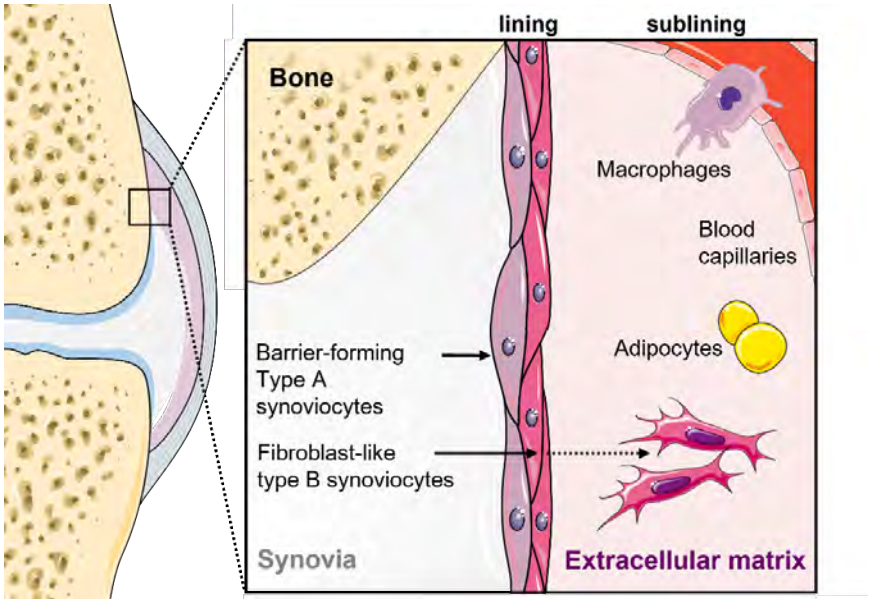

Figure 5: Overview of the synovial membrane architecture. The synovial membrane is made up of two layers: lining and sublining layer. The lining layer consists of barrier-forming synoviocytes type A and synoviocytes type B. The sublining layer is made up of fibrous, areolar, and fatty tissue. The figure contains graphics from Servier Medical Art, licensed under a Creative Common Attribution 3.0 Generic License. http://smart.servier.com/.

Type A synoviocytes can actively phagocytose or pinocytose cell debris, waste in the synovial cavity, and possess an antigen-presenting ability. These type A cells are derived from blood-based mononuclear cells, can be considered resident macrophages and are localized in the intimal and subintimal layer of the synovium (Buckley 2019). Type B synoviocytes or FLSs are

the major stromal cells of the joint synovium that physiologically maintain joints' structural and dynamic integrity. They are of mesenchymal origin and can be defined as non-vascular, non-epithelial cells of the synovium, arise during embryogenesis by local division and are replaced by local division (Li, Tang et al. 2019). Type B synoviocytes synthesize matrix components such as hyaluronic acid, collagens, and fibronectin of the synovial fluid. They perform a lubricating function and allow joint surfaces to smoothly slide across each other. Therefore, they are essential for cartilage integrity and lubrication of the joint (de Sousa, Casado et al. 2014). Large amounts of hyaluronan are found mainly in the intimal layers of normal synovium while disappearing in the subintimal layer. This indicates diffusion of hyaluronan from the surface towards the clearing lymphatic vasculature.

Considering the structural and cellular anatomical features of the joint, it is apparent that mimicking this complex functional unit *in vitro* is a challenge.

1.5. *In vitro* models of arthritis

During the last decade, advances in tissue engineering have improved promising *in vitro* techniques. Thus, the pathogenesis of RA has been studied using a variety of *in vitro* and *in vivo* models. Cell-based *in vitro* assays range from tissue explants and relatively simplified (co)-culture systems to complex engineered three-dimensional (multi)component tissue systems. Therefore, a variety of cell types from cell lines, primary cells, or patient-derived cells, such as MSCs or induced pluripotent stem cells (iPSCs), to study e.g., cell migration, activation, antigen presentation, cell-cell interaction, as well as cell- and matrix-related changes are used. Additionally, microfluidic chip technology and *in silico* approaches are promising techniques to further study the mechanisms underlying RA pathophysiology and to identify potential new targets. Thus, next-generation preclinical *in vitro* screening systems will be based on microphysiological *in vitro* human-joint-on-a-chip systems using primary cells from patients with RA and from different organs, mimicking the systemic nature of the disease and fostering the translational process to humans, while reducing the number of animal experiments. Ultimately, the main goal for all *in vitro* approaches is to achieve the greatest possible physiological proximity to the disease, while ensuring experimental feasibility, breaking down the barrier to translational medicine and thus conducting high-quality, reproducible research (Figure 6) (Damerau and Gaber 2020).

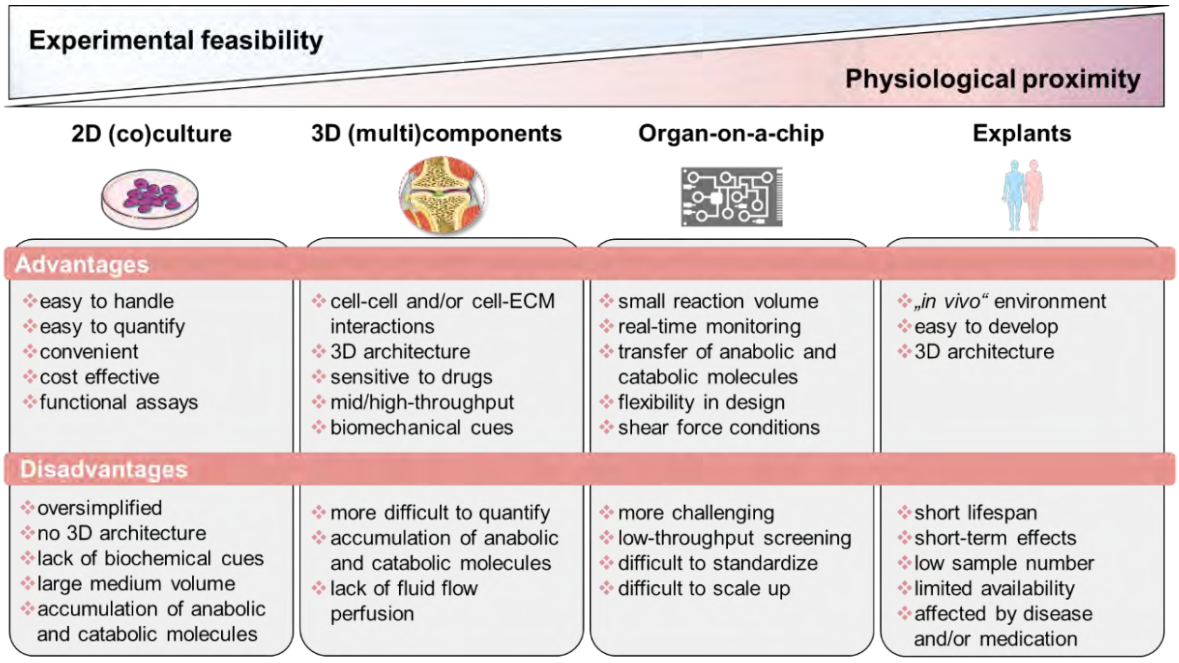

Figure 6: Overview of state-of-the-art *in vitro* models classified according to experimental feasibility and physiological proximity (Damerau and Gaber 2020). The figure contains graphics from Servier Medical Art, licensed under a Creative Common Attribution 3.0 Generic License. http://smart.servier.com/ (Damerau and Gaber 2020).

1.5.1. Tissue Explants: Close physiological proximity but low experimental feasibility

Ex vivo culture models or tissue explants exhibit the closest physiological similarity to pathological tissue due to the nature of their origin. If available in the clinics and ethically justifiable, these models can be easily obtained, are straightforward to develop, and allow the semi-controlled study of the behavior of included cell populations. Although tissue explants reflect human physiology in terms of 3D structure, cell composition, and environment, they are often affected by individual health status, medication, and sample preparation. Nevertheless, tissue explant approaches are still a powerful tool in, e.g., osteochondral bone research due to the ability to retain native bone cell communication and to study cellular responses and extracellular matrix remodeling processes, including disease-specific matrix degradation in a (patho)physiological bone environment (Marino, Staines et al. 2016). In addition to their limited availability (especially in terms of healthy human material), the main limitations of tissue explant models are shortened lifespan due to simultaneous disruption of the supplying vessels and, consequently, induced cell death and necrosis-induced cell death at the explant/wound edges (Gilbert, Singhrao et al. 2009). With synovial tissue, explants can be obtained from patients with RA or OA during joint replacement surgery, as well as by needle and arthroscopic biopsy. These types of samples have been comprehensively examined using molecular and immunohistochemical techniques leading to a better understanding of the pathogenic events

occurring in the course of the disease (Nozaki, Takahashi et al. 2007). Samples of synovial (Chevrel, Garnero et al. 2002) and bone explants (Chabaud and Miossec 2001) have been used to study the efficacy and efficiency of drugs on the (i) production of pro-inflammatory mediators, (ii) expression of matrix-degrading enzymes, and (iii) adhesion molecules. Of note, IL-1β, TNF-α, and IL-17 have been demonstrated to produce many additives and/or synergistic effects *in vitro*. Using synovial explants from patients with RA, therapeutic intervention with a combination of biologicals, e.g., anti-TNF-α antibodies and IL-1Ra, resulted in significantly decreased IL-6 and MMP3 production, indicating the superior efficacy of combinatorial therapy over a single biological treatment (Hosaka, Ryu et al. 2005). As an example, Kirenol, a Chinese herbal active component, was demonstrated to inhibit FLS proliferation, migration, invasion, and secretion of pro-inflammatory IL-6 in explants from RA synovium (Wu, Li et al. 2019, Damerau and Gaber 2020).

Explants, such as articular cartilage discs, have been obtained from patients with RA after knee arthroplasty to examine disease-related expression profiles. Using this approach, Gotoh et al. demonstrated that the interaction of CD40 with CD154 increased the expression of inflammatory cytokines and MMPs, resulting in increased cartilage degradation in patients with RA (Gotoh, Kawaguchi et al. 2004). Based on the aforementioned types of explants, Schultz et al. developed a 3D *in vitro* model to investigate destructive processes in RA (Schultz, Keyszer et al. 1997). Although the explant co-culture system did not address all aspects of RA, such as the presence of immune cells, the authors confirmed the capability of their model to study FLS activity on destructive processes of established joint diseases *in vitro* (Schultz, Keyszer et al. 1997, Damerau and Gaber 2020).

1.5.2. Simplified 2D culture and co-culture approaches

To mimic physiological and pathophysiological biological complexity of tissues and their disorders, the 3D structure of the respective tissue is required and reachable using either 3D tissue explants or *in vitro* models. However, achieving experimental feasibility and ensuring adequate nutrient and oxygen supply are more challenging tasks with 3D designs than 2D cell cultures. Therefore, 2D monolayer cell cultures are a simple and cost-effective alternative, especially for high-throughput screening approaches, which are common in pharmaceutical, industrial, and toxicological research. They are still used to (i) investigate the efficiency and efficacy of therapeutics, (ii) determine their optimal concentration, (iii) analyze disease-related gene expression profiles, and (iv) study cell-cell, cell-microenvironment, or cell-humoral interactions using auto- and paracrine signals, such as in aggregate-cell interactions, in a simplified co-culture system (Turner, Counts et al. 1980, Croft, Naylor et al. 2016, Chen, Li Yim et al. 2019, Lewis, Barnes et al. 2019). Two-dimensional monolayer cell cultures are used for

rapid *in vitro* cell expansion, despite the risk of cellular alterations in terms of morphology, genetic alteration, cell diversity, cell cycle progression, and cell differentiation capacity (von der Mark, Gauss et al. 1977). Accordingly, when trying to mimic cartilage in monolayer, the phenotype of chondrocytes becomes unstable, indicated by a downregulation of type II collagen, with a concomitant increase in the expression of type I collagen. To avoid these artificial changes, an optimized cultivation procedure is required using specific plate coatings, such as poly(L-lactic acid) (Benya, Padilla et al. 1978). When investigating the effects of RA-associated cytokines on cartilage, monolayer chondrocyte cultures are considered an optimal tool due to their easy handling and the rapid response of chondrocytes to pro-inflammatory cytokines. In addition, chondrocytes, when stimulated with, e.g., IL-1β, TNF-α, or IFN-γ, show a classical RA-like phenotype as evidenced by decreased expressions of COL2 and ACAN while both MMP13 expression (Murphy and Lee 2005) and induced apoptosis in chondrocytes increase (Schuerwegh, Dombrecht et al. 2003), reflecting the human *in vivo* situation (Kim and Song 1999, Saito, Murakoshi et al. 2008). Using the 2D approach, Teltow et al. demonstrated that the majority of IL-1β-treated chondrocytes produced collagenase 1 instead of collagenase 3. However, the latter has been assumed to foster the destructive processes of RA joints by degrading collagen type II (Tetlow and Woolley 1998). IL-1β was demonstrated to decrease the expression of COL2 in monolayer cultures (Goldring and Berenbaum 1999, Damerau and Gaber 2020).

Expanding the 2D monolayer cultures using co-culture systems, the interaction between cells growing in the same environment can be cultivated either indirectly (physical barrier) by simple medium transfer and using a trans-well chamber or directly in a mixed culture system providing cell-to-cell contact. Using direct and indirect co-cultivation, Donlin et al. demonstrated that human RA synovial fibroblasts suppress the TNF-α-induced IFN-γ signature in macrophages under both conditions, indicating that no cell contact is required, but rather soluble fibroblast products inhibit the IFN-γ signature of macrophages (Donlin, Jayatilleke et al. 2014). To extend the co-culture systems, Pagani et al. developed an advanced tri-culture model to study the interaction between osteoblasts, osteoclasts, and endothelial cells and the cytokine-induced effects on bone homeostasis concerning RA (Pagani, Torricelli et al. 2018, Damerau and Gaber 2020).

1.5.3. 3D tissue engineering approaches: Mimicking structural features of the joint

In the field of musculoskeletal disorders, simplified 2D cell culture systems have been stepwise replaced by promising *in vitro* 3D tissue engineering approaches, including (i) scaffold-free 3D approaches, such as cell-sheet formation (Kim, Bou-Ghannam et al. 2019), self-assembly, or

self-organization (Weber, Fischer et al. 2020), (ii) natural scaffold-based 3D approaches, such as hyaluronic-acid-based scaffolds (Dhivya, Saravanan et al. 2015), and (iii) synthetic scaffold-based 3D approaches, such as poly-(lactide)-based scaffolds (Scheinpflug, Pfeiffenberger et al. 2018). These 3D approaches offer considerable advantages compared to the above-mentioned 2D approaches because they facilitate cell-cell and cell-matrix interactions, cell proliferation, differentiation, and migration. Finally, they maintain the cell fate as a result of the physiological 3D structure. To mimic the structural features of the joint, which is a prerequisite for simulating the pathogenesis of RA, the various cell-based components, such as synovial membrane and the chondrogenic and osteogenic parts, must be developed for an *in vitro* 3D approach (Damerau and Gaber 2020).

Multicomponent *in vitro* 3D co-cultures systems combining 3D *in vitro* models of articular cartilage and bone (osteochondral unit) with *in vitro* 3D models of the synovial membrane are necessary to study the cartilage degradation and bone erosive processes during RA that are linked to the invasiveness of the hyperplastic synovium (pannus) [132]. Currently, multicomponent engineering approaches are widely used to simulate key features of OA instead of RA or are used to develop suitable artificial matrices that can replace damaged regions and promote tissue regeneration. Thus, many promising *in vitro* approaches have been recently developed using (i) scaffold-based bone and scaffold-free cartilage [133], (ii) different scaffolds for both bone and cartilage, (iii) a heterogeneous (bi-layered) scaffold, or (iv) a homogenous scaffold for both bone and cartilage [134]. Notably, bi-layered systems are most often fixed by adhesives, such as fibrin, creating a barrier for cell–cell contact. To avoid this, Lin et al. encapsulated iPSCs-derived MSCs (iMPCs) in a photo-crosslinkable gelatin scaffold. Using a dual-flow bioreactor, encapsulated iMPCs were chondrogenic (top) and osteogenic (bottom) differentiated to directly form a stable bridging zone between both tissue models [135]. So far, no appropriate multicomponent *in vitro* model exists that is able to mimic the physiologically relevant environment of a healthy or an inflamed joint, including all signaling molecules, cells, and tissue types (Damerau and Gaber 2020).

2. CHAPTER: AIMS

A prerequisite for simulating joint inflammation and destruction as a feature of RA is to mimic the structural anatomical characteristics of the joint including the following cell-based components: the bony part covered by a chondral tissue located close to the synovial membrane. These cell-based components must be designed and engineered accordingly for an *in vitro* 3D approach.

Therefore, the aim of this thesis was to establish and characterize human *in vitro* tissue equivalents of the joint, namely (1) cancellous bone, (2) articular cartilage, and (3) synovial membrane using MSCs to provide the possibility of producing a complete joint model from single donor material thus offering the opportunity of a personalized testing platform.

For this purpose, it was necessary to (i) establish and characterize scaffold-based bone-like constructs solely based on human MSCs. In order to build the osteochondral unit of a healthy joint, (ii) the development and characterization of scaffold-free cartilage constructs at the macro- and microscale was targeted. Once both components are fully established, (iii) their responsiveness to disease-relevant cytokines should be analyzed in terms of arthritis-related changes in cell and matrix composition. Getting more complex, the next aim was (iv) the co-cultivation of these two components of the joint in order to generate a functional osteochondral unit and to test its responsiveness to inflammatory stimuli. Finally, (v) the development of a xeno-free synovial membrane model was aimed at ultimately mimicking all functional units of the joint needed to simulate arthritis.

Ultimately, the established 3D *in vitro* models could serve as a preclinical screening tool providing the opportunity to study cellular processes within the tissue, investigate cytokine-driven key mechanisms of arthritis, and test therapeutic interventions on tissue level *in vitro*.

3. CHAPTER: RESULTS

3.1. Part I: Modeling the osteochondral unit

Degeneration of articular cartilage and disruption of subchondral bone homeostasis, including bone lesions and erosions, are critical features of arthritis. To explore the pathogenesis of arthritis, it is necessary to thoroughly understand the physiology of the major components of the joint. This particularly includes the complex knowledge on the osteochondral unit, which consists of subchondral bone covered by articular cartilage, in terms of anatomy, function and supply (Ostrowska, Maśliński et al. 2018). Articular cartilage is responsible for both smooth joint movement and load bearing capacity, while subchondral bone supports articular cartilage to maintain homeostasis. Cartilage and subchondral bone interact through the exchange of signaling and nutritional molecules within the osteochondral unit (Lepage, Robson et al. 2019). Their importance becomes apparent when cartilage destruction begins, leading to pain and impaired quality of life. Although the physical impairment of patients and the economic burden of arthritis are substantial, the long-lasting problem will increase significantly over years as the population ages (Glyn-Jones, Palmer et al. 2015). Preventing the development of arthritis and treating joints already affected by RA or OA are the focus of current research with the goal of preserving or restoring joint function (Mendes, Katagiri et al. 2018). Therefore, sophisticated *in vitro* and *in vivo* models are required to achieve this goal. Although a variety of models for arthritis, particularly RA, already exist, many of the current model systems for arthritis are of limited predictive value as they either rely on phylogenetically distant species or suffer from oversimplified culture conditions. These limitations pose major challenges to preclinical testing and translation to humans. Various tissue engineering approaches have been pursued for the *in vitro* generation of artificial bone and cartilage, including scaffold-based (synthetic or natural), scaffold-free (cell-sheet technology, self-assembly, or self- organization), and more complex microfluidic model systems (Murdoch, Grady et al. 2007, Weber, Fischer et al. 2020, Pirosa, Gottardi et al. 2021). Most of the established *in vitro* tissue equivalents are derived from primary cells or MSCs. As osteoblasts, chondrocytes, and synovial fibroblasts originate from MSCs, they have been extensively studied for their broad clinical potential. However, an experimental setting of arthritis is still needed to (i) investigate key mechanisms involved in the pathogenesis of e.g., RA, (ii) use this model as a preclinical tool, to test new therapeutic approaches, (iii) facilitate the translatability of results by using human material, and (iv) reduce the number of animal experiments.

Hence, the following peer-reviewed publication presents a ceramic-based bone equivalent and scaffold-free cartilage equivalent that have been successfully used for the *in vitro* generation of a 3D osteochondral unit as a potential part of an artificial joint. Major features of arthritis were induced by regular administration of RA-related cytokines, and the impact of approved drugs on the extent of inflammation was investigated.

3.1.1. Manuscript 1: A human osteochondral tissue model mimicking cytokine-induced key features of arthritis *in vitro*

This is a peer-reviewed version of the following article:

Authors: Alexandra Damerau, Moritz Pfeiffenberger, Marie-Christin Weber, Gerd-Rüdiger Burmester, Frank Buttgereit, Timo Gaber*, Annemarie Lang* (*These authors contributed equally)

Title: A human osteochondral tissue model mimicking cytokine-induced key features of arthritis *in vitro*

Year: 2021

Journal: International Journal of Molecular Sciences (Volume 22, Issue 1, 128)

Final form: https://doi.org/10.3390/ijms22010128

Personal contribution: In this manuscript, I was responsible for conceptualizing, planning, preparing, conducting, analyzing and interpreting the experiments including MSC isolation, expansion and characterization, generation of bone equivalents, cultivation and characterization of bone and cartilage constructs, development of the osteochondral unit, cytokine and drug treatment experiments, histological and immunofluorescence investigations and quantifications, primer design and gene expression analysis using quantitative real-time PCR, viability and metabolic assays, flow cytometry, and scanning electron microscopy. Manuscript design, visualization, writing, and final approval was performed under the supervision of Dr. Annemarie Lang, PhD, Dr. Timo Gaber, and Prof. Dr. Frank Buttgereit.

International Journal of
Molecular Sciences

MDPI

Article

A Human Osteochondral Tissue Model Mimicking Cytokine-Induced Key Features of Arthritis In Vitro

Alexandra Damerau [1,2], Moritz Pfeiffenberger [1,2], Marie-Christin Weber [1], Gerd-Rüdiger Burmester [1,2], Frank Buttgereit [1,2], Timo Gaber [1,2,*,†] and Annemarie Lang [1,2,†]

[1] Charité—Universitätsmedizin Berlin, Corporate Member of Freie Universität Berlin, Humboldt-Universität zu Berlin, and Berlin Institute of Health, Department of Rheumatology and Clinical Immunology, 10117 Berlin, Germany; alexandra.damerau@charite.de (A.D.); moritz.pfeiffenberger@charite.de (M.P.); marie-christin.weber@charite.de (M.-C.W.); gerd.burmester@charite.de (G.-R.B.); frank.buttgereit@charite.de (F.B.); annemarie.lang@charite.de (A.L.)
[2] German Rheumatism Research Centre (DRFZ) Berlin, a Leibniz Institute, 10117 Berlin, Germany
* Correspondence: timo.gaber@charite.de
† These authors contributed equally.

Abstract: Adequate tissue engineered models are required to further understand the (patho)physiological mechanism involved in the destructive processes of cartilage and subchondral bone during rheumatoid arthritis (RA). Therefore, we developed a human in vitro 3D osteochondral tissue model (OTM), mimicking cytokine-induced cellular and matrix-related changes leading to cartilage degradation and bone destruction in order to ultimately provide a preclinical drug screening tool. To this end, the OTM was engineered by co-cultivation of mesenchymal stromal cell (MSC)-derived bone and cartilage components in a 3D environment. It was comprehensively characterized on cell, protein, and mRNA level. Stimulating the OTM with pro-inflammatory cytokines, relevant in RA (tumor necrosis factor α, interleukin-6, macrophage migration inhibitory factor), caused cell- and matrix-related changes, resulting in a significantly induced gene expression of lactate dehydrogenase A, interleukin-8 and tumor necrosis factor α in both, cartilage and bone, while the matrix metalloproteases 1 and 3 were only induced in cartilage. Finally, application of target-specific drugs prevented the induction of inflammation and matrix-degradation. Thus, we here provide evidence that our human in vitro 3D OTM mimics cytokine-induced cell- and matrix-related changes—key features of RA—and may serve as a preclinical tool for the evaluation of both new targets and potential drugs in a more translational setup.

Keywords: mesenchymal stem cells; tissue engineering; osteochondral unit; in vitro model; rheumatoid arthritis

Citation: Damerau, A.; Pfeiffenberger, M.; Weber, M.-C.; Burmester, G.-R.; Buttgereit, F.; Gaber, T.; Lang, A. A Human Osteochondral Tissue Model Mimicking Cytokine-Induced Key Features of Arthritis In Vitro. *Int. J. Mol. Sci.* **2021**, *22*, 128. https://dx.doi.org/10.3390/ijms22010128

Received: 26 November 2020
Accepted: 23 December 2020
Published: 24 December 2020

1. Introduction

The osteochondral unit is an essential part of the joint and commits the functional association of the articular cartilage, calcified cartilage and the subchondral bone. Its main function is to transfer mechanical strain during weight-bearing and to ensure the mechanical and metabolic homeostasis as well as the overall joint integrity. Articular cartilage is surfacing the subchondral bone, adsorbing mechanical loading and distributing forces within the joint, while the subchondral bone provides mechanical stability, maintains the joint shape and supplies nutrient and oxygen for the deeper layers of the avascular cartilage [1].

Several pathologies have been demonstrated to affect the osteochondral unit e.g., microcracks, microedema, microbleeding, the development of subchondral bone cysts and osteophytes co-localizing with regions of articular cartilage damage [2–4]. All these changes are also attributed to the degenerative joint disease osteoarthritis (OA) or chronic

autoimmune-mediated joint inflammation such as found in rheumatoid arthritis (RA), which is a systemic autoimmune disease. OA is principally characterized by articular cartilage degeneration often accompanied with subchondral bone erosions due to a higher load impact and the presence of certain mediators and growth factors [5,6]. On the other hand, the progressive, destructive processes in RA are driven by a persistent inflammation of the joint. The complex pathogenesis of RA involves a diverse interplay between various humoral factors, cell types and tissues, though many underlying triggers and mechanism are still unclear. Beside the production of autoantibodies, the release of pro-inflammatory cytokines, such as tumor necrosis factor (TNF)α, interleukin (IL)-1, -6, -17 and macrophage migration inhibitory factor (MIF) and the induction of matrix degrading enzymes such as matrix metalloproteases (MMPs) drives both inflammation and destructive processes within cartilage and subchondral bone leading to an imbalance in metabolic processes [7]. During RA, MMP1, MMP3, MMP8, and MMP13 are predominantly involved in the extracellular matrix remodeling and degradation of cartilage collagens and proteoglycans but may also affect bone (e.g., MMP3, MMP13) [8,9].

As long as the causes of the disease are unknown, current therapies in clinical application aim to reduce the inflammatory mechanisms in the pathogenesis of RA, whereby their unwanted effects with regard to joint and bone homeostasis are often neglected or accepted, as exemplified by the use of glucocorticoids and their pro-osteoporotic effects [10]. According to current recommendations, today's treatment goal is to achieve remission or at least low disease activity [11]. Despite major progress in the treatment of RA, a strong unmet medical need remains, as not all patients reach the treat-to-target goal, i.e., sustained clinical remission or low disease activity; about 25% still suffer from moderate or even high disease activity [11]. Therefore, preclinical models which reflect the complexity of the functional unit of the joint are essential to improve our understanding of pathophysiological mechanisms, to increase our knowledge on adverse drug effects in clinical use, and to develop and verify new therapeutic approaches.

Until today, animal models represent an integral part of the preclinical drug discovery process. While animals do not develop spontaneously autoimmune conditions such as RA—which constitutes an inherent limitation of these models—arthritis can be induced in these animals by a single agent or by genetic manipulations [12–14]. Finally, non-humanized rodent models are not suitable to test treatment strategies which are highly specific for human target proteins [12]. Understanding the homeostasis within the osteochondral unit as well as RA-related mechanisms is essential for determining treatment strategies. Therefore, different in vitro models have been developed and evaluated during the last years ranging from tissue explants, simplified (co)culture systems and complex tissue engineered three-dimensional (3D) (multi)component systems to chip approaches [14]. Most of the current in vitro cell culture systems in monolayer are used to study the effect of e.g., humoral factors or therapeutics on chondrocytes [15,16], aggregate-cell interactions or cell-cell interplay [14,17], lacking the complexity of (patho)physiologically relevant cell-cell and cell-matrix interactions and nutrient gradients [14,18]. Today, complex 3D in vitro systems include the co-cultivation of e.g., bovine cartilage discs with human synovial fibroblasts mimicking early cartilage destructive processes [19], porcine chondrocytes with an RA-derived cell line [20], RA synovium with bone explants [21] or cartilage explants from either humans or animals [22]. Cartilage and bone differ in matrix characteristics and microenvironmental and mechanical cues. Therefore, osteochondral tissue engineering requires (i) a unique cell and matrix composition, (ii) a certain organization of the artificial tissue with or without scaffold and (iii) specific biological properties. To date, promising in vitro tissue engineering approaches have been developed using (i) scaffold-based bone and scaffold-free cartilage [23], (ii) different scaffolds for both bone and cartilage [24], (iii) a single heterogeneous scaffold [25] or (iv) a single homogenous scaffold for both [26]. A major challenge is the restriction to obtain human primary cells or explants, the limited lifespan of explants [27] and the unstable phenotype of chondrocytes during monolayer expansion [28]. Therefore, mesenchymal stromal cells (MSCs) are often used to engineer

Int. J. Mol. Sci. **2021**, *22*, 128

cartilage and bone equivalents [14]. Despite major progress especially due to emerging techniques such as 3D bioprinting, so far, there is no appropriate in vitro model which is able to mimic an inflamed joint with respect to the osteochondral unit allowing the preclinical testing of a variety of specific therapeutic approaches.

Here, we describe a human in vitro 3D osteochondral tissue model (OTM) as potential part of an artificial joint, comprising a scaffold-free cartilage-like component and a tricalcium phosphate (TCP)-based bone-like component (TBBC). In addition, we aimed at demonstrating that this engineered human OTM can be used as in vitro model to study cytokine-driven cell- and matrix-related changes during osteochondral degradation—key feature of RA. Moreover, we evaluated the feasibility of our OTM by using approved biologics, which prevented these cytokine-related changes. An overview on the experimental setup is given in Figure 1.

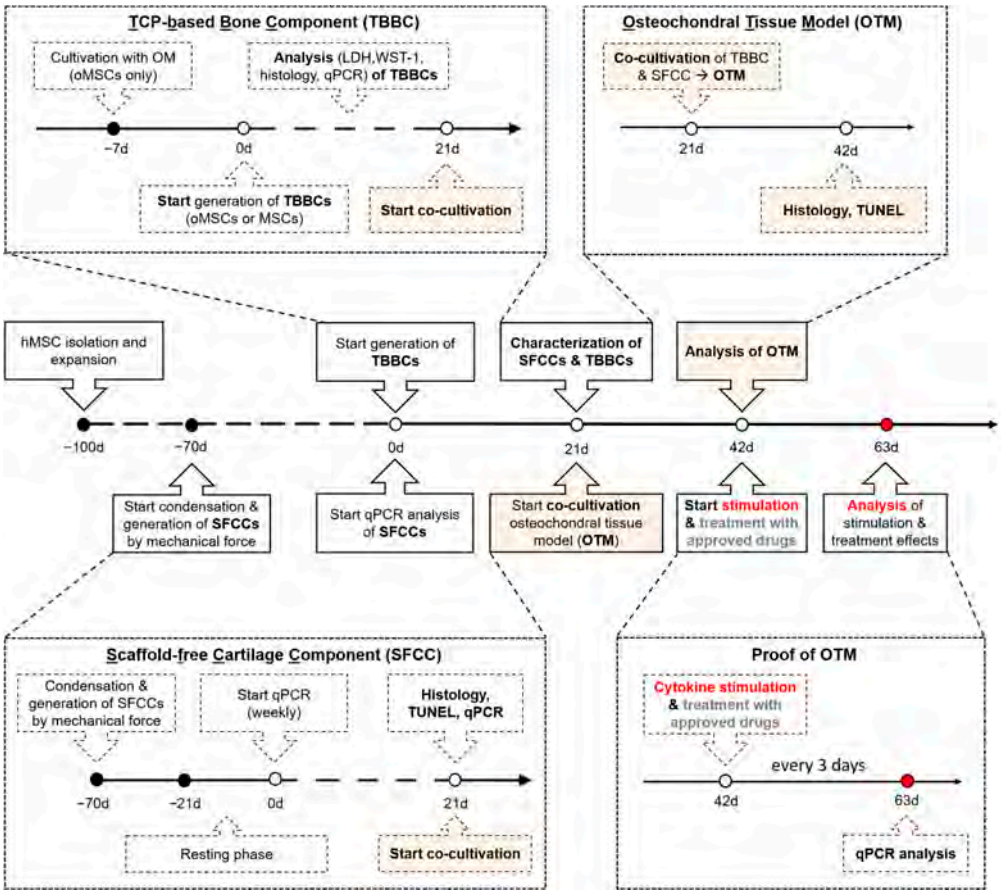

Figure 1. Schematic overview of the timely interlocked processes to generate the human in vitro 3D osteochondral tissue model of arthritis. Based on human bone marrow-derived mesenchymal stromal cells (MSCs), the in vitro 3D TCP-based bone components (TBBCs) and scaffold-free cartilage components (SFCCs) were developed. The osteochondral tissue model (OTM) was engineered by co-cultivation of both tissue components for 21 days. To replicate cytokine-mediated features of rheumatoid arthritis (RA), the osteochondral tissue model was stimulated with typical RA-related cytokines (tumor necrosis factor α, interleukin-6, and macrophage migration inhibitory factor) and finally treated with approved drugs (Proof of OTM). oMSC, one-week osteogenic pre-differentiated MSCs; OM, osteogenic medium; TCP, tricalcium phosphate; LDH, lactate dehydrogenase.

2. Results

2.1. Optimization of the TCP-Based Bone Component Results in a Valid and Sustainable Osteogenic Phenotype Replicating the Subchondral Bone Compartment

Firstly, we determined a cell/TCP ratio of approximately 1×10^6 cells/12 mg (0.8×10^5 cells/mg) as being optimal for the in vitro 3D TCP-based bone component (TBBC) since higher initial cell densities led to increased cell death (Appendix A Figure A1). To test whether osteogenic pre-differentiation of seeded MSCs influences the TBBC formation, we pre-differentiated MSCs using osteogenic differentiation medium for one week (oMSCs) and colonized TCP particles with either MSCs or oMSCs (Figure 2A). Scanning electron microscopy revealed that both MSCs and oMSCs became adherent to the TCP scaffold and invaded the TCP scaffold within 21 days (Figure 2B). Both, MSCs and oMSCs colonized the TCP scaffold within 21 days without any sign of cytotoxicity as demonstrated by the lack of differences in LDH release when compared to the spontaneous release of a TCP-free monolayer (ML), but a significant lower release compared to the positive control (Figure 2C). Analyzing cell viability after 21 days of incubation using LIVE/DEAD staining, we observed a significant lower amount of viable oMSCs (Calcein AM+; green) and an increase in EthD1+ oMSCs (dead, red) when compared to the corresponding MSCs and the respective ML (Figure 2D,E). Analyzing cellular metabolic activity using the WST-1 assay, we detected a significantly reduced metabolic activity in oMSCs compared to MSCs after 21 days (Figure 2F). Interestingly, co-cultivation of MSCs or oMSCs with osteoconductive TCP significantly increased calcium deposition after 7 and 21 days when compared to the monolayer incubated in osteogenic medium but without TCP. Calcification was more pronounced in MSCs than oMSCs (Figure 2G).

Taken together, MSCs and oMSCs colonized the TCP scaffold within 21 days without any sign of cytotoxicity while cell viability, metabolic activity, and calcification were more pronounced in MSCs than oMSCs (Figure 2C–G).

To investigate the spatial distribution, matrix formation and the osteogenic phenotype of either MSCs or oMSCs on the TCP scaffold, we quantified TBBC sections for the expression of actin, laminin and osteopontin (OPN) normalized to the cell nuclei (DAPI) using immunofluorescence staining (Figure 3A). To assess the spatial distribution, the total area of TBBC section was sub-divided into an outer, middle, and inner area and analyzed for the expression of actin. At day 21, seeded MSCs demonstrate a more pronounced and distributed staining for actin throughout the total area of TBBC section than oMSCs as indicated by significantly more actin staining in the total, middle, and inner area (Figure 3A). To assess the matrix formation, we normalized the relative expression of the extracellular protein laminin as quantified at day 21 to day 1. We found an up to 2-fold increase of matrix production in MSCs and oMSCs over time without observing differences between the two groups (Figure 3B). When focusing on the OPN expression as a measure of osteogenic phenotype, we observed significantly more OPN expression per cell in the TBBCs populated with MSCs than those with oMSCs both in the total area and in the middle and inner area (Figure 3C). Together with the observed actin distribution within the TCP, the OPN results indicate that the invading cells differentiate towards the osteogenic lineage. In this line of observation, the upregulation of runt-related transcription factor 2 (*RUNX2*), secreted phosphoprotein 1 (*SPP1*), osteonectin (*ON*), and collagen type 1 alpha 1 (*COL1A1*), respectively, where superior over time in MSCs as compared to oMSCs (Figure 3D). Based on these findings, we proceeded with the use of MSCs for the generation of TBBCs.

Int. J. Mol. Sci. **2021**, *22*, 128

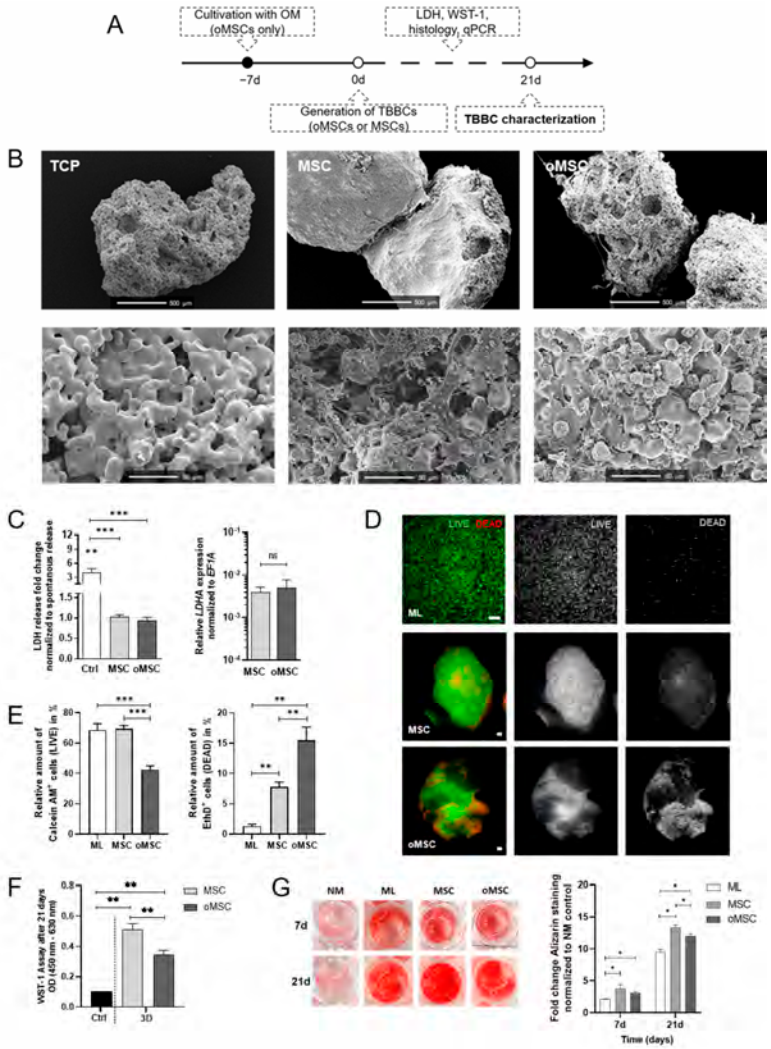

Figure 2. In vitro studies on β-TCP biocompatibility and cell survival comparing the suitability of human mesenchymal stromal cells (MSCs) and osteogenic pre-differentiated MSCs (oMSCs). (**A**) Experimental design of the in vitro TCP-based bone component (TBBC). (**B**) Structural evaluation of β-TCP using scanning electron microscopy. Exemplary images of n = 6. Scale bars show 500 µm and 50 µm as indicated in the images. (**C**) LDH-assay was conducted after 24 h to confirm the biocompatibility of β-TCP. Ctrl = 2% of Triton X-100. Data are shown as mean ± SEM for n = 10–12. Gene expression of lactate dehydrogenase A (*LDHA*) was determined by qPCR and normalized to the housekeeper gene *EF1A*. Data are shown as mean ± SEM for n = 4. Mann-Whitney U-test was used to determine the statistical significance between groups and Wilcoxon signed-ranked test for the spontaneous LDH release control. (**D**) LIVE/DEAD staining was performed after 21 days and (**E**) quantified using ImageJ. As control MSCs in monolayer (ML) were stained. Green and red colors discriminated between living and dead cells (scale bar = 100 µm). Representative images are shown accordingly for n = 4–6. Data are shown as mean ± SEM. (**F**) WST-1 assay was conducted to confirm metabolically active cells after 21 days of 3D cultivation. Ctrl = 2% of Triton X-100. Data are shown as mean ± SEM for n = 6. Mann-Whitney U-test was used. (**G**) MSCs and oMSCs were cultivated for 7 and 21 days in normal medium (NM control), in osteogenic medium without β-TCP (ML) and with β-TCP populated with MSCs (MSC) or pre-differentiated MSCs (oMSC). Alizarin Red staining was quantified (562 nm). Data are shown as mean ± SEM for n = 5. Wilcoxon matched-pairs signed rank test was used to determine the statistical significance. p-values are indicated in the graphs with * $p < 0.05$, ** $p < 0.01$ and *** $p < 0.001$ (ns = not significant). TCP, tricalcium phosphate; LDH, lactate dehydrogenase; *EF1A*, eukaryotic translation elongation factor 1 alpha.

Int. J. Mol. Sci. **2021**, *22*, 128

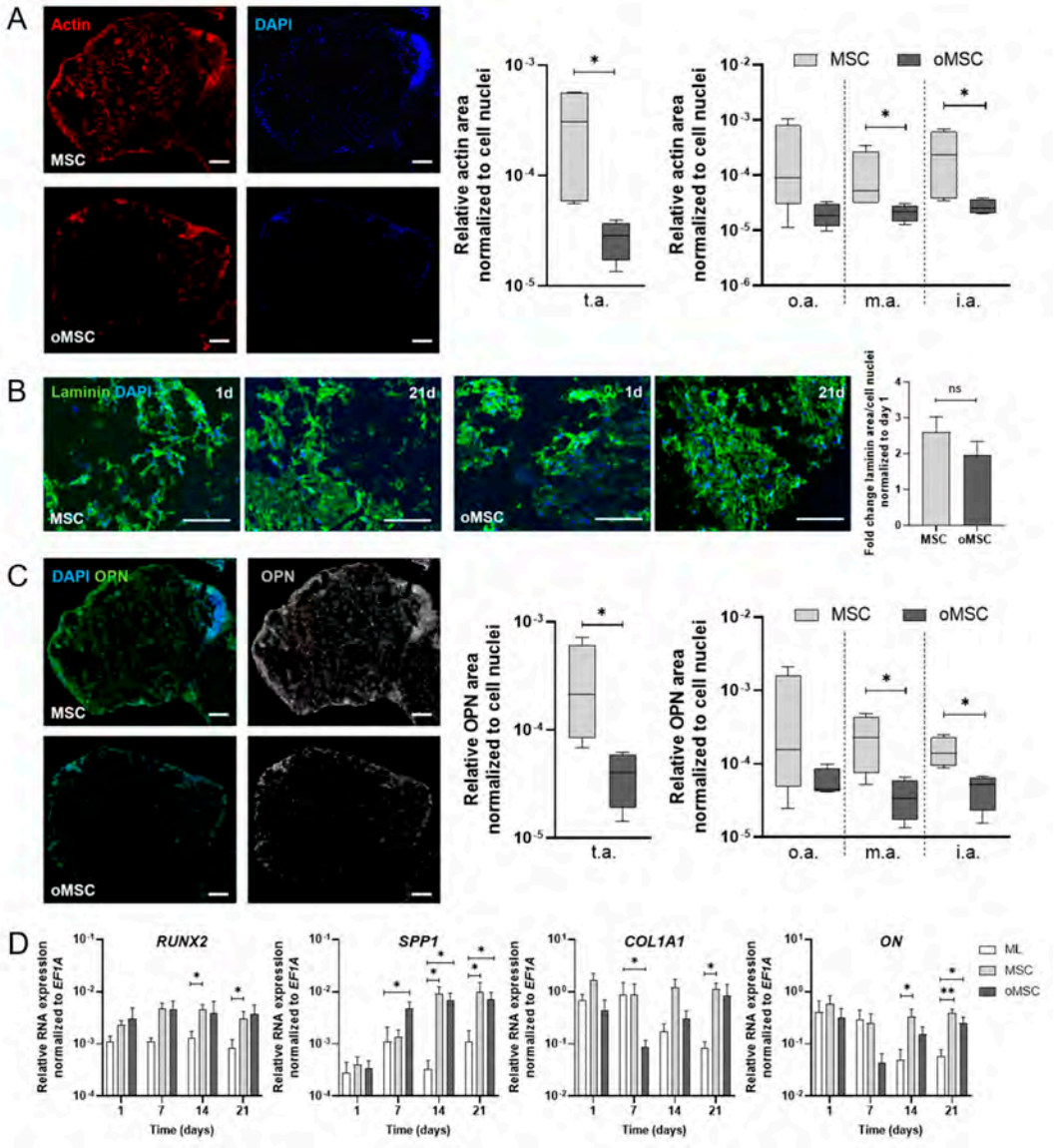

Figure 3. Characterization of the human in vitro tricalcium phosphate-based bone component (TBBC) using both MSCs and oMSCs. (**A**) The amount of actin (in pixels) per cell nuclei (DAPI+) after 21 days within total area (t.a.), outer area (o.a.; outer border determined by a reduction of the diameter by 0.95 for X- and Y-axes), middle area (m.a.; outer area subtracted from total area, diameter reduced by 0.5 for X- and Y-axes) and inner area (i.a.; remaining inner part of the outer area subtracted from total area, diameter reduced by 0.5 for X- and Y-axes) were quantified via ImageJ. Data are shown as Box and Whiskers plot with median ± min/max for $n = 4$. Scale bar indicates 100 µm. (**B**) Laminin and DAPI were stained after day 1 and 21 and quantified via ImageJ. Data are shown as mean ± SEM for $n = 3$. Scale bar indicates 100 µm. (**C**) Osteopontin (OPN) and DAPI were stained after 21 days. The amount of OPN (in pixels) per cell within t.a., o.a., m.a., and i.a. were quantified via ImageJ. Data are shown as Box and Whiskers plot with median ± min/max for $n = 4$. Representative images are shown accordingly (scale bar = 100 µm). (**D**) Total RNA extraction was performed from MSC monolayer (ML) and 3D cultures with MSCs and oMSCs after 1, 7, 14 and 21 days. Gene expression was normalized to the housekeeper gene *EF1A*. Data are shown as mean ± SEM for $n = 4$–6. Mann-Whitney U-test was used to determine the statistical significance; * $p < 0.05$, ** $p < 0.01$ (ns = not significant). MSC, mesenchymal stromal cell; oMSC, one-week osteogenic pre-differentiated MSC; *EF1A*, eukaryotic translation elongation factor 1 alpha.

Int. J. Mol. Sci. **2021**, *22*, 128

The final TBBCs were produced in sizes with a diameter up to 0.5 cm and cultivated for 21 days (Figure 4A). Exemplary images of actin and DAPI immunofluorescence staining over time (day 1, 7, 14, 21) further supported prior endpoint analyses demonstrating the invasion of cells into the TCP scaffold (Figure 4B). Furthermore, TBBCs cultivated for 21 days displayed a cell and matrix formation comparable to native bone as analyzed by scanning electron microscopy (Figure 4C). H&E staining clearly indicated a matrix formation, the interconnection between cells and the TCP particles, and the beginning of osteoid formation at day 21 (Figure 4D). Additionally, seeded MSCs maintained their metabolic activity over 21 days when compared to day 1 and the respective monolayer control (ML; Figure 4E). Analyzing bone formation using µCT, we observed a numerical increase in bone volume at day 21 compared to day 0 (TCP only) and day 14 (Figure 4F). Finally, gene expression of bone specific markers revealed a significant upregulation of *RUNX2*, *SPP1*, *ON*, *COL1A1* and osteocalcin (*OC*) as compared to the osteogenic differentiated ML (Figure 4G). In summary, using MSCs to produce TBBCs is valid to achieve a sustainable osteogenic phenotype and to recapitulate the subchondral bone compartment in our OTM approach.

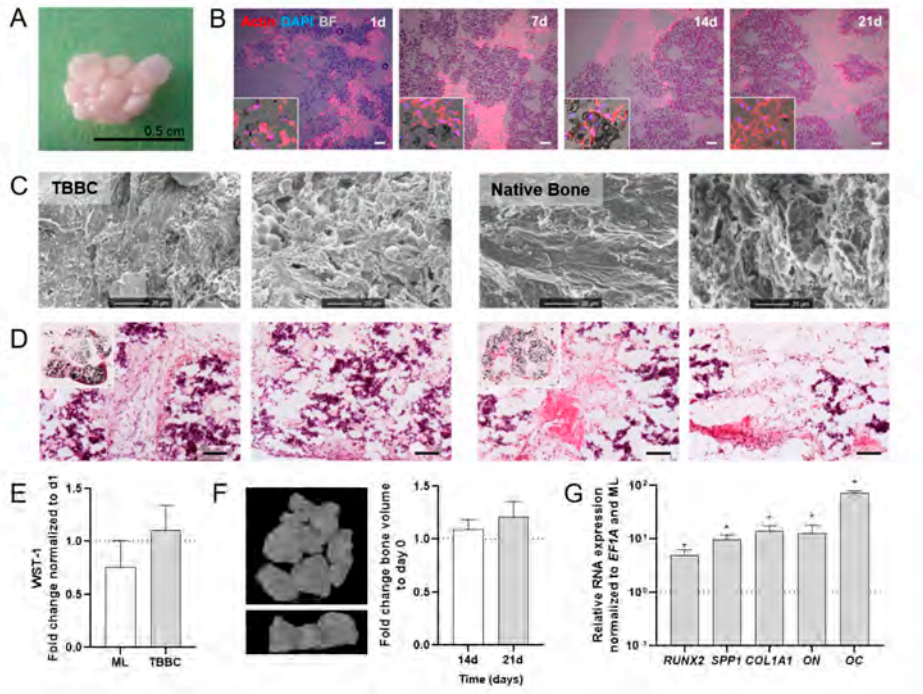

Figure 4. Human in vitro 3D TCP-based bone component (TBBC) based on MSCs. (**A**) Macroscopic overview of the in vitro 3D TBBC. (**B**) Exemplary images to highlight cell localization and extracellular matrix formation as shown by immunofluorescence staining for actin (red) and DAPI (blue) after day 1, 7, 14 and 21. Bright field (BF) shows the β-TCP scaffold. Exemplary images of $n = 4$ (scale bar = 100 µm). (**C**) Structural examination of the TBBC in comparison to native bone using scanning electron microscopy. Exemplary images of $n = 8$ TBBC and $n = 2$ human native bone. (**D**) Histological evaluation of the morphology via H&E staining. Exemplary images for $n = 8$. Scale bars indicate 100 µm. (**E**) WST-1 assay was conducted to confirm metabolically active cells after 21 days of cultivation compared to day 1 and monolayer control (ML). Data are shown as mean ± SEM (duplicates per donor in two independent experiments) for $n = 6$. Mann-Whitney U-test was used to determine the statistical significance. (**F**) In vitro 3D µCT reconstruction and quantitative results. Data are shown as mean ± SEM for $n = 3$. (**G**) Total RNA extraction was performed from ML and TBBCs after 21 days of osteogenic differentiation. The relative gene expression was normalized to the housekeeper gene *EF1A* and osteogenic differentiated ML. Data are shown as mean ± SEM (duplicates per gene) for $n = 6$. Wilcoxon Signed Rank Test was used to determine the statistical significance; p-values are indicated in the graphs with * $p < 0.05$. MSC, mesenchymal stromal cell; TCP, tricalcium phosphate; *EF1A*, eukaryotic translation elongation factor 1 alpha.

2.2. Characterization of the Scaffold-Free Cartilage Component Demonstrates a Valid Cartilage-Like Phenotype Including Zonal Organization

The cartilage-like component was produced as described previously. In short, the procedure is based on mesenchymal condensation and the cyclic application of biomechanical force which finally leads to the self-organized 3D scaffold-free cartilage component (SFCC) [18]. Thus, we were asking the question whether we can maintain a cartilage-like phenotype of the SFCCs for 21 days, which is the time point that coincides with the start of co-cultivation with TBBCs (Figure 1). SFCCs were produced in a diameter sized up to 0.5 cm (Figure 5A). H&E staining of histological sections demonstrated an almost homogenous cell matrix distribution with a higher cell density and more flattened cells in the outer surface area similar to the superficial zone of native cartilage (Figure 5B). Additionally, the inner area was characterized by spherical and randomly oriented cells reflecting characteristics of the middle zone of native cartilage. Using TUNEL staining at day 21, we observed only a low number of apoptotic cells within the SFCC (Figure 5C). Histochemistry and immunohistochemistry revealed the presence of glycosaminoglycans (Alcian blue staining) and collagen type 2 (Figure 5D). We also found collagen type 1 expressed in the tissue, although its extent of expression was clearly lower as compared to the TBBC control. However, mineralization was not present as shown by Alizarin and von Kossa staining (Figure 5D). Comparing the gene expression of SFCCs to undifferentiated MSCs in ML at day 21, we observed an up-regulation of cartilage specific markers such as collagen type 2 alpha 1 (*COL2A1*), aggrecan (*ACAN*) and collagen type 10 alpha 1 (*COL10A1*), while the expression of the bone specific markers *COL1A1* and *RUNX2* was downregulated as compared to the monolayer control (Figure 5E). In addition, the cartilage specific transcription factor *SOX9*, which is an early marker of chondrogenesis during cartilage development, was also downregulated (Figure 5E). However, the temporal course of the analyzed marker gene expression revealed no significant changes over 21 days as assessed weekly (Appendix A Figure A2). Based on our findings, we continued with the in vitro generated SFCCs displaying a stable chondrogenic phenotype and characteristics of native cartilage.

Int. J. Mol. Sci. **2021**, *22*, 128

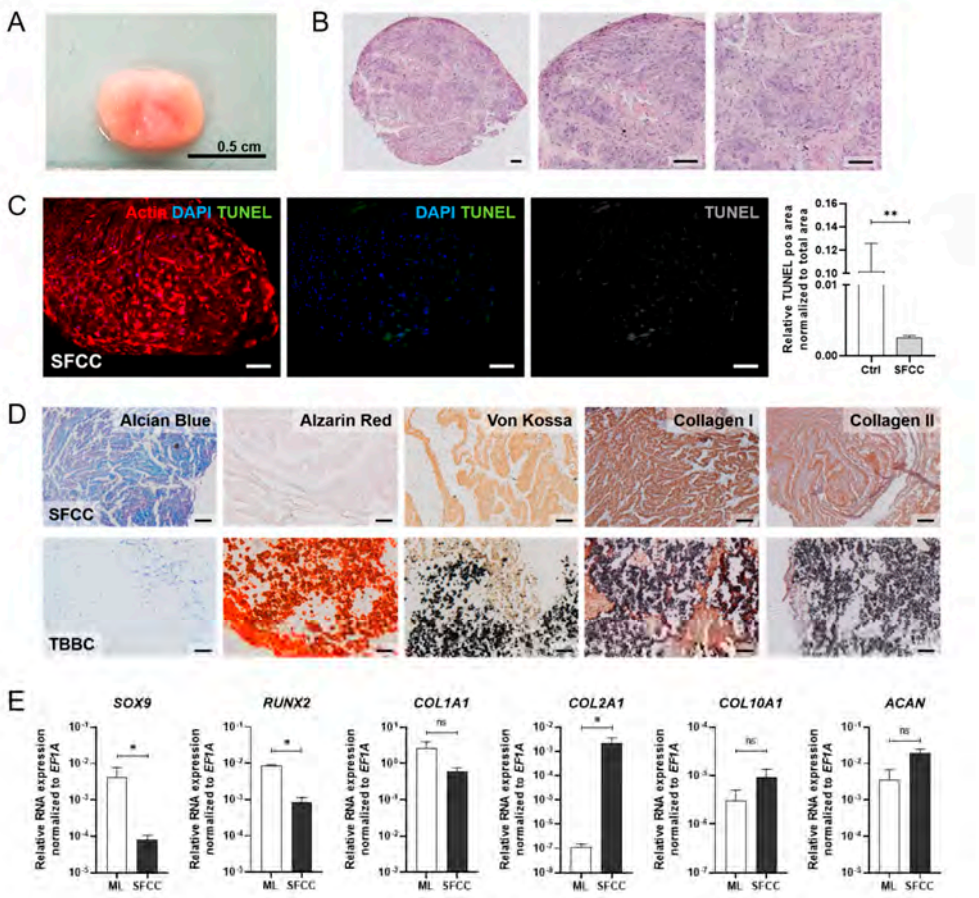

Figure 5. In vitro studies on the 3D scaffold-free cartilage constructs (SFCC) based on human MSCs. (**A**) Macroscopic overview of the in vitro 3D SFCCs. (**B**) Histological evaluation of the morphology via H&E staining. Exemplary images for $n = 6$. Scale bars indicate 200 µm. (**C**) Detecting apoptotic cells (green) using TUNEL staining after 21 days without mechanical force. Exemplary image for $n = 4$. Scale bars indicate 200 µm. Pos. ctrl = incubation with DNase I for 10 min. (**D**) Histological (Alcian Blue, Alizarin Red, von Kossa) and immunohistochemistry staining (collagen type 1 and collagen type 2) of the SFCC in comparison with the tricalcium phosphate-based bone component (TBBC) control. Exemplary images for $n = 4$. Scale bars indicate 200 µm. (**E**) Total RNA extraction was performed from 3D cultures after 21 days. Gene expression was normalized to the housekeeper gene *EF1A*. Data are shown as mean ± SEM (duplicates per gene) for $n = 3$–6. Mann-Whitney U-test was used to determine the statistical significance; *p*-values are indicated in the graphs with * $p < 0.05$, ** $p < 0.01$ (ns = not significant). MSC, mesenchymal stromal cell; *EF1A*, eukaryotic translation elongation factor 1 alpha.

2.3. Co-Cultivation of Scaffold-Free Cartilage Components and In Vitro 3D Tricalcium Phosphate-Based Bone Components Lead to Formation of a Subchondral Bone-Like Zone

Since we aimed to develop a complex human in vitro 3D OTM to mimic the part of a joint which is affected during the late stages of RA, we cultivated the SFCC on top of the TBBC. Therefore, TBBCs and SFCCs were produced as outlined before (Figures 1 and 6A) and cultivated for 21 days before analysis (day 42). H&E staining of OTMs showed that SFCC and TBBC were sticking together without any gap formation (Figure 6B). Although both parts could still be discriminated morphologically by H&E staining, we additionally phenotypically discriminated the SFCC from the TBBC part using Toluidine blue combined with von Kossa staining visualizing the chondrogenic phenotype by Toluidine blue dye attaching to the negative charges of the proteoglycans while calcified tissue phenotype

Int. J. Mol. Sci. **2021**, *22*, 128

was confirmed by von Kossa (Figure 6C). Moreover, we observed a rearrangement of the cytoskeleton after 21 days of co-cultivation in the bridging area between both components reflecting a subchondral bone-like zone of the osteochondral tissue as visualized by actin and DAPI (cytoskeleton, nucleus) staining (Figure 6D). To confirm cellular viability after 21 days of co-cultivation, we conducted a TUNEL staining (green: apoptotic cells) showing only a few apoptotic cells compared to the positive control with induced apoptosis by DNase I treatment (Figure 6E). Taken together, co-cultivation of SFCC and TBBC led to the formation of a connecting OTM with cellular rearrangements in the bridging area.

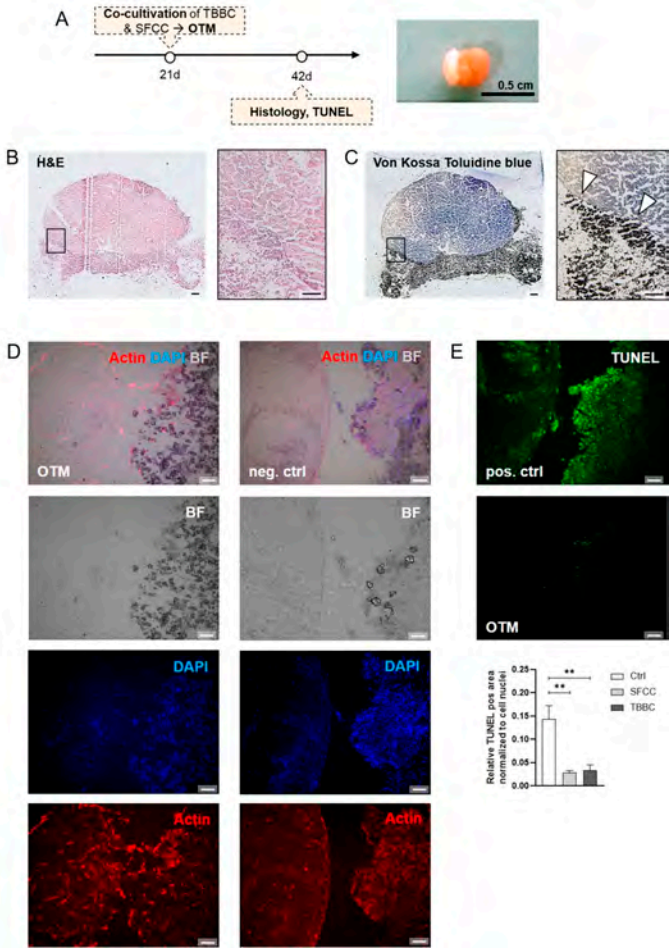

Figure 6. Human in vitro 3D osteochondral tissue model (OTM). Both components were developed independently and subsequently co-cultured in a cell culture insert for 21 days. (**A**) Experimental design of the in vitro 3D OTM. (**B**) Histological evaluation via H&E and (**C**) Toluidine blue combined with von Kossa staining. Exemplary image for $n = 4$. Scale bars indicate 500 µm. White asterisks highlight initial mineralization. (**D**) Actin and DAPI staining were performed to visualize the transitional bridging area between both components. Neg. ctrl = co-cultivation for 1 day, simulating a not unified OTM. Exemplary image for $n = 4$. Scale bars indicate 200 µm. (**E**) The number of apoptotic cells (green; TUNEL staining) normalized to cell nuclei (DAPI+) in both TBBC and SFCC after 21 days of co-cultivation was quantified via ImageJ. Exemplary images for $n = 5$. Scale bars indicate 200 µm. Pos. ctrl = incubation with DNase I for 10 min to induce apoptosis. Mann-Whitney U-test was used to determine the statistical significance compared to the control, p-values are indicated in the graphs with ** $p < 0.01$. TBBC, tricalcium phosphate-based bone component; SFCC, scaffold-free cartilage component.

2.4. The Osteochondral Tissue Model Shows Cell- and Matrix-Related Changes after Cytokine Stimulation Which Were Prevented by Application of Anti-Rheumatic Drugs

To mimic the chronic inflammatory environment of RA, our osteochondral tissue model was treated for a prolonged period of 21 days repetitively (every 3 days) using a cocktail of three major RA-related cytokines, namely TNFα (10 ng/mL), IL-6 (30 ng/mL) and MIF (10 ng/mL) at pathophysiological, non-cytotoxic concentrations (Figure 7A–C). Cytokine concentrations were used as reported from synovial fluid of patients with RA (STIM) or left untreated (CTRL). The cytokine cocktail was applied with or without drugs to quantify both the effects of the cytokines and the preventive potential of the drugs under investigation. To this end, we added a combination of clinically available drugs in their therapeutic dosage (10 µg/mL adalimumab, 8 µg/mL tocilizumab, 5 µg/mL milatuzumab; TREAT). After sustained repetitive treatment for 21 days mimicking chronic inflammation, we analyzed the transcriptional response of our model and identified a significant cytokine-mediated upregulation of the metabolic marker lactate dehydrogenase A (*LDHA*) in the STIM group compared to CTRL which was significantly reduced in both SFCC and TBBC when treated with the combination of chosen drugs (TREAT; Figure 7D,E). Additionally, a cytokine-induced upregulation of the angiogenic marker vascular endothelial growth factor A (*VEGFA*) was observed, which was prevented in the TREAT group. The expression of *IL6* was numerically reduced after both cytokine stimulation (STIM) and therapeutic treatment (TREAT) as compared to CTRL in SFCCs (Figure 7D) but was significantly reduced in TBBCs (Figure 7E). Conversely, *IL8* and *TNF* were significantly upregulated after stimulation, while this effect was prevented by the drugs. In the SFCC model, *MMP1* and *MMP3* were significantly upregulated in the cytokine-treated group compared to the CTRL group (Figure 7D). This effect was reversed in the drug-treated group compared to the STIM group. There were no significant differences in gene expression for *MMP13* within the experimental groups. However, in the bone-like model, *MMP1* expression was numerically diminished in both the STIM and TREAT group compared to the CTRL group (Figure 7E). There was no significant difference in gene expression of *MMP3* within CTRL and STIM, while we observed a significant downregulation in the TREAT group. Moreover, there were no significant differences in gene expression for *MMP13* within the experimental groups. Of note, cartilage and bone component differentially responded to cytokine-mediated stimulation with respect to the significantly upregulated expression of *MMP1* and *MMP3*.

In summary, stimulation with TNFα, IL-6 and MIF lead to cytokine-mediated cartilage degradation, a key feature of arthritis. These findings are in accordance with in vivo data from animal studies and with observations made in human pathophysiology. Cultivation in the presence of immunomodulatory drugs did sufficiently prevent these cytokine-induced changes.

Int. J. Mol. Sci. **2021**, *22*, 128

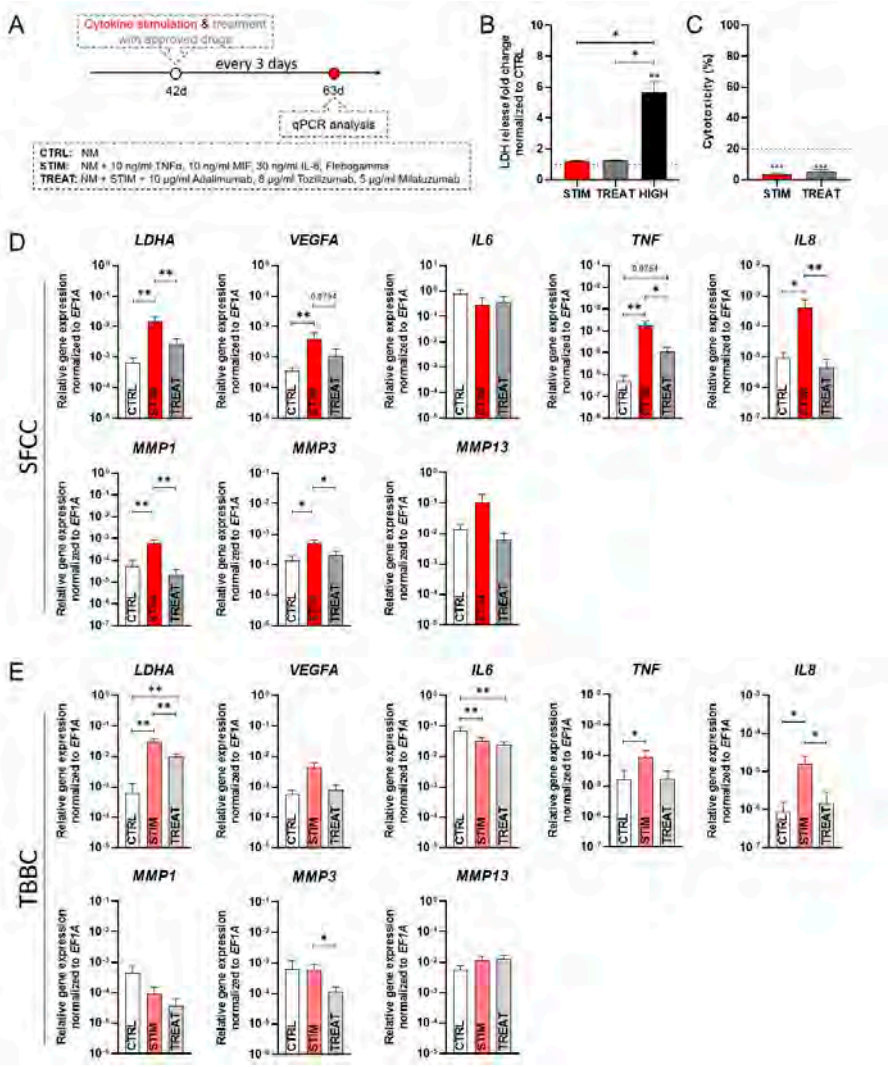

Figure 7. Experimental results of our osteochondral tissue model incubated for 21 days under non-inflammatory conditions (CTRL), repetitive cytokine stimulation with a cocktail of TNFα, IL-6 and MIF (STIM) and under treatment conditions (TREAT). (**A**) Schematic overview of the experimental design. (**B**) LDH-assay was performed after 1 day to cover any cytotoxic effects using supernatant from the OTM treated with cytokines (STIM—10 ng/mL TNFα, 30 ng/mL IL-6, 10 ng/mL MIF) and in combination with clinically available drugs (TREAT—10 µg/mL adalimumab, 8 µg/mL tocilizumab, 5 µg/mL milatuzumab). CTRL = untreated control; HIGH = 2% of Triton X-100 to induce LDH release. Data are shown as mean ± SEM for $n = 5$. Wilcoxon matched-pairs signed rank test was used to determine the statistical significance between groups and One sample t test for the spontaneous LDH release control (CTRL). (**C**) Percentage of cytotoxicity was determined by the following equation [%] = (exp. value − CTRL)/(HIGH − CTRL) × 100 for $n = 5$. Data are shown as mean ± SEM. One sample t test was used with a cytotoxicity cut off of 20% [29]. (**D**) Gene expression studied via qPCR for *LDHA*, *VEGFA*, *IL6*, *TNF*, *IL8*, *MMP1*, *MMP3* and *MMP13* for scaffold-free cartilage components (SFCCs) and (**E**) tricalcium phosphate-based bone components (TBBCs). Data were normalized to the housekeeper gene *EF1A* and are shown as mean ± SEM (duplicates per gene) for $n = 5$. Mann-Whitney U-test was used to determine the statistical significance, p-values are indicated in the graphs with * $p < 0.05$, ** $p < 0.01$, *** $p < 0.001$. LDH, lactate dehydrogenase; TNF, tumor necrosis factor; IL, interleukin; MIF, macrophage migration inhibitory factor; *LDHA*, lactate dehydrogenase A; *VEGFA*, vascular endothelial growth factor A; MMP, matrix metalloproteases; *EF1A*, eukaryotic translation elongation factor 1 alpha.

3. Discussion

Until today, no appropriate human in vitro model exists so far, which can appropriately mimic the (patho)physiological relevant environment of a healthy or an inflamed joint specifically focusing on the later stage of disease involving cartilage matrix degradation and subchondral bone erosion with the need for a crosstalk between bone and cartilage within the osteochondral unit. Simulating such features in a preclinical drug screening tool would be transformative for the translational process necessary for optimizing rheumatological care. Here, we have developed a human MSC-derived OTM and described its capacity to create a RA-like phenotype, which replicated in part the immunomodulatory effect of well-known anti-rheumatic drugs such as adalimumab [30,31] and tocilizumab [32,33], but also the antineoplastic agent milatuzumab [34].

As in our current study, MSCs are widely used as suitable cell source to engineer in vitro tissue owing to their availability, isolation simplicity, high proliferation rate and differentiation capacity towards individual resident cell types of bone and cartilage [35,36]. Since there has been evidence that high-density scaffold-free chondrogenic cultures and ceramic bone scaffolds might lead to the formation of well-integrated OTMs [37], we firstly engineered bone components by using TCP ceramic particles, which mimic the mineral bony part. Comparable in vitro and in vivo approaches to promote osteogenesis and bone regeneration have been published during the last decade [38,39]. With respect to the biocompatibility and prominent osteoconductive activity of TCP [40], our results (Figures 2 and 3) are in line with a study conducted by Herten et al. where both MSCs and osteoblasts were cultivated on TCP particles [41]. Additionally, we confirmed the osteogenic phenotype based on upregulated expressions of early osteoblast-specific genes, including *RUNX2*, *SPP1* and *COL1A1* and enhanced expression of mature osteoblast markers (*SPP1*, *ON*), indicating the mineralization capacity of MSCs within the tissue models (Figure 4) [42,43]. Secondly, in order to generate cartilage-like tissue components, emerging tissue engineering approaches use mesenchymal condensation based on cell-sheet formation, self-assembly or self-organization to engineer scaffold-free constructs [44–47]. Although MSCs are well-known to differentiate into various lineages, their capacity to form mature chondrocytes and full articular cartilage is limited. However, chondrogenic differentiated MSCs still provide sufficient similarities to articular cartilage which renders them eligible to serve as therapeutic option for e.g., cartilage defects [48] or in vitro models [18,49]. Furthermore, Li et al. showed that adding mechanical load additionally promotes chondrogenesis of MSCs by up-regulating TGF-β. An approach which is identical to the procedure we applied here. As a result, chondroblastic cells form a functional network, embedded into their self-synthesized matrix comprising both superficial and middle zone and abundant expression of collagen type 2 but also collagen type 1 (Figure 5). The latter is a prerequisite for chondrogenic MSC differentiation, because MSCs firstly reside within the pre-cartilaginous matrix rich in collagen type 1 inducing cell-cell contact, which finally results in an increased expression of *SOX9* and differentiation [50–52].

The crosstalk between bone and cartilage within the osteochondral unit is supposed to play an important role in the etiopathogenesis of cartilage matrix degradation and subchondral bone erosion and needs, therefore, to be considered in emerging therapeutic strategies and preclinical testing tools. To mimic the osteochondral unit, common in vitro approaches use a bi-layered scaffold where chondrocytes or MSCs are embedded in polymers and the bone layer is based on e.g., ceramics [53]. Both layers are most often fixed by adhesives such as fibrin resulting in a barrier for cell-cell contacts. Conversely, Lin et al. encapsulated iPSCs-derived MSCs in a gelatin scaffold and cultivated these scaffolds in a dual-flow bioreactor [54]. In contrast to our approach, they directly generated a stable bridging zone between the components but neglected the different cellular demands on the given ECM (stiffness, matrix composition) and microenvironment (oxygen supply) [53]. As shown in our study, co-cultivation for 21 days in a static culture system led to the formation of a bridging zone, suggesting a functional interplay between the two tissue components (subchondral bone-like zone; Figure 6).

Studies have shown that synovial fibroblasts and different immune cells (e.g., neutrophils, macrophages, T-cells) are a major source of pro-inflammatory cytokines in RA. For example, TNFα, IL-6 and MIF activate resident chondrocytes to produce TNFα, IL-8, IL-6 and matrix metalloproteases (MMP1, MMP3, MMP13) promoting cartilage degeneration and subsequent bone erosion. In line with our results, Pretzel et al. analyzed cartilage degradation of bovine cartilage discs co-cultivated with human synovial fibroblasts and supplemented IL-1β and TNFα. They were able to demonstrate an upregulation of tissue-degrading enzymes (MMP1, MMP3) and pro-inflammatory cytokines (IL-6, IL-8). In addition, several studies report an increased production of matrix metalloproteinases (MMP3, MMP13) in chondrocytes and cartilage explants after IL-6 treatment, which is in accordance with our results (Figure 7) [55–57]. Moreover, TNFα and IL-6 have been recently shown to have overlapping and synergistic effects, even though some of these effects are regulated by separate mechanisms [58]. Interestingly, Honorati et al. analyzed chondrocytes from non-inflammatory pathology in comparison with RA chondrocytes showing that inflammation seems to play an important role in inducing the chondrocyte-related VEGF secretion [59]. Here, we demonstrate that exposure to TNFα, IL-6 and MIF [60–62] does induce arthritic transformation followed by activation of the angiogenic marker *VEGFA* in the SFCC (Figure 7) [63]. In contrast, we did not observe a cytokine-related upregulation of *IL6* which has been already described after TNFα exposure. It was shown that the self-activation of pY-STAT3 by newly synthesized IL-6 leads to a transient auto-inhibition of further IL-6 transcription [64]. Thus, the supplementation of IL-6 may be responsible for the absence of induced IL-6 expression in our study.

Finally, we provide first evidence that effects of immunomodulatory drug candidates can be demonstrated in our MSC-derived OTM on mRNA level (Figure 7). We used adalimumab [30,31], tocilizumab [32,33] and milatuzumab [34] for proof of concept, as these are clinically used monoclonal antibodies directed against TNFα, IL-6 and MIF. Recent work has indicated that TNFα may mediate its angiogenic effect in RA via IL-8 and VEGF [65]. In fact, treatment strategies aimed at decreasing TNFα resulted in decreased angiogenic IL-8 production in vitro and decreased serum levels of angiogenic VEGF in RA patients [66,67]. We reported that treatment in a pharmacologically relevant dose does prevent pro-inflammatory effects, attenuating the TNF and IL-6 signaling pathway. Preclinical testing of therapeutics towards RA is a major challenge, since current therapeutic approaches target specific molecules or pathways by e.g., antibodies or small molecules which are unique in humans. Nevertheless, recent studies have indicated that there are differences in functionality and binding capacity between the human and murine system leading to the potential failure of promising antibodies during clinical trials as exemplified by anti-IL-17 antibodies (e.g., secukinumab) [68] as an biological disease-modifying antirheumatic drugs or the phosphodiesterase 4 inhibitor apremilast [69] which were both tested successfully in mice but failed to provide clinical efficacy in patients suffering from RA [70–72].

Nevertheless, the model has still some limitations that need to be addressed in the future. So far, the TBBC does not include bone remodeling processes and our current version of the OTM omits circulating cells such as leukocytes and endothelial cells. However, there is the opportunity to expand our model by including e.g., osteoblasts/osteoclasts, selected RA-related leukocyte populations or human umbilical vein endothelial cells. Finally, an approach that offers possibilities to investigate the cellular behavior and intercellular interactions in a perfused 3D context is given by the organ-on-a-chip technology [73].

4. Materials and Methods

4.1. MSC Isolation, Cultivation and Characterization

Primary human mesenchymal stromal cells (MSCs) were isolated from bone marrow obtained from patients undergoing total hip replacement (provided by the Center of Musculoskeletal Surgery, Charité-Universitätsmedizin Berlin, donor list in Table 1). Study design and protocols were approved by the Charité-Universitätsmedizin Ethics Commit-

tee and performed according to the Helsinki Declaration (ethical approval EA1/012/13, 31 January 2013). Briefly, bone marrow was transferred into a T-175 flasks (Greiner Bio-one International GmbH, Kremsmünster, Austria) with Dulbecco's Modified eagle minimal Essential Medium (DMEM) GlutaMAX™ (Gibco, Waltham, MA, USA) supplemented with 10% fetal calf serum (FCS, Biowest, Nuaillé, France), 100 U/mL penicillin (Gibco, Waltham, MA, USA), 100 µg/mL streptomycin (Gibco, Waltham, MA, USA) and 20% StemMACS^{TM} MSC Expansion Media Kit XF (Miltenyi Biotech, Bergisch Gladbach, Germany). After incubation for two days (37 °C, 5% CO_2), medium was changed, remaining tissue parts were removed, and the adherent cells were washed with phosphate-buffered saline (PBS; pH 7.4). Reaching 90% confluency, cells were passaged. MSCs were characterized after three passages using differentiation assays (adipogenic, osteogenic, chondrogenic) and flow cytometry (MSC Phenotyping Kit; Miltenyi Biotech, Bergisch Gladbach, Germany; CD90+, CD105+, CD73+, CD14−, CD20−, CD34−, CD45−, and HLA-DR−, Appendix A Figure A3). Only MSCs successfully passing the characterization were further used for experiments until passage 3–8.

Table 1. Human MSCs donor information and conducted experiments.

Donor	Age	Sex	Type of Experiments	Used Methods
MSC 1	62	m	Characterization of TBBCs	LDH, WST-1, gene expression analysis, histology, immunofluorescence
MSC 2	78	m		
MSC 3	56	w		
MSC 4	69	w		
MSC 5	57	m		
MSC 6	74	w		
MSC 7	75	w		LDH, µCT, SEM, Alizarin Red, histology, immunofluorescence
MSC 8	76	w		
MSC 9	77	m		
MSC 10	77	w		
MSC 11	66	m		
MSC 12	53	m		
MSC 13	63	m		
MSC 14	84	w	Characterization of SFCCs	Gene expression analysis, histology
MSC 15	71	w		
MSC 16	66	m		
MSC 17	59	w		
MSC 18	79	m		
MSC 19	78	m		
MSC 20	64	m	Co-cultivation (OTM), proof of OTM experiments	Gene expression analysis, histology
MSC 21	67	w		
MSC 22	72	w		
MSC 23	76	w		
MSC 24	57	m		

For differentiation, MSCs were seeded at a density of 1×10^4 cells per well in a 96-well plate (Greiner Bio-one International GmbH, Kremsmünster, Austria) and cultivated in appropriate differentiation medium for three weeks (37 °C, 5% CO_2). For adipogenic differentiation, MSCs were incubated in StemMACS^{TM} AdipoDiff medium (Miltenyi Biotech, Bergisch Gladbach, Germany). After 3 weeks, cells were fixed in 4% paraformaldehyde (PFA; Electron Microscopy Sciences, Hatfield, PA, USA) for 15 min. After washing with 60% isopropanol, cells were stained with 60% Oil Red O solution dissolved in ddH_2O (Sigma-Aldrich Chemie GmbH, Munich, Germany: freshly prepared and passed through a 0.45 µm filter; stock solution: 0.3% Oil Red O dissolved in 100% isopropanol) for 15 min, washed with 60% isopropanol. Finally, ddH_2O was added and intracellular lipid droplets were analyzed microscopically.

For osteogenic differentiation, MSCs were cultivated in StemMACS™ OsteoDiff medium (Miltenyi Biotech, Bergisch Gladbach, Germany) for three weeks. Alizarin Red staining was performed according to the following protocol: cells were washed with PBS, fixed with 4% PFA for 15 min, washed with PBS and stained using a 0.5% Alizarin Red S staining solution (pH 4; Sigma-Aldrich Chemie GmbH, Munich, Germany) dissolved in ddH_2O for 15 min. After the final washing step with ddH_2O, calcium deposition was analyzed microscopically.

For chondrogenic differentiation MSCs were transferred in a 3D state (pellet cultivation) via centrifugation for 10 min at 400× *g* and cultivated in StemMACS™ ChondroDiff medium (Miltenyi Biotech, Bergisch Gladbach, Germany). Slices were prepared and Alcian Blue staining was performed to analyze the presence of acidic mucopolysaccharides microscopically.

4.2. Generation of the Osteogenic Component—TCP-Based Bone Component (TBBC)

The 3D cultivation was performed in cell culture inserts (Sarstedt AG, Nümbrecht, Germany) with a 0.3 cm^2 growth area and a polyethylene terephthalate (PET) membrane (8 µm pore size). Approximately 12 mg of β-tricalcium phosphate (TCP) granules (Cerasorb®M, Curasan AG, Kleinostheim, Germany) were preincubated with 1 mL of DMEM GlutaMAX™ supplemented with 10% FCS, 100 U/mL penicillin, 100 µg/mL streptomycin, in the following referred to as normal medium (NM) for one day. To optimize the 3D TCP-based bone component (TBBC), 1×10^6 MSCs or pre-differentiated MSCs (pre-incubated in osteogenic differentiation medium for one week, oMSCs) were seeded onto TCP granules. Cell suspension and TCP particles were gently mixed and cultured in osteogenic medium (OM, NM supplemented with 0.5 mM ascorbic acid, 10^{-8} M dexamethasone, 10 mM L-glycerophosphate). Medium was changed twice a week.

4.3. Generation of the Scaffold-Free Cartilage Component (SFCC)

The 3D scaffold-free cartilage components (SFCCs) were generated based on a patented method (No. 10 2004 001 225, German Patent and Trade Mark Office, 2004) purchased from the Research Center of Medical Technology and Biotechnology (fzmb GmbH), Bad Langensalza, Germany. Briefly, approximately 6×10^6 MSCs were detached and transferred into a 3D state via centrifugation for 10 min at 400× *g*. After 5 to 7 days, biomechanical forces were applied for 3 to 4 weeks to the self-assembled 3D component. SFCCs were then cultivated for up to 21 days without biomechanical forces (resting phase) in NM supplemented with 9.39 mg/L ascorbic acid (Sigma-Aldrich Chemie GmbH, Munich, Germany), in the following referred to as chondrogenic medium (CM).

4.4. Generation of the Osteochondral Tissue Model and Experimental Setup

An overview on the experimental setup is given Figure 1. Co-cultivation of both SFCC and TBBC was performed in cell culture inserts by placing the SFCC on top of the TBBC. Chondrogenic medium was added and both components were cultured for 21 days at 37 °C, 5% CO_2 to develop the osteochondral tissue model by allowing cell-cell interaction. To mimic chronic cytokine-mediated joint inflammation, stimulation was performed using CM (CTRL) supplemented with 10 ng/mL recombinant human macrophage migration inhibitory factor (MIF) [60], 30 ng/mL recombinant human IL-6 [62], 10 ng/mL recombinant human tumor necrosis factor alpha (TNFα; all ImmunoTools GmbH, Friesoythe; Germany) [61] using concentrations as reported from synovial fluid of patients with RA and 23 µg/mL Flebogamma (Grifols, Barcelona, Spain) in the following referred as STIM. To evaluate the impact of specific therapeutic approaches, CM was supplemented with cytokines and well-known clinically available drugs in their therapeutic dosage: 10 µg/mL adalimumab (Amgen, Thousand Oaks, CA, USA) [30,31], 8 µg/mL tocilizumab (Roche, Basel, Switzerland) [32,33] and 5 µg/mL milatuzumab (Immunomedics, Morris Plains, NJ, USA) [34], in the following referred to as TREAT. Medium was changed every

3 days including the respective supplements resulting in a repetitive chronic cytokine stimulation in case of STIM and a repeated counter-treatment in case of TREAT.

4.5. Viability and Cytotoxicity Assay

Cell Proliferation Reagent WST-1 Kit (Sigma-Aldrich Chemie GmbH, Munich, Germany) was used according to the manufacturer's instructions. Samples were mixed with WST-1 solution and incubated for 30 min at 37 °C, 5% CO_2. Supernatants were measured photometrically using a standard 96-well plate reader (Synergy™ HT Reader, BioTek Instruments, Bad Friedrichshall, Germany) at a wavelength of 450 nm (reference wavelength 630 nm). To induce cell death, a control group of cells was incubated with 2% Triton X-100 (Sigma-Aldrich Chemie GmbH, Munich, Germany) for one day (Ctrl). The assay was performed in two independent experiments with duplicates.

Cytotoxicity Detection LDH Kit (Sigma-Aldrich Chemie GmbH, Munich, Germany) was used to detect cytotoxic effects of TCP particles, cell/TCP ratio, cytokine and treatment concentrations. According to the manufacturer's instructions the OD-values were measured at a wavelength of 490 nm (reference wavelength 630 nm). Additionally, to induce LDH release via cell death, cells were incubated with 2% Triton X-100 for one day, in the following referred as high control (Ctrl). The LDH assay was performed in duplicates.

LIVE/DEAD® Viability/Cytotoxicity Kit (Invitrogen AG, Carlsbad, CA, USA) was used to determine cell viability and to visualize 3D cell colonization. Samples were first washed with PBS, transferred to a slide and subsequently incubated with LIVE/DEAD® staining solution (established concentration: 2 µM Calcein AM, 4 µM EthD-1) for 35 min at RT in the dark. Evaluation was performed with the fluorescence microscope BZ-9000 (Keyence, Itasca, IL, USA).

4.6. Alizarin Red Assay

For calcium quantification, Alizarin Red assay was performed. MSCs were seeded at a density of 1×10^4 cells per well in a 96-well plate and cultivated in NM (NM control), in OM without TCP (ML) and in OM with TCP co-cultivating MSCs (MSC) or pre-differentiated MSCs (oMSC). To exclude TCP-related staining, the OD value of TCP cultivated in OM without cells was subtracted from the TCP OD value. Medium was removed and cells were fixed in 4% PFA (10 min) and stained with Alizarin Red S staining solution (10 min), washed with ddH_2O, staining was dissolved with 10% cetylpyridiniumchlorid and OD-values were measured with a plate reader at a wavelength of 562 nm (reference wavelength 630 nm). Data were normalized to the NM OD-values. The assay was performed in duplicates.

4.7. Scanning Electron Microscopy

First, samples were washed twice with PBS and then fixed with 2.5% glutaraldehyde (Sigma-Aldrich Chemie GmbH, Munich, Germany) solved in PBS (10 min, room temperature—RT). After washing with PBS, samples were dewatered using ascending ethanol concentrations 30%, 50%, 70%, 80%, 90%, 95% and twice 100% for 5 min each. Afterwards samples were incubated with hexamethyldisilazane (1×5 min, 2×10 min; Sigma-Aldrich Chemie GmbH, Munich, Germany). Finally, samples were air dried overnight and coated with gold using a Fine Coater JFC-1200 (Jeol GmbH, Freising, Germany). The imaging with the scanning electron microscope JCM-6000 Plus Neo Scope™ (Jeol GmbH, Freising, Germany) was performed under high vacuum.

4.8. Histochemistry

Slices were prepared using the Kawamoto method to allow the embedding of samples without decalcification [74]. Samples were first fixed in 4% PFA for 3 h followed by an ascending sucrose solution treatment (10%, 20% and 30%) for one day each at 4 °C. Afterwards, the samples were embedded with SCEM embedding medium (Sectionlab, Hiroshima, Japan) and stored at −80 °C. We prepared cryo-sections of 7 µm thickness using Kawamoto cryofilm type 2C (Sectionlab, Hiroshima, Japan). Prior to each staining

procedure, slices were dried for 20 min at RT and at the final step covered with DPX Mountant (Sigma-Aldrich Chemie GmbH, Munich, Germany).

Hematoxylin and Eosin (H&E) staining was conducted using the following protocol: fixing with 4% PFA for 10 min, washing with ddH_2O for 5 min, first staining with Harris's hematoxylin for 7 min (Merck, Darmstadt, Germany), washing twice with ddH_2O, differentiating in 0.25 mL HCl solution (37% HCl, Merck, Darmstadt, Germany) in 100 mL of 70% ethanol. After washing with tap water for 10 min, second staining with Eosin (0.2%, 2 min; Chroma Waldeck GmbH & Co KG, Münster, Germany) was performed, differentiation step in 96% ethanol, followed by 100% ethanol (2 × 2 min) and xylol (2 × 2 min) treatments.

Von Kossa Toluidine blue staining was performed according to the following protocol: fixing with 4% PFA (10 min), washing with ddH_2O (5 min), staining in silver nitrate solution (3% in ddH_2O, 10 min), washing with ddH_2O, staining in sodium carbonate/formaldehyde solution (2 min), washing with ddH_2O, followed by a staining step in sodium thiosulfate solution (5% in ddH_2O, 5 min). After washing with tap water for 10 min, slices were washed with ddH_2O, counter stained in Toluidine blue solution for 8 min, washed with ddH_2O, differentiated in 70% ethanol, 100% ethanol and fixed in xylol (each 2 × 2 min).

Alcian Blue staining was performed according to the following protocol: fixing with 4% PFA (10 min), washing with ddH_2O (5 min), treating with 3% acetic acid (3 min), staining step in 1% Alcian Blue for 30 min (Sigma-Aldrich Chemie GmbH, Munich, Germany), washing in 3% acetic acid (pH 2.5), washing with ddH_2O, staining step in nuclear fast red aluminum sulfate for 4 min, washing with ddH_2O, followed by 80%, 96% and 100% ethanol (2 min each) and fixing with xylol (2 × 2 min).

4.9. Immunohistochemistry

Immunohistochemistry was performed according to the following protocol: rehydrating with PBS (10 min), blocking with 3% H_2O_2 (30 min), washing with PBS (5 min), blocking with 5% normal horse serum (Vector Laboratories, Burlingame, CA, USA) in 2% bovine serum albumin (BSA, Sigma-Aldrich Chemie GmbH, Munich, Germany)/PBS, first incubation step with primary antibody for collagen type I (1:500, Abcam plc, Cambridge, UK) or collagen type II (1:10, Quartett GmbH, Berlin, Germany) at 4 °C overnight, washing in PBS (2 × 5 min), second incubation step with 2% biotinylated horse anti-mouse IgG antibody (secondary antibody, Vector Laboratories, Burlingame, CA, USA) diluted in 5% normal horse serum/2% BSA/PBS for 30 min and washing in PBS (2 × 5 min). After incubation with Vecastain® Elite® ABC HRP Kit (Vector Laboratories, Burlingame, CA, USA) for 50 min, slices were washed with PBS (2 × 5 min), incubated with DAB Peroxidase HRP Substrate Kit (microscopic control, Vector Laboratories, Burlingame, CA, USA), thus the reaction was stopped with PBS, followed by washing with ddH_2O, counter staining step in Mayer's hematoxylin (2 min, Sigma-Aldrich Chemie GmbH, Munich, Germany), washing in tap water (10 min) and finally washing in ddH_2O.

4.10. Immunofluorescence Staining

Immunofluorescence staining was performed in a dark, humid chamber at RT. First, slices were air dried and then rehydrated with PBS for 10 min. Subsequently, unspecific binding sites were blocked with PBS/5% FCS for 30 min. Afterwards, primary antibody was diluted in PBS/5% FCS/0.1% Tween® 20 (Qbiogene Inc., Carlsbad, CA, USA) and incubated according to the manufacturer's instructions, followed by washing with PBS/0.1% Tween® 20 (3×). Secondary antibody was diluted in PBS/5% FCS/0.1% Tween® 20 and applied for 2 h, washed with PBS/0.1% Tween® 20 (3×) and nuclei staining was performed using 4′,6-diamidino-2-phenylindole (DAPI; 1 µg/mL diluted in PBS/5% FCS/0.1% Tween® 20, 15 min). After bubble-free covering with FluoroMount (Sigma-Aldrich Chemie GmbH, Munich, Germany) covering medium, imaging was performed with the fluorescence microscope BZ-9000 (Keyence). Image analysis was performed using ImageJ. Primary and secondary antibodies used for immunofluorescence staining are listed in Table 2.

Table 2. Primary and secondary antibodies used for immunofluorescence staining.

Primary Antibody	Dye	Host	ID	Concentration [mg/mL]	Company
Phalloidin	TRITC	-	P1951	1.5	Sigma-Aldrich
Laminin	-	rabbit	NB300	0.8	Novus Biologicals LLC
Osteopontin	A488	rabbit	ab8448	1	Abcam
Collagen 1	-	mouse	ab6308	1.5	Abcam
Collagen 2	-	mouse	CO072	1	Quartett
Secondary Antibody	**Dye**	**Host**	**ID**	**Concentration [mg/mL]**	**Company**
Anti-mouse	Biotin	horse	BA-2000	1.5	Vector Laboratories Inc.
Anti-rabbit	A488	goat	A32731	2	Thermo Fisher Scientific

TUNEL assay (Sigma-Aldrich Chemie GmbH, Munich, Germany) was performed to detect apoptotic cells. As a positive control, slices were treated with desoxyribonuclease (DNase) I (0.34 Kunitz units, Qiagen GmbH, Hilden, Germany) for 10 min and washed twice with PBS. Staining was performed with TUNEL reaction mixture (5 µL TUNEL enzyme + 45 µL TUNEL label) for 1 h at 37 °C and then washed twice with PBS. A negative control was incubated with TUNEL label without TUNEL enzyme.

4.11. Image Analysis with ImageJ

Evaluation of immunofluorescence images was performed using FIJI ImageJ 1.52p (National Institutes of Health, Bethesda, MD, USA). First, a free hand selection tool was used to define the region of interest (ROI) representing the total area (t.a.). The outer area (o.a.) was determined by a reduction of the diameter by 0.95 for X- and Y-axes. Another reduction of the diameter by 0.5 for X- and Y-axes leads to the middle area (m.a.; outer area subtracted from total area, diameter reduced by 0.5 for X- and Y-axes) and inner area (i.a.; remaining inner part). The positive stained areas were defined using the color threshold tool. Finally, the cell count was performed with a combination of the Find Maxima tool in ImageJ and manual counting.

4.12. In Vitro µCT

TBBCs were scanned at a nominal resolution of 4–5 µm, with a Bruker SkyScan 1172 high-resolution microCT (Bruker, Kontich, Belgium). X-ray tube voltage was of 80 kV and a 0.5 mm aluminum filter was employed. The scan orbit was 360 degrees with a rotation step of 0.3 degree. For reconstruction the SkyScan NRecon software was used and Gaussian smoothing, ring artifact reduction, misalignment compensation, and beam hardening correction were applied. CTAn (Bruker MicroCT, Kontich, Belgium) software was used to analyze the total VOI.

4.13. RNA Isolation, cDNA Synthesis and qPCR

Total RNA from the 3D components was isolated according to the manufacturer's instructions using the RNeasy® Fibrous Tissue Mini Kit (Qiagen GmbH, Hilden, Germany) after homogenization with the TissueRuptor II (Qiagen GmbH, Hilden, Germany). Total RNA from monolayer (ML) cultivations was isolated according to the manufacturer's instructions using the RNeasy® Mini Kit (Qiagen GmbH, Hilden, Germany). RNA concentrations were determined via NanoDrop®-ND-1000 Spectrophotometer (Thermo Fisher Scientific, Waltham, MA, USA) and stored at −80 °C. TaqMan® Reverse Transcription Reagents Kit (Applied Biosystems Inc., Foster City, CA, USA) was used for cDNA synthesis with more than 50 ng per reaction whereas Sensiscript Reverse Transcriptase Kit (Qiagen GmbH, Hilden, Germany) was used for cDNA synthesis with less than 50 ng per reaction. Primer were designed using Primer Blast (NCBI, Bethesda, MD, USA). Sequence analyses of qPCR products were confirmed by LGC Genomics GmbH (Berlin, Germany) and evalu-

ated using the Chromas software 2.6.4 (Technelysium Pty Ltd., South Brisbane, Australia). Quantitative PCR (qPCR) was carried out using the DyNAmo ColorFlash SYBR Green qPCR Kit (Thermo Fisher Scientific, Waltham, MA, USA) in the Stratagene Mx3000P™ (Agilent Technologies Inc., Santa Clara, CA, USA). The qPCR was conducted in duplicates with a non-template control (NTC) for each mastermix using the following temperature profile: 7 min initial denaturation at 95 °C, 45 to 60 cycles of 10 s denaturation at 95 °C, 7 s annealing at 60 °C and 9 s elongation at 72 °C. After every run, a melting curve analysis was performed to confirm primer specificity. In cases where the amplification curve did not reach the threshold within the cycles, the value of the maximum cycle number was used. All primers were purchased from TIB Molbiol Berlin, Germany (Table 3).

Table 3. Sequences of primers, fragment size and GenBank ID used for qPCR.

Gene	Sequence of Forward Primer	Sequence of Reverse Primer	GenBank ID
EF1A	GTTGATATGGTTCCTGGCAAGC	TTGCCAGCTCCAGCAGCCT	NM_001402.5
RUNX2	TTACTTACACCCCGCCAGTC	TATGGAGTGCTGCTGGTCTG	NM_001015051.3
SPP1	GCCGAGGTGATAGTGTGGTT	TGAGGTGATGTCCTCGTCTG	NM_001251830.1
COL1A1	CAGCCGCTTCACCTACAGC	TTTTGTATTCAATCACTGTCTTGCC	NM_000088.3
ON	ACCAGCACCCCATTGACG	AGGTCACAGGTCTCGAAAAAGC	NM_001309443.1
SOX9	CGCCTTGAAGATGGCGTTG	GCTCTGGAGACTTCTGAACGA	NM_000346.3
PPARG2	CAAACCCCTATTCCATGCTGTT	AATGGCATCTCTGTGTCAACC	NM_015869.4
COL2A1	GTGGGGCAAGACTGTTATCG	AGGTCAGGTCAGCCATTCAG	NM_033150.3
COL10A1	CCAGCACGCAGAATCCATCT	TATGCCTGTGGGCATTTGGT	NM_000493.4
ACAN	AACGCAGACTACAGAAGCGG	GGCGGACAAATTAGATGCGG	NM_001369268.1
MMP1	CTCTGGAGTAATGTCACACCTCT	TGTTGGTCCACCTTTCATCTTC	NM_001145938.2
MMP3	ATCCTACTGTTGCTGTGCGT	CATCACCTCCAGAGTGTCGG	NM_002422.5
MMP13	TCCTGATGTGGGTGAATACAATG	GCCATCGTGAAGTCTGGTAAAAT	NM_002427.4
TNF	GTCTCCTACCAGACCAAG	CAAAGTAGACCCTGCCCAGACTC	NM_000594.4
IL6	TACCCCCAGGAGAAGATTCC	TTTTCTGCCAGTGCCTCTTT	NM_001371096.1
IL8	GAATGGGTTTGCTAGAATGTGATA	CAGACTAGGGTTGCCAGATTTAAC	NM_000584.4
LDHA	ACCCAGTTTCCACCATGATT	CCCAAAATGCAAGGAACACT	NM_005566.4
VEGFA	AGCCTTGCCTTGCTGCTCTA	GTGCTGGCCTTGGTGAGG	NM_001025366.3

4.14. Statistical Analysis

Statistical analysis was performed using the GraphPad® Prism V.8.4.1 software (GraphPad Software, La Jolla/San Diego, CA, USA). All values are shown as the mean ± SEM if not indicated otherwise. Mann-Whitney U test was applied for independent datasets while dependent datasets were compared by means using the Wilcoxon-signed rank test. Values of $p < 0.05$ were considered as statistically significant.

5. Conclusions

We herein describe a novel alternative approach simulating key features of RA including cartilage destruction and subchondral bone erosion in late stages of disease to be used as preclinical drug screening tool. The 3D osteochondral tissue model replicates the interaction of cells within a physiological matrix and environment, the crosstalk between the major resident cells of human cartilage and anabolic bone, and the option to further expand cellular interactions by the application of e.g., leukocytes.

Author Contributions: Conceptualization, A.D., A.L., T.G.; methodology, A.D.; validation, A.D., A.L., T.G.; formal analysis, A.D., M.P., M.-C.W.; investigation, A.D., T.G., A.L.; data curation, A.D., T.G., A.L., F.B.; writing—original draft preparation, A.D., T.G., A.L., F.B.; writing—review and editing, A.D., T.G., A.L., F.B., G.-R.B., M.P., M.-C.W., visualization, A.D.; supervision, T.G., A.L.; project administration, F.B.; funding acquisition, T.G., A.L., F.B. All authors have read and agreed to the published version of the manuscript.

Funding: This research was funded by the German Federal Ministry for Education and Research (BMBF), project number 031L0070A and Lush Prize Award 2018: Alexandra Damerau—Young Researcher, Rest of World. The work of A.D. was additionally supported by the Studienstiftung des deutschen Volkes. A.L. is currently being supported by the Joachim Herz Foundation (Add-on Fellowship 2019). The work of T.G. was supported by the Deutsche Forschungsgemeinschaft (353142848). Funding bodies did not have any role in designing the study, in collecting, analyzing and interpreting the data, in writing this manuscript, and in deciding to submit it for publication.

Institutional Review Board Statement: The study was conducted according to the guidelines of the Declaration of Helsinki, and approved by the Ethics Committee of the Charité-Universitätsmedizin Berlin (ethical approval EA1/012/13, 31 January 2013).

Informed Consent Statement: Informed consent was obtained from all subjects involved in the study.

Data Availability Statement: The data presented in this study are available on request from the corresponding author. The data are not publicly available due to privacy and ethical restrictions.

Acknowledgments: The authors would like to thank Manuela Jakstadt for excellent technical assistance, and Thomas Leeuw for providing technical advice. Bone-marrow was provided by the Tissue Harvesting Core Facility of the BIH Berlin. A.D., M.P., F.B., T.G. and A.L. are members of Berlin-Brandenburg research platform BB3R and Charité3R.

Conflicts of Interest: The authors declare no conflict of interest.

Appendix A

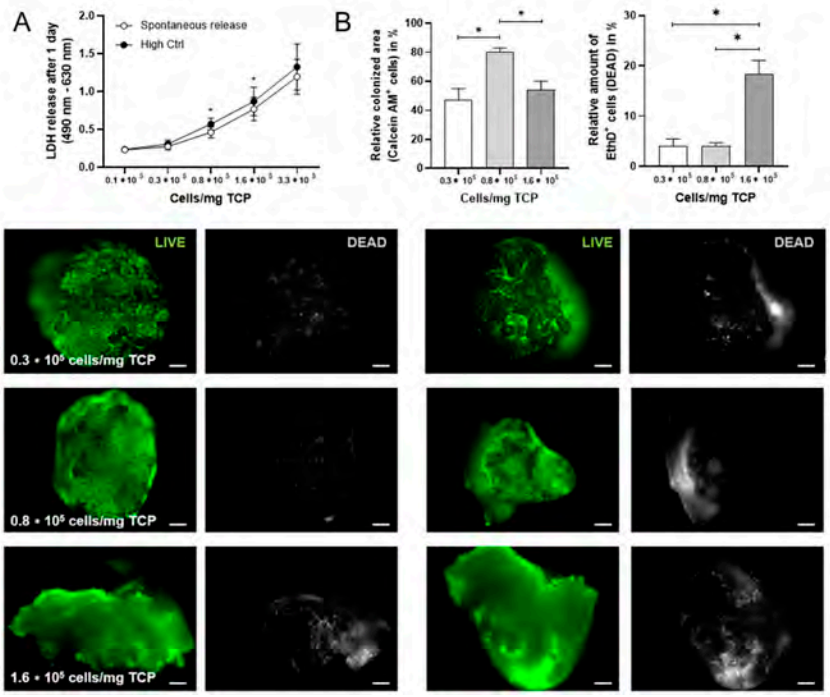

Figure A1. Cell number/mg TCP. (**A**) LDH assay was performed after 1 day and different cell densities (0.1×10^5, 0.3×10^5, 0.8×10^5, 1.6×10^5, 3.3×10^5 cells/mg TCP). High Ctrl = 2% of Triton X-100 to induce LDH release. Data are shown as mean ± SEM (duplicates per donor) for $n = 4$. For statistical analysis the Wilcoxon matched-pairs signed rank test was used; * $p < 0.05$. (**B**) LIVE/DEAD staining was performed after 21 days and different cell densities (0.3×10^5, 0.8×10^5, 1.6×10^5 cells/mg TCP). Images were quantified using ImageJ. Green and grey colors discriminated between living and dead cells (scale bars = 100 µm). Representative images are shown accordingly for $n = 5$. Data are shown as mean ± SEM. For statistical analysis the Wilcoxon matched-pairs signed rank test was used; * $p < 0.05$. TCP, tricalcium phosphate; LDH, lactate dehydrogenase.

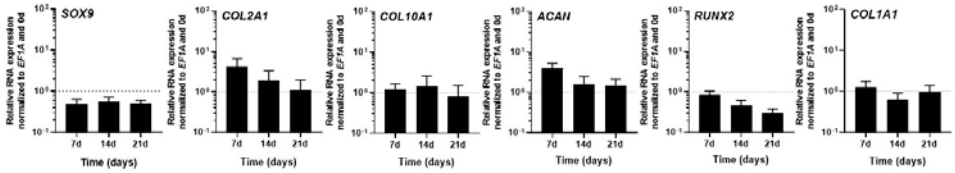

Figure A2. Gene expression analysis of scaffold-free cartilage components for *SOX9*, *COL2A1*, *COL10A1 ACAN*, *RUNX2* and *COL1A1* were performed after 0, 7, 14 and 21 days. The relative gene expression was normalized to the housekeeper gene *EF1A* and day 0. Data are shown as mean ± SEM (duplicates per gene) for $n = 3$. Mann-Whitney U-test was used to determine the statistical significance. *SOX9*, SRY-box transcription factor 9; *COL2A1*, collagen type II alpha 1; *COL10A1*, collagen type X alpha 1; *ACAN*, aggrecan; *RUNX2*, runt-related transcription factor 2; *COL1A1;* collagen type I alpha 1; *EF1A*, eukaryotic translation elongation factor 1 alpha.

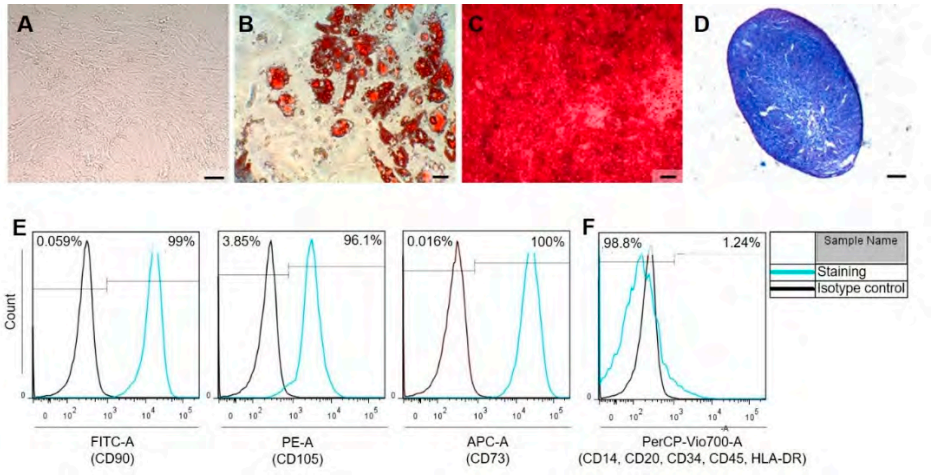

Figure A3. Bone marrow-derived mesenchymal stromal cells are characterized (**A**) by plastic adherence, by their differentiation capacity towards (**B**) adipogenesis using Oil Red O staining, (**C**) osteogenesis using Alizarin Red staining (scale bars = 100 µm), (**D**) chondrogenesis using Alcian Blue staining (scale bar = 200 µm), (**E**) the expression of surface marker CD90, CD105, CD73 and (**F**) lack of CD14, CD20, CD34, CD45 and HLA-DR.

References

1. Lepage, S.I.M.; Robson, N.; Gilmore, H.; Davis, O.; Hooper, A.; St John, S.; Kamesan, V.; Gelis, P.; Carvajal, D.; Hurtig, M.; et al. Beyond Cartilage Repair: The Role of the Osteochondral Unit in Joint Health and Disease. *Tissue Eng. Part. B Rev.* **2019**, *25*, 114–125. [CrossRef]
2. Burr, D.B.; Radin, E.L. Microfractures and Microcracks in Subchondral Bone: Are They Relevant to Osteoarthrosis? *Rheum. Dis. Clin. N. Am.* **2003**, *29*, 675–685. [CrossRef]
3. Goldring, S.R.; Goldring, M.B. Changes in the Osteochondral Unit during Osteoarthritis: Structure, Function and Cartilage–Bone Crosstalk. *Nat. Rev. Rheumatol.* **2016**, *12*, 632–644. [CrossRef]
4. Imhof, H.; Sulzbacher, I.; Grampp, S.; Czerny, C.; Youssefzadeh, S.; Kainberger, F. Subchondral Bone and Cartilage Disease: A Rediscovered Functional Unit. *Investig. Radiol.* **2000**, *35*, 581–588. [CrossRef]
5. Kurz, B.; Lemke, A.K.; Fay, J.; Pufe, T.; Grodzinsky, A.J.; Schünke, M. Pathomechanisms of Cartilage Destruction by Mechanical Injury. *Ann. Anat. Anat. Anz.* **2005**, *187*, 473–485. [CrossRef]
6. Martel-Pelletier, J.; Barr, A.J.; Cicuttini, F.M.; Conaghan, P.G.; Cooper, C.; Goldring, M.B.; Goldring, S.R.; Jones, G.; Teichtahl, A.J.; Pelletier, J.-P. Osteoarthritis. *Nat. Rev. Dis. Primers* **2016**, *2*, 16072. [CrossRef]
7. McInnes, I.B.; Schett, G. The Pathogenesis of Rheumatoid Arthritis. *N. Engl. J. Med.* **2011**, *365*, 2205–2219. [CrossRef] [PubMed]
8. Hardy, E.; Fernandez-Patron, C. Destroy to Rebuild: The Connection between Bone Tissue Remodeling and Matrix Metalloproteinases. *Front. Physiol.* **2020**, *11*, 47. [CrossRef] [PubMed]
9. Otero, M.; Goldring, M.B. Cells of the Synovium in Rheumatoid Arthritis. Chondrocytes. *Arthritis Res. Ther.* **2007**, *9*, 220. [CrossRef] [PubMed]
10. Buttgereit, F. Views on Glucocorticoid Therapy in Rheumatology: The Age of Convergence. *Nat. Rev. Rheumatol.* **2020**, *16*, 239–246. [CrossRef]

11. Burmester, G.R.; Pope, J.E. Novel Treatment Strategies in Rheumatoid Arthritis. *Lancet* **2017**, *389*, 2338–2348. [CrossRef]
12. Schinnerling, K.; Rosas, C.; Soto, L.; Thomas, R.; Aguillón, J.C. Humanized Mouse Models of Rheumatoid Arthritis for Studies on Immunopathogenesis and Preclinical Testing of Cell-Based Therapies. *Front. Immunol.* **2019**, *10*, 203. [CrossRef] [PubMed]
13. Trentham, D.E.; Townes, A.S.; Kang, A.H. Autoimmunity to Type Ii Collagen an Experimental Model of Arthritis. *J. Exp. Med.* **1977**, *146*, 857–868. [CrossRef] [PubMed]
14. Damerau, A.; Gaber, T. Modeling Rheumatoid Arthritis in Vitro: From Experimental Feasibility to Physiological Proximity. *Int. J. Mol. Sci* **2020**, *21*, 7916. [CrossRef] [PubMed]
15. Murphy, G.; Lee, M.H. What Are the Roles of Metalloproteinases in Cartilage and Bone Damage? *Ann. Rheum. Dis.* **2005**, *64*, iv44. [CrossRef]
16. Gaber, T.; Brinkman, A.C.K.; Pienczikowski, J.; Diesing, K.; Damerau, A.; Pfeiffenberger, M.; Lang, A.; Ohrndorf, S.; Burmester, G.R.; Buttgereit, F.; et al. Impact of Janus Kinase Inhibition with Tofacitinib on Fundamental Processes of Bone Healing. *Int. J. Mol. Sci.* **2020**, *21*, 865. [CrossRef]
17. Donlin, L.T.; Jayatilleke, A.; Giannopoulou, E.G.; Kalliolias, G.D.; Ivashkiv, L.B. Modulation of Tnf-Induced Macrophage Polarization by Synovial Fibroblasts. *J. Immunol.* **2014**, *193*, 2373–2383. [CrossRef]
18. Weber, M.C.; Fischer, L.; Damerau, A.; Ponomarev, I.; Pfeiffenberger, M.; Gaber, T.; Gotschel, S.; Lang, J.; Roblitz, S.; Buttgereit, F.; et al. Macroscale Mesenchymal Condensation to Study Cytokine-Driven Cellular and Matrix-Related Changes During Cartilage Degradation. *Biofabrication* **2020**, *12*, 045016. [CrossRef]
19. Pretzel, D.; Pohlers, D.; Weinert, S.; Kinne, R.W. In Vitro Model for the Analysis of Synovial Fibroblast-Mediated Degradation of Intact Cartilage. *Arthritis Res. Ther.* **2009**, *11*, R25. [CrossRef]
20. Lubke, C.; Ringe, J.; Krenn, V.; Fernahl, G.; Pelz, S.; Kreusch-Brinker, R.; Sittinger, M.; Paulitschke, M. Growth Characterization of Neo Porcine Cartilage Pellets and Their Use in an Interactive Culture Model. *Osteoarthr. Cartil.* **2005**, *13*, 478–487. [CrossRef]
21. Chabaud, M.; Miossec, P. The Combination of Tumor Necrosis Factor A Blockade with Interleukin-1 and Interleukin-17 Blockade Is More Effective for Controlling Synovial Inflammation and Bone Resorption in an Ex Vivo Model. *Arthritis Rheum.* **2001**, *44*, 1293–1303. [CrossRef]
22. Kim, T.W.; Lee, M.C.; Bae, H.C.; Han, H.S. Direct Coculture of Human Chondrocytes and Synovium-Derived Stem Cells Enhances in Vitro Chondrogenesis. *Cell J.* **2018**, *20*, 53–60. [PubMed]
23. Kandel, R.A.; Grynpas, M.; Pilliar, R.; Lee, J.; Wang, J.; Waldman, S.; Zalzal, P.; Hurtig, M. Repair of Osteochondral Defects with Biphasic Cartilage-Calcium Polyphosphate Constructs in a Sheep Model. *Biomaterials* **2006**, *27*, 4120–4131. [CrossRef] [PubMed]
24. Schaefer, D.; Martin, I.; Jundt, G.; Seidel, J.; Heberer, M.; Grodzinsky, A.; Bergin, I.; Vunjak-Novakovic, G.; Freed, L.E. Tissue-Engineered Composites for the Repair of Large Osteochondral Defects. *Arthritis Rheum.* **2002**, *46*, 2524–2534. [CrossRef]
25. Schek, R.M.; Taboas, J.M.; Segvich, S.J.; Hollister, S.J.; Krebsbach, P.H. Engineered Osteochondral Grafts Using Biphasic Composite Solid Free-Form Fabricated Scaffolds. *Tissue Eng.* **2004**, *10*, 1376–1385. [CrossRef] [PubMed]
26. Fukuda, A.; Kato, K.; Hasegawa, M.; Hirata, H.; Sudo, A.; Okazaki, K.; Tsuta, K.; Shikinami, Y.; Uchida, A. Enhanced Repair of Large Osteochondral Defects Using a Combination of Artificial Cartilage and Basic Fibroblast Growth Factor. *Biomaterials* **2005**, *26*, 4301–4308. [CrossRef]
27. Gilbert, S.J.; Singhrao, S.K.; Khan, I.M.; Gonzalez, L.G.; Thomson, B.M.; Burdon, D.; Duance, V.C.; Archer, C.W. Enhanced Tissue Integration During Cartilage Repair In Vitro Can Be Achieved by Inhibiting Chondrocyte Death at the Wound Edge. *Tissue Eng. Part. A* **2009**, *15*, 1739–1749. [CrossRef]
28. Darling, E.M.; Athanasiou, K.A. Rapid Phenotypic Changes in Passaged Articular Chondrocyte Subpopulations. *J. Orthop. Res.* **2005**, *23*, 425–432. [CrossRef]
29. Vinken, M.; Blaauboer, B.J. In Vitro Testing of Basal Cytotoxicity: Establishment of an Adverse Outcome Pathway from Chemical Insult to Cell Death. *Toxicol. Vitr.* **2017**, *39*, 104–110. [CrossRef]
30. Nguyen, D.X.; Cotton, A.; Attipoe, L.; Ciurtin, C.; Dore, C.J.; Ehrenstein, M.R. Regulatory T Cells as a Biomarker for Response to Adalimumab in Rheumatoid Arthritis. *J. Allergy Clin. Immunol.* **2018**, *142*, 978–980.e979. [CrossRef]
31. Pattacini, L.; Boiardi, L.; Casali, B.; Salvarani, C. Differential Effects of Anti-Tnf-A Drugs on Fibroblast-Like Synoviocyte Apoptosis. *Rheumatology* **2009**, *49*, 480–489. [CrossRef] [PubMed]
32. Gaber, T.; Hahne, M.; Strehl, C.; Hoff, P.; Dörffel, Y.; Feist, E.; Burmester, G.-R.; Buttgereit, F. Disentangling the Effects of Tocilizumab on Neutrophil Survival and Function. *Immunol. Res.* **2016**, *64*, 665–676. [CrossRef] [PubMed]
33. Shin, B.-H.; Ge, S.; Mirocha, J.; Jordan, S.C.; Toyoda, M. Tocilizumab (Anti-Il-6r) Suppressed Tnfα Production by Human Monocytes in an in Vitro Model of Anti-Hla Antibody-Induced Antibody-Dependent Cellular Cytotoxicity. *Transplant. Direct* **2017**, *3*, e139. [CrossRef] [PubMed]
34. Stein, R.; Smith, M.R.; Chen, S.; Zalath, M.; Goldenberg, D.M. Combining Milatuzumab with Bortezomib, Doxorubicin, or Dexamethasone Improves Responses in Multiple Myeloma Cell Lines. *Clin. Cancer Res.* **2009**, *15*, 2808. [CrossRef] [PubMed]
35. Gimble, J.M.; Guilak, F.; Nuttall, M.E.; Sathishkumar, S.; Vidal, M.; Bunnell, B.A. In Vitro Differentiation Potential of Mesenchymal Stem Cells. *Transfus. Med. Hemother.* **2008**, *35*, 228–238. [CrossRef]
36. Larson, B.L.; Ylöstalo, J.; Prockop, D.J. Human Multipotent Stromal Cells Undergo Sharp Transition from Division to Development in Culture. *Stem Cells* **2008**, *26*, 193–201. [CrossRef]
37. Tuli, R.; Nandi, S.; Li, W.-J.; Tuli, S.; Huang, X.; Manner, P.A.; Laquerriere, P.; Nöth, U.; Hall, D.J.; Tuan, R.S. Human Mesenchymal Progenitor Cell-Based Tissue Engineering of a Single-Unit Osteochondral Construct. *Tissue Eng.* **2004**, *10*, 1169–1179. [CrossRef]

38. Boukhechba, F.; Balaguer, T.; Michiels, J.-F.; Ackermann, K.; Quincey, D.; Bouler, J.-M.; Pyerin, W.; Carle, G.F.; Rochet, N. Human Primary Osteocyte Differentiation in a 3d Culture System. *J. Bone Miner. Res.* **2009**, *24*, 1927–1935. [CrossRef]
39. Gao, P.; Zhang, H.; Liu, Y.; Fan, B.; Li, X.; Xiao, X.; Lan, P.; Li, M.; Geng, L.; Liu, D.; et al. Beta-Tricalcium Phosphate Granules Improve Osteogenesis in Vitro and Establish Innovative Osteo-Regenerators for Bone Tissue Engineering in Vivo. *Sci. Rep.* **2016**, *6*, 23367. [CrossRef]
40. Liu, G.; Zhao, L.; Cui, L.; Liu, W.; Cao, Y. Tissue-Engineered Bone Formation Using Human Bone Marrow Stromal Cells and Novel B-Tricalcium Phosphate. *Biomed. Mater.* **2007**, *2*, 78–86. [CrossRef]
41. Herten, M.; Rothamel, D.; Schwarz, F.; Friesen, K.; Koegler, G.; Becker, J. Surface- and Nonsurface-Dependent In Vitro Effects of Bone Substitutes on Cell Viability. *Clin. Oral Investig.* **2009**, *13*, 149–155. [CrossRef] [PubMed]
42. Kulterer, B.; Friedl, G.; Jandrositz, A.; Sanchez-Cabo, F.; Prokesch, A.; Paar, C.; Scheideler, M.; Windhager, R.; Preisegger, K.-H.; Trajanoski, Z. Gene Expression Profiling of Human Mesenchymal Stem Cells Derived from Bone Marrow During Expansion and Osteoblast Differentiation. *BMC Genom.* **2007**, *8*, 70. [CrossRef] [PubMed]
43. Wrobel, E.; Leszczynska, J.; Brzoska, E. The Characteristics of Human Bone-Derived Cells (Hbdcs) during Osteogenesis In Vitro. *Cell. Mol. Biol. Lett.* **2016**, *21*, 26. [CrossRef]
44. DuRaine, G.D.; Brown, W.E.; Hu, J.C.; Athanasiou, K.A. Emergence of Scaffold-Free Approaches for Tissue Engineering Musculoskeletal Cartilages. *Ann. Biomed. Eng.* **2015**, *43*, 543–554. [CrossRef] [PubMed]
45. Furukawa, K.S.; Suenaga, H.; Toita, K.; Numata, A.; Tanaka, J.; Ushida, T.; Sakai, Y.; Tateishi, T. Rapid and Large-Scale Formation of Chondrocyte Aggregates by Rotational Culture. *Cell Transplant.* **2003**, *12*, 475–479. [CrossRef]
46. Gilpin, D.A.; Weidenbecher, M.S.; Dennis, J.E. Scaffold-Free Tissue-Engineered Cartilage Implants for Laryngotracheal Reconstruction. *Laryngoscope* **2010**, *120*, 612–617. [CrossRef]
47. Park, I.-S.; Jin, R.L.; Oh, H.J.; Truong, M.-D.; Choi, B.H.; Park, S.-H.; Park, D.Y.; Min, B.-H. Sizable Scaffold-Free Tissue-Engineered Articular Cartilage Construct for Cartilage Defect Repair. *Artif. Organs* **2019**, *43*, 278–287. [CrossRef]
48. Bhumiratana, S.; Eton, R.E.; Oungoulian, S.R.; Wan, L.Q.; Ateshian, G.A.; Vunjak-Novakovic, G. Large, Stratified, and Mechanically Functional Human Cartilage Grown In Vitro by Mesenchymal Condensation. *Proc. Natl. Acad. Sci. USA* **2014**, *111*, 6940–6945. [CrossRef]
49. Addo, R.K.; Heinrich, F.; Heinz, G.A.; Schulz, D.; Sercan-Alp, Ö.; Lehmann, K.; Tran, C.L.; Bardua, M.; Matz, M.; Löhning, M.; et al. Single-Cell Transcriptomes of Murine Bone Marrow Stromal Cells Reveal Niche-Associated Heterogeneity. *Eur J. Immunol.* **2019**, *49*, 1372–1379. [CrossRef]
50. Kim, I.G.; Ko, J.; Lee, H.R.; Do, S.H.; Park, K. Mesenchymal Cells Condensation-Inducible Mesh Scaffolds for Cartilage Tissue Engineering. *Biomaterials* **2016**, *85*, 18–29. [CrossRef]
51. Xia, H.; Liang, C.; Luo, P.; Huang, J.; He, J.; Wang, Z.; Cao, X.; Peng, C.; Wu, S. Pericellular Collagen I Coating for Enhanced Homing and Chondrogenic Differentiation of Mesenchymal Stem Cells in Direct Intra-Articular Injection. *Stem Cell Res. Ther.* **2018**, *9*, 174. [CrossRef] [PubMed]
52. Raghothaman, D.; Leong, M.F.; Lim, T.C.; Toh, J.K.C.; Wan, A.C.A.; Yang, Z.; Lee, E.H. Engineering Cell Matrix Interactions in Assembled Polyelectrolyte Fiber Hydrogels for Mesenchymal Stem Cell Chondrogenesis. *Biomaterials* **2014**, *35*, 2607–2616. [CrossRef] [PubMed]
53. Ng, J.; Bernhard, J.; Vunjak-Novakovic, G. Mesenchymal Stem Cells for Osteochondral Tissue Engineering. *Methods Mol. Biol.* **2016**, *1416*, 35–54. [PubMed]
54. Lin, Z.; Li, Z.; Li, E.N.; Li, X.; Del Duke, C.J.; Shen, H.; Hao, T.; O'Donnell, B.; Bunnell, B.A.; Goodman, S.B.; et al. Osteochondral Tissue Chip Derived from Ipscs: Modeling Oa Pathologies and Testing Drugs. *Front. Bioeng. Biotechnol.* **2019**, *7*, 411. [CrossRef]
55. Choy, E.H.S.; Panayi, G.S. Cytokine Pathways and Joint Inflammation in Rheumatoid Arthritis. *N. Engl. J. Med.* **2001**, *344*, 907–916. [CrossRef]
56. Hashizume, M.; Mihara, M. High Molecular Weight Hyaluronic Acid Inhibits Il-6-Induced Mmp Production from Human Chondrocytes by up-Regulating the Erk Inhibitor, Mkp-1. *Biochem. Biophys. Res. Commun.* **2010**, *403*, 184–189. [CrossRef]
57. Latourte, A.; Cherifi, C.; Maillet, J.; Ea, H.-K.; Bouaziz, W.; Funck-Brentano, T.; Cohen-Solal, M.; Hay, E.; Richette, P. Systemic Inhibition of Il-6/Stat3 Signalling Protects against Experimental Osteoarthritis. *Ann. Rheum. Dis.* **2017**, *76*, 748. [CrossRef]
58. Fox, D.A. Cytokine Blockade as a New Strategy to Treat Rheumatoid Arthritis: Inhibition of Tumor Necrosis Factor. *Arch. Intern. Med.* **2000**, *160*, 437–444. [CrossRef]
59. Honorati, M.C.; Cattini, L.; Facchini, A. Il-17, Il-1 and Tnf Stimulate Vegf Production by Dedifferentiated Chondrocytes. *Osteoarthr. Cartil.* **2004**, *12*, 683–691. [CrossRef]
60. Leech, M.; Metz, C.; Hall, P.; Hutchinson, P.; Gianis, K.; Smith, M.; Weedon, H.; Holdsworth, S.R.; Bucala, R.; Morand, E.F. Macrophage Migration Inhibitory Factor in Rheumatoid Arthritis: Evidence of Proinflammatory Function and Regulation by Glucocorticoids. *Arthritis Rheum.* **1999**, *42*, 1601–1608. [CrossRef]
61. Manicourt, D.H.; Poilvache, P.; Van Egeren, A.; Devogelaer, J.P.; Lenz, M.E.; Thonar, E.J. Synovial Fluid Levels of Tumor Necrosis Factor Alpha and Oncostatin M Correlate with Levels of Markers of the Degradation of Crosslinked Collagen and Cartilage Aggrecan in Rheumatoid Arthritis but Not in Osteoarthritis. *Arthritis Rheum.* **2000**, *43*, 281–288. [CrossRef]
62. Wright, H.L.; Mewar, D.; Bucknall, R.C.; Edwards, S.W.; Moots, R.J. Synovial Fluid Il-6 Concentrations Associated with Positive Response to Tocilizumab in an Ra Patient with Failed Response to Anti-Tnf and Rituximab. *Rheumatology* **2015**, *54*, 743–744. [CrossRef] [PubMed]

63. Koch, A.E.; Volin, M.V.; Woods, J.M.; Kunkel, S.L.; Connors, M.A.; Harlow, L.A.; Woodruff, D.C.; Burdick, M.D.; Strieter, R.M. Regulation of Angiogenesis by the C-X-C Chemokines Interleukin-8 and Epithelial Neutrophil Activating Peptide 78 in the Rheumatoid Joint. *Arthritis Rheum.* **2001**, *44*, 31–40. [CrossRef]
64. Verboogen, D.R.J.; Revelo, N.H.; ter Beest, M.; van den Bogaart, G. Interleukin-6 Secretion Is Limited by Self-Signaling in Endosomes. *J. Mol. Cell Biol.* **2018**, *11*, 144–157. [CrossRef] [PubMed]
65. Yoshida, S.; Ono, M.; Shono, T.; Izumi, H.; Ishibashi, T.; Suzuki, H.; Kuwano, M. Involvement of Interleukin-8, Vascular Endothelial Growth Factor, and Basic Fibroblast Growth Factor in Tumor Necrosis Factor Alpha-Dependent Angiogenesis. *Mol. Cell. Biol.* **1997**, *17*, 4015. [CrossRef]
66. Paleolog, E.M.; Hunt, M.; Elliott, M.J.; Feldmann, M.; Maini, R.N.; Woody, J.N. Deactivation of Vascular Endothelium by Monoclonal Anti-Tumor Necrosis Factor Alpha Antibody in Rheumatoid Arthritis. *Arthritis Rheum.* **1996**, *39*, 1082–1091. [CrossRef]
67. Paleolog, E.M.; Young, S.; Stark, A.C.; McCloskey, R.V.; Feldmann, M.; Maini, R.N. Modulation of Angiogenic Vascular Endothelial Growth Factor by Tumor Necrosis Factor Alpha and Interleukin-1 in Rheumatoid Arthritis. *Arthritis Rheum.* **1998**, *41*, 1258–1265. [CrossRef]
68. Koenders, M.I.; van den Berg, W.B. Secukinumab for Rheumatology: Development and Its Potential Place in Therapy. *Drug Des. Dev. Devel Ther.* **2016**, *10*, 2069–2080. [CrossRef]
69. Genovese, M.C.; Jarosova, K.; Cieslak, D.; Alper, J.; Kivitz, A.; Hough, D.R.; Maes, P.; Pineda, L.; Chen, M.; Zaidi, F. Apremilast in Patients with Active Rheumatoid Arthritis: A Phase Ii, Multicenter, Randomized, Double-Blind, Placebo-Controlled, Parallel-Group Study. *Arthritis Rheumatol.* **2015**, *67*, 1703–1710. [CrossRef]
70. Nakae, S.; Nambu, A.; Sudo, K.; Iwakura, Y. Suppression of Immune Induction of Collagen-Induced Arthritis in Il-17-Deficient Mice. *J. Immunol.* **2003**, *171*, 6173–6177. [CrossRef]
71. Lubberts, E.; Koenders, M.I.; Oppers-Walgreen, B.; van den Bersselaar, L.; Coenen-de Roo, C.J.; Joosten, L.A.; van den Berg, W.B. Treatment with a Neutralizing Anti-Murine Interleukin-17 Antibody after the Onset of Collagen-Induced Arthritis Reduces Joint Inflammation, Cartilage Destruction, and Bone Erosion. *Arthritis Rheum.* **2004**, *50*, 650–659. [CrossRef] [PubMed]
72. Tahir, H.; Deodhar, A.; Genovese, M.; Takeuchi, T.; Aelion, J.; Van den Bosch, F.; Haemmerle, S.; Richards, H.B. Secukinumab in Active Rheumatoid Arthritis after Anti-Tnfalpha Therapy: A Randomized, Double-Blind Placebo-Controlled Phase 3 Study. *Rheumatol. Ther.* **2017**, *4*, 475–488. [CrossRef]
73. Piluso, S.; Li, Y.; Abinzano, F.; Levato, R.; Moreira Teixeira, L.; Karperien, M.; Leijten, J.; van Weeren, R.; Malda, J. Mimicking the Articular Joint with in Vitro Models. *Trends Biotechnol.* **2019**, *37*, 1063–1077. [CrossRef] [PubMed]
74. Kawamoto, T.; Kawamoto, K. Preparation of Thin Frozen Sections from Nonfixed and Undecalcified Hard Tissues Using Kawamot's Film Method (2012). *Methods Mol. Biol.* **2014**, *1130*, 149–164. [PubMed]

3.2. Part II: Optimization of the osteochondral building blocks

More than four decades have passed since the term "tissue engineering" was introduced to describe a new concept focused on the generation of de novo synthesized tissues from cells using growth factors and biomaterials. While scaffold-free tissue formation is still restricted to the self-assembly of cells into spheroids and organoids, scaffold-based tissue formation is limited to the seeding of cells onto a specific type of non-degradable or biodegradable scaffold (Ikada 2006, Causa, Netti et al. 2007). Scaffold-free and scaffold-based approaches are usually generated in a small scale format and with few cell spheroids or scaffold particles. Therefore, optimal strategies for cell seeding and down-sizing or up-scaling without changing the manufacturing conditions are major challenges in the production of *in vitro* 3D models.

Hence, the following manuscripts present the optimization of the building blocks of the osteochondral unit.

(i) The bone model was further optimized by combining the ceramic-based scaffold with cell-sheet technology to improve the efficiency of cell colonization and differentiation (3.2.1).

(ii) The macroscale scaffold-free chondrogenic construct was optimized by reducing the number of cells, while maintaining morphology during differentiation, in order to adapt culture size to mid/high-throughput that resulted in the development of microscale scaffold-free chondrogenic components (miniSFCCs) (3.2.2).

3.2.1. Manuscript 2: Optimization of a tricalcium phosphate-based bone model using cell-sheet technology to simulate bone disorders

This is a peer-reviewed version of the following article:

Authors: Alexandra Damerau, Frank Buttgereit, Timo Gaber

Title: Optimization of a tricalcium phosphate-based bone model using cell-sheet technology to simulate bone disorders

Year: 2022

Journal: Processes (Volume 10, Issue 3, 550)

Final form: https://doi.org/10.3390/pr10030550

Personal contribution: In this manuscript, I was responsible for conceptualizing, planning, preparing, conducting, analyzing, and interpreting the experiments including cell isolation, expansion and characterization, generation and cultivation of bone equivalents using β-TCP scaffold particles and sheet technology, treatment experiments, histological and immunofluorescence investigations and quantifications, gene expression analysis, and scanning electron microscopy. Manuscript design, visualization, writing, reviewing, and final approval under the supervision of Dr. Timo Gaber and Prof. Dr. Frank Buttgereit.

processes

MDPI

Article

Optimization of a Tricalcium Phosphate-Based Bone Model Using Cell-Sheet Technology to Simulate Bone Disorders

Alexandra Damerau [1,2], Frank Buttgereit [1,2] and Timo Gaber [1,2,*]

[1] Department of Rheumatology and Clinical Immunology, Charité-Universitätsmedizin Berlin, Corporate Member of Freie Universität Berlin, Humboldt-Universität zu Berlin, 10117 Berlin, Germany; alexandra.damerau@charite.de (A.D.); frank.buttgereit@charite.de (F.B.)
[2] Deutsches Rheuma-Forschungszentrum (DRFZ), Institute of the Leibniz Association, 10117 Berlin, Germany
* Correspondence: timo.gaber@charite.de

Abstract: Bone diseases such as osteoporosis, delayed or impaired bone healing, and osteoarthritis still represent a social, financial, and personal burden for affected patients and society. Fully humanized in vitro 3D models of cancellous bone tissue are needed to develop new treatment strategies and meet patient-specific needs. Here, we demonstrate a successful cell-sheet-based process for optimized mesenchymal stromal cell (MSC) seeding on a β-tricalcium phosphate (TCP) scaffold to generate 3D models of cancellous bone tissue. Therefore, we seeded MSCs onto the β-TCP scaffold, induced osteogenic differentiation, and wrapped a single osteogenically induced MSC sheet around the pre-seeded scaffold. Comparing the wrapped with an unwrapped scaffold, we did not detect any differences in cell viability and structural integrity but a higher cell seeding rate with osteoid-like granular structures, an indicator of enhanced calcification. Finally, gene expression analysis showed a reduction in chondrogenic and adipogenic markers, but an increase in osteogenic markers in MSCs seeded on wrapped scaffolds. We conclude from these data that additional wrapping of pre-seeded scaffolds will provide a local niche that enhances osteogenic differentiation while repressing chondrogenic and adipogenic differentiation. This approach will eventually lead to optimized preclinical in vitro 3D models of cancellous bone tissue to develop new treatment strategies.

Keywords: mesenchymal stromal cell; cell sheet; osteogenesis; β-TCP; tricalcium phosphate; tissue engineering; in vitro 3D model

Citation: Damerau, A.; Buttgereit, F.; Gaber, T. Optimization of a Tricalcium Phosphate-Based Bone Model Using Cell-Sheet Technology to Simulate Bone Disorders. *Processes* **2022**, *10*, 550. https://doi.org/10.3390/pr10030550

Academic Editor: Clayton Jeffryes

Received: 4 February 2022
Accepted: 7 March 2022
Published: 11 March 2022

1. Introduction

Bone defects and healing disorders arise from various causes such as fractures, other traumas, tumors, infections, dental restorations, healing disorders, and congenital malformations. They can lead to pain and significant loss of quality of life [1–3]. The prevalence of bone diseases and healing disorders increases with life expectancy [4,5]. Both regenerating bone defects and treating healing disorders represent considerable challenges for clinicians. Autologous grafts from the iliac crest remain the gold standard; even though their availability is limited, they carry a risk of infection, and there is only little autologous bone material available [6,7]. Over the past two decades, significant progress has been achieved in developing tissue engineering concepts for the production of synthetic bone substitutes that overcome these challenges by adding new possibilities to standard surgical procedures for the treatment of these patients [2,3].

Clinically, tissue-engineered bone restoration relies on the generation of neo-tissues from osteogenic progenitor cells alone or with the support of osteoconductive bone substitutes for bone ingrowth and osteoinductive growth factors, with and without the need of supportive metal implants [2,3,8]. Although preclinical data from animal studies are often promising, the clinical failure of implants, bone substitutes, and osteoinductive agents is apparent because of limited animal-to-human predictability due to differences in, for

example, physiology, genetics, epigenetics, and molecular biology between species [9,10]. This is also a problem when dealing with bone substitutes coated with osteoinductive growth factors that work in animal models but fail in humans.

Preclinically, tissue-engineered in vitro 3D bone models can improve our understanding of bone biology's physiological and pathophysiological mechanisms (e.g., avascular osteonecrosis). These models may also serve as predictive models of implant success or failure concerning osteoconductive properties of novel biomaterials for bone regeneration. In addition, in vitro 3D bone models provide the opportunity to test, verify, and evaluate novel osteoinductive substances or other therapeutical attempts (e.g., anti-osteoporotic drugs) in a human-based laboratory setting or may directly be used as a clinical implant [11]. However, due to the lack of sophisticated in vitro 3D models, animal models still remain the gold standard, even though great differences in (patho) physiology led to low transferability [12,13].

To simulate native bone in vitro, various tissue engineering approaches have been pursued, including scaffold-based, scaffold-free, and more sophisticated microfluidic model systems that implement a variety of cell or tissue types [14,15]. The most common in vitro 3D approach involves seeding osteogenic progenitor cells on synthetic bone graft substitutes that mimic the mineral bone part, followed by static cultivation, perfused cultivation, or dynamic mechanical loading during cultivation. Artificial bone graft substitutes differ in biocompatibility, immunogenicity, biological activity, cell–biomaterial interactions, and mechanical properties [16]. Additional limitations include low cell attachment efficiency and heterogeneous cellular distribution [17]. Calcium phosphate-based bioceramics that mimic the inorganic bone component have been extensively studied for their applicability. The most common bioceramics are β-tricalcium phosphate (β-TCP), hydroxyapatite (HA), and a mixture of the two known as biphasic calcium phosphate (BCP)-HA/β-TCP—which are well researched and have been reported to support cell adhesion, tissue formation, and differentiation [18–20].

Conventional approaches usually focus on the injection of isolated cell suspensions or the use of pre-seeded biodegradable scaffolds to support tissue formation, depriving cells of their endogenous extracellular matrix (ECM). However, it is challenging to ensure reproducible cell-seeding efficiency [21,22]. In addition, scaffold-based and scaffold-free models are often produced on a small scale with few scaffold particles or cell spheroids. Thus, optimized cell seeding and up-sizing without altering manufacturing conditions are significant challenges in the fabrication of complex in vitro models. Moreover, in the clinical situation, the microenvironment of the bone and surrounding cells are involved in the regeneration process [7]. These conditions are missing and need to be mimicked in developing preclinical models, enhancing translational and clinical success [2,3].

The cell-sheet technology offers the possibility to compensate for these deficits in conventional approaches. This technology enables the generation of viable, transplantable cell sheets from monolayer cell cultures, e.g., using temperature-dependent plates [17,22]. These plates allow cells to be harvested while preserving cell–cell junctions and the ECM without using proteolytic enzymes, allowing for cell-dense tissues [22–25]. Cell-sheet technology has already been successfully used for proper tissue regeneration in periosteum [26], corneal epithelial, myocardial, and—of note—in bone tissues [24,27–29]. However, the development of grafts for bone regeneration is still in its infancy. The difficulty is replicating the high level of bone hierarchical organization while considering the anabolic and catabolic processes.

In bone regeneration, adult mesenchymal stromal cells (MSCs)—the progenitor cells of the anabolic bone compartment—are well suited for the cell-sheet technology approach. MSCs are "self-renewable, multipotent, easily accessible and culturally expandable in vitro with exceptional genomic stability and few ethical issues, marking its importance in cell therapy, regenerative medicine and tissue repairment" [30]. Moreover, MSCs own the potential to modulate and suppress immune responses and thus reduce graft rejection or graft-versus-host reactions [31–33]. Therefore, MSC-based cell-sheets have attracted increasing attention

as a tool to accelerate bone healing, treat chronic pain and infection, and minimize immunological reactions associated with allogeneic bone graft substitutes [24,34]. Interestingly, thin MSC-based cell-sheets can spontaneously form vascular or pre-vascularized capillaries with endothelial (progenitor) cells to facilitate vascularization and integration into the host anatomy [35,36]. Finally, the envelopment of osteoclasts and osteoblasts/osteocytes and immune cells in the MSC-based cell sheets in vitro allows mapping both catabolic and anabolic processes and immunological processes in the bone marrow.

In a previous study, we used a scaffold-based model and seeded MSCs on the biodegradable β-TCP scaffold to mimic cancellous bone [37]. We could demonstrate that these MSCs showed osteogenic properties in vitro, evidenced by the high expression of collagen type 1 (*COL1A1*), osteocalcin (*OC*), osteonectin (*ON*), and bone formation via µCT analysis. However, we observed that porous scaffolds, such as β-TCP, are hardly populated by cells. Given this background, we evaluated osteogenically induced MSC-based cell sheets wrapped around a human in vitro 3D bone model comprising a pre-seeded β-TCP scaffold for cell seeding and differentiation efficiency.

To evaluate our human sheet-based in vitro 3D bone model, we analyzed its response to osteoinductive deferoxamine (DFO). Several studies have already demonstrated the efficacy of DFO in promoting bone fracture healing in a variety of animal models (mouse, rat, and rabbit) with different bone defects (calvaria defect or critical size defect) [38–51]. DFO treatment promotes angiogenesis/vessel formation and bone regeneration independent of the species, model, and evaluation methods [39–57]. Using well-characterized MSCs, we previously demonstrated that HIF-1 promotes osteogenesis and suppresses adipogenesis by loss of function experiments and by pharmacological intervention using DFO [58]. Therefore, we investigated the applicability and response to DFO in this human MSC-sheet-based in vitro 3D bone model, ultimately serving as a human-based preclinical model providing transferability and reducing the number of animal experiments.

2. Materials and Methods

2.1. Bone Marrow-Derived MSC Isolation and Cultivation

Human bone marrow was provided by the Center of Musculoskeletal Surgery, Charité-Universitätsmedizin Berlin, and obtained from patients undergoing total hip replacement (Table 1). Protocols and study design were performed according to the Helsinki Declaration and approved by the Charité-Universitätsmedizin Ethics Committee (ethical approval EA1/146/21; EA1/012/13).

Table 1. Data on age and sex of human MSCs used.

Donor	Age	Sex	Donor	Age	Sex
1	56	male	6	62	female
2	69	female	7	77	male
3	71	male	8	64	female
4	81	female	9	65	male
5	75	female	10	58	male

For isolation of MSCs, bone marrow was placed in a T-175 flask (Greiner Bio-one International GmbH, Kremsmünster, Austria). MSCs—ability to adhere to plastic—were cultured in Dulbecco's Modified eagle Minimal Essential Medium with GlutaMAX™ (DMEM, Gibco, Waltham, MA, USA) supplemented with 10% fetal calf serum (FCS, Biowest, Nuaillé, France), 100 U/mL penicillin (Gibco), 100 µg/mL streptomycin (Gibco, Waltham, MA, USA), and 20% StemMACS™ MSC Expansion Media Kit XF (Miltenyi Biotech, Bergisch Gladbach, Germany). The remaining bone marrow tissue parts were removed after 48 h. The medium was changed weekly, and passaging was performed when reaching 85–90% confluence. Cells were used until passage 6. MSC characterization was performed as described previously in detail [37,59].

2.2. Fabrication of 3D Bone Models: β-TCP Wrapped with an Osteogenically Induced MSC Sheet

To mimic the mineral part of cancellous bone most closely, we used clinical-grade, biocompatible and resorbable β-TCP (Cerasorb®M, Curasan AG, Kleinostheim, Germany) with a particle size range from 1000 to 2000 µm, which provides an interconnecting, open multiporosity with micro-, meso- and macropores (5–500 µm) and total porosity of approximately 65%. Notably, particles of this size most closely mimicked the properties of cancellous bone about bone formation trabecular numbers and thickness in a model of bone formation, whereas the chemical composition had only a minor influence [60].

We preincubated 12 mg of β-TCP with DMEM GlutaMAX™ supplemented with 10% FCS, 100 U/mL penicillin, and 100 µg/mL streptomycin for 24 h. Subsequently, we preseeded β-TCP with a suspension of 1×10^6 MSCs and cultured them in tissue culture inserts in a 24-well plate (Sarstedt, Nümbrecht, Germany) to ensure adequate nutrient supply (in the following abbreviated as 'TCP'). Osteogenic differentiation was induced using DMEM supplemented with 10% FCS, 100 U/mL penicillin, 100 µg/mL streptomycin, 0.5 mM ascorbic acid, 10^{-8} M dexamethasone, and 10 mM L-glycerophosphate (osteogenic medium). A single osteogenically induced MSC sheet was developed by culturing 1×10^6 cells in a 35 mm temperature-responsive dish (Nunc™, Merck, Darmstadt, Germany) with an osteogenic medium for 7 days. On day 7, the single cell-sheet was harvested by decreasing the temperature under 32 °C and then wrapped around the pre-seeded β-TCP scaffold (cell-sheet-based β-TCP, in the following abbreviated as 'csTCP'). In total, the TCP and csTCP model was osteogenically differentiated for 21 days.

2.3. Live/Dead Staining

To visualize the colonization of viable cells in 3D, LIVE/DEAD® Viability/Cytotoxicity Kit (Invitrogen AG, Carlsbad, CA, USA) was performed: After a washing step with 1 × PBS, the staining solution consisting of 2 µM Calcein-AM and 4 µM EthD-1 was added to the 3D models and incubated for 35 min at room temperature in the dark. Imaging was performed using the fluorescence microscope BZ-9000 (Keyence, Neu-Isenburg, Germany).

2.4. TUNEL Assay

Detecting apoptotic cells, TUNEL staining (Sigma-Aldrich, Munich, Germany) was performed with 5 µL TUNEL enzyme and 45 µL TUNEL label for one hour at 37 °C. After washing with 1 × PBS (twice), images were acquired using a BZ-9000 fluorescence microscope (Keyence). Slices treated with deoxyribonuclease (DNase) I (0.34 Kunitz units, Qiagen, Hilden, Germany) for 10 min were positive, while the negative control was incubated without the TUNEL enzyme.

2.5. Scanning Electron Microscopy (SEM)

Using SEM, scaffolds seeded with cells with and without an additional MSC sheet were examined for cellular colonialization, distribution, and cell morphology. After a washing step with 1 × PBS, samples were fixed with 2.5% glutaraldehyde (Sigma-Aldrich) for 10 min and then washed again. Afterward, samples were stepwise dewatered in an ascending ethanol order—30%, 50%, 70%, 80%, 90%, 95%, and twice 100%—for 5 min each, followed by hexamethyldisilazane (1 × 5 min, 2 × 10 min; Sigma-Aldrich). Finally, all samples were dried overnight. After gold coating using the Fine Coater JFC 1200 (Jeol GmbH, Freising, Germany), images were acquired using the scanning electron microscope JCM-6000 Plus Neo Scope™ (Jeol GmbH).

2.6. (Immun)Histochemistry

Kawamoto cryofilm type 2C (Sectionlab, Hiroshima, Japan) was used to prepare 7 µm cryo-sections. Slices were air-dried before each staining protocol, then fixed in 4% paraformaldehyde (PFA, Electron Microscopy Sciences, Hatfield, PA, USA), and subsequently washed with ddH_2O. After every staining protocol, cryo-sections were covered with DPX Mountant (Sigma-Aldrich).

Hematoxylin and Eosin (H & E) staining was performed using Harris's hematoxylin (Merck, Darmstadt, Germany) for 7 min, then washed with ddH_2O, followed by a differentiation step with 0.25% HCl–ethanol (Merck). Eosin staining (0.2%, 2 min; Chroma Waldeck GmbH & Co. KG, Münster, Germany) was performed after 10 min in tap water, followed by 96% ethanol, 100% ethanol, and xylol (2 min, twice).

Collagen type I staining was performed as follows: 3% H_2O_2 for 30 min, washing step with 1 × PBS for 5 min. After a blocking step with 1 × PBS/5% normal horse serum (HS, Vector Laboratories, Burlingame, CA, USA)/2% bovine serum albumin (BSA, Sigma-Aldrich), staining with anti-collagen type I (1:500, Abcam, Cambridge, UK) was performed overnight at 4 °C. Slices were washed with 1 × PBS, followed by an incubation step with 2% biotinylated horse anti-mouse IgG antibody (Vector Laboratories; diluted in 1 × PBS/5% HS/2% BSA) at room temperature for 30 min. After a washing step, slices were incubated with Vecastain® Elite® ABC HRP Kit (Vector Laboratories) for 50 min, washed with 1 × PBS, and set with DAB Peroxidase HRP Substrate Kit (Vector Laboratories). Finally, counterstaining was performed with Mayer's hematoxylin (2 min, Sigma-Aldrich).

2.7. Immunofluorescence Staining

For the immunofluorescence staining, slices were rehydrated with 1 × PBS for 10 min and permeabilized with 0.1% Tween 20® (Sigma-Aldrich) in 1 × PBS for 20 min. After a blocking step with 5% FCS in 1 × PBS for 30 min, cells were washed three times with 1 × PBS/0.1% Tween 20® and incubated with phalloidin-TRITC (Sigma-Aldrich; working solution: 10 µg/mL in 1 × PBS/0.1% Tween 20®/5% FCS) for 45 min or the primary osteopontin antibody (Abcam; 1:50 in 1 × PBS/5% FCS/0.1% Tween 20®) for 2 h. After a washing step, the secondary donkey anti-goat A568 antibody (Thermo Fisher Scientific, Waltham, MA, USA; 1:500 in 1 × PBS/5% FCS/0.1% Tween 20®) was applied for 1 h. Finally, after washing with 1 × PBS/0.1% Tween 20®, the visualization of nuclear DNA was performed using 1 µg/mL 4′,6-diamidino-2-phenylindo (DAPI; Life Technologies, Carlsbad, CA, USA; diluted in 1 × PBS/0.1% Tween 20®/5% FCS) for 15 min. Cryosections were covered with Fluoromount™ (Sigma-Aldrich). Images were performed using a fluorescence microscope (BZ-9000; Keyence).

2.8. Gene Expression Analysis

TCPs were transferred to 300 µL RLT-buffer (Qiagen) with 1% 2-mercaptoethanol (Serva Electrophoresis GmbH, Heidelberg, Germany) and homogenized using the TissueRuptor II (Qiagen). According to the manufacturer's instructions, total RNA was isolated using the RNeasy® Fibrous Tissue Mini Kit (Qiagen). Nanodrop ND-1000 (Peqlab Biotechnologie GmbH, Erlangen, Germany) was used to determine the RNA concentration. cDNA synthesis was performed using TaqMan® Reverse Transcription Reagents Kit (Applied Biosystems Inc., Waltham, MA, USA). The DyNAmo ColorFlash SYBR Green qPCR Kit (Thermo Fisher Scientific) and the Stratagene Mx3000P™ (Agilent Technologies Inc., Santa Clara, CA, USA) were used to perform qPCR. Gene expression analysis was performed in duplicate with a non-template control for each master mix using the following temperature profile: initial denaturation for 7 min at 95 °C, denaturation for 60 cycles of 10 s at 95 °C, annealing for 7 s at 60 °C, and elongation for 9 s at 72 °C. All primers (Table 2) were purchased from TIB Molbiol and verified by sequence analysis performed by LGC Genomics.

Table 2. Sequences of primers used for qPCR.

Gene	Sequence of Forward Primer	Sequence of Reverse Primer
EF1A	GTTGATATGGTTCCTGGCAAGC	TTGCCAGCTCCAGCAGCCT
RUNX2	TTACTTACACCCCGCCAGTC	TATGGAGTGCTGCTGGTCTG
SPP1	GCCGAGGTGATAGTGTGGTT	TGAGGTGATGTCCTCGTCTG
COL1A1	CAGCCGCTTCACCTACAGC	TTTTGTATTCAATCACTGTCTTGCC
ON	ACCAGCACCCCATTGACG	AGGTCACAGGTCTCGAAAAAGC
SOX9	CGCCTTGAAGATGGCGTTG	GCTCTGGAGACTTCTGAACGA
PPARγ2	CAAACCCCTATTCCATGCTGTT	AATGGCATCTCTGTGTCAACC
IL6	TACCCCCAGGAGAAGATTCC	TTTTCTGCCAGTGCCTCTTT
IL8	GAATGGGTTTGCTAGAATGTGATA	CAGACTAGGGTTGCCAGATTTAAC
LDHA	ACCCAGTTTCCACCATGATT	CCCAAAATGCAAGGAACACT
VEGFA	AGCCTTGCCTTGCTGCTCTA	GTGCTGGCCTTGGTGAGG
PGK1	ATGGATGAGGTGGTGAAAGC	CAGTGCTCACATGGCTGACT

2.9. Statistical Analysis

Statistical analyses were performed using the software GraphPad® Prism Version 9.3.0 (La Jolla, San Diego, CA, USA). Data are shown as box plots with all data points (centerline, median; box limits, upper and lower quartiles; whiskers, maximum and minimum). For independent datasets, the Mann–Whitney U test was applied. Concerning the deferoxamine study, differences between the groups were determined with the two-tailed Wilcoxon matched-pairs signed-rank test. p-values of <0.05 were considered to be statistically significant.

3. Results

3.1. MSC-Based Cell-Sheet Wrapping Enhanced Survival Rate of MSCs Seeded on β-TCP

Since it is essential to achieve flexibility in the size of the preclinical in vitro bone model to allow for high throughput, use in a perfused cell culture chamber, or regeneration of different sized bone defects, we investigated the FDA-approved synthetic β-TCP-based bone graft substitute (1–2 mm particle size). We previously determined an optimal cell source of 0.8×10^5 cells/mg and readout parameters, such as SEM, RT-qPCR, and histology after 21 days of differentiation [37].

To enhance the handling, reproducibility, and quality of β-TCP-based cancellous bone models, we used a technique known as cell-sheet technology. We used bone-marrow-derived MSCs obtained from patients undergoing surgery for total hip replacement as a cell source. MSCs were seeded at a high density onto a temperature-responsive cell culture surface and in parallel on biodegradable β-TCP scaffolds (Figure 1A). The cell-sheet reached confluence within 2 or 3 days and formed a thin cellular sheet at 7 days. To investigate the survival of differentiated MSCs in 3D, LIVE/DEAD® and TUNEL staining was performed on day 21. Results indicated a higher survival rate—relative area of living (Calcein-AM+) cells—of osteogenically induced MSCs populated on β-TCP wrapped with a single MSC-sheet (csTCP) to the unwrapped MSC-populated β-TCP (TCP; Figure 1B,C). Taken together, combining cell-sheet technology with conventional β-TCP leads to improved survival without causing apoptosis.

3.2. CsTCPs Exhibit Higher MSC Seeding Density than Unwrapped Pre-Seeded TCPs

Next, we investigated cell adhesion to the β-TCP scaffold, morphological differences, and ECM development between the MSC-populated TCPs and csTCPs using SEM. MSCs adhered and spread on the surface of the scaffold by forming a cell layer covering the pores of the scaffold. SEM images qualitatively but reproducibly highlight that MSCs entirely colonized the biodegradable β-TCP scaffold when an additional cell sheet was used, as indicated by more significant amounts of ECM on the scaffold (Figure 2A, asterisk). Scanning the scaffold surface at specific locations and higher magnifications revealed the presence of a microstructure deposit exhibiting a unique spherical morphology. After three weeks of differentiation, the morphology of these deposits was similar to the typical calcium phosphate microstructures, demonstrating osteogenic differentiation as reported previously [61]. The proportion of cells covered with spherical deposits showed osteogenic

Processes **2022**, *10*, 550

differentiation in both approaches, although osteogenesis appears to be more pronounced in csTCPs (Figure 2A, arrow). Furthermore, fluorescence analysis of the actin filaments confirmed a high cell density within the β-TCP particles, which was considerably higher when using the cell-sheet technology (Figure 2B). The histological evaluation of the in vitro bone model was consistent with the results of the SEM examination and immunofluorescence analysis, demonstrating a high cell density, uniform cell distribution (Figure 3A), and the presence of more significant amounts of ECM, especially in the csTCP models (Figure 3B). In summary, using cell-sheet technology, isolated MSCs attached and differentiated on and in the β-TCP scaffold.

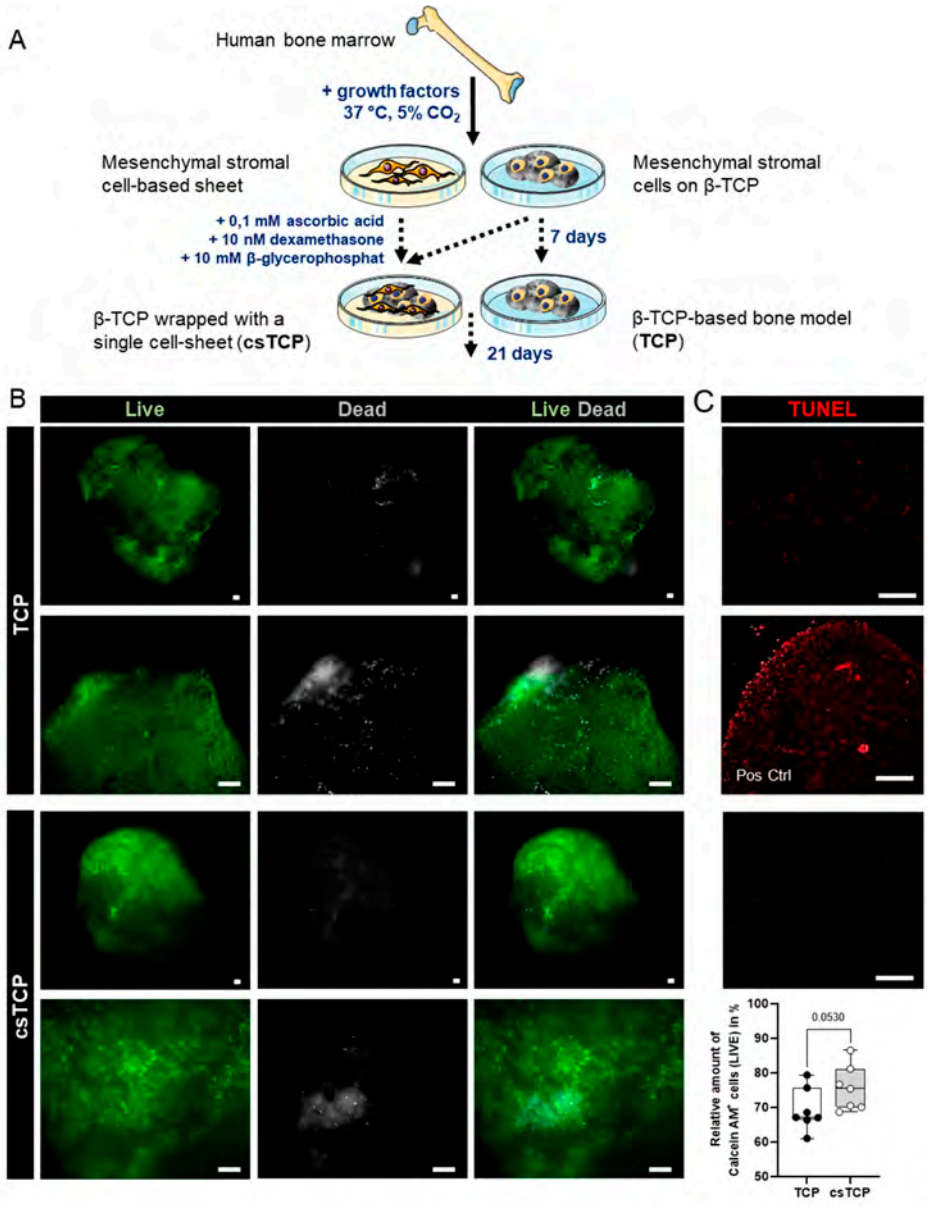

Figure 1. MSC-based cell-sheet wrapping enhanced the survival rate of MSCs seeded on TCP. (**A**) MSCs were seeded on (i) β-TCP particles (TCP) and (ii) temperature-responsive dishes. The latter

was osteogenically differentiated for 7 days, then wrapped around TCP (csTCP), and differentiated for 21 days. (**B**) Representative images of LIVE/DEAD staining were conducted at 21 days and quantified using ImageJ. Living cells are presented in green (Calcein-AM+) and dead cells in grey (EthD+). (**C**) Detection of apoptotic cells (red) using TUNEL staining at day 21 with and without cell-sheet technology. Pos Ctrl = DNase I treatment for 10 min. Data are shown as box plots (centerline, median; box limits, upper and lower quartiles; whiskers, maximum and minimum values; all data points); n = 7. Scale bars show 100 µm. Statistics: Two-tailed Mann–Whitney U test.

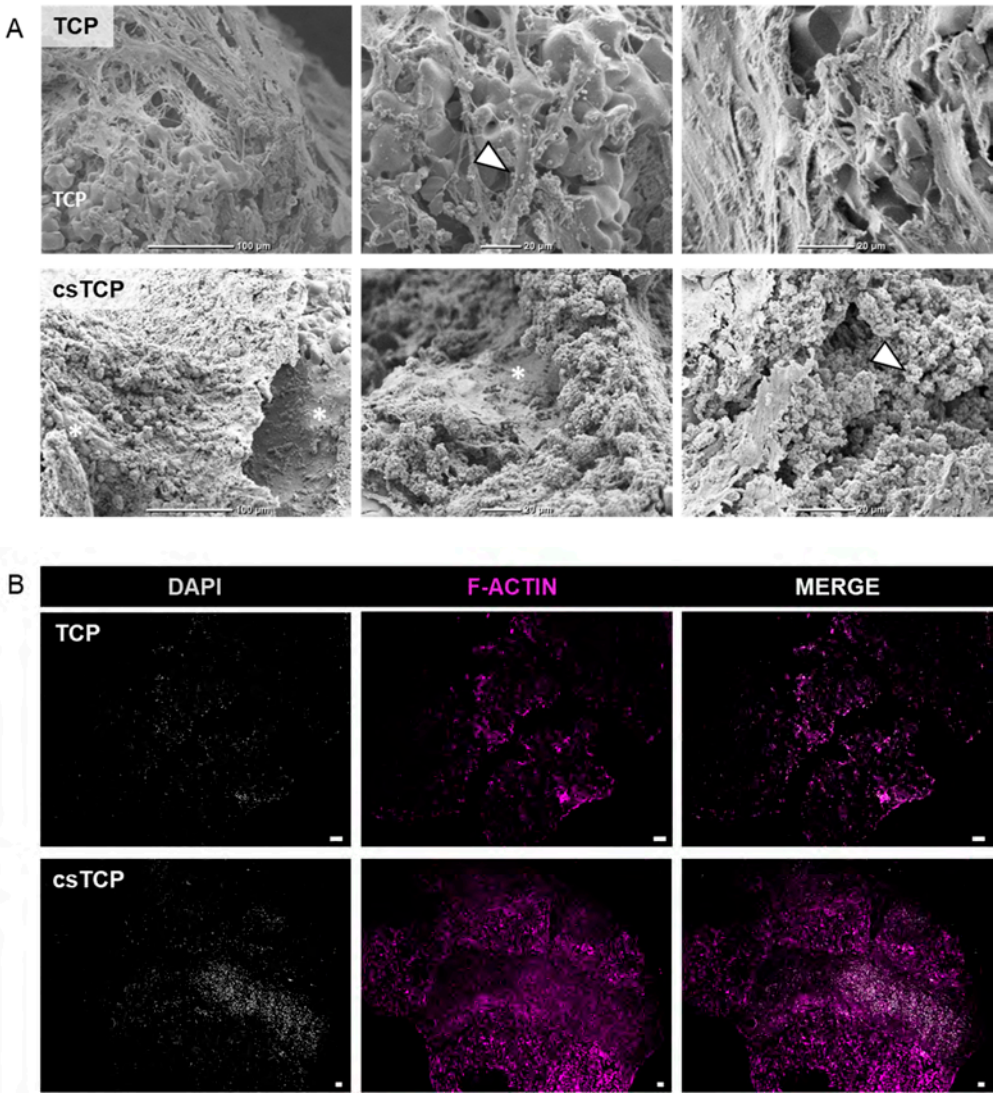

Figure 2. Comparing csTCPs and MSC-populated TCPs regarding cell density and morphology. (**A**) Exemplary SEM images at three magnifications highlighting cell adhesion, ECM content, phenotypic features at day 21 comparing TCP and csTCP. Cells well adhered to and spread on the surfaces of β-TCP. (**B**) Immunofluorescence staining for F-actin and DAPI to visualize cell density through the β-TCP particles. Exemplary images for n = 5. Scale bars show 100 µm. Legend: asterisk = highlighting ECM; arrow = highlighting microstructure deposition; TCP = highlighting the scaffold material.

Processes **2022**, *10*, 550

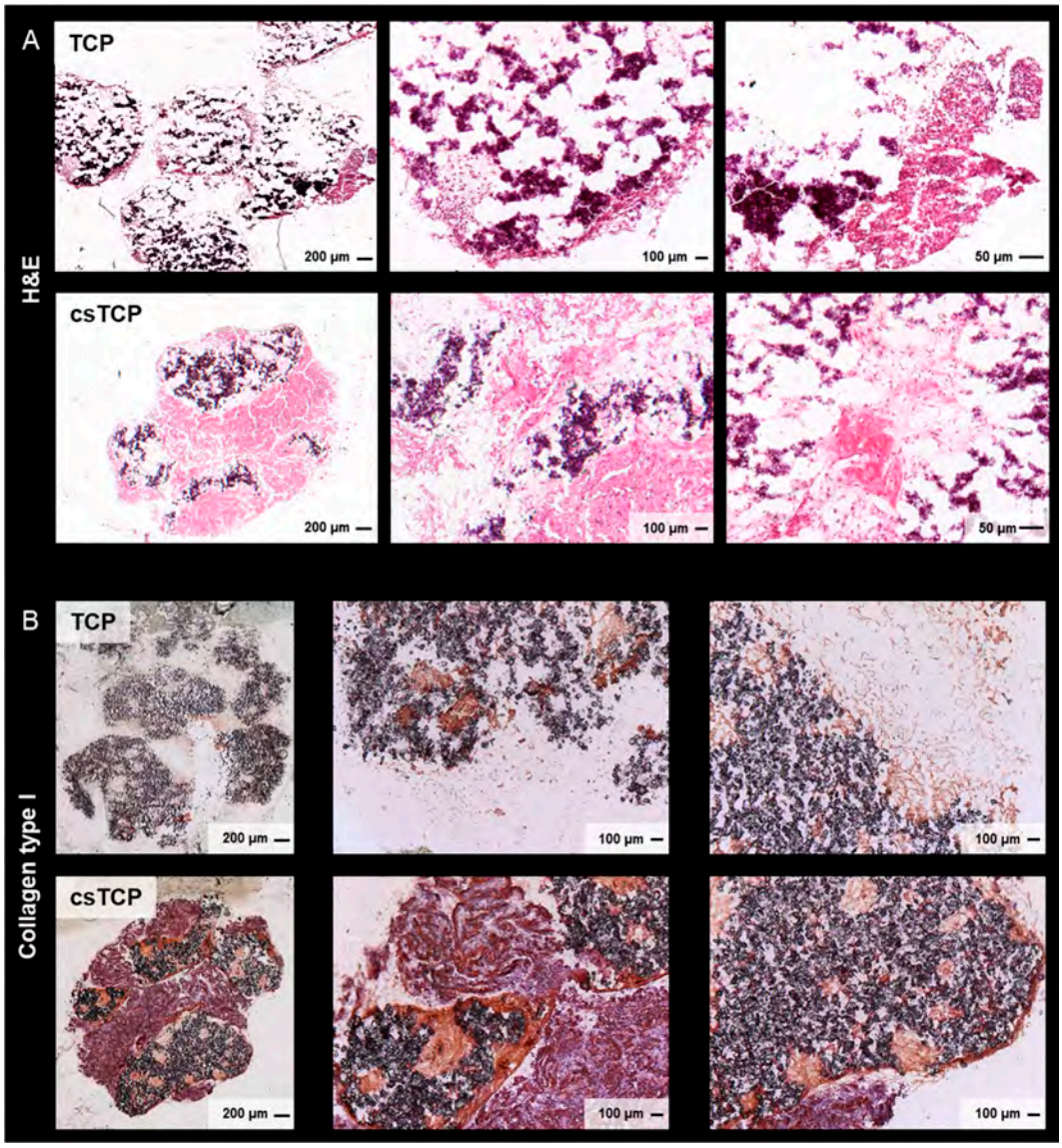

Figure 3. Comparing csTCPs and MSC-populated TCPs regarding uniform cell distribution and ECM at 21 days. (**A**) Representative images of hematoxylin and eosin (H & E) staining. (**B**) Exemplary images of histological sections stained for collagen type I and visualized using brightfield microscopy.

3.3. Sheet Technology Slightly Enhance Osteogenic Tissue Formation In Vitro

To analyze whether the combination of cell-sheet technology with β-TCP promotes osteogenic differentiation of MSCs, we monitored the relative mRNA expression levels of osteogenic marker genes, such as runt-related transcription factor 2 (*RUNX2*), osteopontin (*SPP1*), *COL1A1*, *OC*, alkaline phosphatase (*ALP*), and *ON* at 21 days using quantitative PCR. As a result, we observed a similar expression pattern of *RUNX2*—an early osteogenic marker—and *ALP* between TCP and csTCP. The expression of *SPP1*, *COL1A1*, and *ON* tended to be higher in csTCP, whereas the late-stage bone marker *OC* was significantly more highly expressed, compared to TCP.

In this line of observation, *PPARG* as an adipogenic marker gene and *SOX9* as a chondrogenic marker gene tended to be expressed less and significantly less, respectively, when TCP scaffolds were combined with sheet technology (Figure 4A). We further confirmed the *SPP1* gene expression result with immunofluorescence staining and noticed an intense staining of osteopontin at csTCP, as shown in Figure 4B. In summary, a clear osteogenic differentiation was achieved when using cell-sheet technology.

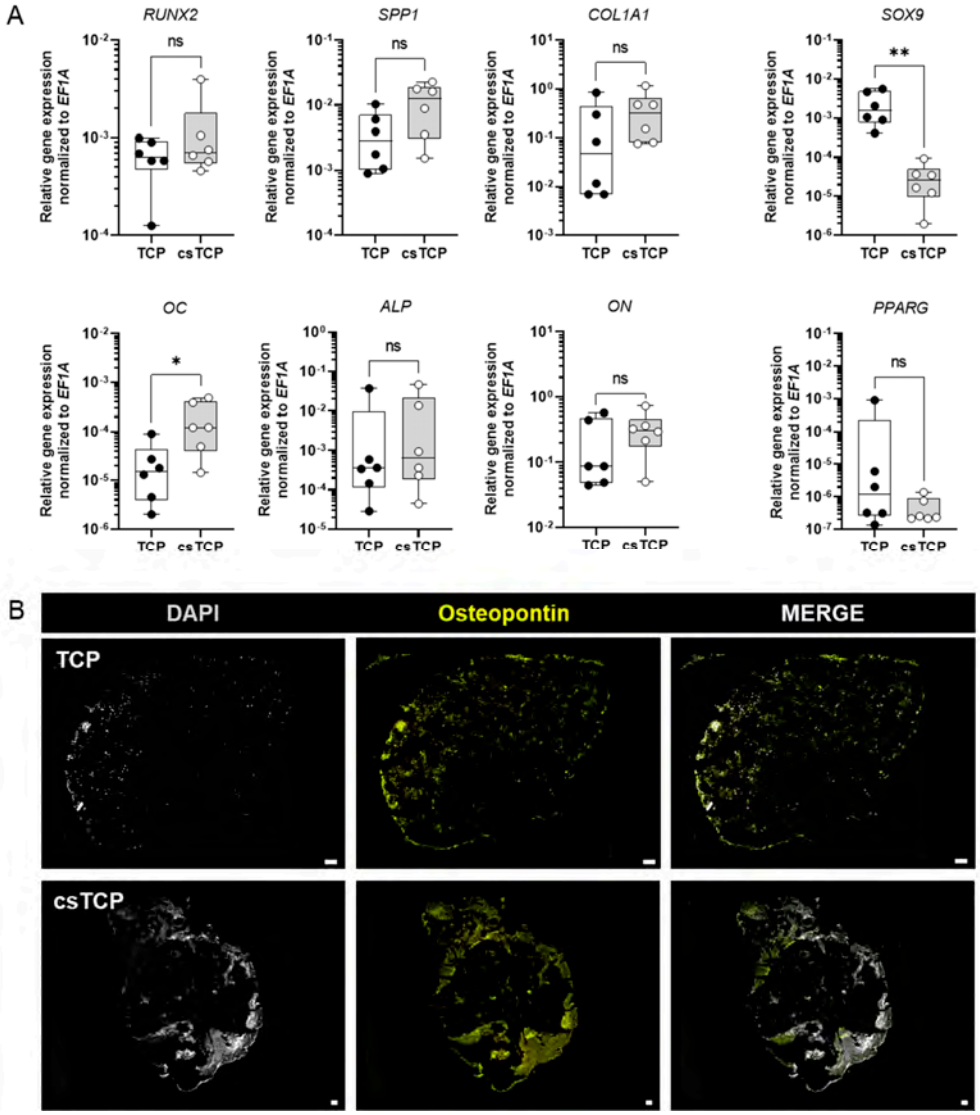

Figure 4. RNA expression analysis at day 21 showed that sheet technology slightly enhances osteogenic tissue formation in vitro. (**A**) Relative expression of osteogenic marker genes. Total RNA extraction was performed on day 21. Data are normalized to the housekeeper gene *EF1A*. Data are shown as box plots (centerline, median; box limits, upper and lower quartiles; whiskers, maximum and minimum values; all data points); $n = 6$. Statistics: Two-tailed Mann Whitney U test. p-values are indicated in the graphs with * $p < 0.05$, ** $p < 0.01$, ns = not significant. (**B**) Exemplary images of histological sections stained for osteopontin and visualized using a BZ-9000 fluorescence microscope ($n = 5$). Scale bars show 100 µm.

3.4. Deferoxamine Promotes Osteogenesis In Vitro

To confirm the responsiveness of our cell-sheet-based TCP bone model to modifying substances (e.g., therapeutics), we used DFO, which is well known to induce cellular hypoxia-adaptive, osteogenic, and angiogenic processes within the differentiated MSCs of the cell-sheet-based TCP bone model. Therefore, we treated csTCPs with 250 µM DFO for 3 days at day 21, compared them with the untreated control, and assessed the expression of selected marker genes. We observed an upregulation of osteogenic (*RUNX2*, *SPP1*), hypoxia-related (*LDHA*, *PGK1*, *VEGFA*), and pro-angiogenic (*VEGFA*, *IL8*) markers, while *IL6* was similarly expressed as compared to the untreated control (Figure 5). These experiments demonstrate the responsiveness of our cell-sheet-based TCP bone model to modifying substances, such as DFO.

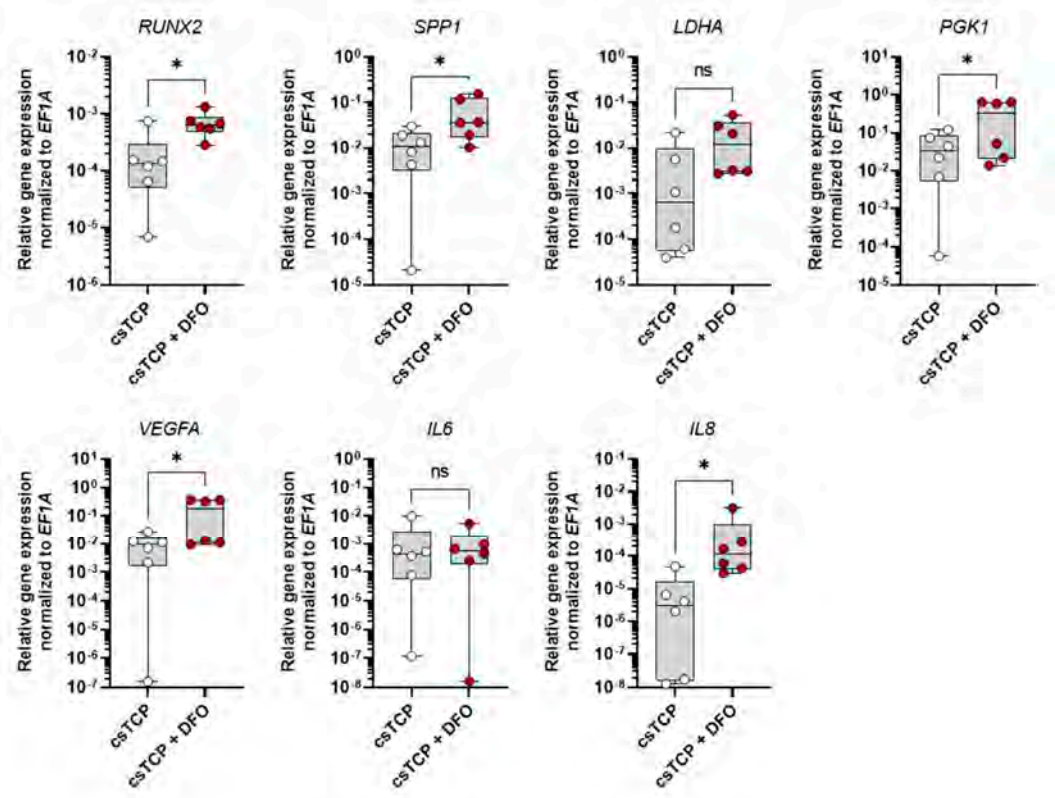

Figure 5. Deferoxamine (DFO) conditioned medium further promotes osteogenesis of the csTCP bone model verified on mRNA level using RT-qPCR. csTCP was treated after 21 days with 250 µM DFO for 72 h. Relative expression of *RUNX2*, *SPP1*, *LDHA*, *PGK1*, *VEGFA*, *IL6*, and *IL8* was normalized to the housekeeper gene *EF1A*. Data are shown as box plots (centerline, median; box limits, upper and lower quartiles; whiskers, maximum and minimum values; all data points); $n = 6$. Statistics: Two-tailed Wilcoxon matched-pairs signed-rank test. p-values are indicated in the graphs with * $p < 0.05$ and ns = not significant.

4. Discussion

In recent years, new advances have been made in bone tissue engineering to overcome the challenges of bone defect regeneration. Cell-sheet technology has become a promising tool, as its application to ectopic sites or bone defects promotes bone formation in vivo without using an additional scaffold [62,63]. Transplantation of mechanically generated osteogenic cell-sheets to the site of bone defects resulted in significantly improved new bone formation [64–66]. Fracture healing is characterized by initial inflammation, callus

formation, and bone remodeling, resulting in scar-free bone regeneration. In some cases, bone-healing disorders may occur, leading to delayed or non-union. Transplantation of osteogenic cell-sheets into a fractured rat femur showed improved bone formation at the fracture site, providing a treatment option for bone-healing disorders [67].

However, recapitulating the complex process of continuous bone remodeling in an adequate preclinical in vitro 3D model remains a significant challenge in the field of preclinical and basic musculoskeletal research [14]. Preclinical bone models as an alternative to the current gold standard—in vivo animal models—require the (co-)culture of bone-relevant cells under bone-like physiological conditions. Cell-sheets alone have poor mechanical properties and limited spatial support [16]. These obstacles can be surmounted by combining cell sheets with biodegradable scaffolds that mimic the mineral cancellous bone part.

The most common biodegradable scaffolds used as synthetic bone graft substitutes that closely resemble the native bone matrix are β-TCP, HA, and BCP (HA: β-TCP), well-known to be osteoconductive [68]. These materials facilitate cell adhesion, differentiation, and homogeneous cell distribution. The model or implant must be adjusted in particle size, pore size, porosity, and mechanical strength to the target natural bone, considering the different requirements of, for example, cortical and trabecular bone [60,69–71]. Macropores allow for cell proliferation due to the enhanced nutrient supply and oxygen transportation, while in vitro osteogenesis does not seem to be affected by pore size [72]. Trabecular bone has a porosity in the range of 50%–90% and a pore size up to 1000 µm in diameter [73].

In vitro bone models are used to mimic native cortical or trabecular bone to study physiological processes (e.g., metabolism of bone turnover), pathophysiological processes (e.g., cellular processes in bone healing), the effects of agents on bone homeostasis and regeneration (e.g., glucocorticoids or BMPs), implant integration (e.g., the interaction of bone and implant surfaces), or the suitability of the model as an implant itself (e.g., load-bearing capacity and stability) [2]. To evaluate substances or implant materials (evaluation of osteoconductive properties) in high-throughput format about toxicology, biocompatibility, tolerability, and osteoinductivity, simple, easy-to-handle scaffold-free spheroid cultures (osteospheres) with a 3D architecture but without mechanical strength are used [74–79]. In contrast, scaffold- or hydrogel-based models own load-bearing capacity and the option for a trabecular-like structure [80–87]. These models are more complex and bear the capability to add bone marrow cells, including immune cells, a supplying vascular-like system [86,87]. Typically scaffold-based models closely mimicking native bone are used to study physiological and pathophysiological processes and implant integration or serve as an implant itself. However, there is still space for optimization left.

The present study demonstrated that the biodegradable pre-seeded β-TCP scaffold or bone graft substitute wrapped with osteogenically induced MSC sheets exhibited higher expression of osteogenic genes and proteins in vitro. csTCP also showed sufficient matrix formation. Here, we evidenced that pre-seeded biodegradable β-TCP scaffolds wrapped with osteogenic MSC-sheets provide superior osteogenic performance in vitro and, therefore, may represent an elegant and physiologically relevant preclinical 3D alternative. Up-sizing of scaffold-based bone constructs becomes feasible through sheet technology. In addition, sheets combining different cell types can be fabricated, as demonstrated by Zhang et al. using MSC-derived endothelial progenitor cells on MSC sheets [88] and Kawamura et al. adding MSCs to human-induced pluripotent stem cell-derived cardiomyocyte sheets [89]. This provides the opportunity to combine osteoblast and osteoclast progenitor cells.

Artificial bone scaffold materials, such as TCP, are biodegradable and can be replaced by autologous bone after implantation. The β-TCP scaffold is one the most used and potent synthetic bone graft substitute known to be osteoconductive and osteoinductive [90,91]. The 3D structure with interconnected pores and an optimal porosity of 65% allows for sufficient nutrient supply, cell proliferation, and ingrowth of cells [92]. Ueha et al. demonstrated the promising osteogenic potential of pre-seeded TCP with osteogenic cell-sheets in a femoral defect model in rats [93]. A similar approach was applied to treat patients with osteoarthritis and/or osteonecrosis by using differentiated osteoblasts in combination with

scaffolds. Importantly, seeding cells on an artificial bone scaffold leads to bone formation, but only in their pores, resulting in single separated constructs without any bridging area. Considering the need for sophisticated preclinical in vitro 3D models, a physiologically similar bone with sufficient cell colonization and strong osteogenic potential should be developed to ensure the transferability of results. By confirming the cell adherence, cell phenotype, morphology, and cell density of differentiated MSCs on β-TCP with and without cell sheets, we successfully demonstrated an optimized cell seeding and the differentiation of MSCs using cell-sheet technology. Usually, the number of cells combined with artificial bone substitutes, such as β-TCP, is limited because most suspended cells remain in the pores and do not homogeneously and reproducibly populate the β-TCP scaffold as demonstrated here. Adding the cell sheet resulted in a large number of loaded cells on the β-TCP scaffold, thereby providing a microenvironment that facilitates cell seeding and differentiation. A strategy that optimizes seeding and production, up-sizing and osteogenic properties of small scale and small amounts of particles such as β-TCP particles. In this line of observation, Ueha et al. showed bone formation on the surface of sheet/TCP constructs, assuming facilitation in bridging the fracture gap and promoting bone formation [93]. Another sophisticated optimization approach of complex bone models in tissue engineering strategy is the functionalization of bioinspired scaffold systems. Functionalization with growth factors promoting angiogenesis and osteogenesis has shown great therapeutic potential in preclinical models and clinical applications [94,95]. They promote tissue ingrowth and proliferation. Growth factors such as VEGF, fibroblast growth factor (FGF) (involved in angiogenesis) as well as transforming growth factor-beta (TGF-β) and bone morphogenetic proteins (BMPs) (involved in healing and new bone formation) are commonly applied [96]. The latter is probably the most essential protein to enhance neo-bone formation in bone defects, such as tibia fracture reconstruction and spinal fusion surgery [97,98]. BMPs can be delivered to a surgical site by scaffold-based carrier systems, such as fibrous glass, HA granules, and β-TCP granules. Nowadays, these systems are chemically modified to enable the controlled, precise, sustained, and localized release of such proteins. Taken together, functionalized scaffolds allow mimicking hierarchical architectures and ECM components with high cell affinity and bioactivity, bringing the model closer to natural bone. In contrast, cell seeding and ingrowth can be optimized by enveloping them with an additional cell layer.

5. Conclusions

Our data demonstrate that the colonization of β-TCP scaffolds with MSCs and the additional wrapping of the colonized scaffolds creates a local niche. This niche promotes osteogenic but not chondrogenic and adipogenic differentiation and allows for the combination of multiple models. In addition, we have shown that our in vitro human MSC-sheet-based 3D bone model is responsive to modifying agents such as DFO. This finding suggests that optimization provides all the requirements to serve as an alternative personalized preclinical model of cancellous bone tissue for predicting and developing therapeutic strategies for treating bone healing disorders.

Although preclinical data from in vitro bone models and animal studies are often promising, the clinical failure of cell-based implants, osteoconductive bone substitutes, and osteoinductive growth factors cannot be predicted or generally excluded. Humans are complex systems that are more than the sum of their parts, which cannot be represented in all aspects by animal models or preclinical in vitro 3D models. Nevertheless, while animal models still remain models, preclinical in vitro 3D models can directly serve as bone graft substitutes for clinical application.

Author Contributions: Conceptualization, A.D. and T.G.; methodology, A.D.; validation, A.D.; formal analysis, A.D.; investigation, A.D.; data curation, A.D. and T.G.; writing—original draft preparation, A.D., T.G. and F.B.; writing—review and editing, A.D., T.G. and F.B.; visualization, A.D.; supervision, T.G.; project administration, F.B.; funding acquisition, T.G. and F.B. All authors have read and agreed to the published version of the manuscript.

Funding: This research was funded by the German Federal Ministry for Education and Research (BMBF), project number 031L0070A and Lush Prize Award 2018: Alexandra Damerau—Young Researcher, Rest of World. The work of A.D. was additionally supported by the German Academic Scholarship Foundation (Studienstiftung des deutschen Volkes) and by the Joachim Herz Foundation (Add-on Fellowship 2020). We acknowledge support from the German Research Foundation (DFG) and the Open Access Publication Fund of Charité-Universitätsmedizin Berlin.

Institutional Review Board Statement: The study was conducted in accordance with the Declaration of Helsinki, and approved by the Ethics Committee of the Charité-Universitätsmedizin Berlin (ethical approval EA1/012/13, January 2013; EA1/146/21, May 2021).

Informed Consent Statement: Informed consent was obtained from all subjects involved in the study.

Data Availability Statement: The data presented in this study are available on request from the corresponding author. The data are not publicly available due to privacy and ethical restrictions.

Acknowledgments: Bone marrow was provided by the Tissue Harvesting Core Facility of the BIH Berlin. A.D., F.B. and T.G. are members of the Berlin-Brandenburg research platform BB3R and Charité3R.

Conflicts of Interest: The authors declare no conflict of interest.

References

1. Alonzo, M.; Primo, F.A.; Kumar, S.A.; Mudloff, J.A.; Dominguez, E.; Fregoso, G.; Ortiz, N.; Weiss, W.M.; Joddar, B. Bone tissue engineering techniques, advances and scaffolds for treatment of bone defects. *Curr. Opin. Biomed. Eng.* **2021**, *17*, 100248. [CrossRef] [PubMed]
2. Pfeiffenberger, M.; Damerau, A.; Lang, A.; Buttgereit, F.; Hoff, P.; Gaber, T. Fracture Healing Research-Shift towards In Vitro Modeling? *Biomedicines* **2021**, *9*, 748. [CrossRef] [PubMed]
3. Einhorn, T.A.; Gerstenfeld, L.C. Fracture healing: Mechanisms and interventions. *Nat. Rev. Rheumatol* **2015**, *11*, 45–54. [CrossRef] [PubMed]
4. Collaborators, G.B.D.F. Global, regional, and national burden of bone fractures in 204 countries and territories, 1990–2019: A systematic analysis from the Global Burden of Disease Study 2019. *Lancet Healthy Longev.* **2021**, *2*, e580–e592. [CrossRef]
5. Salari, N.; Darvishi, N.; Bartina, Y.; Larti, M.; Kiaei, A.; Hemmati, M.; Shohaimi, S.; Mohammadi, M. Global prevalence of osteoporosis among the world older adults: A comprehensive systematic review and meta-analysis. *J. Orthop. Surg. Res.* **2021**, *16*, 669. [CrossRef]
6. Banaszkiewicz, P.A.; Kader, D.F. *Classic Papers in Orthopaedics*; Springer: London, UK, 2014; p. 624.
7. Zhu, G.; Zhang, T.; Chen, M.; Yao, K.; Huang, X.; Zhang, B.; Li, Y.; Liu, J.; Wang, Y.; Zhao, Z. Bone physiological microenvironment and healing mechanism: Basis for future bone-tissue engineering scaffolds. *Bioact. Mater.* **2021**, *6*, 4110–4140. [CrossRef] [PubMed]
8. Roddy, E.; DeBaun, M.R.; Daoud-Gray, A.; Yang, Y.P.; Gardner, M.J. Treatment of critical-sized bone defects: Clinical and tissue engineering perspectives. *Eur. J. Orthop. Surg. Traumatol.* **2018**, *28*, 351–362. [CrossRef]
9. Leenaars, C.H.C.; Kouwenaar, C.; Stafleu, F.R.; Bleich, A.; Ritskes-Hoitinga, M.; De Vries, R.B.M.; Meijboom, F.L.B. Animal to human translation: A systematic scoping review of reported concordance rates. *J. Transl. Med.* **2019**, *17*, 223. [CrossRef]
10. Bracken, M.B. Why animal studies are often poor predictors of human reactions to exposure. *J. R. Soc. Med.* **2009**, *102*, 120–122. [CrossRef]
11. Fong, E.L.S.; Toh, T.B.; Yu, H.; Chow, E.K. 3D Culture as a Clinically Relevant Model for Personalized Medicine. *SLAS Technol.* **2017**, *22*, 245–253. [CrossRef]
12. Mestas, J.; Hughes, C.C. Of mice and not men: Differences between mouse and human immunology. *J. Immunol.* **2004**, *172*, 2731–2738. [CrossRef] [PubMed]
13. Seok, J.; Warren, H.S.; Cuenca, A.G.; Mindrinos, M.N.; Baker, H.V.; Xu, W.; Richards, D.R.; McDonald-Smith, G.P.; Gao, H.; Hennessy, L.; et al. Genomic responses in mouse models poorly mimic human inflammatory diseases. *Proc. Natl. Acad. Sci. USA* **2013**, *110*, 3507–3512. [CrossRef] [PubMed]
14. Scheinpflug, J.; Pfeiffenberger, M.; Damerau, A.; Schwarz, F.; Textor, M.; Lang, A.; Schulze, F. Journey into Bone Models: A Review. *Genes* **2018**, *9*, 247. [CrossRef]
15. Roseti, L.; Parisi, V.; Petretta, M.; Cavallo, C.; Desando, G.; Bartolotti, I.; Grigolo, B. Scaffolds for Bone Tissue Engineering: State of the art and new perspectives. *Mater. Sci. Eng. C Mater. Biol. Appl.* **2017**, *78*, 1246–1262. [CrossRef] [PubMed]
16. Yorukoglu, A.C.; Kiter, A.E.; Akkaya, S.; Satiroglu-Tufan, N.L.; Tufan, A.C. A Concise Review on the Use of Mesenchymal Stem Cells in Cell Sheet-Based Tissue Engineering with Special Emphasis on Bone Tissue Regeneration. *Stem Cells Int.* **2017**, *2017*, 2374161. [CrossRef]
17. Owaki, T.; Shimizu, T.; Yamato, M.; Okano, T. Cell sheet engineering for regenerative medicine: Current challenges and strategies. *Biotechnol. J.* **2014**, *9*, 904–914. [CrossRef] [PubMed]

18. Murphy, M.B.; Suzuki, R.K.; Sand, T.T.; Chaput, C.D.; Gregory, C.A. Short Term Culture of Human Mesenchymal Stem Cells with Commercial Osteoconductive Carriers Provides Unique Insights into Biocompatibility. *J. Clin. Med.* **2013**, *2*, 49–66. [CrossRef]
19. Lomelino Rde, O.; Castro, S., II; Linhares, A.B.; Alves, G.G.; Santos, S.R.; Gameiro, V.S.; Rossi, A.M.; Granjeiro, J.M. The association of human primary bone cells with biphasic calcium phosphate (βTCP/HA 70:30) granules increases bone repair. *J. Mater. Sci. Mater. Med.* **2012**, *23*, 781–788. [CrossRef]
20. Bernhardt, A.; Lode, A.; Peters, F.; Gelinsky, M. Optimization of culture conditions for osteogenically-induced mesenchymal stem cells in β-tricalcium phosphate ceramics with large interconnected channels. *J. Tissue Eng. Regen. Med.* **2011**, *5*, 444–453. [CrossRef]
21. Shimizu, T.; Yamato, M.; Kikuchi, A.; Okano, T. Cell sheet engineering for myocardial tissue reconstruction. *Biomaterials* **2003**, *24*, 2309–2316. [CrossRef]
22. Yang, J.; Yamato, M.; Kohno, C.; Nishimoto, A.; Sekine, H.; Fukai, F.; Okano, T. Cell sheet engineering: Recreating tissues without biodegradable scaffolds. *Biomaterials* **2005**, *26*, 6415–6422. [CrossRef] [PubMed]
23. Takezawa, T.; Mori, Y.; Yoshizato, K. Cell culture on a thermo-responsive polymer surface. *Biotechnology* **1990**, *8*, 854–856. [CrossRef] [PubMed]
24. Li, M.; Ma, J.; Gao, Y.; Yang, L. Cell sheet technology: A promising strategy in regenerative medicine. *Cytotherapy* **2019**, *21*, 3–16. [CrossRef] [PubMed]
25. Moschouris, K.; Firoozi, N.; Kang, Y. The application of cell sheet engineering in the vascularization of tissue regeneration. *Regen. Med.* **2016**, *11*, 559–570. [CrossRef] [PubMed]
26. Ma, D.; Yao, H.; Tian, W.; Chen, F.; Liu, Y.; Mao, T.; Ren, L. Enhancing bone formation by transplantation of a scaffold-free tissue-engineered periosteum in a rabbit model. *Clin. Oral Implants Res.* **2011**, *22*, 1193–1199. [CrossRef] [PubMed]
27. Gao, Z.; Chen, F.; Zhang, J.; He, L.; Cheng, X.; Ma, Q.; Mao, T. Vitalisation of tubular coral scaffolds with cell sheets for regeneration of long bones: A preliminary study in nude mice. *Br. J. Oral Maxillofac. Surg.* **2009**, *47*, 116–122. [CrossRef] [PubMed]
28. Chen, F.; Zhou, Y.; Barnabas, S.T.; Woodruff, M.A.; Hutmacher, D.W. Engineering tubular bone constructs. *J. Biomech.* **2007**, *40* (Suppl. S1), S73–S79. [CrossRef]
29. Probst, F.A.; Fliefel, R.; Burian, E.; Probst, M.; Eddicks, M.; Cornelsen, M.; Riedl, C.; Seitz, H.; Aszodi, A.; Schieker, M.; et al. Bone regeneration of minipig mandibular defect by adipose derived mesenchymal stem cells seeded tri-calcium phosphate-poly(D,L-lactide-co-glycolide) scaffolds. *Sci. Rep.* **2020**, *10*, 2062. [CrossRef]
30. Ullah, I.; Subbarao, R.B.; Rho, G.J. Human mesenchymal stem cells—Current trends and future prospective. *Biosci. Rep.* **2015**, *35*, e00191. [CrossRef]
31. Bartholomew, A.; Sturgeon, C.; Siatskas, M.; Ferrer, K.; McIntosh, K.; Patil, S.; Hardy, W.; Devine, S.; Ucker, D.; Deans, R.; et al. Mesenchymal stem cells suppress lymphocyte proliferation in vitro and prolong skin graft survival in vivo. *Exp. Hematol.* **2002**, *30*, 42–48. [CrossRef]
32. Di Nicola, M.; Carlo-Stella, C.; Magni, M.; Milanesi, M.; Longoni, P.D.; Matteucci, P.; Grisanti, S.; Gianni, A.M. Human bone marrow stromal cells suppress T-lymphocyte proliferation induced by cellular or nonspecific mitogenic stimuli. *Blood* **2002**, *99*, 3838–3843. [CrossRef] [PubMed]
33. Stagg, J. Immune regulation by mesenchymal stem cells: Two sides to the coin. *Tissue Antigens* **2007**, *69*, 1–9. [CrossRef] [PubMed]
34. Ansari, S.; Ito, K.; Hofmann, S. Cell Sources for Human In vitro Bone Models. *Curr. Osteoporos. Rep.* **2021**, *19*, 88–100. [CrossRef] [PubMed]
35. Kang, Y.; Ren, L.; Yang, Y. Engineering vascularized bone grafts by integrating a biomimetic periosteum and β-TCP scaffold. *ACS Appl. Mater. Interfaces* **2014**, *6*, 9622–9633. [CrossRef] [PubMed]
36. Zhang, H.; Zhou, Y.; Zhang, W.; Wang, K.; Xu, L.; Ma, H.; Deng, Y. Construction of vascularized tissue-engineered bone with a double-cell sheet complex. *Acta Biomater.* **2018**, *77*, 212–227. [CrossRef] [PubMed]
37. Damerau, A.; Pfeiffenberger, M.; Weber, M.C.; Burmester, G.R.; Buttgereit, F.; Gaber, T.; Lang, A. A Human Osteochondral Tissue Model Mimicking Cytokine-Induced Key Features of Arthritis In Vitro. *Int. J. Mol. Sci* **2020**, *22*, 128. [CrossRef] [PubMed]
38. Wan, C.; Gilbert, S.R.; Wang, Y.; Cao, X.; Shen, X.; Ramaswamy, G.; Jacobsen, K.A.; Alaql, Z.S.; Eberhardt, A.W.; Gerstenfeld, L.C.; et al. Activation of the hypoxia-inducible factor-1α pathway accelerates bone regeneration. *Proc. Natl. Acad. Sci. USA* **2008**, *105*, 686–691. [CrossRef]
39. Donneys, A.; Ahsan, S.; Perosky, J.E.; Deshpande, S.S.; Tchanque-Fossuo, C.N.; Levi, B.; Kozloff, K.M.; Buchman, S.R. Deferoxamine restores callus size, mineralization, and mechanical strength in fracture healing after radiotherapy. *Plast. Reconstr. Surg.* **2013**, *131*, 711e–719e. [CrossRef]
40. Donneys, A.; Nelson, N.S.; Page, E.E.; Deshpande, S.S.; Felice, P.A.; Tchanque-Fossuo, C.N.; Spiegel, J.P.; Buchman, S.R. Targeting angiogenesis as a therapeutic means to reinforce osteocyte survival and prevent nonunions in the aftermath of radiotherapy. *Head Neck* **2015**, *37*, 1261–1267. [CrossRef]
41. Donneys, A.; Nelson, N.S.; Perosky, J.E.; Polyatskaya, Y.; Rodriguez, J.J.; Figueredo, C.; Vasseli, C.A.; Ratliff, H.C.; Deshpande, S.S.; Kozloff, K.M.; et al. Prevention of radiation-induced bone pathology through combined pharmacologic cytoprotection and angiogenic stimulation. *Bone* **2016**, *84*, 245–252. [CrossRef]
42. Donneys, A.; Weiss, D.M.; Deshpande, S.S.; Ahsan, S.; Tchanque-Fossuo, C.N.; Sarhaddi, D.; Levi, B.; Goldstein, S.A.; Buchman, S.R. Localized deferoxamine injection augments vascularity and improves bony union in pathologic fracture healing after radiotherapy. *Bone* **2013**, *52*, 318–325. [CrossRef] [PubMed]

43. Drager, J.; Ramirez-Garcia Luna, J.L.; Kumar, A.; Gbureck, U.; Harvey, E.J.; Barralet, J.E. Hypoxia Biomimicry to Enhance Monetite Bone Defect Repair. *Tissue Eng. Part A* **2017**, *23*, 1372–1381. [CrossRef] [PubMed]
44. Drager, J.; Sheikh, Z.; Zhang, Y.L.; Harvey, E.J.; Barralet, J.E. Local delivery of iron chelators reduces in vivo remodeling of a calcium phosphate bone graft substitute. *Acta Biomater.* **2016**, *42*, 411–419. [CrossRef] [PubMed]
45. Farberg, A.S.; Jing, X.L.; Monson, L.A.; Donneys, A.; Tchanque-Fossuo, C.N.; Deshpande, S.S.; Buchman, S.R. Deferoxamine reverses radiation induced hypovascularity during bone regeneration and repair in the murine mandible. *Bone* **2012**, *50*, 1184–1187. [CrossRef] [PubMed]
46. Guzey, S.; Aykan, A.; Ozturk, S.; Avsever, H.; Karslioglu, Y.; Ertan, A. The Effects of Desferroxamine on Bone and Bone Graft Healing in Critical-Size Bone Defects. *Ann. Plast. Surg.* **2016**, *77*, 560–568. [CrossRef] [PubMed]
47. Matsumoto, T.; Sato, S. Stimulating angiogenesis mitigates the unloading-induced reduction in osteogenesis in early-stage bone repair in rats. *Physiol. Rep.* **2015**, *3*, e12335. [CrossRef] [PubMed]
48. Shen, X.; Wan, C.; Ramaswamy, G.; Mavalli, M.; Wang, Y.; Duvall, C.L.; Deng, L.F.; Guldberg, R.E.; Eberhart, A.; Clemens, T.L.; et al. Prolyl hydroxylase inhibitors increase neoangiogenesis and callus formation following femur fracture in mice. *J. Orthop. Res. Off. Publ. Orthop. Res. Soc.* **2009**, *27*, 1298–1305. [CrossRef] [PubMed]
49. Stewart, R.; Goldstein, J.; Eberhardt, A.; Chu, G.T.; Gilbert, S. Increasing vascularity to improve healing of a segmental defect of the rat femur. *J. Orthop. Trauma* **2011**, *25*, 472–476. [CrossRef]
50. Yao, Q.; Liu, Y.; Tao, J.; Baumgarten, K.M.; Sun, H. Hypoxia-Mimicking Nanofibrous Scaffolds Promote Endogenous Bone Regeneration. *ACS Appl. Mater. Interfaces* **2016**, *8*, 32450–32459. [CrossRef] [PubMed]
51. Zhang, W.; Li, G.; Deng, R.; Deng, L.; Qiu, S. New bone formation in a true bone ceramic scaffold loaded with desferrioxamine in the treatment of segmental bone defect: A preliminary study. *J. Orthop. Sci. Off. J. Jpn. Orthop. Assoc.* **2012**, *17*, 289–298. [CrossRef]
52. Kang, H.; Yan, Y.; Jia, P.; Yang, K.; Guo, C.; Chen, H.; Qi, J.; Qian, N.; Xu, X.; Wang, F.; et al. Desferrioxamine reduces ultrahigh-molecular-weight polyethylene-induced osteolysis by restraining inflammatory osteoclastogenesis via heme oxygenase-1. *Cell Death Dis.* **2016**, *7*, e2435. [CrossRef] [PubMed]
53. Kusumbe, A.P.; Ramasamy, S.K.; Adams, R.H. Coupling of angiogenesis and osteogenesis by a specific vessel subtype in bone. *Nature* **2014**, *507*, 323–328. [CrossRef] [PubMed]
54. Li, J.; Fan, L.; Yu, Z.; Dang, X.; Wang, K. The effect of deferoxamine on angiogenesis and bone repair in steroid-induced osteonecrosis of rabbit femoral heads. *Exp. Biol. Med.* **2015**, *240*, 273–280. [CrossRef] [PubMed]
55. Liu, X.; Tu, Y.; Zhang, L.; Qi, J.; Ma, T.; Deng, L. Prolyl hydroxylase inhibitors protect from the bone loss in ovariectomy rats by increasing bone vascularity. *Cell Biochem. Biophys.* **2014**, *69*, 141–149. [CrossRef] [PubMed]
56. Wang, L.; Jia, P.; Shan, Y.; Hao, Y.; Wang, X.; Jiang, Y.; Yuan, Y.; Du, Q.; Zhang, H.; Yang, F.; et al. Synergistic protection of bone vasculature and bone mass by desferrioxamine in osteoporotic mice. *Mol. Med. Rep.* **2017**, *16*, 6642–6649. [CrossRef] [PubMed]
57. Donneys, A.; Yang, Q.; Forrest, M.L.; Nelson, N.S.; Zhang, T.; Ettinger, R.; Ranganathan, K.; Snider, A.; Deshpande, S.S.; Cohen, M.S.; et al. Implantable hyaluronic acid-deferoxamine conjugate prevents nonunions through stimulation of neovascularization. *NPJ Regen. Med.* **2019**, *4*, 11. [CrossRef] [PubMed]
58. Wagegg, M.; Gaber, T.; Lohanatha, F.L.; Hahne, M.; Strehl, C.; Fangradt, M.; Tran, C.L.; Schonbeck, K.; Hoff, P.; Ode, A.; et al. Hypoxia promotes osteogenesis but suppresses adipogenesis of human mesenchymal stromal cells in a hypoxia-inducible factor-1 dependent manner. *PLoS ONE* **2012**, *7*, e46483. [CrossRef] [PubMed]
59. Pfeiffenberger, M.; Damerau, A.; Ponomarev, I.; Bucher, C.H.; Chen, Y.; Barnewitz, D.; Thone-Reineke, C.; Hoff, P.; Buttgereit, F.; Gaber, T.; et al. Functional Scaffold-Free Bone Equivalents Induce Osteogenic and Angiogenic Processes in a Human In Vitro Fracture Hematoma Model. *J. Bone Miner. Res.* **2021**, *36*, 1189–1201. [CrossRef]
60. Stokovic, N.; Ivanjko, N.; Erjavec, I.; Milosevic, M.; Oppermann, H.; Shimp, L.; Sampath, K.T.; Vukicevic, S. Autologous bone graft substitute containing rhBMP6 within autologous blood coagulum and synthetic ceramics of different particle size determines the quantity and structural pattern of bone formed in a rat subcutaneous assay. *Bone* **2020**, *141*, 115654. [CrossRef] [PubMed]
61. Kazemzadeh-Narbat, M.; Kindrachuk, J.; Duan, K.; Jenssen, H.; Hancock, R.E.; Wang, R. Antimicrobial peptides on calcium phosphate-coated titanium for the prevention of implant-associated infections. *Biomaterials* **2010**, *31*, 9519–9526. [CrossRef]
62. Shimizu, K.; Ito, A.; Yoshida, T.; Yamada, Y.; Ueda, M.; Honda, H. Bone tissue engineering with human mesenchymal stem cell sheets constructed using magnetite nanoparticles and magnetic force. *J. Biomed. Mater. Res. B Appl. Biomater.* **2007**, *82*, 471–480. [CrossRef] [PubMed]
63. Ma, D.; Ren, L.; Liu, Y.; Chen, F.; Zhang, J.; Xue, Z.; Mao, T. Engineering scaffold-free bone tissue using bone marrow stromal cell sheets. *J. Orthop. Res.* **2010**, *28*, 697–702. [CrossRef] [PubMed]
64. Ueyama, Y.; Yagyuu, T.; Maeda, M.; Imada, M.; Akahane, M.; Kawate, K.; Tanaka, Y.; Kirita, T. Maxillofacial bone regeneration with osteogenic matrix cell sheets: An experimental study in rats. *Arch. Oral Biol.* **2016**, *72*, 138–145. [CrossRef] [PubMed]
65. Xie, Q.; Wang, Z.; Huang, Y.; Bi, X.; Zhou, H.; Lin, M.; Yu, Z.; Wang, Y.; Ni, N.; Sun, J.; et al. Characterization of human ethmoid sinus mucosa derived mesenchymal stem cells (hESMSCs) and the application of hESMSCs cell sheets in bone regeneration. *Biomaterials* **2015**, *66*, 67–82. [CrossRef]
66. Wang, F.; Hu, Y.; He, D.; Zhou, G.; Ellis, E., 3rd. Scaffold-free cartilage cell sheet combined with bone-phase BMSCs-scaffold regenerate osteochondral construct in mini-pig model. *Am. J. Transl. Res.* **2018**, *10*, 2997–3010.

67. Nakamura, A.; Akahane, M.; Shigematsu, H.; Tadokoro, M.; Morita, Y.; Ohgushi, H.; Dohi, Y.; Imamura, T.; Tanaka, Y. Cell sheet transplantation of cultured mesenchymal stem cells enhances bone formation in a rat nonunion model. *Bone* **2010**, *46*, 418–424. [CrossRef] [PubMed]
68. Zimmermann, G.; Moghaddam, A. Allograft bone matrix versus synthetic bone graft substitutes. *Injury* **2011**, *42* (Suppl. S2), S16–S21. [CrossRef]
69. Kasten, P.; Beyen, I.; Niemeyer, P.; Luginbuhl, R.; Bohner, M.; Richter, W. Porosity and pore size of β-tricalcium phosphate scaffold can influence protein production and osteogenic differentiation of human mesenchymal stem cells: An in vitro and in vivo study. *Acta Biomater.* **2008**, *4*, 1904–1915. [CrossRef]
70. Zhang, H.; Mao, X.; Du, Z.; Jiang, W.; Han, X.; Zhao, D.; Han, D.; Li, Q. Three dimensional printed macroporous polylactic acid/hydroxyapatite composite scaffolds for promoting bone formation in a critical-size rat calvarial defect model. *Sci. Technol. Adv. Mater.* **2016**, *17*, 136–148. [CrossRef]
71. Lee, D.J.; Kwon, J.; Kim, Y.I.; Wang, X.; Wu, T.J.; Lee, Y.T.; Kim, S.; Miguez, P.; Ko, C.C. Effect of pore size in bone regeneration using polydopamine-laced hydroxyapatite collagen calcium silicate scaffolds fabricated by 3D mould printing technology. *Orthod. Craniofac. Res.* **2019**, *22* (Suppl. S1), 127–133. [CrossRef]
72. Takahashi, Y.; Tabata, Y. Effect of the fiber diameter and porosity of non-woven PET fabrics on the osteogenic differentiation of mesenchymal stem cells. *J. Biomater. Sci. Polym. Ed.* **2004**, *15*, 41–57. [CrossRef] [PubMed]
73. Keaveny, T.M.; Morgan, E.F.; Niebur, G.L.; Yeh, O.C. Biomechanics of trabecular bone. *Annu. Rev. Biomed. Eng.* **2001**, *3*, 307–333. [CrossRef]
74. Kronemberger, G.S.; Matsui, R.A.M.; Miranda, G.d.A.S.d.C.E.; Granjeiro, J.M.; Baptista, L.S. Cartilage and bone tissue engineering using adipose stromal/stem cells spheroids as building blocks. *World J. Stem Cells* **2020**, *12*, 110–122. [CrossRef] [PubMed]
75. Shen, F.H.; Werner, B.C.; Liang, H.; Shang, H.; Yang, N.; Li, X.; Shimer, A.L.; Balian, G.; Katz, A.J. Implications of adipose-derived stromal cells in a 3D culture system for osteogenic differentiation: An in vitro and in vivo investigation. *Spine J.* **2013**, *13*, 32–43. [CrossRef]
76. Laschke, M.W.; Schank, T.E.; Scheuer, C.; Kleer, S.; Shadmanov, T.; Eglin, D.; Alini, M.; Menger, M.D. In vitro osteogenic differentiation of adipose-derived mesenchymal stem cell spheroids impairs their in vivo vascularization capacity inside implanted porous polyurethane scaffolds. *Acta Biomater.* **2014**, *10*, 4226–4235. [CrossRef] [PubMed]
77. Murata, D.; Tokunaga, S.; Tamura, T.; Kawaguchi, H.; Miyoshi, N.; Fujiki, M.; Nakayama, K.; Misumi, K. A preliminary study of osteochondral regeneration using a scaffold-free three-dimensional construct of porcine adipose tissue-derived mesenchymal stem cells. *J. Orthop. Surg. Res.* **2015**, *10*, 35. [CrossRef] [PubMed]
78. Fennema, E.M.; Tchang, L.A.H.; Yuan, H.; van Blitterswijk, C.A.; Martin, I.; Scherberich, A.; de Boer, J. Ectopic bone formation by aggregated mesenchymal stem cells from bone marrow and adipose tissue: A comparative study. *J. Tissue Eng. Regen. Med.* **2018**, *12*, e150–e158. [CrossRef]
79. Brochado, A.C.B.; de Souza, V.H.; Correa, J.; Dos Anjos, S.A.; de Almeida Barros Mourao, C.F.; Cardarelli, A.; Montemezzi, P.; Gameiro, V.S.; Pereira, M.R.; Mavropoulos, E.; et al. Osteosphere Model to Evaluate Cell-Surface Interactions of Implantable Biomaterials. *Materials* **2021**, *14*, 5858. [CrossRef]
80. Ishaug-Riley, S.L.; Crane, G.M.; Gurlek, A.; Miller, M.J.; Yasko, A.W.; Yaszemski, M.J.; Mikos, A.G. Ectopic bone formation by marrow stromal osteoblast transplantation using poly(DL-lactic-co-glycolic acid) foams implanted into the rat mesentery. *J. Biomed. Mater. Res.* **1997**, *36*, 1–8. [CrossRef]
81. Chen, L.J.; Wang, M. Production and evaluation of biodegradable composites based on PHB-PHV copolymer. *Biomaterials* **2002**, *23*, 2631–2639. [CrossRef]
82. Yaszemski, M.J.; Payne, R.G.; Hayes, W.C.; Langer, R.; Mikos, A.G. Evolution of bone transplantation: Molecular, cellular and tissue strategies to engineer human bone. *Biomaterials* **1996**, *17*, 175–185. [CrossRef]
83. Hu, Y.; Grainger, D.W.; Winn, S.R.; Hollinger, J.O. Fabrication of poly(α-hydroxy acid) foam scaffolds using multiple solvent systems. *J. Biomed. Mater. Res.* **2002**, *59*, 563–572. [CrossRef] [PubMed]
84. Sheikh, F.A.; Ju, H.W.; Moon, B.M.; Lee, O.J.; Kim, J.-H.; Park, H.J.; Kim, D.W.; Kim, D.-K.; Jang, J.E.; Khang, G.; et al. Hybrid scaffolds based on PLGA and silk for bone tissue engineering. *J. Tissue Eng. Regen. Med.* **2016**, *10*, 209–221. [CrossRef] [PubMed]
85. Yao, Q.; Cosme, J.G.; Xu, T.; Miszuk, J.M.; Picciani, P.H.; Fong, H.; Sun, H. Three dimensional electrospun PCL/PLA blend nanofibrous scaffolds with significantly improved stem cells osteogenic differentiation and cranial bone formation. *Biomaterials* **2017**, *115*, 115–127. [CrossRef] [PubMed]
86. Bose, S.; Tarafder, S. Calcium phosphate ceramic systems in growth factor and drug delivery for bone tissue engineering: A review. *Acta Biomater.* **2012**, *8*, 1401–1421. [CrossRef] [PubMed]
87. Matsuno, T.; Hashimoto, Y.; Adachi, S.; Omata, K.; Yoshitaka, Y.; Ozeki, Y.; Umezu, Y.; Tabata, Y.; Nakamura, M.; Satoh, T. Preparation of injectable 3D-formed β-tricalcium phosphate bead/alginate composite for bone tissue engineering. *Dent. Mater. J.* **2008**, *27*, 827–834. [CrossRef] [PubMed]
88. Zhang, R.; Gao, Z.; Geng, W.; Yan, X.; Chen, F.; Liu, Y. Engineering vascularized bone graft with osteogenic and angiogenic lineage differentiated bone marrow mesenchymal stem cells. *Artif. Organs* **2012**, *36*, 1036–1046. [CrossRef]
89. Kawamura, M.; Miyagawa, S.; Fukushima, S.; Saito, A.; Miki, K.; Funakoshi, S.; Yoshida, Y.; Yamanaka, S.; Shimizu, T.; Okano, T.; et al. Enhanced Therapeutic Effects of Human iPS Cell Derived-Cardiomyocyte by Combined Cell-Sheets with Omental Flap Technique in Porcine Ischemic Cardiomyopathy Model. *Sci. Rep.* **2017**, *7*, 8824. [CrossRef]

90. Bohner, M.; Santoni, B.L.G.; Dobelin, N. Beta-Tricalcium phosphate for bone substitution: Synthesis and properties. *Acta Biomater.* **2020**, *113*, 23–41. [CrossRef]
91. Liu, G.; Zhao, L.; Cui, L.; Liu, W.; Cao, Y. Tissue-Engineered bone formation using human bone marrow stromal cells and novel beta-tricalcium phosphate. *Biomed. Mater.* **2007**, *2*, 78–86. [CrossRef]
92. Gao, P.; Zhang, H.; Liu, Y.; Fan, B.; Li, X.; Xiao, X.; Lan, P.; Li, M.; Geng, L.; Liu, D.; et al. Beta-Tricalcium phosphate granules improve osteogenesis in vitro and establish innovative osteo-regenerators for bone tissue engineering in vivo. *Sci. Rep.* **2016**, *6*, 23367. [CrossRef] [PubMed]
93. Ueha, T.; Akahane, M.; Shimizu, T.; Uchihara, Y.; Morita, Y.; Nitta, N.; Kido, A.; Inagaki, Y.; Kawate, K.; Tanaka, Y. Utility of tricalcium phosphate and osteogenic matrix cell sheet constructs for bone defect reconstruction. *World J. Stem Cells* **2015**, *7*, 873–882. [CrossRef] [PubMed]
94. Wang, Z.; Wang, K.; Lu, X.; Li, M.; Liu, H.; Xie, C.; Meng, F.; Jiang, O.; Li, C.; Zhi, W. BMP-2 encapsulated polysaccharide nanoparticle modified biphasic calcium phosphate scaffolds for bone tissue regeneration. *J. Biomed. Mater. Res. A* **2015**, *103*, 1520–1532. [CrossRef]
95. Zhang, H.; Migneco, F.; Lin, C.Y.; Hollister, S.J. Chemically-Conjugated bone morphogenetic protein-2 on three-dimensional polycaprolactone scaffolds stimulates osteogenic activity in bone marrow stromal cells. *Tissue Eng. Part A* **2010**, *16*, 3441–3448. [CrossRef] [PubMed]
96. Blumenfeld, I.; Srouji, S.; Lanir, Y.; Laufer, D.; Livne, E. Enhancement of bone defect healing in old rats by TGF-beta and IGF-1. *Exp. Gerontol.* **2002**, *37*, 553–565. [CrossRef]
97. Seeherman, H.; Wozney, J.M. Delivery of bone morphogenetic proteins for orthopedic tissue regeneration. *Cytokine Growth Factor Rev.* **2005**, *16*, 329–345. [CrossRef] [PubMed]
98. Dimar, J.R.; Glassman, S.D.; Burkus, K.J.; Carreon, L.Y. Clinical outcomes and fusion success at 2 years of single-level instrumented posterolateral fusions with recombinant human bone morphogenetic protein-2/compression resistant matrix versus iliac crest bone graft. *Spine* **2006**, *31*, 2534–2539; discussion 2540. [CrossRef]

3.2.2. Manuscript 3: Microscale scaffold-free *in vitro* 3D cartilage constructs replicate inflammation-mediated cartilage degeneration

The following manuscript has been submitted to the Journal *Frontiers in Bioengineering and Biotechnology*.

Authors: Alexandra Damerau, Duc Ha Do Nguyen, Christina Lubahn, Madeleine Jenning, Moritz Pfeiffenberger, Timo Gaber, Frank Buttgereit

Title: Microscale scaffold-free *in vitro* 3D cartilage constructs replicate inflammation-mediated cartilage degeneration

Personal contribution: Conceptualization, planning, validation, preparing, interpreting, analyzing, and conducting of MSC isolation, expansion and characterization, generation of miniaturized scaffold-free cartilage components, characterization and stimulation of miniSFCCs, histological and immunofluorescence investigations and quantifications, gene expression analysis, viability and metabolic assays, ELISA, scanning electron microscopy, immune cell isolation, flow cytometry, and pO_2 measurements. Manuscript visualization, design, writing, reviewing, and final approval under the supervision of Dr. Timo Gaber and Prof. Dr. Frank Buttgereit.

Microscale scaffold-free *in vitro* 3D cartilage constructs replicate inflammation-mediated cartilage degeneration

Alexandra Damerau[1,2], Duc Ha Do Nguyen[1,2], Christina Lubahn[1,2], Madeleine Jenning[2], Moritz Pfeiffenberger[1,2], Timo Gaber[1,2]* and Frank Buttgereit[1,2]

[1] Charité – Universitätsmedizin Berlin, corporate member of Freie Universität Berlin and Humboldt-Universität zu Berlin, Department of Rheumatology and Clinical Immunology, Berlin, Germany

[2] German Rheumatism Research Centre (DRFZ) Berlin, a Leibniz Institute, Berlin, Germany

*** Correspondence:**
Dr. rer. nat. Timo Gaber
timo.gaber@charite.de

Keywords: chondrogenic model, TNF-α, pro-inflammatory cytokine, mesenchymal stromal cell, CD4 T helper (Th) cells, articular cartilage breakdown

Abstract

The articular surface of joints is covered by hyaline cartilage characterized by a uniquely layered structure that resists compressive forces and enhances bone resilience. However, severe traumatic and repeated excessive stress can damage cartilage. The same is true for prolonged inflammation that also prevents cartilage regeneration. Therefore, progressive cartilage destruction is one of the main features of rheumatic diseases such as degenerative osteoarthritis (OA) and chronic inflammatory rheumatoid arthritis (RA). Current preclinical approaches to study cartilage degeneration rely on in vivo models, not allowing precise representation of the microenvironment. Therefore, human-based model approaches that properly incorporate complex biological properties are needed to investigate disease-specific mechanisms and identify promising targets to address unmet therapeutic needs.

Here, we aimed at establishing an *in vitro* approach to investigate the effect of TNF-α and activated CD4+ T helper (Th) cells on specific targets in arthritis-mediated cartilage degradation in a preclinical mid-throughput format. To this end, we have developed scaffold-free *in vitro* 3D cartilage-like constructs (SFCCs) based on mesenchymal condensation of bone marrow-derived mesenchymal stromal cells (MSCs) of different sizes – microscale (ø ~1.4 mm) and macroscale (ø ~5 mm). We show that (i) microscale mesenchymal condensation leads to the formation of viable, cell-dense miniSFCCs with collagen type 2 and GAG-rich extracellular matrix. This was comparable to that observed in generated macroSFCCs by intermittent mechanical stimulation. In addition, (ii) miniSFCCs and macroSFCCs show a similar chondrogenic phenotype, and (iii) TNF-α stimulation leads to apoptosis, metabolic changes, an inflammatory gene expression pattern, and IL-6 production, mimicking characteristic features of arthritis. Finally, stimulation by activated Th cells, which more closely resembles the *in vivo* situation, increased glycolysis. We conclusively demonstrate that miniSFCCs, as opposed to macroSFCCs, can be used as an *in vitro* model to study cytokine-induced cell- and matrix-related alterations during cartilage degradation at a faster rate, enabling medium- to high-throughput investigation of the effects of potential therapeutics on specific targets.

Microscale *in vitro* cartilage breakdown

1 Introduction

Progressive cartilage destruction is one of the key features of rheumatic diseases such as osteoarthritis (OA) and rheumatoid arthritis (RA). The high prevalence of both age-related diseases (OA: 5% / RA: 0.5-1%) leads to enormous individual and economic burden (1, 2). Moreover, the situation is exacerbated by increasing life expectancy and an aging population (1, 2). While OA is the most common degenerative joint disease, RA is the most common autoimmune-mediated joint disease. The pathogenesis of RA is characterized by systemic inflammation, progressive cartilage degeneration, and bone destruction driven by inflammatory processes (3-5). As hyaline cartilage does not regenerate, there is a growing need for innovative cell therapies to restore degenerative articular cartilage (1, 2, 6). Hence, various preclinical tissue engineering approaches have been developed to understand the pathophysiological mechanisms and to develop and verify novel therapeutic approaches. Articular cartilage is characterized by a unique layered structure that withstands shear stress and compressive loads and enables frictionless joint motion. It is an avascular, extracellular matrix (ECM)-rich tissue composed of 60-80% water, 20% proteoglycans/aggrecans, 5% collagen (Col) type II and 1-5% chondrocytes (7). In preclinical research, animal models remain the gold standard for studying cartilage degradation (8). However, RA-induced joint damage in animal models heals on its own when the affected joint is surrounded by open growth plates (9). Growth plate germinal cells can supply the regenerating cartilage and change the study results. In addition, mice's biomechanical properties and thin cartilage diverge from humans' (10). Therefore, small animal joints cannot adequately mimic human joints. Consequently, *in vitro* developed 3D cartilage-like tissue of human origin has become increasingly important in preclinical research.

Mainly native or autologous chondrocytes are used in 3D cartilage tissue engineering and regenerative medicine approaches (11-13). In a first surgical operation, chondrocytes are removed from the injured cartilage and cultivated in the laboratory for up to 6 weeks. The cultivated chondrocytes are then implanted into the defect in a second operation, where they grow into the entire cartilage. These cells are only available in minimal numbers in the healthy state, must originate from young patients, and can undergo rapid dedifferentiation during *in vitro* expansion, resulting in the formation of fibrocartilage with altered mechanical properties. (14). Mesenchymal stromal cells (MSCs) are a promising alternative cell source for 3D cartilage tissue engineering due to their high chondrogenic potential, availability from various sources, allogenic applicability, and increased proliferative capacity (15, 16). Upon exposure to chondrogenic factors in 3D, they produce glycosaminoglycan (GAG)- and COL2-rich ECM, like native cartilage (17, 18).

Today, MSCs are used in a variety of *in vitro* models. However, these models vary in complexity, although more sophisticated research questions require more complex *in vitro* models. Hence, 3D approaches providing cell-cell interactions facilitate the investigation of matrix production and degradation mechanisms. However, most 3D models involve scaffolds such as hyaluronic acid (HA) (19), agarose (20), alginate (21, 22), and hybrids such as HA/collagen (23). These improve chondrogenesis and serve as carriers of the cells. However, their distinct effects on cells are often completely neglected or at least insufficiently considered (24, 25). Therefore, researchers aim to produce scaffold-free tissue-engineered cartilage. 3D pellet approaches could be promising for both in vivo cartilage repair and in vitro modeling, as ECM remodeling can be studied without the involvement of scaffolds (26-28). Spheroids from human autologous matrix-associated chondrocytes ─ co.don chondrosphere® ─ are already approved for clinical use in reconstructing cartilage defects. Despite considerable progress, a fine-balanced and precisely elaborated strategy is needed to keep complexity in *in vitro* systems allowing both the examination of basic research questions and the development of new therapeutic approaches, and to enhance translation in biomedical research.

Microscale *in vitro* cartilage breakdown

Here, we propose a scaffold-free *in vitro* 3D chondrogenic model produced from human bone marrow-derived MSCs. We aimed at demonstrating that this pellet culture can be used as an *in vitro* model to study cytokine-mediated alterations in cells and ECM during cartilage degradation, a major feature of rheumatic joint diseases such as OA and RA. This study was designed to precisely characterize the MSC-based chondrogenic model concerning its phenotype and spatial distribution compared to the previously developed macroscale approach concerning the gene expression levels of chondrogenic markers. Moreover, the effects of the pro-inflammatory cytokine tumor necrosis factor (TNF)-α and CD4+ Th cells on e.g., cell viability, glycolysis, and matrix metalloprotease (MMP) expression were determined to confirm a replication of RA-mediated cartilage degeneration.

2 Materials and methods

2.1 Mesenchymal stromal cell cultivation and ethical approval

MSCs were obtained from the bone marrow of patients undergoing total hip replacement. Bone marrow was provided by the Center for Musculoskeletal Surgery, Charité–Universitätsmedizin Berlin, and distributed by the "Tissue Harvesting" core facility of the Berlin-Brandenburg Center for Regenerative Therapies (donor list in **Table 1**). Protocols and study design were approved by the Charité–Universitätsmedizin Ethics Committee and performed according to the Helsinki Declaration (EA1/012/13, January 2013, EA1/146/21, May 2021). Cell isolation, expansion, and characterization were performed as previously described (29). MSCs were cultured with Dulbecco`s Modified eagle Minimal Essential Medium (DMEM) GlutaMAX™ (Gibco, Waltham, MA, USA), 10% fetal calf serum (FCS, Biowest, Nuaillé, France), 20% StemMACS^{TM} MSC Expansion Media Kit XF (Miltenyi Biotech, Bergisch Gladbach, Germany), 100 U/mL penicillin (1% Pen, Gibco, Waltham, MA, USA), and 100 µg/mL streptomycin (1% Step, Gibco, Waltham, MA, USA) as previously described (29).

2.2 Generation of macro and microscale scaffold-free cartilage-like constructs (SFCCs)

Macroscale scaffold-free cartilage-like constructs (macoSFCCs) were obtained from the Research Center of Medical Technology and Biotechnology (fzmb GmbH, Bad Langensalza, Germany). They were prepared as previously described (29, 30), using a patented process (no. 10 2004 001 225, German Patent and Trade Mark Office, 2004). Briefly, around 6-10×10^6 MSCs were transferred into a 3D state via centrifugation. After one week, biomechanical forces were applied for 4 weeks to initiate maturation. Before the experiments, macroSFCCs were cultivated for 3 weeks without biomechanical forces in DMEM GlutaMAX™ supplemented with 10% FCS, 1% Pen/Strep, in the following referred to as normal medium (NM), and 9.39 mg/L ascorbic acid (Sigma-Aldrich Chemie GmbH, Munich, Germany).

MiniSFCCs were generated based on MSCs. Reaching a confluence of >85%, cells were detached using Trypsin/EDTA (Gibco, Waltham, MA, USA). Subsequently, 2x10^5 cells were transferred to a 1.5 mL tube and centrifuged at 400*xg* for 4 min. The tube was filled up with 500 µL NM. Cell pellets were left untreated within the first two days for self-organized mesenchymal condensation forming a microscale 3D pellet state. Afterward, cell pellets were transferred to a U-bottom 96-well plate (Corning, New York, USA) and the differentiation process started by adding 100% StemMACS^{TM} ChondroDiff medium (Miltenyi Biotec, Bergisch Gladbach, Germany) for one week (in the following referred to as CD_{100}), followed by DMEM GlutaMAX™ supplemented with 2% FCS, 1% Pen/Strep and 20% StemMACS^{TM} ChondroDiff medium, in the following referred to as CD_{20}.

2.3 Experimental setup for miniSFCCs stimulation

TNF-α (ImmunoTools GmbH, Friesoythe, Germany) was solved in NM to reach the final concentrations: 10 ng/mL, 100 ng/mL, and 1000 ng/mL. Incubation was conducted at 37 °C in a 5% CO_2 atmosphere with approximately 18% O_2. Investigating TNF-α-mediated cell- and matrix-related changes, miniSFCCs were daily stimulated for three days with a non-cytotoxic, pathophysiological dose of TNF-α (100 ng/mL). Endpoint measurements (e.g., viability assays, qPCR) were performed on day 21 compared to the untreated control group. In addition, CD4+ T helper (Th) cells were isolated by MACS using anti-human CD4 conjugated magnetic beads (Miltenyi Biotec, Bergisch Gladbach, Germany) and activated with TransAct™ (Miltenyi Biotec, Bergisch Gladbach, Germany) for 24 h (Gating strategy shown in **Supplementary Figure 1**). $4x10^5$ activated CD4+ Th cells (>98% purity and >95% viability) were seeded onto the polycarbonate membrane of an HTS Transwell® 96-well plate (Corning, New York, USA) and incubated for three days.

2.4 Viability Assays

Cytotoxicity Detection LDH Kit (Sigma-Aldrich, Munich, Germany) was used to detect the cytotoxic effects of the TNF-α treatment concentration. According to the manufacturer's instructions and as previously described (29, 31), 100 µL of the supernatants were incubated with a 100 µL working solution for 30 min at RT in the dark. Absorption was measured at 490 nm (correction wavelength 630 nm). To induce cell death resulting in LDH release, cells were incubated with 4% (v/v) Triton™ X-100 (Sigma-Aldrich, Munich, Germany) for 24 h. LDH Assay was performed in duplicates.

According to the manufacturer's instructions, the Cell Proliferation Reagent WST-1 Kit (Sigma-Aldrich) was used as previously described (29). Samples mixed with WST-1 solution were incubated for 30 min at 37 °C, 5% CO_2, and measured photometrically at 450 nm (reference wavelength 630 nm).

2.5 External pO_2 measurement

Oxygen consumption (pO_2) was measured using a Clark electrode (SI130 Microcathode electrode, Strathkelvin Instruments Limited, North Lanarkshire, Scotland) connected to a control unit (SI782 Meter, Strathkelvin Instruments Limited, North Lanarkshire, Scotland). The connected, warm water system (Pilot-One™) was used to maintain a temperature of 37 °C. The electrode was covered with a fluorinated ethylene propylene membrane (FEP, Strathkelvin Instruments Limited, North Lanarkshire, Scotland). Equilibration was performed for at least 8 h. Before each daily measurement, the electrode was calibrated by two-point calibration:

(i) Zero point: 2% (w/v) sodium sulfite solution.
(ii) 100%: Experimental medium saturated with atmospheric oxygen overnight.

A voltage range between 400-1000 mV was used for measurements. However, a sample volume of 50 µL was given into the chamber and directly sealed with a polycarbonate plug. After 10 s of stable values, the value obtained was logged.

2.6 Glucose and lactate measurements

To quantify glycolysis, glucose and lactate concentrations were measured. Therefore, miniSFCCs were cultured with and without 100 ng/mL TNF-α (37 °C, 5% CO_2). Daily, 20 µL supernatant was mixed with 1 mL PBS and analyzed using the Biosen C-Line Glucose and Lactate analyzer (EKF-diagnostic GmbH, Barleben, Germany). Instrument calibration and electrode validation were performed before the measurements, using the manufacturer's calibration and control solutions.

2.7 ApoTox-Glo™ Triplex Assay

The ApoTox-Glo™ Triplex Assay was performed according to the manufacturer's instructions (Promega Corporation, Walldorf, Germany) to measure cell viability, cytotoxicity, and apoptosis. To this end, samples were incubated with phenol red-free DMEM (Gibco, Waltham, MA, USA). To induce cell death, samples were incubated with 4% (v/v) Triton™ X-100 for 4 h or 100 µg/mL digitonin (Boehringer Mannheim GmbH, Mannheim, Germany) for 30 min. As a positive control for apoptosis, samples were incubated with 0.1 mM camptothecin (Sigma-Aldrich) for 4 h.

Readout	**Control**	**Measurement**
Viability	100 µg/mL Digitonin (*Neg. Ctrl*)	360/40 Excitation, 460/40 Emission
Cytotoxicity	4% (v/v) Triton™ X-100 (*Pos. Ctrl*)	485/20 Excitation, 528/20 Emission
Apoptosis	0.1 mM Camptothecin (*Pos. Ctrl*)	Luminescence, bottom

2.8 Histology: Cryo-embedding and sectioning

Samples were cryo-embedded for histological and immunofluorescence analysis. Tissues were carefully washed with PBS, fixed in 4% (v/v) paraformaldehyde (PFA; Electron Microscopy Sciences, Hatfield, PA, USA) in PBS for 2 h, and treated with 10%, 20%, and 30% (w/v) sucrose solution at 4 °C for 24 h each. Tissues were embedded in the SCEM embedding medium (Sectionlab, Hiroshima, Japan) and frozen by n-hexane using acetone and dry ice as a cooling agent. Embedded tissue samples were stored at -80 °C until cryostat microtome sectioning. Cryo-embedded samples were sectioned using the Microm Cryo Star HM 560 Cryostat (Thermo Fisher Scientific, Waltham, MA, USA). Samples were adhered to the sample plate using Tissue-Tek® O.C.T.™ Compound (Sakura Finetek Germany GmbH, Staufen, Germany). Cryosections of 7 µm thickness were prepared using the Kawamoto cryofilm type 2C (Sectionlab, Hiroshima, Japan). Hematoxylin and Eosin staining, alcian blue staining, and scanning electron microscopy were performed as previously described (29).

2.9 Histomorphometry using ImageJ

To provide quantitative data on tissue appearance, images were analyzed with FIJI ImageJ 1.52p (National Institutes of Health, Bethesda, MD, US). Brightness and contrast were adjusted to remove background noise. The surveyed areas are depicted in **Figure 1**. Gained results were normalized to the corresponding area: total area (t.a.), outer area (o.a), middle area (m.a.), and inner area (i.a.). Cell count was determined using 'Find Maxima', while mean fluorescence intensities were determined by threshold. The analysis pipeline was adapted to every staining.

2.10 Immunofluorescence staining

Immunofluorescence staining was performed using target-specific antibodies that are listed in **Table 2**. All stainings were performed in a humid chamber in the dark at RT as previously described (29). Before each staining, slices were dried, rimmed using a hydrophobic pen (Dako Pen; Agilent Technologies, Santa Clara, CA, USA), and then rehydrated with PBS for 10 min. Permeabilization was performed with 1x PBS/0.1% (v/v) Tween® 20 (Qbiogene Inc., Carlsbad, CA, USA) for 10 min, followed by blocking the unspecific binding sites with 1x PBS/5% (v/v) FCS for 30 min. Afterward, the primary antibody was diluted in 1x PBS/5% (v/v) FCS/0.1% (v/v) Tween® 20 and incubated according to the manufacturer's instructions, followed by a washing step with PBS/0.1% (v/v) Tween® 20 (3×). All secondary antibodies were diluted 1:500 in PBS/5% (v/v) FCS/0.1% (v/v) Tween® 20 for 2 h. Nuclei staining was performed using 4,6-diamidino-2-phenylindole (DAPI; 1 µg/mL diluted in PBS/0.1% (v/v) Tween® 20 for 15 min). Samples were transferred on a new slide and covered with FluoroMount-G™ (Sigma-Aldrich, Munich, Germany). Immunofluorescence imaging was performed with the

fluorescence microscope BZ-9000 (Keyence) or Zeiss LSM 710 Confocal Microscope (Carl Zeiss AG, Oberkochen, Germany). Image analysis was performed using ImageJ.

2.11 Enzyme-linked immunosorbent assay (ELISA)

TNF-α, interleukin (IL)-6, and IL-6/IL-6 receptor α (Ra) complex DuoSet® ELISA were performed according to the manufacturer's instructions in duplicates (R&D Systems, Minneapolis, USA). Briefly, Nunc MaxiSorp™ high protein-binding capacity 96-well flat-bottomed plates (Thermo Fisher Scientific, Waltham, MA, USA) were incubated overnight at RT with 100 µL of the specific capture antibody diluted in PBS. After a washing step (3x) with the washing buffer (0.05% (v/v) Tween® 20 in 1x PBS), unspecific binding sites were blocked by adding 200 µL reagent diluent (1% (w/v) bovine serum albumin (BSA; Sigma-Aldrich) in PBS, filtrated 0.22 µm, pH 7.2-7.4) for 1 h at RT, followed by a washing step. Standards and samples were diluted and incubated for 2 h. After a washing step, 100 µL of the biotinylated detection antibody ─ binding a specific epitope of the target ─ diluted in 1x PBS was applied for 1 h, followed by 20 min incubation with Streptavidin-HRP conjugate. Finally, the TMB Chromogen Solution was added, and the reaction was stopped after 20 min (RT, dark) using 2N H_2SO_4. Absorption was measured with the Synergy™ HT plate reader (BioTek Instruments Inc., Winooski, USA) at 450 nm and 630 nm (wavelength correction). A four-parameter logistic curve fit was used to plot the standard curve.

2.12 RNA isolation, cDNA synthesis, and qPCR

RNA isolation, cDNA synthesis, and quantitative PCR (qPCR) were performed as previously described (29). Briefly, RNA was isolated using the RNeasy® Fibrous Tissue Mini Kit (Qiagen GmbH, Hilden, Germany). The cDNA synthesis was performed using TaqMan® Reverse Transcription Reagents Kit (Applied Biosystems Inc., Waltham, MA, USA), while the Stratagene Mx3000P (Agilent Technologies Inc., Santa Clara, CA, USA) was used for qPCR with the DyNAmo ColorFlash SYBR Green qPCR Kit (Thermo Fisher Scientific, USA). Duplicates per gene were performed with the temperature profile: 7 min initial denaturation at 95 °C, 60 cycles of 10 s at 95 °C, 7 s at 60 °C, and 9 s at 72 °C. Melting curve analysis was performed after each run to confirm primer specificity (primer sequences listed in **Table 3**).

2.13 Statistical analysis

GraphPad® Prism Version 9.3.0 (La Jolla, San Diego, CA, USA) was used for statistical analyses. Mann-Whitney U test was used for direct comparisons of two independent datasets. For comparisons of more than two independent datasets, one-way analysis using Kruskal-Wallis with Dunn's multiple comparisons test was performed. Two-tailed Wilcoxon matched-pairs signed-rank test was applied for dependent datasets. For comparisons of more than two dependent datasets, one-way analysis using Friedman with Dunn's multiple comparisons test was performed. For two-way analysis, the mixed-effect analysis with Šídák's multiple comparisons test was performed. The statistical tests used are indicated in the figure legends. P-values of <0.05 were considered as statistically significant (*$p < 0.05$, **$p < 0.01$, ***$p < 0.005$). Data are shown as box plots (centerline, median; box limits, upper and lower quartiles; whiskers, maximum and minimum) if not indicated otherwise.

3 RESULTS

3.1 Microscale mesenchymal condensation results in viable, matrix-rich, and cell-dense 3D constructs

To mimic cartilage degradation and allow for studying the effect of preclinical drugs in a mid-throughput way, an *in vitro* microscale scaffold-free chondrogenic component was generated using human bone marrow-derived MSCs. MSCs were isolated and characterized according to previously published protocols (29). Chondrogenic equivalents were developed without supporting materials, e.g., hydrogels. $2x10^5$ cells were identified as the optimal seeding number since higher initial cell densities led to increased cell death. The adherent mesenchymal cells condensate within the first two days and form a 3D microscale structure easily transferable to a U-bottom 96-well plate (**Figure 2A**). The size of the miniSFCCs changed during culture from approximately 2.2 mm on day 3 to 1.4 mm after 21 days, while the spherical appearance was maintained over time (**Figure 2B**). Small, compact, almost round constructs were formed during this cultivation period. To analyze the viability of MSCs differentiated in 3D, LIVE/DEAD® and TUNEL staining were performed after three weeks. The results showed viable chondrogenic differentiated MSCs in 3D with only a few TUNEL-positive cells in the outer region (**Figure 2C, D**).

SEM analysis of the mature miniSFCCs revealed that chondrogenic differentiation of the MSCs after pellet formation resulted in a round, homogeneous, ECM-rich spheroid (**Figure 2E**). Scanning the surface with higher magnification did not reveal any microstructural deposits characteristic of bone-like structures. Chondrogenically differentiated miniSFCCs showed high cell density with elongated cells in the outer region (**Figure 2F**, arrow) and more round cells in the inner part (**Figure 2F**, asterisk). In addition, these cells were embedded in ECM as shown by hematoxylin and eosin staining (**Figure 2G**). They were capable of depositing glycosaminoglycan (GAG)-rich matrix, as alcian blue staining was more intense than in the undifferentiated control (**Figure 2H**). The matrix-to-cell ratio increased from the outside to the inside.

3.2 Microscale and macroscale SFCCs demonstrate a similar chondrogenic phenotype

Since the aim was to optimize the scaffold-free chondrogenic constructs in terms of cell number, size, homogeneous cell distribution, and differentiation for mid-/high-throughput analysis of potential drug targets, miniSFCCs were developed in this study. To analyze whether these miniSFCCs differentiate similarly to the mechanically stimulated macroscale ones, the expression of genes involved in chondrogenesis was analyzed on day 21 by qPCR. As a result, chondrogenic marker genes, such as *COL2A1* and *ACAN*, were significantly upregulated in miniSFCCs compared to the 2D monolayer control. In this line of observation, *COL1A1* — an osteogenic marker gene — was expressed significantly lower in miniSFCCs than in the control (**Figure 3A**). These results highlight the chondrogenic phenotype of the miniSFCCs. Moreover, this chondrogenic phenotype is comparable to the macroscale approach (**Figure 3B**). Immunofluorescence evaluation of miniSFCCs was consistent with the SEM examination and gene expression results, demonstrating the presence of significant amounts of ECM consisting of collagen type 2 (**Figure 3C**).

3.3 Mimicking arthritis using TNF-α stimulation leads to programmed cell death in miniSFCCs

A suitable *in vitro* model should be able to reflect disease-relevant changes; we therefore analyzed the responsiveness of miniSFCCs by simulating the inflammatory milieu of arthritic diseases by TNF-α treatment. This pro-inflammatory cytokine is one of the major cytokines during arthritic diseases such

as RA and OA. For this reason, TNF-α was administered at a concentration of 100 ng/mL, representing a non-cytotoxic but intense proinflammatory stimulation, to achieve maximal effects within a short stimulation period of three days (**Figure 4A**). Cell survival – relative number of Calcein AM+ cells – tended to be reduced by TNF-α stimulation **Figure 4B, C**). Concomitantly, TUNEL staining revealed more TUNEL-positive cells in the TNF-α stimulated group, whereas only a few TUNEL-positive cells were observed in the unstimulated group (**Figure 4D**). This finding suggests that MSCs undergo TNF-driven apoptosis, a key feature of inflammation. In addition, the density of cell nuclei per area was significantly reduced by TNF-α treatment (**Figure 4E**).

Programmed cell death (apoptosis) is well-known to be mediated by TNF-α. Indeed, TNF-α treatment for three days enhanced caspase activity levels in human arthritic miniSFCCs as analyzed by ApoTox-Glo^{TM} assay (**Figure 5A**). Of note, TNF-α mediated death signaling induces B-cell lymphoma (BCL)2-associated X protein (BAX) complex formation in mitochondrial membranes that are associated with propagated death signaling through cytochrome c and caspase-9 activity (32). Indeed, three-day short-term exposure tended to reduce the *BCL2-BAX*-ratio compared to the untreated control group (**Figure 5B**).

3.4 TNF-α stimulation leads to metabolic changes, inflammatory gene expression, and cytokine production

Measurements of oxygen saturation, glucose uptake, and lactate production were conducted to investigate metabolic changes. Oxygen consumption showed a similar course over time, not affected by TNF-α (**Figure 6A**). The amount of the water-soluble formazan product at the cell surface in an NADPH-dependent manner showed a significant increase within the TNF-α treated group (**Figure 6B**). As a parameter of glycolysis, glucose uptake was significantly downregulated upon cytokine stimulation. Accordingly, this resulted in reduced lactate production (**Figure 6C**).

Since TNF-α causes degradation of both aggrecan and type II collagen by inducing the expression of MMPs (33), we investigated whether these effects could be mimicked in miniSFCCs *in vitro*. At mRNA level, the expression of *ACAN* and *COL2A1* tended to be downregulated by cytokine stimulation (**Figure 7A**). This statistical trend was also detectable at the protein level using immunohistochemical analysis. Here, a statistically significantly lower content of aggrecan and collagen type II was observed in both the outer area (o.a.) and the total area (t.a.) of miniSFCCs compared to the untreated control group (**Figure 7B**). Histologically, the outer area containing elongated cells disappeared with stimulation, thereby demonstrating a sign of maceration of the superficial cell layer (**Figure 7C**, arrow). In line with this, expression of MMP13 tended to be higher at mRNA and on protein level, while the expression of *MMP1* was significantly higher at the gene level after TNF-α stimulation (**Figure 8A, B, C**). Moreover, gene expression levels of cartilage oligomeric matrix protein (*COMP*) as a measure of matrix turnover and *TNFA*, *IL8*, and *TGFB* as a measure of inflammation were significantly higher than the untreated control (**Figure 8D**). At the same time, *IL6* only tended to be higher. However, these results indicate that miniSFCCs are sensitive to an inflammatory trigger, as observed in RA.

TNF-α-mediated IL-6 secretion is a well-known feature of inflammation and thus RA (34). Therefore, we examined the supernatants of miniSFCCs for IL-6, which increased after stimulation over time and compared to the untreated control (**Figure 9A**). Additionally, TNF-α was measured to monitor (i) TNF-α uptake and (ii) inflammatory activity. The decrease of TNF-α correlated with increased IL-6 secretion over time but remained unchanged in the corresponding untreated control (**Figure 9B**). Of note, soluble IL-6R, which provides IL-6-responsiveness to cells lacking IL-6R, was unaffected by stimulation

(**Figure 9C**). In summary, in this microscale *in vitro* system, essential cytokine-mediated cell- and matrix-related changes ─ typical for arthritides ─ could be simulated.

3.5 Mimicking the pathophysiology of arthritis by activated CD4 Th cells results in IL-6 secretion and metabolic response of miniSFCCs

To further investigate the Th cell-mediated humoral impact on the pathogenesis of RA in our model, anti-CD3/CD28-activated CD4+ Th cells were seeded onto a transwell membrane with a pore size of 0.4 μm. In contrast to TNF-α stimulation, cytokine release from CD4+ Th cells significantly increased glucose uptake and lactate secretion as a measure of glycolysis (**Figure 10A**). In addition, WST-1 was significantly higher than the untreated control after 72 h (**Figure 10B**). Finally, we demonstrate that CD4+ Th cell stimulation induced IL-6 secretion as observed for TNF-α-mediated stimulation, whereas TNF-α secretion remained low (**Figure 10C, D**). On the other hand, gene expression levels of MMPs and pro-inflammatory cytokines were in mean numerically higher for *IL6, IL8, MMP1*, and *MMP3* than in the untreated control (**Figure 10E**).

4 Discussion

Our study aimed to develop a human *in vitro* model for degenerative cartilage processes based on cell condensation of MSCs without any scaffold materials. We show that (i) microscale mesenchymal condensation results in the formation of a viable, cell-rich, densely-packed miniaturized MSC-based *in vitro* 3D scaffold-free cartilage-like constructs. In addition, (ii) miniSFCCs and previously developed macroSFCCs (29) demonstrate a similar chondrogenic phenotype. Mimicking arthritis by (iii) cytokine stimulation with TNF-α and (iv) secreted molecules from anti-CD3/CD28-activated CD4+ Th cells seeded onto a transwell membrane resulted in apoptosis, metabolic changes, inflammatory gene expression, and cytokine production of miniSFCCs.

Previous reports have illustrated that a critical step in engineering functional chondrogenic equivalents is the condensation of mesenchymal cells, which initiates cell-cell communication before chondrogenic differentiation (35-37). Intercellular communication is closely related to the transfer of small molecules. Disturbances in the transfer of, e.g., GDF5 due to its mutation lead to the disruption of mesenchymal condensation and, consequently, brachypodism, i.e., an alteration in the length and number of bones in the limbs of mice (38-40). In the current study, human MSCs were condensed from a cell concentration of 2×10^5 cells. It is assumed that a high cell density is required for the extent of chondrogenesis to permit enough cell-cell contacts (36, 41). However, many studies have reported apoptosis or necrosis in the central region of the pellet culture ─ a phenomenon that usually occurs during endochondral ossification or as a result of exceeding the perfusion limit in large organoids. This was not observed in our miniSFCCs. (42-44). Here, mesenchymal condensation, even with low cell numbers, resulted in a solid pellet formation with viable cells and a higher cell density per area than our previously developed macroSFCCs (29). In general, our miniSFCCs, differentiated for 3 weeks, exhibited a chondrogenic phenotype on gene and protein levels as verified by the expression of cartilage-related genes such as *COL2A1* and *ACAN* (45), COL2 – an important marker for functional articular cartilage – and the expression of GAGs – a major component of the cartilage ECM. Previous reports have shown that the formation of MSC pellets leads to fibrocartilage characterized by, e.g., the expression of collagen type I and osteopontin (46, 47). Although osteopontin expression was not analyzed, cell differentiation decreased *COL1A1* expression in miniSFCCs compared to the monolayer control, confirming the observations in chondrogenic micromass pellet cultures of bone marrow-derived MSCs reported by Kafienah et al. (48). Comparing miniSFCCs with the macroSFCCs that were developed for more than 7 weeks demonstrated similar *COL2A1/COL1A1*- and *ACAN/COL1A1*-ratios within a shorter incubation time and fewer cell numbers (29). This emphasizes the superiority of mesenchymal pellet formation on a microscale-based approach regarding the velocity of chondrogenic differentiation, the applicability in mid-/high-throughput drug toxicity and efficacy assays. Grigull et al. compared pellet cultures with high-density cultures on a cellulose hydrogel and also showed an increased *COL2A1/COL1A1*-ratio, higher ECM deposits, and no increase in degenerative markers (41). Therefore, there is no need for additional scaffolds that facilitate cell seeding but might affect cell-cell communication and, thus cell differentiation.

TNFα-transgenic mice (heterozygous for the transgene of human soluble TNF) are commonly used to model RA *in vivo*. These mice develop destructive arthritis caused by TNF-α, one of the major proinflammatory cytokines in RA (49). To investigate the suitability of our miniSFCCs to serve as a mid-/high-throughput cartilage degradation model, we administered TNF-α at a high but non-cytotoxic dose for three days. TNF-α plays a pivotal role in apoptosis, tissue damage, and inflammation. We observed a decrease in cell number upon nuclear staining, with a tendency for DNA fragmentation to increase upon TNF treatment, as shown by the nick-end labeling (TUNEL) method (50). Matsuo et al. demonstrated the role of caspase-3 in cell apoptosis and cartilage destruction, which correlates with the severity of OA (51). Our *in vitro* data agree with this finding and demonstrate that caspase-3 or -7

are involved in TNF-α stimulated apoptosis – a hallmark of degenerative arthritis (50, 52). In addition, we could show that oxygen consumption is independent of TNF-α stimulation. In contrast, glucose uptake and lactate excretion as a measure of glycolysis was decreased. However, CD4+ Th cell-mediated stimulation increased glycolysis in a similar way as reported for e.g., IL-1β stimulation or other stressors (53, 54). Usually, chondrocytes shift from oxidative phosphorylation to glycolysis under environmental stress, as observed in RA or OA (54). These results indicate that TNF-α stimulation alone is insufficient to alter chondrocyte metabolism induced by an inflammatory environment.

Recent studies have also shown that MMP1, 3, and 13 can degrade proteoglycans, while MMP1 and MMP13 specifically break down collagen types 1-4 (55-57). Resembling cartilage destruction, treating *in vitro* miniSFCCs with TNF-α resulted in collagen type 2 breakdown, a major and early event mainly affecting the outer area – superficial layer (58). We observed a significant increase in MMP1 expression on protein and gene levels upon treatment, with MMP1 expressed predominantly in the superficial layer. This is consistent with the observation of Wu et al. demonstrating the highest expression of MMP1 in the superficial zone of cartilage in an anterior cruciate ligament transection (ACLT) rabbit model for traumatic osteoarthritis (59). A comparison of the expression levels of MMP1 and MMP13 in the center of the miniSFCCs showed that MMP13 is predominant (60). *MMP3* is known to activate other MMPs, such as proMMP1, and is significantly more expressed in the treated miniSFCCs than in the untreated control (61, 62). The fragmentation of collagen type 2, aggrecan, and COMP was detected during cartilage degradation in patients with OA and RA (63). COMP is a putative substrate for MMP1 and MMP13 but has also been shown to block apoptosis in the presence of TNF in HeLa cells (64). Here, we show a significant TNF-dependent increase in *COMP* gene expression. Usually, serum COMP levels are used as a diagnostic marker for arthritis, as they correlate closely with disease severity (63, 65). Furthermore, Li et al. investigated the expression of *COMP* and *COL2A1* during chondrogenesis using MSCs differentiated by pellet culture (66). They showed that *COMP* expression precedes *COL2A1* expression (66). In support of this, miniSFCCs also showed higher *COMP* expression, which may indicate its role in early chondrogenesis. Interestingly, the results of Li et al. also suggest that TGF-β rapidly mediates the induction of *COMP* (66). In our study, TNF stimulation increased *TGFB* expression, which may affect *COMP* expression. Our *in vitro* miniSFCC further showed TNF-α-mediated expression of *IL8* observed in various cells (67-69). TNF-α-induced *IL8* expression is associated with ERK2 and JNK1 signaling pathways, with JNK finally activating *BAX*, which induces apoptosis (68, 70). Since it is well known that TNF-α mediates IL-6 secretion, its release was measured daily during the stimulation period of three days (71-73). Interestingly, CD4+ T cell-mediated humoral stimulation increased IL-6 but not TNF-α secretion. Although IL-6 secretion increased, the IL-6 receptor remained unchanged after TNF-α stimulation. These results demonstrate that the MSCs-based miniSFCC can map various pathways and may serve as a preclinical tool in a high throughput format.

Our model has limitations that need to be addressed in the future. These include the use of (i) FCS instead of human sera and (ii) a high TNF-α dose to achieve results within a short-term exposure of three days. In addition, (iii) the microenvironment is usually characterized by hypoxia and limited nutrient supply. Therefore, mechanical forces are essential modulators in maintaining cartilage integrity and quality of developed tissue, which was not considered in this study. Bioreactors would therefore provide the opportunity to apply mechanical forces, whose effects could be studied by continuous monitoring.

Despite these limitations, we conclude that our scaffold-free *in vitro* 3D chondrogenic model sourcing from human bone marrow-derived MSCs can be used as an *in vitro* model to study cytokine-driven cell- and matrix-related changes during cartilage degradation, replicating a key feature of rheumatic joint diseases such as OA and RA.

5 Acknowledgments

Bone marrow was provided by the Tissue Harvesting Core Facility of the BIH Berlin. A.D., M.P., T.G., and F.B. are members of the Berlin-Brandenburg research platform BB3R and Charité3R.

6 Author Contributions

Conceptualization, A.D., T.G.; F.B., methodology, A.D., D.H.D.N, C.L.; validation, A.D., D.H.D.N.; formal analysis, A.D., D.H.D.N., C.L., M.J., M.P.; investigation, A.D.; data curation, A.D., T.G.; writing—original draft preparation, A.D., T.G., F.B.; writing—review and editing, A.D., D.H.D.N., C.L., M.J., M.P., T.G., F.B.; visualization, A.D.; supervision, A.D., T.G., F.B.; project administration, F.B.; funding acquisition, A.D., T.G., F.B. All authors have read and agreed to the published version of the manuscript.

7 Funding statement

This research was funded by the German Federal Ministry for Education and Research (BMBF; project no. 031L0070A), and the Lush Prize Award 2018 from Alexandra Damerau — Young Researcher, Rest of World. A.D. was additionally supported by the German Academic Scholarship Foundation (Studienstiftung des deutschen Volkes) and by the Joachim Herz Foundation (Add-on Fellowship 2020).

8 Conflict of interest statement

The authors declare that the research was conducted in the absence of any commercial or financial relationships that could be construed as a potential conflict of interest.

9 Data availability statement

The data presented in this study are available on request from the corresponding author. The data are not publicly available due to privacy and ethical restrictions.

10 References

1. Firestein GS, McInnes IB. Immunopathogenesis of Rheumatoid Arthritis. Immunity. 2017;46(2):183-96.
2. Sanchez-Lopez E, Coras R, Torres A, Lane NE, Guma M. Synovial inflammation in osteoarthritis progression. Nat Rev Rheumatol. 2022;18(5):258-75.
3. Burmester GR, Feist E, Dorner T. Emerging cell and cytokine targets in rheumatoid arthritis. Nat Rev Rheumatol. 2014;10(2):77-88.
4. Smolen JS, Aletaha D, Barton A, Burmester GR, Emery P, Firestein GS, et al. Rheumatoid arthritis. Nat Rev Dis Primers. 2018;4:18001.
5. Iannone F, Lapadula G. The pathophysiology of osteoarthritis. Aging clinical and experimental research. 2003;15(5):364-72.
6. Glyn-Jones S, Palmer AJ, Agricola R, Price AJ, Vincent TL, Weinans H, et al. Osteoarthritis. Lancet. 2015;386(9991):376-87.
7. Poole AR, Kojima T, Yasuda T, Mwale F, Kobayashi M, Laverty S. Composition and structure of articular cartilage: a template for tissue repair. Clinical orthopaedics and related research. 2001(391 Suppl):S26-33.
8. Moudgil KD, Kim P, Brahn E. Advances in rheumatoid arthritis animal models. Curr Rheumatol Rep. 2011;13(5):456-63.
9. Chu CR, Szczodry M, Bruno S. Animal models for cartilage regeneration and repair. Tissue Eng Part B Rev. 2010;16(1):105-15.
10. Esdaille CJ, Ude CC, Laurencin CT. Regenerative Engineering Animal Models for Knee Osteoarthritis. Regenerative Engineering and Translational Medicine. 2021.
11. Anderson DE, Markway BD, Weekes KJ, McCarthy HE, Johnstone B. Physioxia Promotes the Articular Chondrocyte-Like Phenotype in Human Chondroprogenitor-Derived Self-Organized Tissue. Tissue Engineering Part A. 2017;24(3-4):264-74.
12. Bhattacharjee M, Coburn J, Centola M, Murab S, Barbero A, Kaplan DL, et al. Tissue engineering strategies to study cartilage development, degeneration and regeneration. Adv Drug Deliv Rev. 2015;84:107-22.
13. Bhumiratana S, Eton RE, Oungoulian SR, Wan LQ, Ateshian GA, Vunjak-Novakovic G. Large, stratified, and mechanically functional human cartilage grown in vitro by mesenchymal condensation. Proc Natl Acad Sci U S A. 2014;111(19):6940-5.
14. Ma B, Leijten JC, Wu L, Kip M, van Blitterswijk CA, Post JN, et al. Gene expression profiling of dedifferentiated human articular chondrocytes in monolayer culture. Osteoarthritis Cartilage. 2013;21(4):599-603.
15. Chou CL, Rivera AL, Williams V, Welter JF, Mansour JM, Drazba JA, et al. Micrometer scale guidance of mesenchymal stem cells to form structurally oriented large-scale tissue engineered cartilage. Acta Biomater. 2017;60:210-9.
16. Pittenger MF, Mackay AM, Beck SC, Jaiswal RK, Douglas R, Mosca JD, et al. Multilineage potential of adult human mesenchymal stem cells. Science. 1999;284(5411):143-7.
17. Music E, Klein TJ, Lott WB, Doran MR. Transforming growth factor-beta stimulates human bone marrow-derived mesenchymal stem/stromal cell chondrogenesis more so than kartogenin. Scientific Reports. 2020;10(1):8340.

18. Xia P, Wang X, Qu Y, Lin Q, Cheng K, Gao M, et al. TGF-β1-induced chondrogenesis of bone marrow mesenchymal stem cells is promoted by low-intensity pulsed ultrasound through the integrin-mTOR signaling pathway. Stem Cell Research & Therapy. 2017;8(1):281.
19. Unterman SA, Gibson M, Lee JH, Crist J, Chansakul T, Yang EC, et al. Hyaluronic acid-binding scaffold for articular cartilage repair. Tissue Eng Part A. 2012;18(23-24):2497-506.
20. Buschmann MD, Gluzband YA, Grodzinsky AJ, Kimura JH, Hunziker EB. Chondrocytes in agarose culture synthesize a mechanically functional extracellular matrix. J Orthop Res. 1992;10(6):745-58.
21. Paige KT, Cima LG, Yaremchuk MJ, Schloo BL, Vacanti JP, Vacanti CA. De novo cartilage generation using calcium alginate-chondrocyte constructs. Plast Reconstr Surg. 1996;97(1):168-78; discussion 79-80.
22. Saygili E, Kaya E, Ilhan-Ayisigi E, Saglam-Metiner P, Alarcin E, Kazan A, et al. An alginate-poly(acrylamide) hydrogel with TGF-beta3 loaded nanoparticles for cartilage repair: Biodegradability, biocompatibility and protein adsorption. Int J Biol Macromol. 2021;172:381-93.
23. Mohammadi F, Mohammadi Samani S, Tanideh N, Ahmadi F. Hybrid Scaffolds of Hyaluronic Acid and Collagen Loaded with Prednisolone: an Interesting System for Osteoarthritis. Adv Pharm Bull. 2018;8(1):11-9.
24. Wasyleczko M, Sikorska W, Chwojnowski A. Review of Synthetic and Hybrid Scaffolds in Cartilage Tissue Engineering. Membranes (Basel). 2020;10(11).
25. Chang YH, Wu KC, Wang CC, Ding DC. Enhanced chondrogenesis of human umbilical cord mesenchymal stem cells in a gelatin honeycomb scaffold. J Biomed Mater Res A. 2020;108(10):2069-79.
26. DuRaine GD, Brown WE, Hu JC, Athanasiou KA. Emergence of scaffold-free approaches for tissue engineering musculoskeletal cartilages. Annals of biomedical engineering. 2015;43(3):543-54.
27. Murdoch AD, Grady LM, Ablett MP, Katopodi T, Meadows RS, Hardingham TE. Chondrogenic differentiation of human bone marrow stem cells in transwell cultures: generation of scaffold-free cartilage. Stem cells (Dayton, Ohio). 2007;25(11):2786-96.
28. Yasui Y, Ando W, Shimomura K, Koizumi K, Ryota C, Hamamoto S, et al. Scaffold-free, stem cell-based cartilage repair. Journal of clinical orthopaedics and trauma. 2016;7(3):157-63.
29. Damerau A, Pfeiffenberger M, Weber MC, Burmester GR, Buttgereit F, Gaber T, et al. A Human Osteochondral Tissue Model Mimicking Cytokine-Induced Key Features of Arthritis In Vitro. Int J Mol Sci. 2020;22(1).
30. Weber MC, Fischer L, Damerau A, Ponomarev I, Pfeiffenberger M, Gaber T, et al. Macroscale mesenchymal condensation to study cytokine-driven cellular and matrix-related changes during cartilage degradation. Biofabrication. 2020;12(4):045016.
31. Damerau A, Buttgereit F, Gaber T. Optimization of a Tricalcium Phosphate-Based Bone Model Using Cell-Sheet Technology to Simulate Bone Disorders. 2022;10(3):550.
32. Sundararajan R, Cuconati A, Nelson D, White E. Tumor necrosis factor-alpha induces Bax-Bak interaction and apoptosis, which is inhibited by adenovirus E1B 19K. J Biol Chem. 2001;276(48):45120-7.

33. Mirastschijski U, Lupse B, Maedler K, Sarma B, Radtke A, Belge G, et al. Matrix Metalloproteinase-3 is Key Effector of TNF-alpha-Induced Collagen Degradation in Skin. Int J Mol Sci. 2019;20(20).

34. Valin A, Del Rey MJ, Municio C, Usategui A, Romero M, Fernández-Felipe J, et al. IL6/sIL6R regulates TNFα-inflammatory response in synovial fibroblasts through modulation of transcriptional and post-transcriptional mechanisms. BMC Molecular and Cell Biology. 2020;21(1):74.

35. Ofek G, Revell CM, Hu JC, Allison DD, Grande-Allen KJ, Athanasiou KA. Matrix development in self-assembly of articular cartilage. PLoS One. 2008;3(7):e2795.

36. DeLise AM, Fischer L, Tuan RS. Cellular interactions and signaling in cartilage development. Osteoarthritis Cartilage. 2000;8(5):309-34.

37. Yoo JU, Barthel TS, Nishimura K, Solchaga L, Caplan AI, Goldberg VM, et al. The Chondrogenic Potential of Human Bone-Marrow-Derived Mesenchymal Progenitor Cells*. JBJS. 1998;80(12).

38. Duke J, Elmer W. Effect of brachypod mutation on cell adhesion and chondrogenesis in aggregates of mouse limb mesenchyme. J Embryol Exp Morph. 1977;42.

39. Duke J, Elmer WA. Cell adhesion and chondrogenesis in brachypod mouse limb mesenchyme: fragment fusion studies. J Embryol Exp Morphol. 1978;48:161-8.

40. Storm EE, Huynh TV, Copeland NG, Jenkins NA, Kingsley DM, Lee SJ. Limb alterations in brachypodism mice due to mutations in a new member of the TGF beta-superfamily. Nature. 1994;368(6472):639-43.

41. Grigull NP, Redeker JI, Schmitt B, Saller MM, Schonitzer V, Mayer-Wagner S. Chondrogenic Potential of Pellet Culture Compared to High-Density Culture on a Bacterial Cellulose Hydrogel. Int J Mol Sci. 2020;21(8).

42. Steinert AF, Ghivizzani SC, Rethwilm A, Tuan RS, Evans CH, Nöth U. Major biological obstacles for persistent cell-based regeneration of articular cartilage. Arthritis Res Ther. 2007;9(3):213.

43. Steinert AF, Weissenberger M, Kunz M, Gilbert F, Ghivizzani SC, Gobel S, et al. Indian hedgehog gene transfer is a chondrogenic inducer of human mesenchymal stem cells. Arthritis Res Ther. 2012;14(4):R168.

44. Steinert AF, Proffen B, Kunz M, Hendrich C, Ghivizzani SC, Nöth U, et al. Hypertrophy is induced during the in vitrochondrogenic differentiation of human mesenchymal stem cells by bone morphogenetic protein-2 and bone morphogenetic protein-4 gene transfer. Arthritis Research & Therapy. 2009;11(5):R148.

45. Trowe M-O, Shah S, Petry M, Airik R, Schuster-Gossler K, Kist R, et al. Loss of Sox9 in the periotic mesenchyme affects mesenchymal expansion and differentiation, and epithelial morphogenesis during cochlea development in the mouse. Developmental Biology. 2010;342(1):51-62.

46. Pelttari K, Steck E, Richter W. The use of mesenchymal stem cells for chondrogenesis. Injury. 2008;39 Suppl 1:S58-65.

47. Zhang L, Su P, Xu C, Yang J, Yu W, Huang D. Chondrogenic differentiation of human mesenchymal stem cells: a comparison between micromass and pellet culture systems. Biotechnology Letters. 2010;32(9):1339-46.

48. Kafienah W, Mistry S, Dickinson SC, Sims TJ, Learmonth I, Hollander AP. Three-dimensional cartilage tissue engineering using adult stem cells from osteoarthritis patients. Arthritis Rheum. 2007;56(1):177-87.

49. Pap T, Korb-Pap A. Cartilage damage in osteoarthritis and rheumatoid arthritis—two unequal siblings. Nature Reviews Rheumatology. 2015;11(10):606-15.

50. Yang H, Zhang M, Wang X, Zhang H, Zhang J, Jing L, et al. TNF Accelerates Death of Mandibular Condyle Chondrocytes in Rats with Biomechanical Stimulation-Induced Temporomandibular Joint Disease. PloS one. 2015;10(11):e0141774-e.

51. Matsuo M, Nishida K, Yoshida A, Murakami T, Inoue H. Expression of caspase-3 and -9 relevant to cartilage destruction and chondrocyte apoptosis in human osteoarthritic cartilage. Acta medica Okayama. 2001;55(6):333-40.

52. Zhao X, Bausano B, Pike BR, Newcomb-Fernandez JK, Wang KK, Shohami E, et al. TNF-alpha stimulates caspase-3 activation and apoptotic cell death in primary septo-hippocampal cultures. J Neurosci Res. 2001;64(2):121-31.

53. Ohashi Y, Takahashi N, Terabe K, Tsuchiya S, Kojima T, Knudson CB, et al. Metabolic reprogramming in chondrocytes to promote mitochondrial respiration reduces downstream features of osteoarthritis. Sci Rep. 2021;11(1):15131.

54. Zheng L, Zhang Z, Sheng P, Mobasheri A. The role of metabolism in chondrocyte dysfunction and the progression of osteoarthritis. Ageing Res Rev. 2021;66:101249.

55. Nagase H, Woessner JFJTJoBC. Matrix Metalloproteinases*. 1999;274:21491 - 4.

56. Shi L, Liang T, Yang F, Zhu F-F, Liu J, Jiang J-Q, et al. Matrix Metalloproteinase-3 induces proteoglycan degradation in gouty arthritis model. Gene. 2021;765:145120.

57. Wang M, Sampson ER, Jin H, Li J, Ke QH, Im H-J, et al. MMP13 is a critical target gene during the progression of osteoarthritis. Arthritis Research & Therapy. 2013;15(1):R5.

58. Wu W, Billinghurst RC, Pidoux I, Antoniou J, Zukor D, Tanzer M, et al. Sites of collagenase cleavage and denaturation of type II collagen in aging and osteoarthritic articular cartilage and their relationship to the distribution of matrix metalloproteinase 1 and matrix metalloproteinase 13. Arthritis Rheum. 2002;46(8):2087-94.

59. Wu H, Du J, Zheng Q. Expression of MMP-1 in cartilage and synovium of experimentally induced rabbit ACLT traumatic osteoarthritis: immunohistochemical study. Rheumatology International. 2008;29(1):31.

60. Moldovan F, Pelletier JP, Hambor J, Cloutier JM, Martel-Pelletier J. Collagenase-3 (matrix metalloprotease 13) is preferentially localized in the deep layer of human arthritic cartilage in situ: in vitro mimicking effect by transforming growth factor beta. Arthritis Rheum. 1997;40(9):1653-61.

61. Ra H-J, Parks WC. Control of matrix metalloproteinase catalytic activity. Matrix Biol. 2007;26(8):587-96.

62. Troeberg L, Nagase H. Proteases involved in cartilage matrix degradation in osteoarthritis. Biochimica et biophysica acta. 2012;1824(1):133-45.

63. Lai Y, Yu XP, Zhang Y, Tian Q, Song H, Mucignat MT, et al. Enhanced COMP catabolism detected in serum of patients with arthritis and animal disease models through a novel capture ELISA. Osteoarthritis and Cartilage. 2012;20(8):854-62.

64. Gagarina V, Carlberg AL, Pereira-Mouries L, Hall DJ. Cartilage oligomeric matrix protein protects cells against death by elevating members of the IAP family of survival proteins. J Biol Chem. 2008;283(1):648-59.

65. Tseng S, Reddi AH, Di Cesare PE. Cartilage Oligomeric Matrix Protein (COMP): A Biomarker of Arthritis. Biomark Insights. 2009;4:33-44.

66. Li H, Haudenschild DR, Posey KL, Hecht JT, Di Cesare PE, Yik JH. Comparative analysis with collagen type II distinguishes cartilage oligomeric matrix protein as a primary TGFβ-responsive gene. Osteoarthritis Cartilage. 2011;19(10):1246-53.

67. Wu L, Chen H, Chen Y, Wang B. [Effects of TNF-alpha on IL-8 mRNA expression in endothelial cells]. Sheng wu yi xue gong cheng xue za zhi = Journal of biomedical engineering = Shengwu yixue gongchengxue zazhi. 2001;18(1):105-7, 10.

68. Namba S, Nakano R, Kitanaka T, Kitanaka N, Nakayama T, Sugiya H. ERK2 and JNK1 contribute to TNF-alpha-induced IL-8 expression in synovial fibroblasts. PLoS One. 2017;12(8):e0182923.

69. Hasan A, Akhter N, Al-Roub A, Thomas R, Kochumon S, Wilson A, et al. TNF-α in Combination with Palmitate Enhances IL-8 Production via The MyD88- Independent TLR4 Signaling Pathway: Potential Relevance to Metabolic Inflammation. International journal of molecular sciences. 2019;20(17):4112.

70. Dhanasekaran DN, Reddy EP. JNK signaling in apoptosis. Oncogene. 2008;27(48):6245-51.

71. Pearson MJ, Herndler-Brandstetter D, Tariq MA, Nicholson TA, Philp AM, Smith HL, et al. IL-6 secretion in osteoarthritis patients is mediated by chondrocyte-synovial fibroblast cross-talk and is enhanced by obesity. Scientific reports. 2017;7(1):3451-.

72. Jiao Z, Wang W, Ma J, Wang S, Su Z, Xu H. Notch signaling mediates TNF-α-induced IL-6 production in cultured fibroblast-like synoviocytes from rheumatoid arthritis. Clinical & developmental immunology. 2012;2012:350209.

73. Yokota K, Miyazaki T, Hirano M, Akiyama Y, Mimura T. Simvastatin inhibits production of interleukin 6 (IL-6) and IL-8 and cell proliferation induced by tumor necrosis factor-alpha in fibroblast-like synoviocytes from patients with rheumatoid arthritis. J Rheumatol. 2006;33(3):463-71.

11 Figures

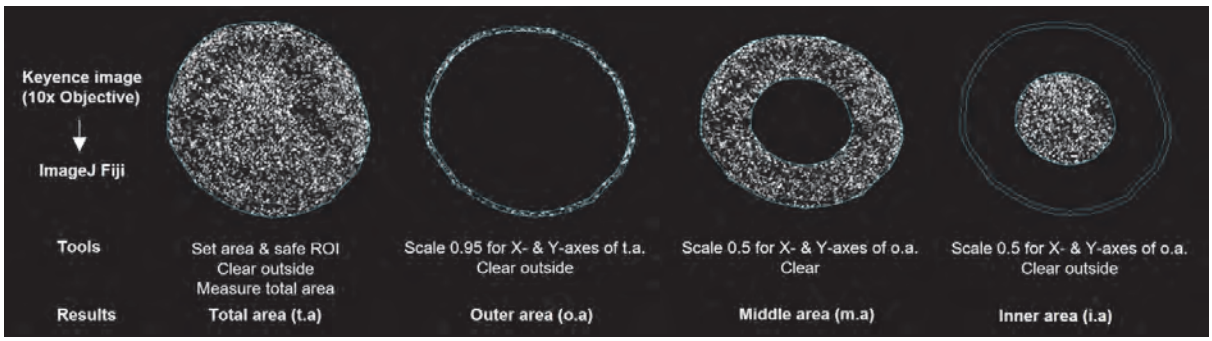

Figure 1: Image analysis pipeline using FIJI ImageJ.

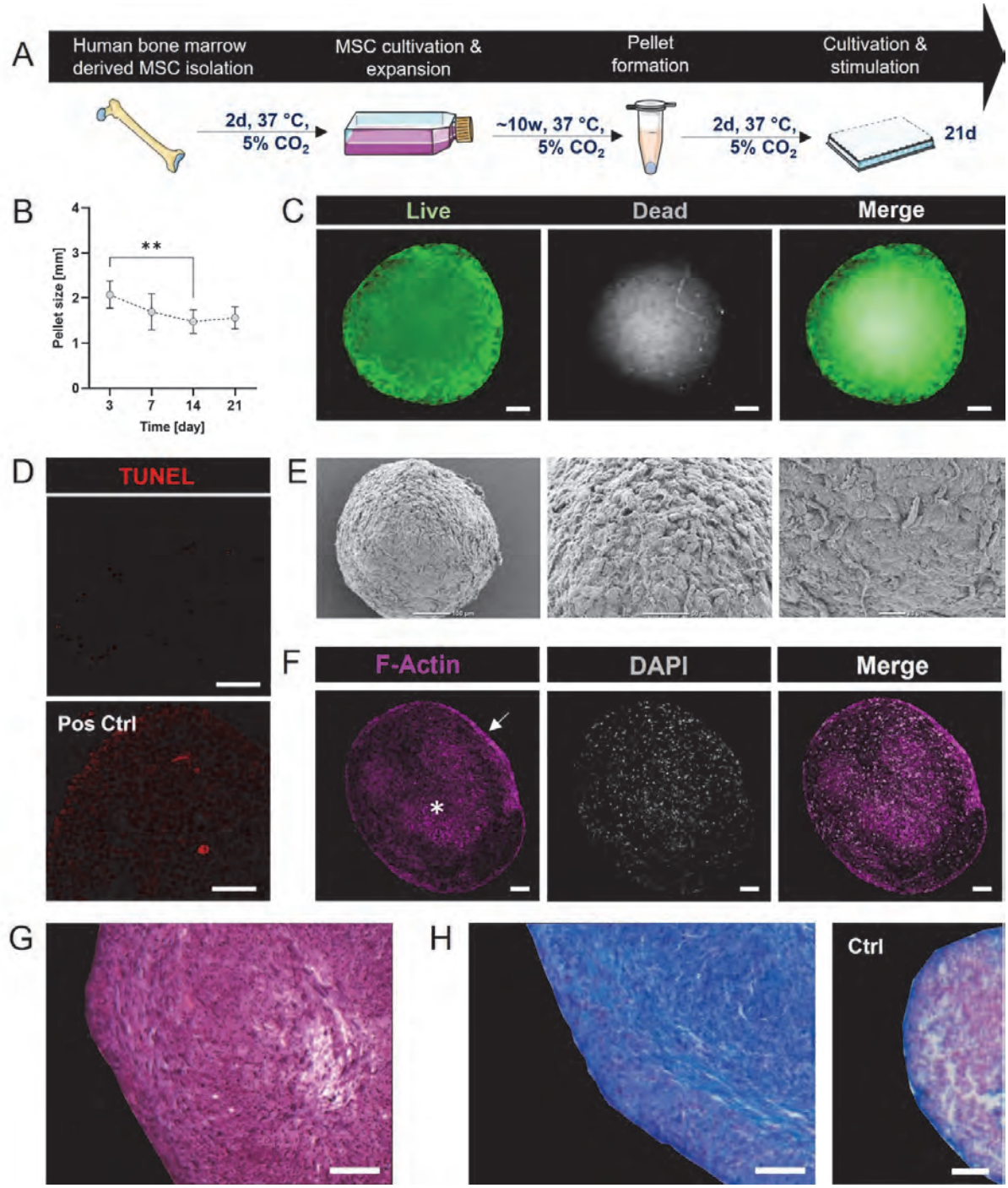

Figure 2: The formation of MSC-based *in vitro* 3D scaffold-free cartilage-like constructs (miniSFCCs). (A) Schematic overview of the experimental procedure of miniSFCC formation. MSCs at a density of 2×10^5 formed a pellet culture within 48 h and were then transferred to a U-bottom 96-well plate. **(B)** Diameter of miniSFCCs during a 3-week culture analyzed using ImageJ. Data are shown as dot plots (error bars ± SD for n=4; duplicates). **(C)** Representative images of LIVE/DEAD staining on day 21. Living cells are presented in green (Calcein-AM+) and dead cells in grey (EthD+), n=6. **(D)** Detection of apoptotic cells (red) using TUNEL staining. Pos Ctrl = 10 min DNase I (n=6). **(E)**

Microscale *in vitro* cartilage breakdown

Exemplary SEM images at three magnifications (scale bars show 100, 50, and 20 µm) highlighting cell formation and ECM content on day 21. **(F)** Immunofluorescence staining for F-actin (magenta) and DAPI (grey) to visualize cell morphology and spatial distribution (n=5). **(G)** Hematoxylin and eosin staining, demonstrating a cell-dense SFCC, with the outer zone showing the most elevated cell density. **(H)** MSC-based miniSFCCs after 21 days of chondrogenic differentiation compared with an undifferentiated control for alcian blue with nuclear fast red staining. Scale bars show 100 µm. Legend: asterisk = highlighting round cells; arrow = highlighting elongated cells. Statistics: Friedman with Dunn's multiple comparisons test, p-values are shown in the graphs with **p <0.01.

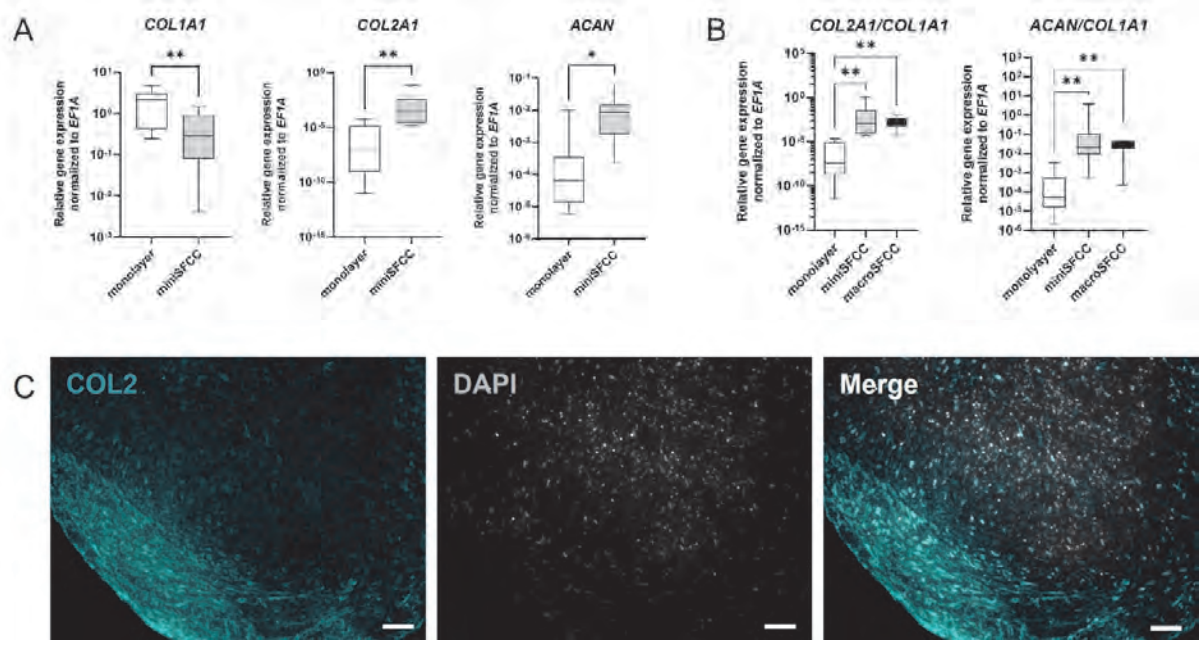

Figure 3: Mesenchymal condensation resulted in a sustained chondrogenic phenotype independent of model scaling. (A) Relative expression of chondrogenic marker genes. Total RNA extraction was performed on day 21. Data are normalized to the housekeeping gene *EF1A* (n=8). **(B)** The ratio of relative gene expression of *COL2A1* and *ACAN* to *COL1A1* normalized to *EF1A* (n=6-8). **(C)** Representative images for collagen type 2 (COL2; cyan) and DAPI (grey) staining. The scale bar shows 100 µm. Data are shown as box plots (centerline, median; box limits, upper and lower quartiles; whiskers, maximum and minimum values). Statistics: Two-tailed Wilcoxon matched-pairs signed-rank test for data in (A) and Kruskal-Wallis with Dunn's multiple comparisons test in (B). Significances are indicated in the graphs with *p <0.05, **p <0.01.

Microscale *in vitro* cartilage breakdown

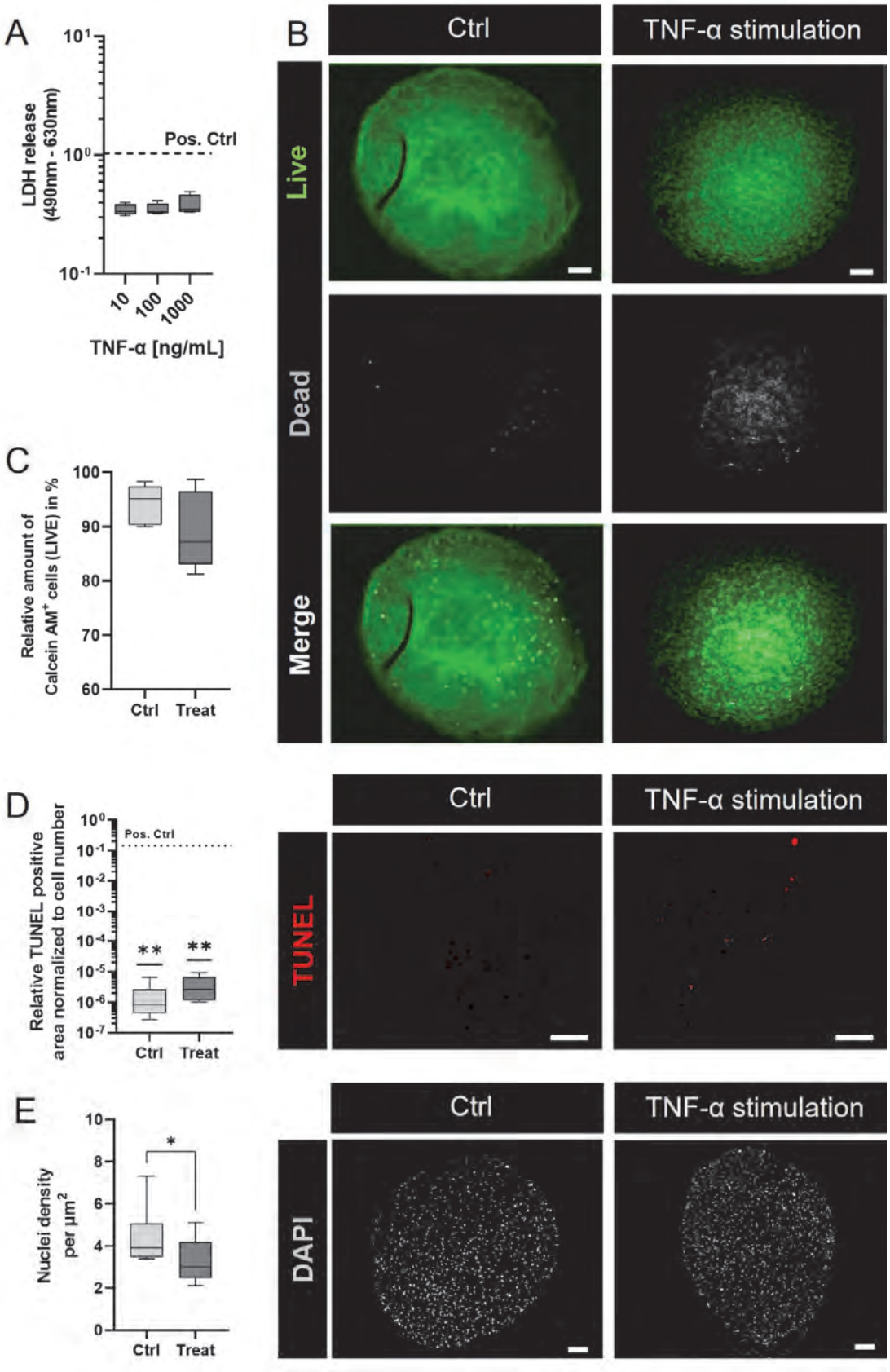

21

Figure 4: Short-term exposure of miniSFCCs to 100 ng/mL TNF-α for three days induced apoptosis. (A) LDH-assay was performed after 24 h to cover any cytotoxic effects using supernatant from the miniSFCCs treated with TNF-α at 10, 100, and 1000 ng/mL (n=4); pos Ctrl = 4% (v/v) Triton™ X-100. **(B)** LIVE/DEAD staining - Calcein AM (green, alive) and EthD (grey, dead) - was performed after 21 days and **(C)** quantified using ImageJ (n=8). **(D)** TUNEL staining to visualize apoptotic cells (red). Quantified using ImageJ and normalized to the cell number (DAPI staining). Exemplary images for n=8. Pos. Ctrl = 10 min DNase I. **(E)** Nuclei density in µm² was quantified using ImageJ (n=6). Data are shown in box plots (centerline, median; box limits, upper and lower quartiles; whiskers, maximum and minimum values). Statistics: Two-tailed Wilcoxon matched-pairs signed-rank test (C, D, and E) and Wilcoxon signed-rank test to the ctrl (B and D); p-values are shown in the graphs with *p <0.05 and **p <0.01.

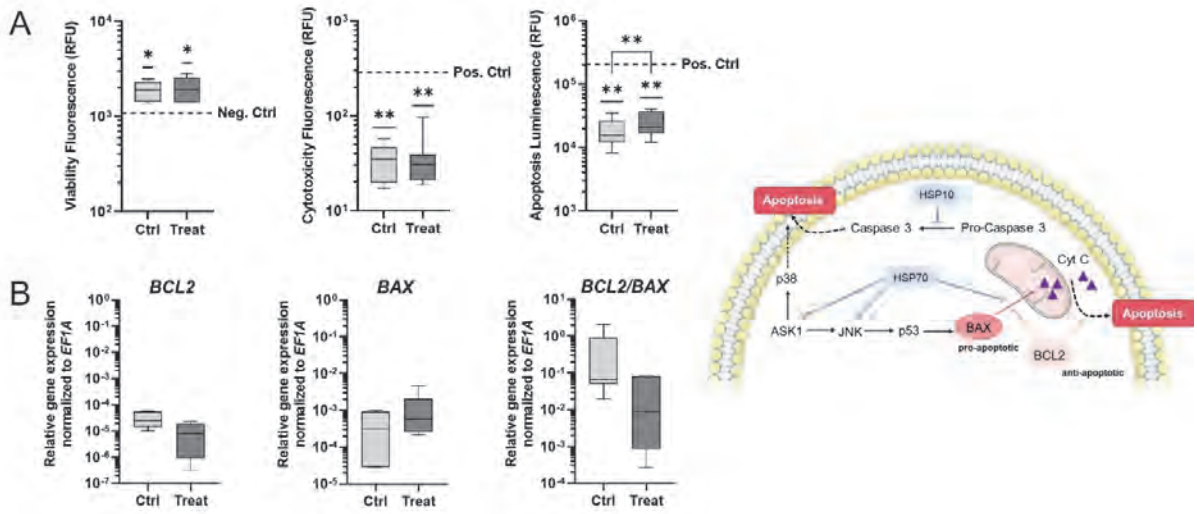

Figure 5: TNF-α induced programmed cell death (apoptosis). (A) ApoTox-Glo™ Assay analyzing cell viability, cytotoxicity, and apoptosis level for n=8. Neg. Ctrl for viability: 100 µg/mL Digitonin; Pos. Ctrl for cytotoxicity: 4% Triton™ X-100; Pos. Ctrl for apoptosis: 0.1 mM Camptothecin. **(B)** Gene expression of *BCL2* and *BAX* normalized to the housekeeping gene *EF1A* (n=6). Data are shown as box plots (centerline, median; box limits, upper and lower quartiles; whiskers, maximum and minimum values). Statistics: Two-tailed Wilcoxon matched-pairs signed-rank test and Wilcoxon signed-rank test to the ctrl; p-values are indicated in the graphs with *p <0.05 and **p <0.01. The figure contains graphics from Servier Medical Art, licensed under a Creative Common Attribution 3.0 Generic License. http://smart.servier.com/.

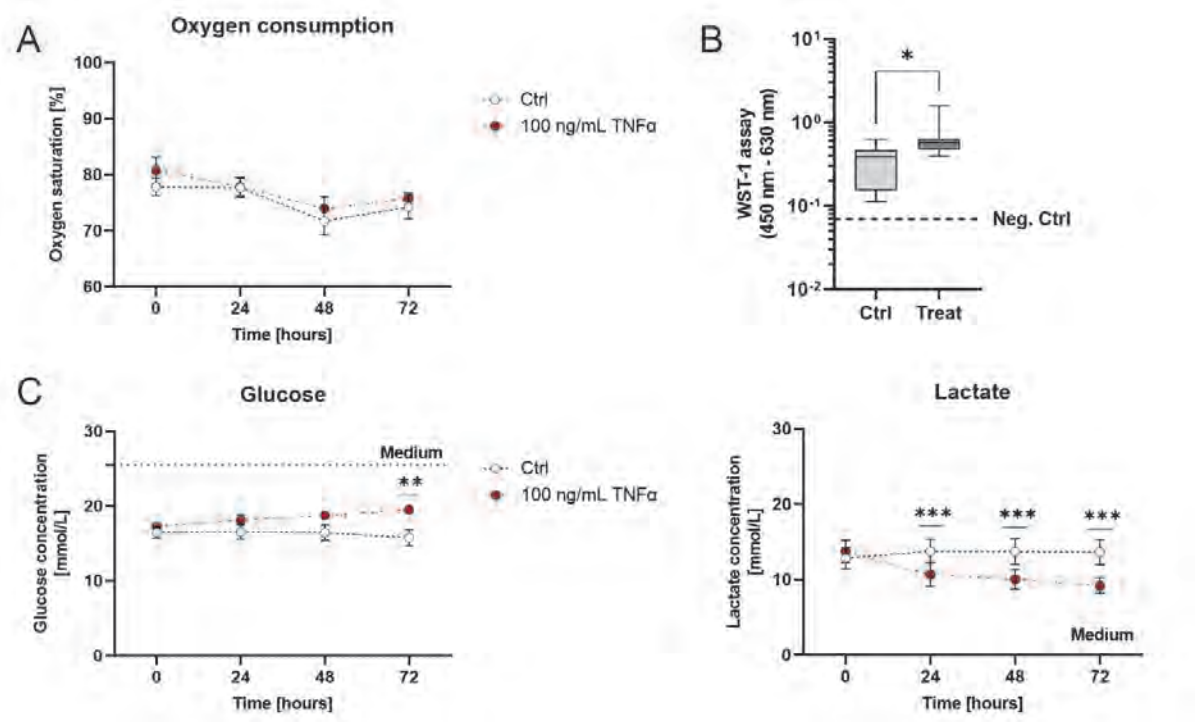

Figure 6: TNF-α did not affect oxygen consumption but reduced glycolysis within three days. (A) Daily measurement of oxygen consumption using a Clark electrode (n=12). **(B)** WST-1 Assay was performed on day 21 without and with three days of TNF-α stimulation (n=8). The NADPH-dependent formazan production was measured at 450 nm (reference wavelength: 630 nm). Neg. Ctrl: treatment with 4% Triton™ X-100 for 24 h. **(C)** Glucose and lactate concentration [mmol/L] within the supernatant was measured using the Biosen C-line analyzer (n=12). Medium line: Glucose and lactate concentration within the cell-free culture medium. A and C are shown as dot plots (error bars ± SEM). Data of B are shown as box plots (centerline, median; box limits, upper and lower quartiles; whiskers, maximum and minimum values). Statistics: Mixed-effect analysis with Šídák's multiple comparisons test (A and C) and Two-tailed Wilcoxon matched-pairs signed-rank test (B). P-values are indicated in the graphs with *p <0.05 and **p <0.01.

Microscale *in vitro* cartilage breakdown

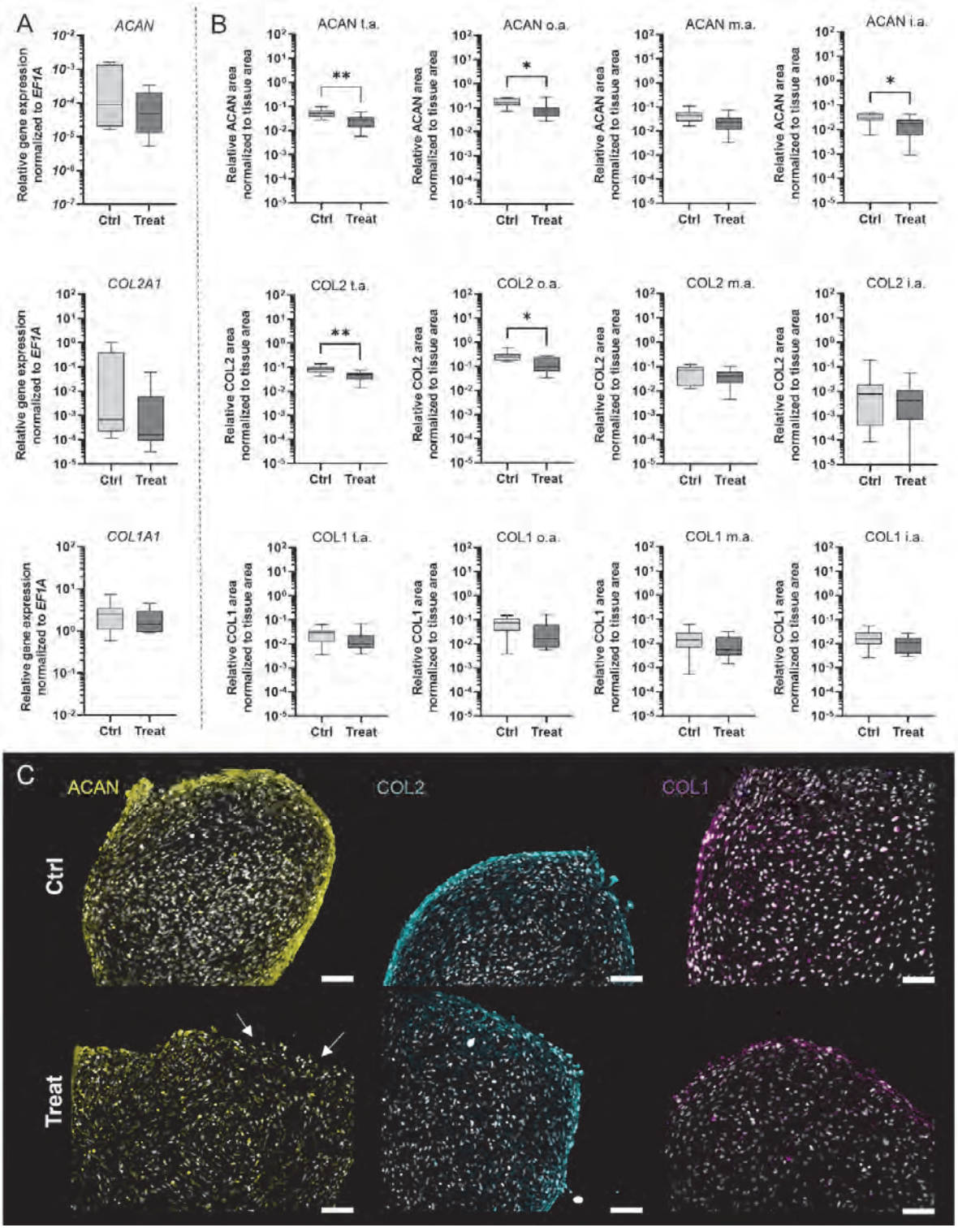

Figure 7: Protein and gene expression profile of miniSFCCs stimulated with TNF-α simulating the pathophysiology of arthritis. (A) Total RNA extraction was performed from miniSFCCs. Gene expression of chondrogenic markers such as aggrecan (*ACAN*), collagen type 2 alpha 1 (*COL2A1*), and type 1 (*COL1A1*) was performed using SYBR Green and normalized to the housekeeping gene *EF1A*

(n=7). **(B)** Image quantification was performed to determine the stained area normalized to the tissue area (duplicates per data point) using ImageJ (n=9). **(C)** Exemplary images for ACAN (yellow), COL2 (cyan), COL1 (magenta), and DAPI (gray) are shown. Arrow indicates alterations in the outer area. Scale bars show 100 µm. Data are shown as box plots (center centerline, median; box limits, upper and lower quartiles; whiskers, maximum and minimum values). Statistics: Two-tailed Mann-Whitney U test; p-values are indicated in the graphs with *p <0.05, **p <0.01.

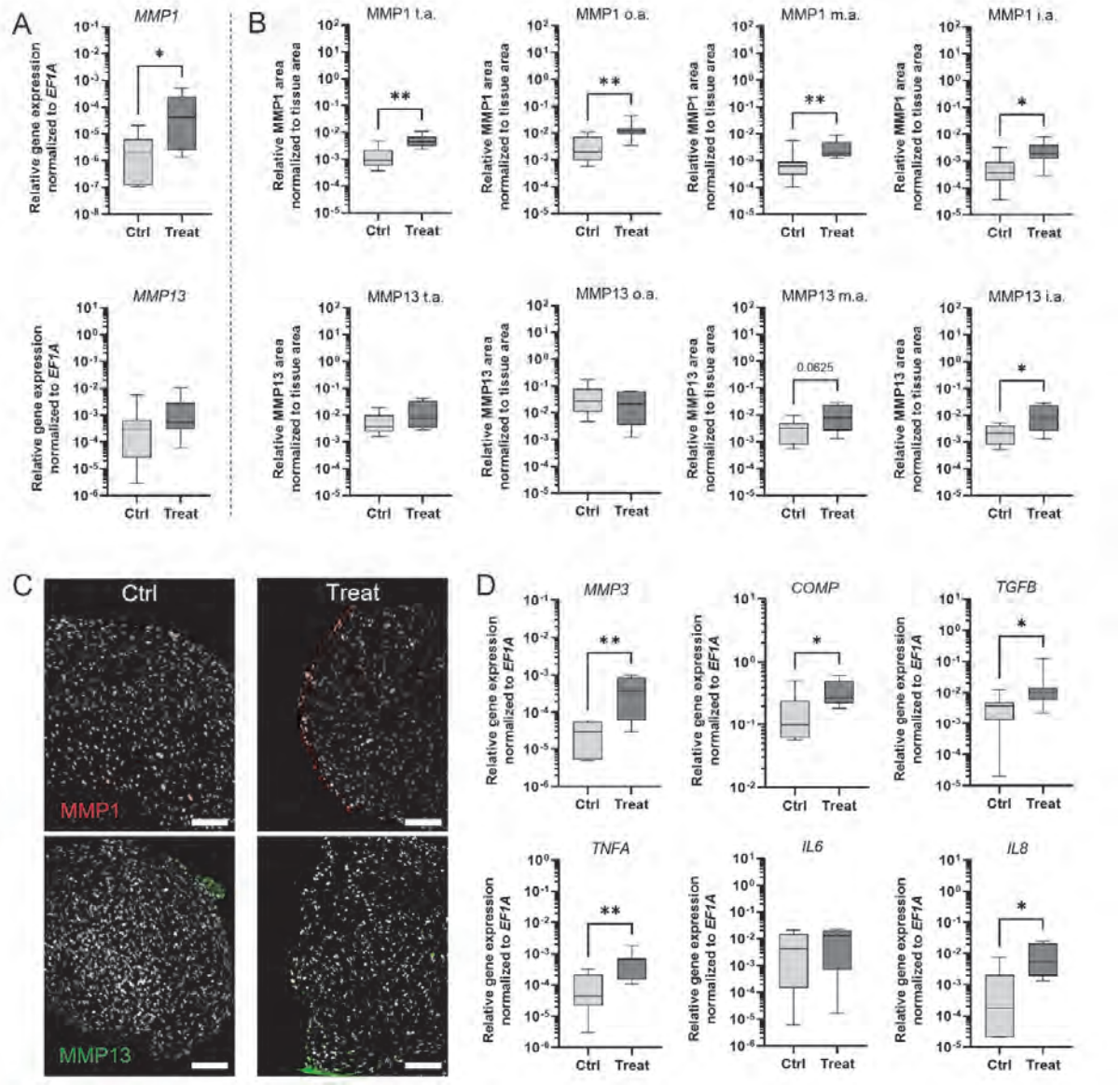

Figure 8: Profile of MMPs and proinflammatory cytokines after TNF-α simulation. (A) Relative gene expression of matrix metalloproteases (MMPs) normalized to the housekeeping gene *EF1A* (n=7). **(B)** Image quantification was performed to determine the stained area normalized to the tissue area

using ImageJ (n=9). **(C**) Exemplary images for MMP1 (red), MMP13 (green), and DAPI (gray) are shown. Scale bars show 100 µm. **(D)** mRNA expression of proinflammatory cytokines normalized to the housekeeper gene *EF1A* (n=7). Data are shown as box plots (center centerline, median; box limits, upper and lower quartiles; whiskers, maximum and minimum values). Statistics: Two-tailed Mann-Whitney U test; p-values are indicated in the graphs with *p <0.05, **p <0.01.

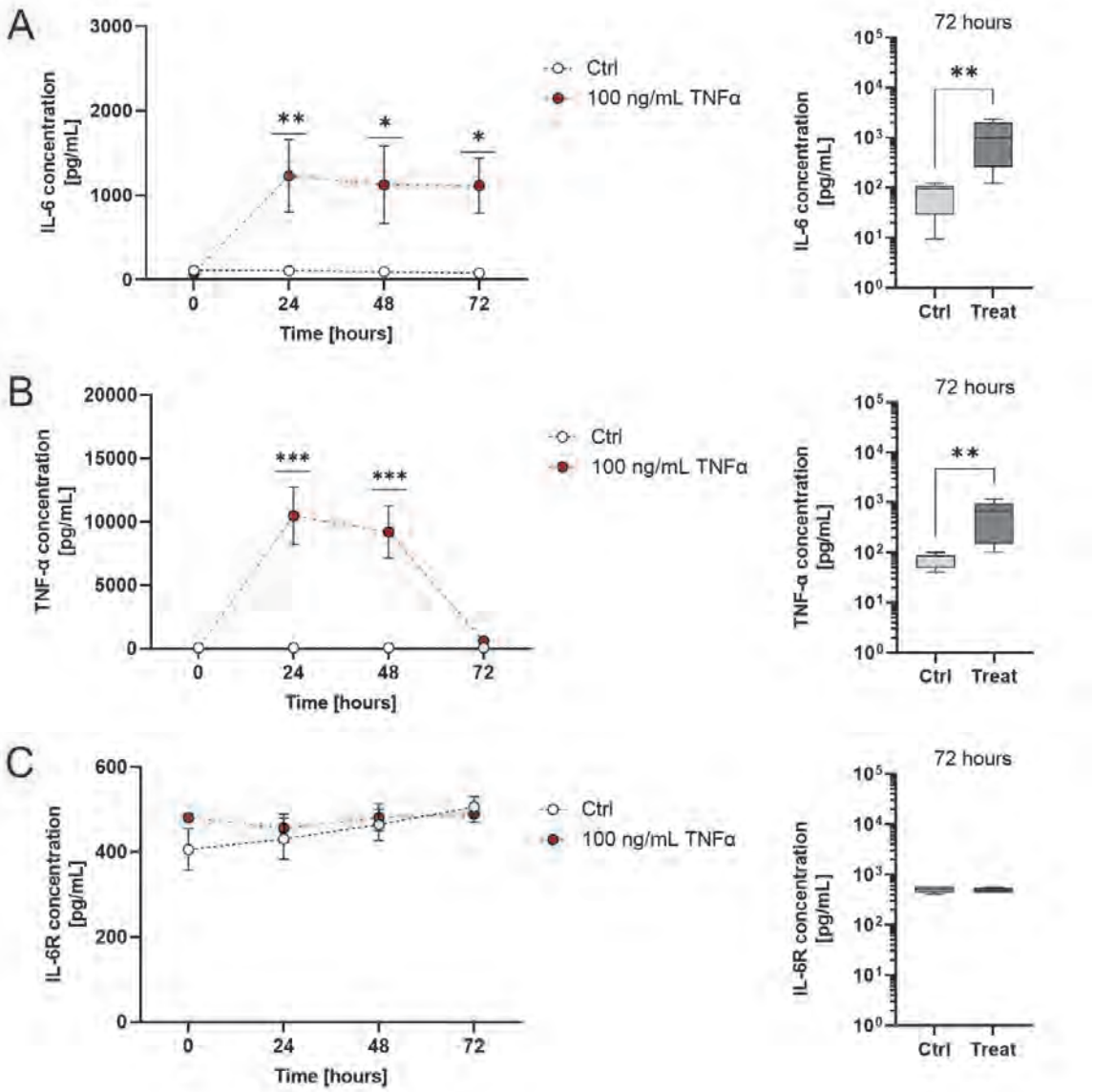

Figure 9: Cytokine levels comparing a healthy, unstimulated, and arthritic, TNF-stimulated environment. (A) Quantification of soluble IL-6, **(B)** TNF-α, and **(C)** IL-6R (n=6-8). Data are shown as dot plots (error bars ± SEM) and box plots (center centerline, median; box limits, upper and lower quartiles; whiskers, maximum and minimum values). Statistics: Mixed-effect analysis with Šídák's multiple comparisons test and two-tailed Wilcoxon matched-pairs signed-rank test; p-values are indicated in the graphs with *p <0.05, **p <0.01, ***p <0.001.

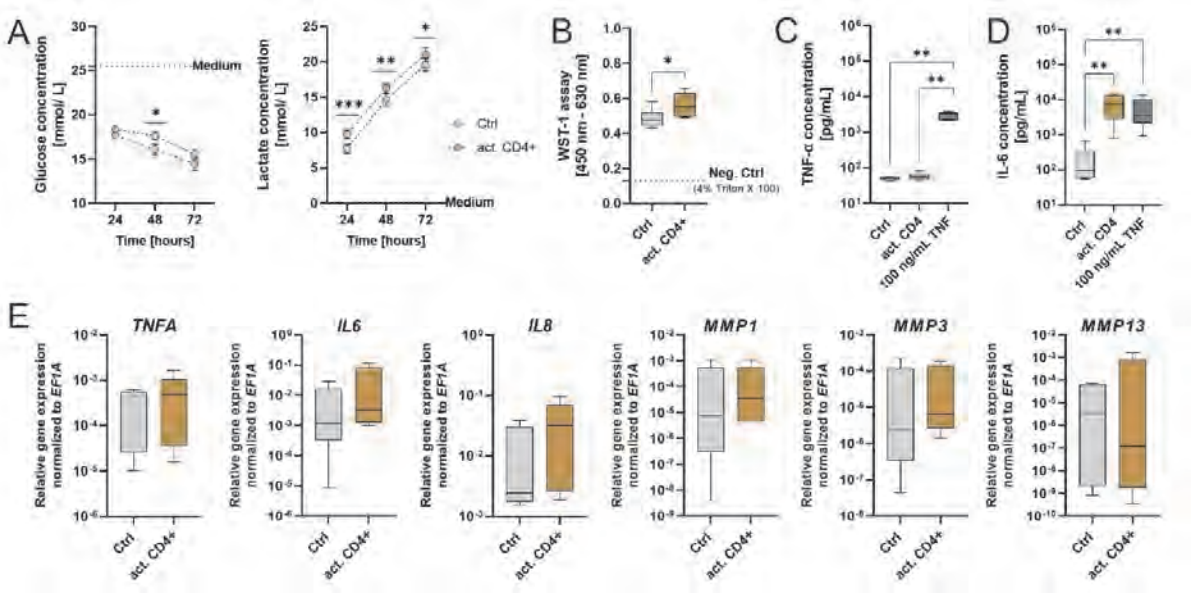

Figure 10: Short-term stimulation with activated CD4+ Th cell-induced IL-6 secretion and metabolic response of the miniSFCCs. (A) Glucose and lactate concentration [mmol/L] within the supernatant was measured using the Biosen C-line analyzer. Medium line: Glucose and lactate concentration within the cell-free culture medium (n=6). **(B)** WST-1 Assay was performed after 72 h (n=6). The NADPH-dependent formazan production was measured at 450 nm (reference wavelength: 630 nm). Neg. Ctrl: treatment with 4% Triton^{TM} X-100 for 24 h. **(C)** Quantification of TNF-α and **(D)** soluble IL-6 after 72 h (n=6). **(E)** Relative gene expression normalized to the housekeeping gene *EF1A* (n=5). Data are shown as dot plots (error bars ± SEM) and box plots (center centerline, median; box limits, upper and lower quartiles; whiskers, maximum and minimum values). Statistics: Mixed-effect analysis with Šídák's multiple comparisons test (A), Mann-Whitney U test (B-E); p-values are indicated in the graphs with *p <0.05, **p <0.01, ***p <0.001.

12 Tables

Table 1: MSC information and conducted experiments.

Donor	Age	Gender		Type of experiment
1	84	f	miniSFCCs characterization	Gene expression, SEM, histology
2	71	f		Gene expression, SEM, histology
3	66	m		Gene expression, SEM, histology, LIVE DEAD & TUNEL staining
4	59	f		Gene expression, SEM, histology, LIVE DEAD & TUNEL staining
5	79	m		Gene expression, histology, LIVE DEAD & TUNEL staining
6	78	m		Gene expression, histology, LIVE DEAD & TUNEL staining
7	64	m		Gene expression, histology, LIVE DEAD & TUNEL staining
8	67	w		Gene expression, histology, LIVE DEAD & TUNEL staining
9	72	w	Stimulated miniSFCCs	Gene expression, histology, pO_2, glucose & lactate, WST-1
10	76	w		Gene expression, histology, pO_2, glucose & lactate, WST-1
11	57	m		Gene expression, histology, pO_2, glucose & lactate, WST-1
12	86	f		Gene expression, histology, pO_2, glucose & lactate, WST-1
13	82	f		Gene expression, histology, pO_2, glucose & lactate, WST-1, ELISA
14	58	m		Gene expression, histology, pO_2, glucose & lactate, WST-1, ELISA
15	46	f		Gene expression, histology, pO_2, glucose & lactate, WST-1, ELISA
16	78	m		Gene expression, histology, pO_2, glucose & lactate, WST-1, ELISA
17	74	w		Histology, pO_2, glucose & lactate, ELISA,
18	70	m		Histology, pO_2, glucose & lactate, ELISA
19	56	w		Histology, pO_2, glucose & lactate, ELISA
20	73	w		Histology, pO_2, glucose & lactate, ELISA

Table 2: List of antibodies, kits, and staining solutions.

Description	Dye	Host	Working concentration	Manufacturer
Immunofluorescence antibodies				
DAPI		-	1 µg/mL	German Rheumatism Research Center
Phalloidin	TRITC	-	50 µg/mL	Sigma-Aldrich
Aggrecan	-	rabbit	5 µg/mL	
Collagen I	-	mouse	6 µg/mL	Abcam
Collagen II	-	rabbit	10 µg/mL	
MMP1	-	mouse	#MA5-15872 1:200	Invitrogen / Thermo Fisher Scientific
MMP13	-	mouse	1 µg/mL	
anti-mouse IgG (H+L)	A594	goat	2 µg/mL	Abcam
anti-rabbit IgG (H+L)	A488	donkey	4 µg/mL	
anti-rabbit IgG (H+L)	A546	goat	4 µg/mL	Invitrogen / Thermo Fisher Scientific
anti-mouse IgG (H+L)	A546	goat	4 µg/mL	
anti-rat IgG (H+L)	A647	goat	4 µg/mL	
Kits and solutions				
LIVE/DEAD® Viability/Cytotoxicity	2 µM Calcein AM, 4 µM EthD-1			Invitrogen / Thermo Fisher Scientific
TUNEL staining kit	5 µL enzyme + 45 µL TUNEL label			Sigma-Aldrich
FluoroMount-G™	Mounting slides for immunofluorescence			
Tween® 20	0.1% for permeabilization			Qbiogene Inc.

Table 3: Sequences of primers used for qPCR.

Gene	Gene name	Sequence of the forward primer	Sequence of the reverse primer
ACAN	Aggrecan	AACGCAGACTACAGAAGCGG	GGCGGACAAATTAGATGCGG
BAX	Bcl-2-associated X protein	TCTGACGGCAACTTCAACTG	ACAGGGACATCAGTCGCTTC
BCL2	B-cell lymphoma 2	GGGATTCCTGCGGATTGACA	GTCTACTTCCTCTGTGATGTTGTA
COL1A1	Collagen type 1 α 1	CAGCCGCTTCACCTACAGC	TTTTGTATTCAATCACTGTCTTGCC
COL2A1	Collagen type 2 α 1	GTGGGGCAAGACTGTTATCG	AGGTCAGGTCAGCCATTCAG
COMP	Cartilage oligomeric matrix protein	CCGTAAGGACAACTGCGTGA	ACTTGTCCTCGTCCGTGTTG
EF1A	Elongation factor 1-α	TGTGCTGTCCTGATTGTTGC	GTAGGGTGGCTCAGTGGAAT
IL6	Interleukin-6	TACCCCCAGGAGAAGATTCC	TTTTCTGCCAGTGCCTCTTT
IL8	Interleukin-8	GAATGGGTTTGCTAGAATGTGATA	CAGACTAGGGTTGCCAGATTTAAC
MMP1	Matrix metalloproteinase 1	CTCTGGAGTAATGTCACACCTCT	TGTTGGTCCACCTTTCATCTTC
MMP13	Matrix metalloproteinase 13	TCCTGATGTGGGTGAATACAATG	GCCATCGTGAAGTCTGGTAAAAT
MMP3	Matrix metalloproteinase 3	ATCCTACTGTTGCTGTGCGT	CATCACCTCCAGAGTGTCGG
TGFB	Transforming growth factor-β	CTAATGGTGGAAACCCACAACG	TATCGCCAGGAATTGTTGCTG
TNFA	Tumor necrosis factor α	GTCTCCTACCAGACCAAG	CAAAGTAGACCCTGCCCAGACTC

frontiers

Supplementary Material

1 Supplementary Figures

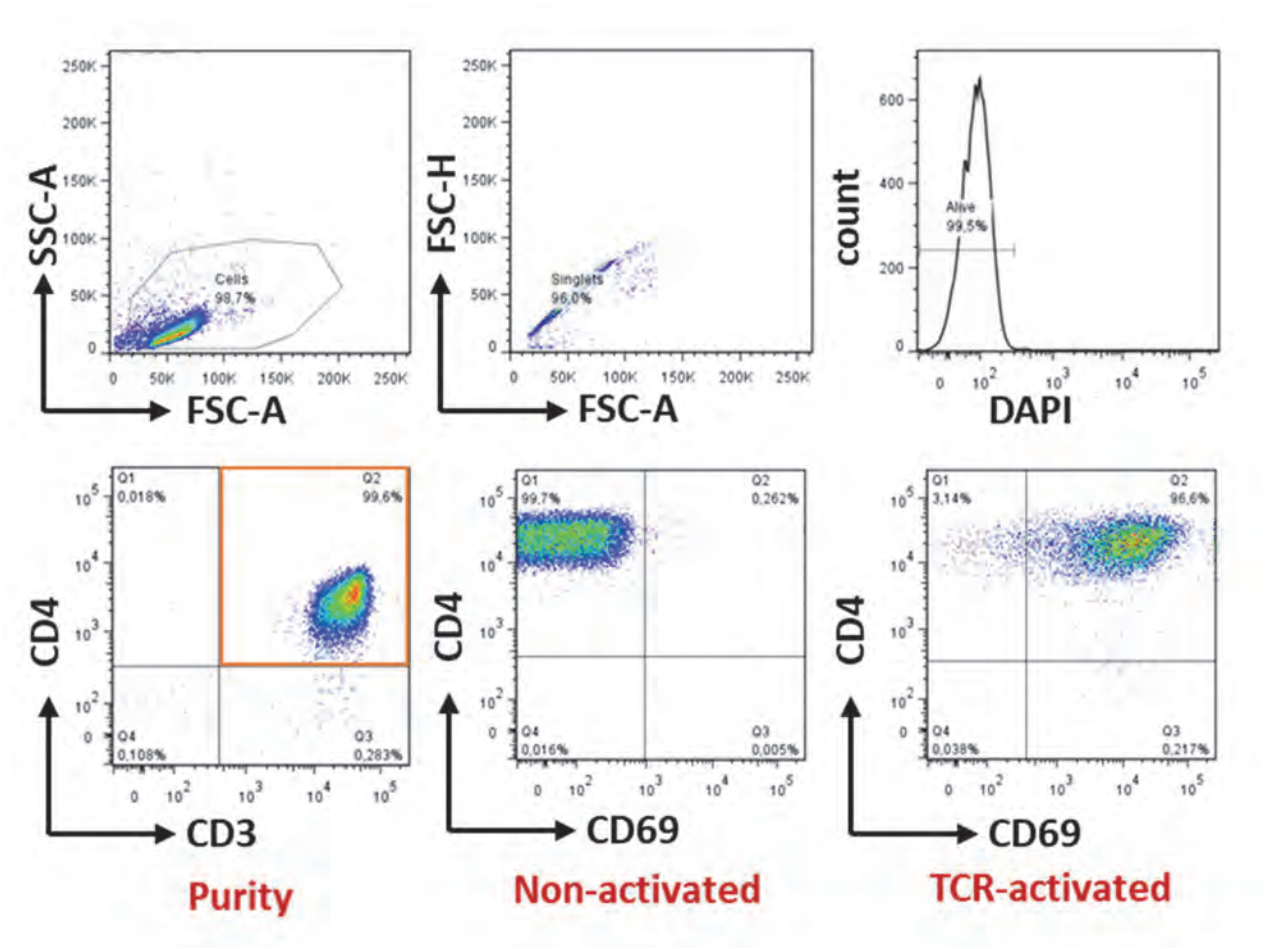

Supplementary Figure 1: Flow cytometric characterization of the purity of isolated CD4 T helper cells. Cells were gated using a forward-scatter and side-scatter plot. Doublets were excluded according to the side-scatter area and height pattern. Purity was analyzed by CD3/CD4, and cell activation by CD69 staining using the MACSQuant® Analyzer 10.

3.3. Part III: The complementary building block – the synovial membrane

Rheumatoid arthritis is maintained by three distinct pathomechanisms: (i) autoimmunological persistent synovitis, (ii) joint destruction by tumor-like proliferation of synovial tissue (pannus formation), and (iii) progressive extra-articular destruction (Burmester, Feist et al. 2014, Smolen, Aletaha et al. 2018). In recent years, fibroblasts, which physiologically maintain the structural and dynamic integrity of joints, have been identified as key drivers in disease pathogenesis because of their unexpected complexity in phenotype and function (Mizoguchi, Slowikowski et al. 2018, Stephenson, Donlin et al. 2018, Cai, Ming et al. 2019, Zhang, Wei et al. 2019, Wei, Korsunsky et al. 2020). Moreover, the extent of synovitis may appear almost indistinguishable between OA and RA tissues, while RA is associated with systemic autoimmune-mediated inflammation (Zhang, Wei et al. 2019, Sanchez-Lopez, Coras et al. 2022).

So far, only few tissue-engineered human *in vitro* synovial membrane models have been developed to mimic synovitis (Kiener, Watts et al. 2010, Broeren, Waterborg et al. 2019). Moreover, these models are mainly based on RA-FLSs or OA-FLSs combined with animal-derived Matrigel™ (Kiener, Watts et al. 2010, Karonitsch, Beckmann et al. 2018, Broeren, Waterborg et al. 2019). These models apparently do not reflect the physiological or 'healthy' state of the synovial membrane. To study the (i) pathophysiologically altered processes of synovitis compared to the 'healthy' state, (ii) overcome species-specific differences, (iii) improve transferability by using appropriate human cells, and (iv) test novel therapeutic approaches, including biologics *in vitro*, human-centered approaches to mimic the synovial membrane are required.

The synovial membrane consists of the lining and sublining layer. The former is one to four cell layers thick and is in constant contact with the intraarticular cavity (Smith 2011). Hence, a human-based synovial membrane model based on a synthetic hydrogel as the final component of an artificial joint was generated. To confirm MSCs as an optimal cell source to mimic quiescent non-inflamed FLSs they were evaluated for their phenotypic properties compared to trauma-FLSs.

3.3.1. Manuscript 4: A functional xeno-free 3D synovial membrane model to study synovitis *in vitro*

The following manuscript has been drafted.

Authors: Alexandra Damerau, Marieluise Kirchner, Julia Beißel, Moritz Pfeiffenberger, Philipp Mertins, Frank Buttgereit, Timo Gaber

Title: A functional xeno-free 3D synovial membrane model to study synovitis *in vitro*

Personal contribution: In this manuscript, I was responsible for conceptualizing, planning, preparing, conducting, analyzing and interpreting the experiments including the isolation expansion and characterization of MSCs and synovial fibroblasts from trauma and OA patients, analyzing the CTGF-induced MSC differentiation, generation and characterization of synovial membrane equivalents, cytokine treatment experiments, immunofluorescence investigations, gene expression analysis, viability assays, proliferation assay, immune cell isolation, flow cytometry, migration assay, sample preparation for proteome analysis, and scanning electron microscopy. Manuscript design, visualization, writing, and final approval under the supervision of Dr. Timo Gaber and Prof. Dr. Frank Buttgereit.

Article Type: Full-length article

Short Title: Xeno-free 3D synovitis model

Full Title: A functional xeno-free 3D synovial membrane model to study synovitis *in vitro*

Authors: Alexandra Damerau[1,2], Marieluise Kirchner[3], Julia Beißel[1,2], Moritz Pfeiffenberger[1,2], Philipp Mertins[3], Frank Buttgereit[1,2] and Timo Gaber[1,2]

Affiliations

[1] Charité – Universitätsmedizin Berlin, corporate member of Freie Universität Berlin and Humboldt-Universität zu Berlin, Department of Rheumatology and Clinical Immunology, Berlin, Germany

[2] German Rheumatism Research Centre (DRFZ) Berlin, a Leibniz Institute, Berlin, Germany

[3] Berlin Institute of Health and Max-Delbrück-Centrum for Molecular Medicine, Germany

Abstract

Musculoskeletal disorders such as rheumatoid arthritis (RA) and osteoarthritis (OA) are the most prevalent forms of inflammatory joint diseases, characterized by synovitis and, in late stages, cartilage and bone degradation. Fibroblast-like synoviocytes (FLSs) of the synovial membrane are critical drivers of arthritis. However, knowledge about the impact of FLSs in the early stages of cartilage degradation is still limited. The pathogenesis of inflammatory joint diseases is primarily studied using animal models, which represent an integral part of the preclinical drug discovery process. Although these animal models have limited predictive value and are accompanied by severe suffering for laboratory animals, they are still the gold standard due to the lack of human-centered *in vitro* alternatives. Most *in vitro* models of the synovial membrane are based on RA-FLSs or OA-FLSs suspended in animal-derived Matrigel™, hence not reflecting the 'healthy' state. To overcome this research gap, we developed a xeno-free, human-centered 3D synovial membrane model based on bone marrow-derived mesenchymal stromal cells (MSCs) embedded in a synthetic hydrogel. We identified MSCs as a suitable cell source since we could show that MSCs share pronounced similarities with human knee-derived FLSs from trauma patients. In addition, differentiation of MSCs into a fibroblastic phenotype using connective tissue growth factor (CTGF) showed no substantial advantages in using these cells for model development. Rather, CTGF-triggered MSCs shifted their phenotype toward fibrosis and are therefore less suitable here.

To characterize the synovial membrane model, we analyzed its geometry and demonstrated two to four cell layers that reflect the native synovial lining *in vivo*. Regarding the stratification process, we simulated an arthritic environment such as in RA by exposing the synovial membrane model to inflammatory stimuli, namely tumor necrosis factor-α, interleukin-6, and macrophage migration inhibitory factor. Cytokine stimulation led to an enhanced gene expression of pro-inflammatory, pro-angiogenic, and matrix-degrading enzymes, hyperproliferation, and a rise in cells' glucose consumption within the synovial membrane model similar to that observed in human arthritis. These results indicate that our xeno-free *in vitro* model can mimic cytokine-driven cellular changes observed during arthritis. We propose that the xeno-free 3D synovial membrane model can be a good alternative for preclinical drug screening to reduce the number of animal experiments and improve the transferability of results to human patients.

Keywords

in vitro synovitis model, arthritis, trauma-fibroblast, MSC, CTGF, cytokines, TNF, MIF, IL-6

Introduction

The synovial membrane (synovium) is critical in joint homeostasis and diseases such as rheumatoid arthritis (RA) and osteoarthritis (OA). It encloses the joint, consists of the intimal lining and sublining layer, and determines synovial fluid composition by filtrating and synthesizing nutrients and lubricants [1-3]. Under physiological conditions, the intimal lining is in direct contact with the synovial fluid-filled joint cavity. It is one to four cell layers thick and composed of 90% fibroblast-like (type B) synoviocytes (FLSs) and 10% macrophage-like (type A) synoviocytes (MLSs) [4]. In contrast, the sublining layer is paucicellular connective tissue with fibrous and collagenous extracellular matrix (ECM) and adipose tissue areas with few blood vessels [3, 5].

Under inflamed conditions, typically associated with RA but also crucial in OA, the synovium thickens into a pannus-like structure with an increase in cellularity (hyperplasia) e.g., immune cell infiltration, vascularity, fibrosis, and innervation. During the last decade, fibroblasts, which physiologically maintain the structural integrity of joints, have been identified as key drivers in disease pathogenesis, linking synovial inflammation to increased cartilage loss and the progression of joint degeneration [3, 6, 7].

To mimic synovitis, few tissue-engineered human *in vitro* synovial membrane models have been developed, each with relative strengths and weaknesses [8-10]. For example, synovial explants have the advantage of their native ECM, FLSs, and MLSs spatial distribution, but the availability of “healthy” clinical specimens is limited [11]. Instead, clinical samples are usually collected from advanced-stage OA patients and are phenotypically and functionally altered due to disease state, donor variability, medication, and collection site [12]. In contrast, 2D monolayer models lack the dense ECM and three-dimensional (3D) architecture of the lining and sublining layer that play a crucial role in the function of the native tissue. Using 3D synovial organoids constructed from micromass cultures of RA- or OA-FLSs embedded in animal-derived Matrigel™ provides ECM-like and cellular features of the intima. It becomes hyperplastic in the presence of inflammatory cytokines [8, 9, 13]. However, it lacks the geometry to facilitate polarized cell migration and solute transport. In addition, FLSs from patients with RA or OA may have an intrinsic imprinted pathological phenotype or be influenced by medication, not reflecting the physiological state of the synovial membrane [14-17]. Thus, a “normal” or “healthy” FLS source would be ideal for establishing a xeno-free 3D synovial membrane model that provides the physiological geometry.

Traditionally, mesenchymal stromal cells (MSCs) are considered the progenitor cells of FLSs and share many characteristics, such as the ability to maintain and regenerate tissues through ECM

components and respond to various inflammatory and non-inflammatory factors. However, recent research indicates that human MSCs and FLSs are indistinguishable, as they share the same morphology, highly similar surface marker profile, and multi-lineage differentiation potential, suggesting the assumption of an identical cell type [18, 19]. Conversely, other reports have shown that various growth factors, such as connective tissue growth factor (CTGF) [20-23], fibroblast growth factor (FGF) [24, 25], and transforming growth factor (TGF)-β [26, 27], are capable of promoting the differentiation of MSCs into FLSs, as evidenced by the expression of classical fibroblast markers, e.g., vimentin (VIM), fibroblast-specific protein 1 (FSP1), and tenascin-C (TNC) [28, 29]. However, in contrast to other well-studied mesenchymal lineages, e.g., osteoblasts, adipocytes, or chondrocytes, the differentiation pathway from MSCs to FLSs ─ if one exists ─ has been poorly defined and is still controversially discussed.

Consequently, we first compared the phenotypic characteristics of FLSs derived from trauma patients with human bone marrow-derived MSCs to identify a suitable cell type for simulating the synovial membrane *in vitro*. In addition, we present the results of the phenotypic comparison of these MSCs with either human FLSs or CTGF-differentiated MSCs on both the transcriptomic and proteomic levels to demonstrate whether, e.g., CTGF promotes MSC differentiation toward the fibroblast lineage. After defining MSCs as the optimal cell source to fabricate a human-based 3D synovial membrane model, we used MSCs combined with a synthetic hydrogel to mimic the geometry of the synovial lining. Next, we applied inflammatory stimuli generating the human-based xeno-free 3D synovitis model, as confirmed by increased inflammatory gene expression and enhanced cell proliferation mimicking pannus formation. This model provides a starting point for adding complexity, such as MLSs or immune cells, that infiltrate the model and other joint components, such as the osteochondral unit, to mimic the complexity of the pathogenesis of arthritis.

Material and Methods

Cells and ethic statement

Table 1: Information and conducted experiments.

	Donor	Age	Gender		Type of experiment
MSCs	1	62	w	**Synovial membrane model**	Gene expression, proliferation, cytokine secretion
	2	52	m		Gene expression, proliferation, cytokine secretion, glucose & lactate, CTGF treatment, migration
	3	58	m		Proliferation, cytokine secretion, CTGF treatment, migration
	4	71	m		Proliferation, cytokine secretion, CTGF treatment, migration
	5	48	w		Proliferation, cytokine secretion, CTGF treatment, migration
	6	76	w		Proliferation, cytokine secretion, CTGF treatment, migration
	7	86	m		Gene expression, glucose & lactate, migration
	8	63	w		Gene expression, glucose & lactate, migration
	9	65	m		Gene expression, glucose & lactate, migration
Trauma-FLS	1	26	m	**Healthy FLS control**	Gene expression analysis, proliferation
	2	25	w		Gene expression analysis, histology, proliferation, cytokine secretion
	3	28	m		Gene expression analysis, histology, proliferation, cytokine secretion
	4	29	w		Gene expression analysis, histology, proliferation, cytokine secretion
	5	43	m		Gene expression analysis, histology
	6	41	m		Gene expression analysis, proliferation
	7	20	w		Gene expression analysis, histology
	8	21	m		Gene expression analysis, cytokine secretion
	9	27	w		Histology, proliferation, cytokine secretion
OA-FLS	1	83	m	**OA-FLS control**	Gene expression analysis
	2	70	m		
	3	67	m		
	4	71	w		
	5	81	w		
	6	70	w		
	7	71	w		
	8	66	w		
	9	59	m		

Since age, sex and comorbidities can affect the behavior of cells *in vitro;* we collected donor-related information. MSCs isolation, expansion, and characterization were performed as described previously [30]. Bone marrow was obtained from patients undergoing total hip replacement, provided by the Center for Musculoskeletal Surgery (Charité–Universitätsmedizin), and distributed by the “Tissue Harvesting” core facility of the Berlin-Brandenburg Center for Regenerative Therapies (BCRT). FLSs were isolated from synovial tissue sections of (i) trauma patients collected during anterior cruciate ligament (ACL) reconstruction and (ii) OA patients excised during knee arthroplasty. Synovial tissue was provided by the Center of Musculoskeletal Surgery (Charité–Universitätsmedizin). The study design and protocols were approved by the

Charité-Universitätsmedizin Ethics Committee and performed according to the Helsinki Declaration (ethical approval EA1/012/13, January 2013, EA1/146/21, May 2021).

Isolation of human synovial fibroblasts

The synovium was washed with 0.5% (w/v) BSA (Sigma-Aldrich, Munich, Germany) and 5 mM EDTA (Gibco, Waltham, MA, USA) in phosphate-buffered saline (PBS; DRFZ, Berlin, Germany; PBS/BSA/EDTA; pH 7.4) and dissected into small pieces. The small tissue pieces were filtered through a pre-wetted 100 µm MACS® SmartStrainer (Miltenyi Biotec, Bergisch Gladbach, Germany), transferred to a 25 cm^2 (trauma synovium) or 75 cm^2 flask (OA synovium), and cultured in a humidified atmosphere (37 °C, 5% CO_2). Dulbecco`s Modified Eagle Minimal Essential Medium (DMEM) GlutaMAX™ (Gibco, Waltham, MA, USA) supplemented with 10% FCS (FCS, Biowest, Nuaillé, France) and 1% penicillin/streptomycin (Gibco, Waltham, MA, USA) was changed weekly. This medium is referred to as normal medium (NM).

Stimulation with growth factors for MSC differentiation

To differentiate MSCs toward the fibroblast lineage, cells were cultured for three weeks using NM supplemented with (i) 25 ng/mL recombinant human (rh) FGF (ImmunoTools GmbH, Friesoythe, Germany), (ii) 5 and 10 ng/mL rhFGF + rhTGF-β (R&D Systems, Inc., Minneapolis, USA), (iii) 100 ng/mL rhCTGF (PeproTech, Hamburg, Germany) and 50 µg/mL ascorbic acid (Sigma-Aldrich, Munich, Germany), or (iv) unstimulated.

Generation of the synovial membrane model

The synovial membrane model was developed using the xeno-free VitroGel® RGD hydrogel (TheWell Bioscience Inc., North Brunswick Township, USA). To allow for sufficient nutrient supply, the model was cultured in a 24-well plate hanging insert with a pore size of 8 µm (Sarstedt, Hildesheim, Germany). Therefore, the polycarbonate membrane was coated with 100 µL hydrogel (1:3 gel-solution) containing $1x10^5$ cells and polymerized for 30 min at RT. Synovial membrane models were cultivated for up to 21 days in a humidified atmosphere (37 °C, 5% CO_2). The medium contains DMEM GlutaMAX™ supplemented with 2% human AB serum (Capricorn Scientific, Ebsdorfergrund, Germany) and 1% penicillin/streptomycin, in the following referred to as NM-XF.

Short- and long-term exposure to inflammatory stimuli

To mimic cytokine-mediated joint inflammation, stimulation was performed in NM-XF using 10 ng/mL rh macrophage migration inhibitory factor (MIF), 30 ng/mL rh interleukin (IL)-6, and

10 ng/mL rh tumor necrosis factor (TNF)-α (all ImmunoTools GmbH, Friesoythe; Germany), referred as +Cyt. The medium was changed every three days, including the respective supplements resulting in a repetitive chronic cytokine stimulation. Incubation was conducted for 3 days (short-term) and 21 days (long-term) at 37 °C in a 5% CO_2 atmosphere.

Cytotoxicity and viability assay

Cytotoxicity Detection LDH Kit (Sigma-Aldrich, Munich, Germany) was performed according to the manufacturer's instructions and as previously described [30, 31]. Cell death was induced by 4% (v/v) Triton™ X-100 (Sigma-Aldrich, Munich, Germany) for 24 h (high control).

ApoTox-Glo™ Triplex Assay was performed according to the instructions of Promega Corporation (Walldorf, Germany) using phenol red-free DMEM (Gibco, Waltham, MA, USA). Cell death was induced by 4% (v/v) Triton™ X-100 for 4 h or 100 µg/mL digitonin (Boehringer Mannheim GmbH, Mannheim, Germany) for 30 min, whereas apoptosis was induced by 0.1 mM camptothecin (Sigma-Aldrich) for 4 h.

BrdU proliferation assay

According to the manufacturer's instructions, the proliferation assay was performed using the BrdU (colorimetric) assay (Roche, Mannheim, Germany). The BrdU labeling solution was added to the cell culture medium on the synovial membrane model 20 h before endpoint measurement. Cells were fixed for 30 min at RT, followed by the addition of an anti-BrdU-POD working solution. After 90 min, cells were washed three times with 1x PBS, substrate solution was added, and incubation was stopped with 25 µL 2N H_2SO_4 after 30 min. Measurement was performed at 450 nm (reference wavelength 630 nm). In addition, cells were treated with 1 µg/mL actinomycin D (Sigma-Aldrich, Munich, Germany) to suppress proliferation (negative control).

Glucose and lactate concentration

Glucose and lactate content – as a measure of glycolysis – were analyzed using the Biosen C-Line Glucose and Lactate analyzer (EKF-diagnostic GmbH, Barleben, Germany). For this, 20 µL supernatant was mixed with 1 mL PBS, while instrument calibration and electrode validation were performed with the manufacturer's solutions before the measurements.

Flow cytometry analysis

Characterizing synovial fibroblasts regarding their surface marker pattern, flow cytometry staining was performed using $5x10^4$ cells per well of a U-bottom 96-well plate. After a washing step with PBS/BSA/Azide, unspecific binding sites of the Fc-receptors were blocked using 10 mg/mL

Flebogamma® (IgG1 66.6%, IgG2 28.5%, IgG3 2.7%, IgG4 2.2%; Grifols, Barcelona, Spain) for 10 min on ice. Subsequently, cells were stained with the antibodies according to the manufacturer's instructions (antibodies listed in Table 2). Cells were washed, centrifuged (400 × *g*, 4 min, 4 °C), and suspended in PBS/BSA/Azide. Apoptotic polymorphonuclear leukocytes (PMNs) were analyzed using annexin V (BD, Heidelberg, Germany). Cells were washed with PBS, resuspended in binding buffer with annexin V (1:100), and incubated for 15 min on ice. Measurement was performed using the MACSQuant® Analyzer 10 (Miltenyi Biotec, Bergisch Gladbach, Germany) and analyzed with FlowJo™ software (version 7.6.4 and 10.7.1, Tree Star).

Table 2: Donor information and conducted experiments.

Description	Dye	Species/Clone	Manufacturer	City, State
Anti-human CD73	APC	REA804	Miltenyi Biotec	Bergisch Gladbach, Germany
Anti-human CD90	FITC	REA897		
Anti-human CD105	APC-Vio770	REA794		
Anti-human CD14	PE	REA599		
Anti-human CD20	PE	REA780		
Anti-human CD34	PE	REA1164		
Anti-human CD45	PE	REA747		
Anti-human HLA-DR	PE	REA805		
Anti-human CD15	FITC	Mouse (VIMC6)		

CD15+ polymorphonuclear leukocyte preparation and magnetic cell separation

Blood from healthy donors was collected using 10 mL Heparin Vacutainers (Becton Dickinson, Franklin Lakes, USA) to isolate CD15+ PMNs. Protocols were approved by the Charité-Universitätsmedizin Ethics Committee and performed according to the Helsinki Declaration (ethical approval EA1/367/14). Briefly, blood was mixed 1:5 with erythrocyte lysis buffer and incubated on ice for 5 min, followed by a centrifugation step at 400 *x g*, 5 min, 4 °C, and resuspension in 1 mL PBS/BSA/EDTA. This procedure was repeated until erythrocytes were lysed completely. The cell number was determined and adjusted with PBS/BSA/EDTA: 80 µL buffer per 10^7 total cells. CD15 MACS® MicroBeads (Miltenyi Biotec, Bergisch Gladbach, Germany) were added to the cells: 20 µL per 10^7 cells and incubated for 15 min in the refrigerator at 4-8 °C. After washing with 2 mL PBS/BSA/EDTA, cells were centrifuged (300 *x g*, 10 min, 4 °C) and resuspended in ice-cold 500 µL PBS/BSA/EDTA. A pre-cooled MACS Cell Separation LS column (Miltenyi Biotec, Bergisch Gladbach, Germany) was placed in the magnetic field of a MACS Separator and rinsed with ice-cold 3 mL PBS/BSA/EDTA buffer. The cell suspension was applied to the column, washed three times with 3 mL PBS/BSA/EDTA, and discarded the unlabeled cells. Finally, the column was removed from the separator and placed on a 15 mL

collection tube. Labeled CD15+ cells were collected by flushing the column with 5 mL buffer and pushing the plunger into the column. The purity of CD15+ cells was confirmed after every isolation using flow cytometry (Figure 1).

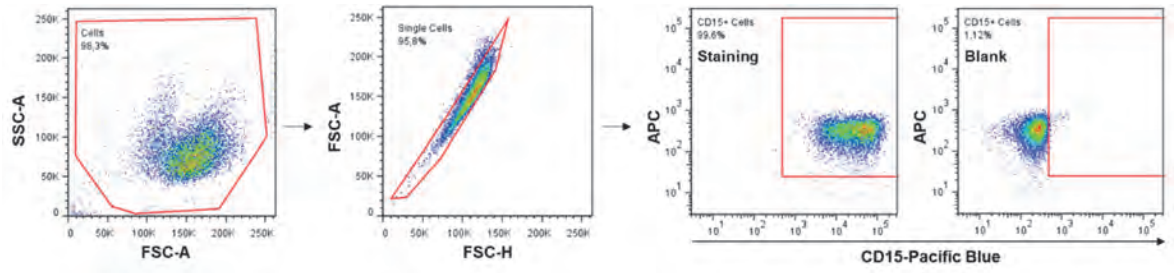

Figure 1: Confirmation of CD15 purity after MACS® MicroBead isolation using flow cytometry. As a first step, cells were gated, and cell debris was excluded. Then, within the CD15+gate, the purity CD15+ cells isolated by MicroBeads were analyzed.

Protein isolation and mass spectrometry (LC-MS/MS)

Protein isolation and mass spectrometry were performed by Dr. Marieluise Kirchner (BIH Proteomics Core Facility) and have been previously described [32]. Briefly, proteins were extracted from $2x10^5$ cells comparing untreated and CTGF treated MSCs. Cells were washed with cold 1x PBS twice and stored at -80 °C. For statistical analyses, 5 biological replicates for each condition (untreated MSCs, CTGF treated MSCs) were defined as groups. A minimum of 3 LFQ intensity values in at least one group was required. Missing values were imputed with low-intensity values simulating the detection limit of the mass spectrometer. Differences in protein abundance between the groups were calculated using the two-sample Student´s t-test. Proteins passing the FDR-based significance cut-off of 5% were considered differentially expressed.

Migration assay

The ChemoTx® Disposable Chemotaxis System (Gaithersburg, MD, USA) with a polycarbonate membrane of 8 µm pore size was used to analyze the ability of MSCs and PMNs to migrate through the membrane toward an attractant. Studying the spontaneous and directed migration of MSCs, $3x10^4$ cells/membrane/30 µL hydrogel were incubated for 24 h using medium (ctrl) and IL-6 (10 ng/mL) as attractants, respectively. To investigate the ability of PMNs to migrate through the synovial model, MSCs were applied 24 h before PMNs. The cell density of $9x10^4$ PMNs (1:4) was applied, and migration was investigated after 24 h via cell count using the Neubauer chamber (Paul Marienfeld GmbH & Co. KG, Lauda Königshofen, Germany). Directed migration was induced by 10 ng/mL IL-6 as a positive control.

Immunofluorescence staining

Immunofluorescence staining was performed as previously described [30] using target-specific antibodies listed in Table 3. All staining were performed in a humid chamber. Imaging was performed with the Zeiss LSM 710 Confocal Microscope (Carl Zeiss AG, Oberkochen, Germany).

Table 3: List of antibodies, kits, and staining solutions.

Description	Dye	Host	Working concentration	Manufacturer
Immunofluorescence antibodies				
DAPI		-	1 µg/mL	German Rheumatism Research Center
Phalloidin	TRITC	-	50 µg/mL	Sigma-Aldrich
Tubulin	A647	mouse	5 µg/mL	Invitrogen / Thermo Fisher Scientific
Vimentin	A488	rabbit	5 µg/mL	Abcam
THY1	A568	rabbit	5 µg/mL	
PDPN	-	rat	2.5 µg/mL	BioLegend
anti-mouse IgG (H+L)	A594	goat	2 µg/mL	Abcam
anti-rabbit IgG (H+L)	A488	donkey	4 µg/mL	
anti-rabbit IgG (H+L)	A546	goat	4 µg/mL	Invitrogen / Thermo Fisher Scientific
anti-mouse IgG (H+L)	A546	goat	4 µg/mL	
anti-rat IgG (H+L)	A647	goat	4 µg/mL	
Kits and solutions				
LIVE/DEAD® Viability/Cytotoxicity	2 µM Calcein AM, 4 µM EthD-1			Invitrogen / Thermo Fisher Scientific
FluoroMount-G™	Mounting slides for immunofluorescence			Sigma-Aldrich
Tween® 20	0.1% for permeabilization			Qbiogene Inc.

RNA isolation, cDNA synthesis, and qPCR

RNA isolation using RNeasy® Fibrous Tissue Mini Kit (Qiagen GmbH, Germany), cDNA synthesis using TaqMan® Reverse Transcription Reagents Kit (Applied Biosystems Inc., USA), and quantitative PCR (qPCR) with the DyNAmo ColorFlash SYBR Green qPCR Kit (Thermo Fisher Scientific, USA) were performed as previously described [30]. The Stratagene Mx3000PTM (Agilent Technologies Inc., USA) was used for qPCR (duplicates per gene) with the following profile: 7 min at 95 °C, 60 cycles of 10 s at 95 °C, 7 s at 60 °C, and 9 s at 72 °C. Primer specificity was confirmed after every run (sequences listed in Table 4).

Table 4: Donor information and conducted experiments.

Gene symbol	Gene name	Sequence of the forward primer	Sequence of the reverse primer
COL3A1	Collagen, type III, alpha 1	CTTTGTGCAAAAGGGGAGCT	TGGGTTGGGGCAGTCTAATT
CXCR4	C-X-C chemokine receptor type 4	GCATGACGGACAAGTACAGGCT	AAAGTACCAGTTTGCCACGGC
DCN	Decorin	CCTTTGGTGAAGTTGGAACG	TCGCACTTTGGTGATCTCAT
EF1A	Elongation factor 1 alpha 1	TGTGCTGTCCTGATTGTTGC	GTAGGGTGGCTCAGTGGAAT
FN1	Fibronectin 1	GGTGACACTTATGAGCGTCCTAAA	AACATGTAACCACCAGTCTCATGTG
FSP1	Fibroblast-specific protein 1	TCTTGGTTTGATCCTGACTGCT	TCACCCTCTTTGCCCGAGTA
GLUT1	Glucose transporter 1	AACCACTGCAACGGCTTAGA	TCACGGCTGGCACAAAACTA
HAS2	Hyaluronan synthase 2	TGTCGAGTTTACTTCCCGCC	CAGCGTCAAAAGCATGACCC
HIF1A	Hypoxia-inducible factor 1	CCATTAGAAAGCAGTTCCGC	TGGGTAGGAGATGGAGATGC
IL1b	Interleukin 1b	AGCTACGAATCTCCGACCAC	CGTTATCCCATGTGTCGAAGAA
IL6	Interleukin 6	AAGCAGCAAAGAGGCACTGG	TGGGTCAGGGGTGGTTATTG
IL8	Interleukin 8	CAGAGACAGCAGAGCACACA	TGGGGTGGAAAGGTTTGGAG
LDHA	Lactate dehydrogenase A	ACCCAGTTTCCACCATGATT	CCCAAAATGCAAGGAACACT
MMP1	Matrix metallopeptidase 1	CTCTGGAGTAATGTCACACCTCT	TGTTGGTCCACCTTTCATCTTC
MMP13	Matrix metallopeptidase 13	TCCTGATGTGGGTGAATACAATG	GCCATCGTGAAGTCTGGTAAAAT
MMP3	Matrix metallopeptidase 3	ATCCTACTGTTGCTGTGCGT	CATCACCTCCAGAGTGTCGG
PGK1	Phosphoglycerate Kinase 1	ATGGATGAGGTGGTGAAAGC	CAGTGCTCACATGGCTGACT
TNFA	Tumor necrosis factor-alpha	TCTGGGCAGGTCTACTTTGG	ATCCCAGGTTTCGAAGTGGT
VEGFA	Vascular endothelial growth factor A	AGCCTTGCCTTGCTGCTCTA	GTGCTGGCCTTGGTGAGG
VIM	Vimentin	GGACCAGCTAACCAACGACA	AAGGTCAAGACGTGCCAGAG

Statistics

Statistical analyses were performed using the software GraphPad® Prism Version 9.3.0 (La Jolla, San Diego, CA, USA). Since the data sets were not normally distributed, non-parametric tests were performed. Mann-Whitney U test was used for direct comparisons of two independent datasets. For comparisons of more than two independent datasets, one-way analysis using Kruskal-Wallis with Dunn's multiple comparisons test was performed. Two-tailed Wilcoxon matched-pairs signed-rank test was applied for dependent datasets. For comparisons of more than two dependent datasets, one-way analysis using Friedman with Dunn's multiple comparisons test was performed. P-values of <0.05 were considered as statistically significant (*p <0.05, **p <0.01, ***p <0.005). Data are shown as box plots (centerline, median; box limits, upper and lower quartiles; whiskers, maximum and minimum) if not indicated otherwise.

Results

Human knee-derived FLS from trauma patients exhibit a stem cell-like phenotype similar to that of human bone marrow-derived MSCs

To confirm MSCs as an optimal cell source, we first evaluated their phenotypic properties compared with FLSs derived from trauma patients. Therefore, a standardized protocol was applied to characterize the isolated cells according to their mesenchymal nature. Characterization was performed during the second passaging. Following the international recommendations [33], the isolated MSCs and FLSs were analyzed for their plastic adherence, the presence and absence of defined surface markers, and multilineage differentiation potential ─ adipogenic and osteogenic lineage. MSCs and FLSs adhered to plastic and showed the characteristic spindle-shaped cell morphology using brightfield microscopy (Figure 2A). Moreover, 21-day differentiation showed their ability to differentiate into mesenchymal lineages such as adipogenic (Figure 2B) and osteogenic (Figure 2C). Flow cytometric analysis revealed a similar expression pattern of stem cell markers CD105, CD73, and CD90, while negative markers such as CD14, CD20, CD34, CD45, and HLA-DR accounted for <5% (Figure 2D).

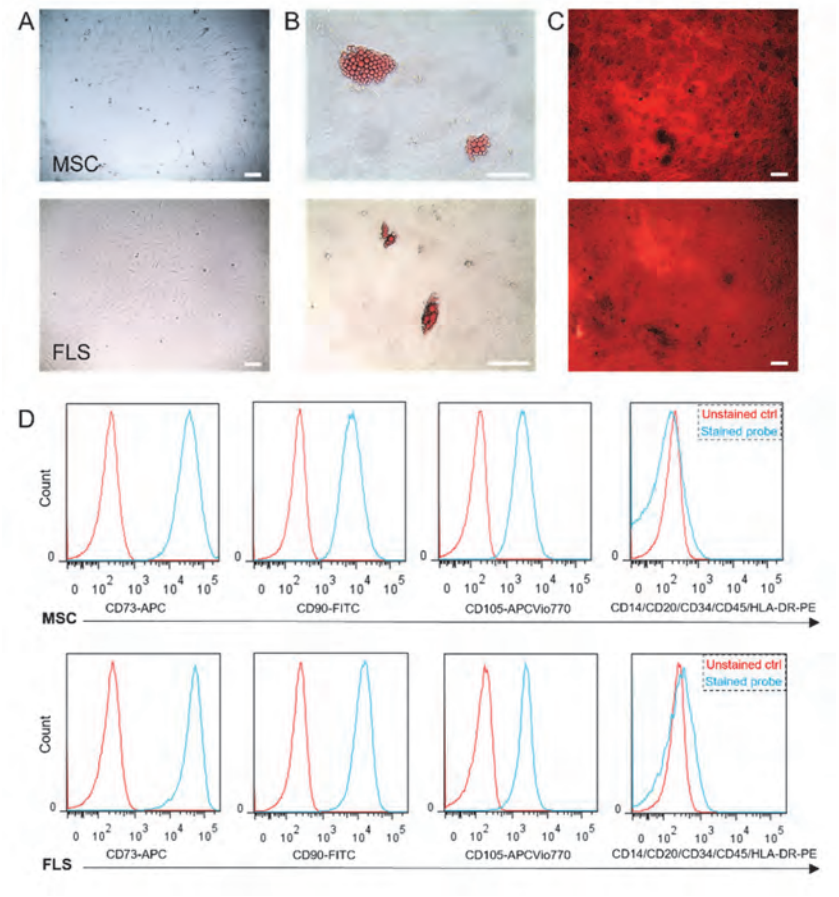

Figure 2: Characterization of trauma-FLSs compared with bone marrow-derived MSCs. (A) MSCs and FLSs adhere to plastic and show spindle-shaped cell morphology. (B) Representative images of the Oil Red (adipogenesis) and (C) Alizarin Red S (osteogenesis) staining demonstrate their ability to differentiate into multiple lineages. Scale bars = 100 µm. (D) Flow cytometry was used to investigate the expression of CD73, CD90, and CD105 and the absence of CD14, CD20, CD34, CD45, and HLA-DR.

Due to their heterogeneity and lack of a specific marker, FLSs and MSCs are challenging to identify. Traditionally, FLSs have been recognized by the mesenchymal marker VIM. However, recent research on RA-FLS has shown that subpopulations differ by thymic cell antigen 1 (THY1, CD90), while podoplanin (PDPN) is associated with a severe course of chronic inflammation [32, 34, 35]. Furthermore, visualization of THY1+ cells confirmed the flow cytometry results and showed similar expression of PDPN in both cell types (Figure 3). Therefore, the comparable PDPN expression argues for the suitability of MSCs as a cell source for developing a healthy synovial membrane.

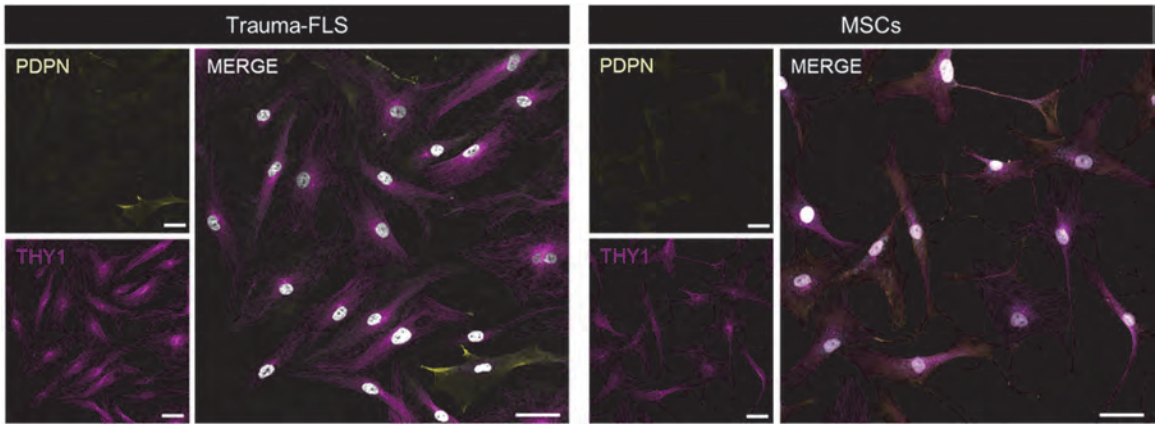

Figure 3: Exemplary images comparing trauma-FLS and MSCs regarding THY1 and PDPN. THY1 (magenta), PDPN (yellow), and DAPI (gray); scale bars show 50 μm.

CTGF induces the differentiation of human MSCs toward fibrotic fibroblast phenotype

To confirm the ability of specific growth factors such as CTGF to promote MSC differentiation toward the fibroblast lineage, MSCs were treated with (i) FGF, (ii) FGF + TGF-β, and (iii) CTGF for three weeks and analyzed in comparison with the untreated control group. Spindle-shaped cell morphology and vimentin expression are hallmarks of FLSs. Therefore, growth factor effects on cell morphology, vimentin expression, and the major component of microtubules were investigated. A concentration-dependent effect of FGF and TGF-β on the cell shape was detectable. Treatment with 5 ng/mL FGF + TGF-β or 25 ng/mL FGF resulted in fluffy morphology. On the other hand, treatment with CTGF and 10 ng/mL FGF + TGF-β showed thin, spindle-shaped, elongated cells, with the CTGF group resembling the untreated group and trauma-FLS' morphology (Figure 4). However, vimentin stability and microtubule polymerization were not affected regardless of treatment (Figure 4). In summary, CTGF seems to be the most promising candidate for promoting fibroblast differentiation of MSCs.

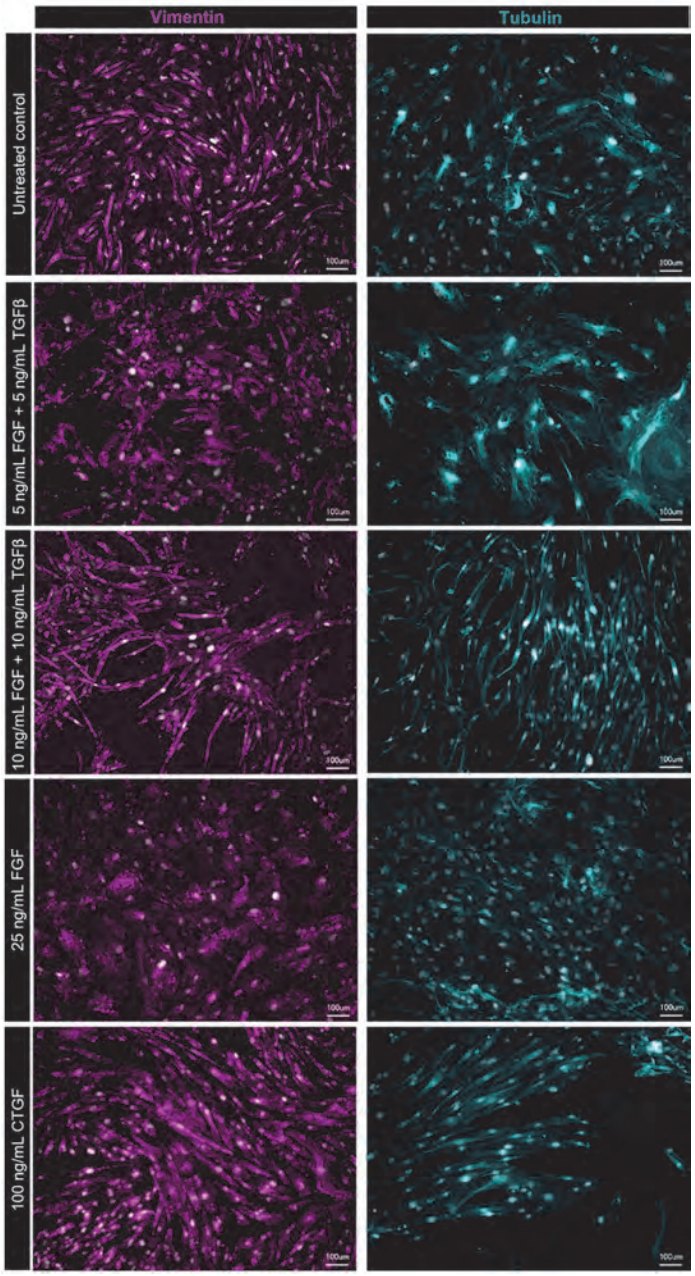

Figure 4: Cell morphology is affected by long-term exposure of MSCs to FGF, TGF-β, and CTGF. Exemplary image for the untreated control group of mesenchymal stromal cells, cells treated with FGF + TGF-β at 5 ng/mL and 10 ng/mL, respectively, and FGF as well as CTGF alone. Vimentin (magenta), tubulin (cyan), and DAPI (gray). The scale bar shows 100 µm.

Analyzing the impact of CTGF on MSCs, a global proteome comparison revealed 57 differentially expressed proteins when applying a two-sample t-test (paired) with a false discovery rate (FDR) of 5% cut-off (Figure 5A, B). CTGF affects the expression of, e.g., serpin family B member 2 (SERPINB2), lysyl oxidase-like 4 (LOXL4) (Figure 5A, B), and collagen type 4 and 6 (Figure 5C), which are known to be associated with fibrosis [36, 37]. In addition, neither the expression of fibroblast markers such as VIM, TNC, decorin (DCN), and COL1A1 (Figure 5D) nor the expression

of MSC markers such as THY1 and Ecto-5′-nucleotidase (NT5E; CD73) was affected by CTGF stimulation (Figure 5E).

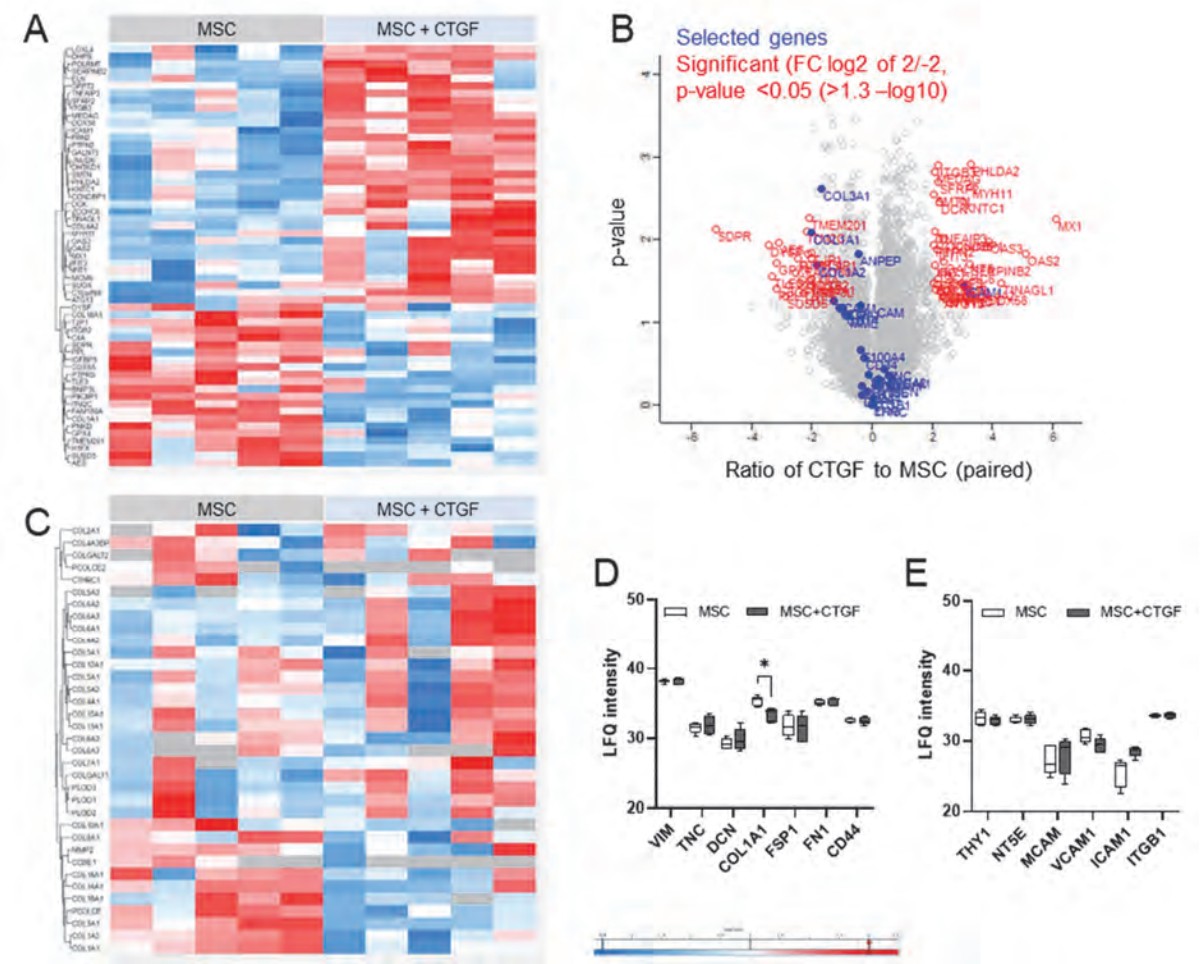

Figure 5: Distinct protein expression between CTGF treated and untreated MSCs. (A) Heatmap shows 57 significant differentially expressed proteins, comparing untreated and CTGF-treated MSCs after 21 days (n=5). (B) Volcano plot of proteome data (LFQ intensities) comparing CTGF-treated MSCs and untreated MSCs. The colored dots indicate significant differentially expressed proteins (red; false discovery rate (FDR) of 5% cut-off) and selected cell-specific marker genes (blue). (C) Heatmap with non-imputed data showing collagen-specific marker genes. Grey color indicates missing value; NA = not detected, under limit of detection (n=5). (D) Protein abundance of classical fibroblast and (E) MSC-related markers (n=5). Shown are log2 transformed LFQ intensity values. Data are shown as box plots (centerline, median; box limits, upper and lower quartiles; whiskers, maximum and minimum values). Statistics: Paired two-sample t-test; FDR of 5% cut-off (A) and Šídák's multiple comparisons test (D, E); p-values are indicated in the graphs with *p <0.05.

Examination of marker genes revealed a similar expression profile of ‘classical fibroblast markers’ such as *FSP1*, *DCN*, *VIM*, and *COL3A1* on protein and mRNA levels, whereas hyaluronan synthase 2 (*HAS2*) tended to be higher expressed on RNA level after CTGF treatment (Figure 6). Notably, fibronectin (*FN1*) is downregulated in OA-FLSs at both the protein [32] and RNA levels,

which appears to be related to disease status. In summary, the results are consistent with previous observations showing no significant differences between MSCs and trauma-FLSs.

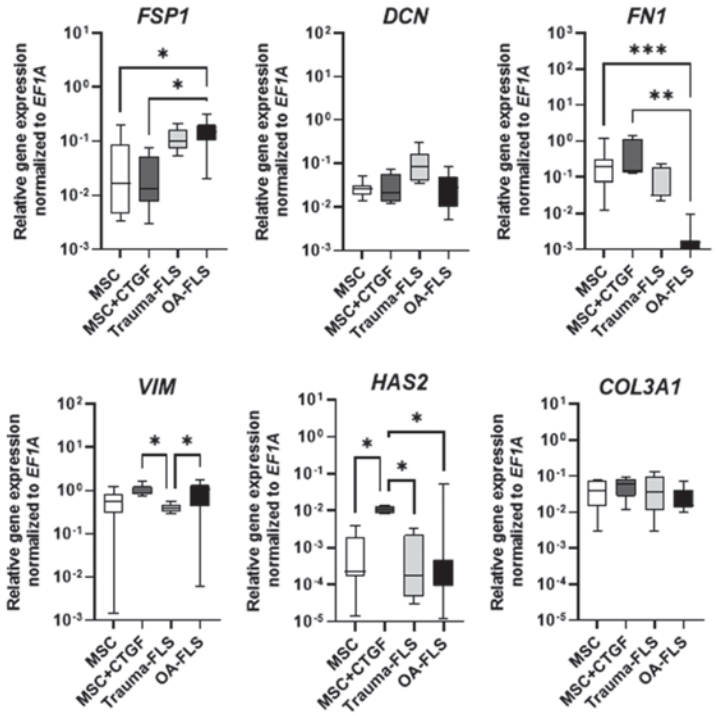

Figure 6: Transcriptome level demonstrated a similar expression profile. (A) Total RNA extraction was performed from undifferentiated MSCs and after differentiation, with 100 ng/mL CTGF after three weeks compared with FLS from trauma and OA patients (n=5-10). Gene expression of classical fibroblast markers was performed using SYBR Green and normalized to the housekeeper gene *EF1A*. Data are shown as box plots (centerline, median; box limits, upper and lower quartiles; whiskers, maximum and minimum values). Statistics: Kruskal-Wallis with Dunn's multiple comparisons tests; p-values are indicated in the graphs with *p <0.05, **p <0.01, ***p <0.001.

Mimicking the geometry of the synovial membrane using a biocompatible 3D hydrogel construct that allows neutrophil migration

The synovial membrane is marked by a confluent synovial lining layer lacking a basement membrane and tight junctions [38]. Therefore, it is a loose composite of cells embedded in an amorphous matrix composed of collagens such as collagen type I and III [38, 39]. The intimal lining is usually one to four cell layers thick and in contact with the synovial fluid within the intraarticular cavity. To simulate a simplified synovial membrane *in vitro*, cells were embedded in a thin layer of synthetic hydrogel. The 3D model was cultured on a polycarbonate-based hanging insert and supplied apically and basally. Firstly, we determined 1×10^5 cells within the hydrogel as an optimal cell number leading to a confluent layer of viable cells. Next, an LDH assay was performed to confirm the hydrogel's biocompatibility, demonstrating no sign of induced LDH release compared to the high control (Figure 7A). Analyzing cell viability, cytotoxicity, and programmed cell death (apoptosis) after 21 days of incubation revealed viable, non-cytotoxic, non-apoptotic cells within the synthetic hydrogel (Figure 7B). In this line, LIVE/DEAD staining showed a confluent cell layer of viable Calcein AM+ cells (Figure 7C, D). Horizontal and vertical

tissue sections were stained with F-actin to visualize cell density and distribution in the 3D state. The horizontal analysis confirmed the homogeneous cell distribution with two to three layers, as indicated on the z-axis, which was approved by the vertical sections (Figure 7E, F).

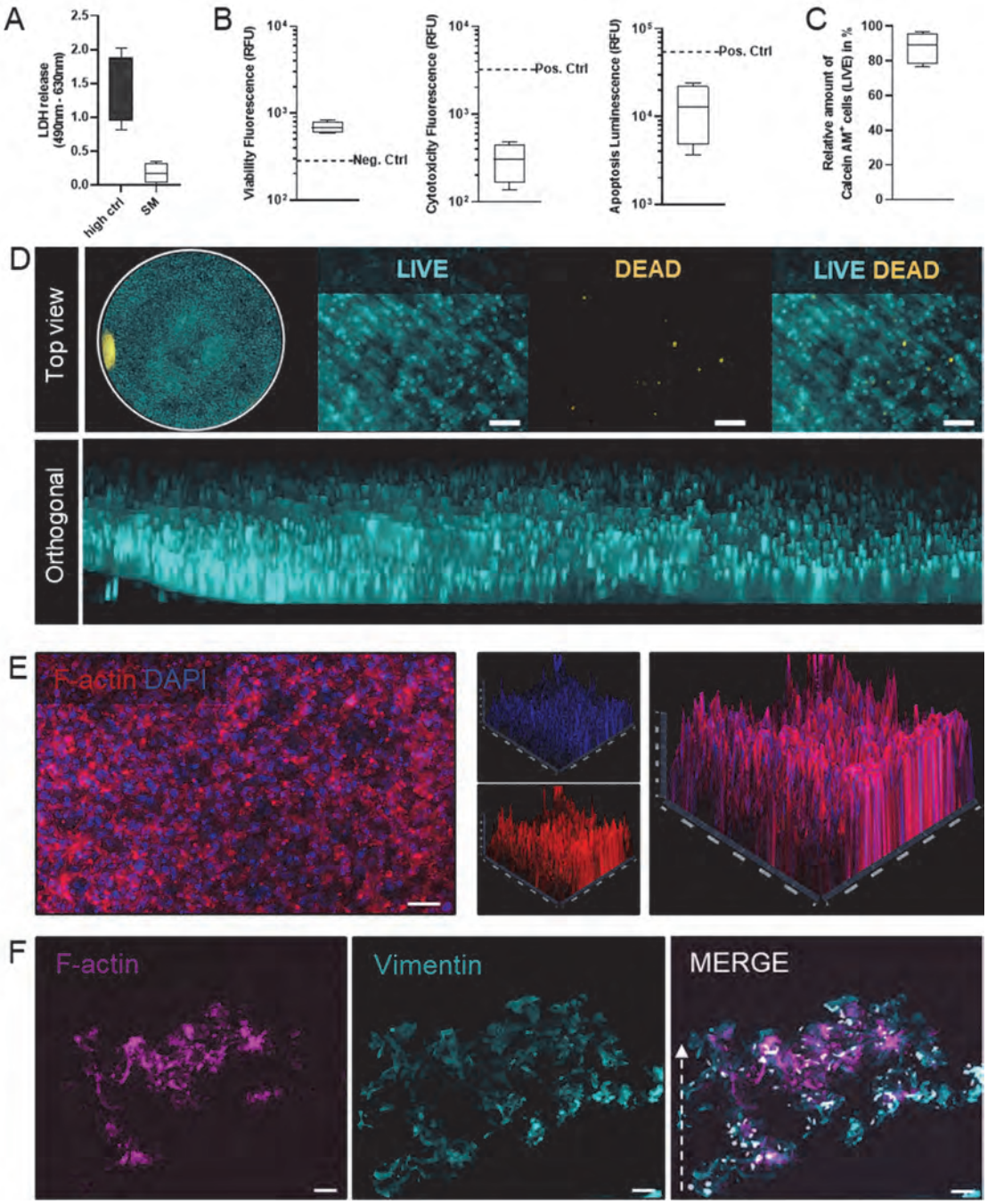

Figure 7: The RGD-based synovial membrane results in a biocompatible 3D construct with a homogenous one to four cell layers thick lining. (A) LDH cytotoxicity assay was conducted after 24 h to confirm the biocompatibility of the synthetic hydrogel. High ctrl = 4% Triton™ X-100 for 24 h; SM = synovial membrane model (n=4). (B) ApoTox-Glo™ Assay analyzing cell viability, cytotoxicity, and apoptosis level for n=4. Neg. Ctrl for viability: 100 µg/mL Digitonin. Pos.

Ctrl for cytotoxicity: 4% Triton™ X-100. Pos. Ctrl for apoptosis: 0.1 mM Camptothecin. (C) Relative number of viable cells was visualized using LIVE/DEAD staining. The staining was performed after 21 days and quantified using ImageJ (n=8). (D) Exemplary image of LIVE/DEAD staining. Living cells are presented in cyan (Calcein-AM+) and dead cells in yellow (EthD+). (E) Horizontal analysis of the synovial membrane. F-actin (red), DAPI (blue). (F) Vertical histological section. F-actin (magenta), vimentin (cyan), DAPI (grey). Scale bars = 100 µm. Statistics: Two-tailed Wilcoxon matched-pairs signed-rank test and Wilcoxon signed-rank test to the ctrl.

Since the aim is to simulate the pathogenesis of arthritic diseases *in vitro*, it was essential to investigate if immune cells could migrate through the synovial membrane model, as the migration of immune cells is evident in human arthritic joints. Analysis of the migration rate of MSCs toward either medium (ctrl) or the attractant IL-6 (10ng/mL) revealed that even when an attractant was used, only a few cells migrated, indicating the stability of the hydrogel-based system for immune cell-based studies in the future (Figure 8A). Polymorphonuclear leukocytes (PMNs), cells of the innate immune system, are the first cells at the site of inflammation and are much larger than cells of the adaptive immune system. Based on the lowest apoptosis rate and the highest survival rate in a co-culture setup, a ratio of MSCs to PMNs of 1:4 was determined, which is suitable to simulate the course of synovitis (Figure 8B). Furthermore, the ability of PMNs to migrate through the synovial membrane layer toward IL-6 could be confirmed (Figure 8C). This was the prerequisite for the subsequent simulation of the arthritic joint, in which immune cells migrate through the synovial membrane.

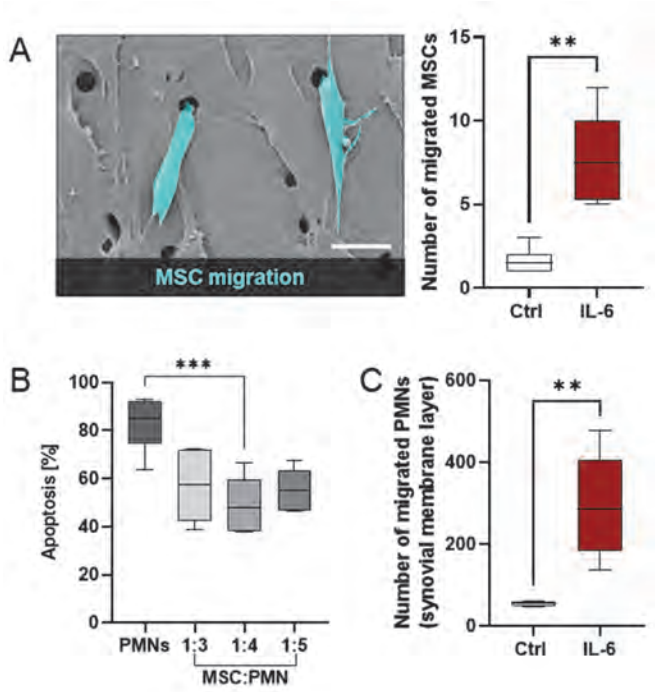

Figure 8: The polycarbonate-based model system allows for immune cell migration. (A) Exemplary SEM image highlighting the ability of MSCs (cyan) to migrate through the polycarbonate membrane. The scale bar shows 20 µm. A migration assay was performed after 24 h to analyze spontaneously and induced MSC migration using IL-6 (10 ng/mL) as an attractant (n=8). (B) Determining the optimal MSC:PMN ratio and the apoptosis rate using annexin V was investigated by flow cytometry (n=6). (C) Migration assay was performed to analyze spontaneous and induced PMN migration through the 3D MSC-based synovial membrane model (n=8). Data are shown as box plots (centerline, median; box limits, upper and lower quartiles; whiskers, maximum and minimum values). Statistics: Friedman test with Dunn's multiple comparisons tests (B), two-tailed Wilcoxon signed-rank test (A, C); p-values are indicated in the graphs with **p <0.01, ***p <0.001.

Short-term exposure to inflammatory stimuli leads to an inflammatory gene expression, while long-term exposure results in hyperproliferation of the synovial membrane model

To confirm the responsiveness of the xeno-free 3D synovial membrane model to pro-inflammatory cytokines, a cytokine cocktail of TNF-α, IL-6, and MIF was applied at non-cytotoxic concentrations, as tested previously [30]. These cytokines are well known to induce cellular hypoxia-adaptive, angiogenic, and invasive processes within the synovial membrane. Therefore, the synovial membrane was stimulated for 3 and 21 days and compared with the untreated control group. Proliferation and glucose uptake as markers of glycolysis were significantly increased after short-term exposure (Figure 9A, B). In addition, exposure resulted in increased cell thickening with enhanced PDPN expression (Figure 9C). Investigating the expression of selected marker genes, cytokine stimulation significantly induced the expression of pro-inflammatory markers such as *Il6* and *IL8*. At the same time, *TNFA* tended to be higher expressed after short-term exposure than in the untreated control (Figure 9D). In addition, the inflammatory environment significantly increased vascular endothelial growth factor A (*VEGFA*) and phosphoglycerate kinase 1 (*PGK1*) expression, while *LDHA* tended to increase. Glucose transporter 1 (*GLUT1*) was similarly expressed compared to the untreated control (Figure 9E).

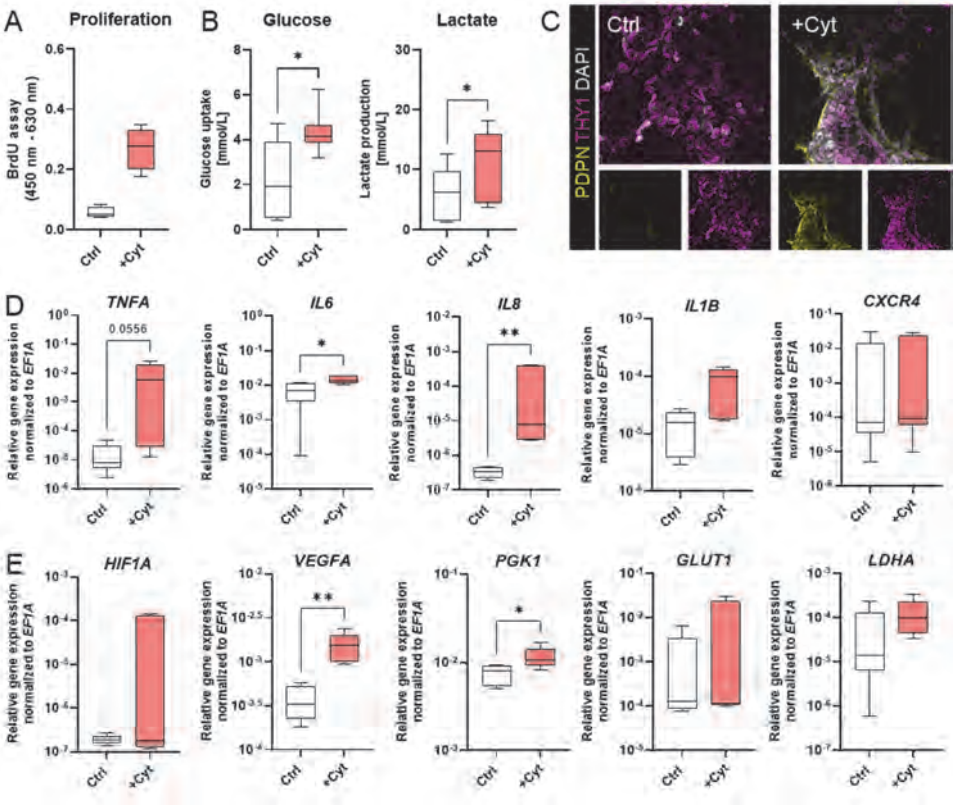

Figure 9: Short-term exposure to inflammatory stimuli leads to enhanced glycolysis and induced gene expression of pro-inflammatory markers. (A) BrdU assay was conducted to explore the proliferation rate (n=4). (B) Glucose uptake and lactate production was analyzed after day 3 days (n=7). (C) Exemplary top view images comparing short-term exposure with the unstimulated control regarding THY1 (magenta), PDPN (yellow), and DAPI (gray). (D)The expression of pro-inflammatory cytokine marker genes, (E) hypoxia-related and pro-angiogenic genes was studied via qPCR and normalized to the housekeeper gene *EF1A* (n=5). Data are shown as box plots (centerline, median; box limits, upper and lower quartiles; whiskers, maximum and minimum values). Statistics: Two-tailed Wilcoxon matched-pairs signed-rank test (A, B), Mann-Whitney U test (D, E); p-values are indicated in the graphs with *p <0.05 and **p <0.01.

In addition, we investigated the inflammatory response of the xeno-free synovial membrane model to repetitive long-term exposure. Since synovial hyperplasia is a hallmark of arthritis, we compared the proliferation rate after short-term and long-term exposure demonstrating the increased lining layer proliferation after 21 days (Figure 10A). We still observed a significant increase in *IL8* expression on gene expression level, while pro-inflammatory markers such as *TNFA*, *IL6*, and *IL1B* were not significantly increased (Figure 10B). Furthermore, since the invasiveness of synoviocytes during inflammation is distinctive, marker genes such as matrix metalloproteinases (*MMPs*) were also analyzed. Long-term exposure significantly increased the *MMP1* and *MMP13* expression compared to the untreated control (Figure 10C). Moreover, hypoxia as a feature of inflammation is marked by the interaction of MIF and hypoxia-inducible factor (HIF)-1. The latter is significantly upregulated upon long-term exposure (Figure 10D).

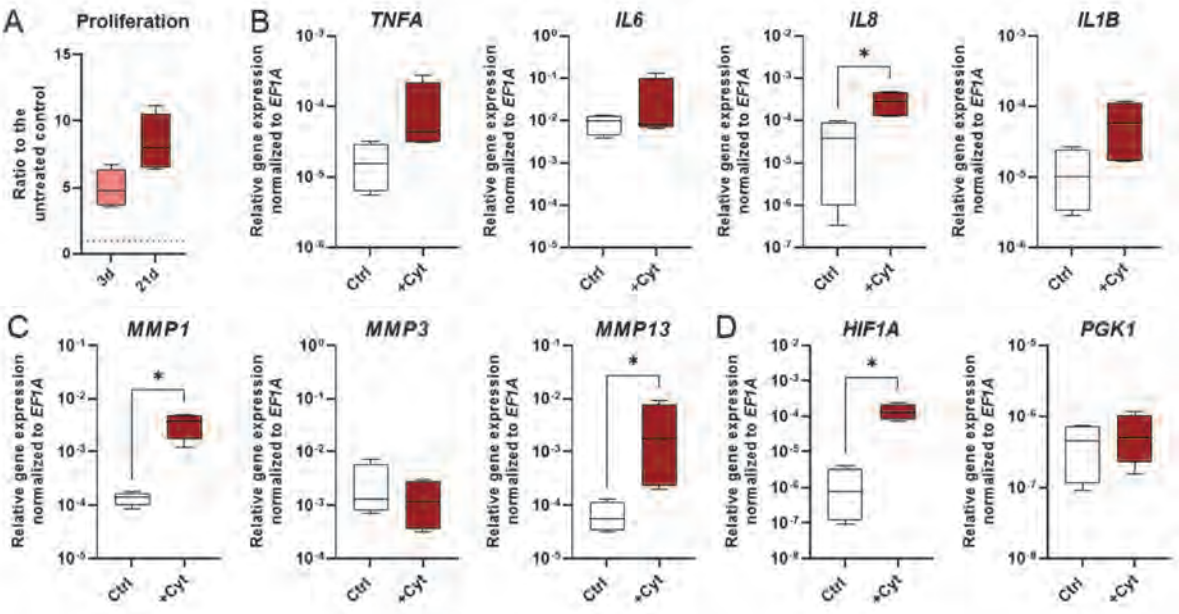

Figure 10: Gene expression after long-term exposure to inflammatory stimuli. (A) BrdU assay was conducted to explore the proliferation rate of short- and long-term exposure as a ratio to the untreated control (n=4). (B) Expression of pro-inflammatory cytokine marker genes, (C) invasive, and (D) hypoxia-related was studied via qPCR and normalized to the housekeeper gene *EF1A* (n=4). Data are shown as box plots (centerline, median; box limits, upper and lower quartiles; whiskers, maximum and minimum values). Statistics: Wilcoxon Signed Rank Test compared to the control (A); Mann-Whitney U test (A-C); p-values are indicated in the graphs with *p <0.05.

Discussion

In this study, we developed and characterized for the first time a xeno-free, human-centered MSC-hydrogel-based multilayered synovial membrane model that mimics the morphology, functionality, and response to inflammatory stimuli observed in native tissue. This model may be used as an alternative to animal experiments in both RA and OA research. Within the study, (i) we could mimic the geometry of the synovial membrane demonstrating a biocompatible, synthetic hydrogel 3D construct supporting cell arrangement in a lining layer-like structure that allows neutrophil migration, while (ii) the exposure to inflammatory stimuli lead to an enhanced gene expression of pro-inflammatory, pro-angiogenic, and matrix-degrading proteins, increased proliferation and a rise in glucose consumption of cells within the synovial membrane model similar to that observed in human arthritis. Furthermore, we revealed that (iii) human knee-derived FLS from trauma patients exhibit a stem cell-like phenotype similar to that of human bone marrow-derived MSCs, and (iv) CTGF induced the differentiation of MSCs toward the fibrotic fibroblast phenotype, both underlining the profound suitability of MSCs in the development of both healthy and diseased *in vitro* models of the synovial membrane.

During inflammatory joint diseases, activated FLSs of the synovial membrane have been identified as critical drivers of persistent inflammation and cartilage degradation. However, profound insights into the pathogenic mechanisms and the impact of FLSs in the early stages of cartilage degradation are still limited. To study processes that occur in the synovium during rheumatic diseases, various *in vitro* alternative approaches to mimic the synovial membrane have been developed to overcome current limitations of experiments using phylogenetically distant species (e.g., rodents) and to break the barrier to translation. A 3D synovial membrane micromass based on primary FLSs from RA patients was first explored by Kiener et al. [38]. They demonstrated that RA-FLSs suspended in an ice-cold Matrigel™ matrix formed a lining layer architecture at the interface between the matrix and liquid phase. The extension of this model by including monocytes further demonstrated that RA-FLSs promote monocyte survival and accumulation in the lining layer [8, 9]. However, these *in vitro* models of the synovial membrane are based on RA-FLSs and animal-derived Matrigel™, which do not reflect the ‘healthy’ state.

In a previous study, we observed that FLSs from patients with OA, even after prolonged culture, have a disease imprint, demonstrated by the release of pro-inflammatory cytokines, a high proliferation rate, and an altered metabolism [32]. Although fibroblasts are assumed to be of mesenchymal origin, we first verified the stem cell-like phenotype of synovial tissue-derived

trauma-FLSs compared to bone marrow-derived MSCs. The latter is the most suitable chronic inflammatory-unexposed control, as FLSs from healthy patients are not justifiable for ethical reasons. Both cells were indistinguishable in terms of plastic adherence, the characteristic elongated, spindle-shaped morphology, and the presence of mesenchymal-specific markers, coupled with the absence of hematopoietic-specific markers [18, 40-44]. Traditionally, differentiation ability was used to distinguish FLSs from MSCs, with FLSs being the negative control [45]. Recent research revealed that FLSs from various tissues such as skin, bronchial, and synovium could differentiate into lineages of the mesenchyme – e.g., adipogenic and osteogenic [32, 44, 46-48]. However, until today, both cell types cannot be clearly distinguished due to the lack of a specific marker [33, 49].

In contrast, studies reported that the addition of CTGF promotes MSC differentiation into FLSs, at least regarding markers such as COL1, COL3, FN1, FSP1, and TNC [50-53]. However, our unbiased global proteome analysis revealed that fibroblast markers such as COL1A1, COL1A2, and COL1A3 tended to be reduced by CTGF, while features such as VIM, FN1, FSP1, TNC, and DCN remained unchanged. Activated fibroblasts and myofibroblasts are the leading producers of structural proteins of the ECM [54]. In this line, induced COL4 and COL6 expression is a driver and biomarker in fibrosis associated with pro-fibrotic myofibroblasts [55-57]. The upregulation of *HAS2* by CTGF stimulation suggests the improved ability to synthesize hyaluronic acid. This expression is not comparable to fibroblasts from trauma and OA patients but was observed in myofibroblasts induced by TGF-β1 [58]. In addition, overexpression of HAS is associated with fibroblast invasiveness, which promotes fibrosis [59]. CTGF also induced the expression of LOXL4, an indicator of fibrosis that correlates with tissue stiffness [60]. Interestingly, Elsafadi et al. identified *SERBINB2* as a gene repressed by TGF-β, whereas CTGF tended to induce it at the protein level [61]. It is known that FLSs display characteristic gene expression patterns depending on their origin [62]. However, our data showed that MSCs are a suitable cell source to mimic the healthy synovial membrane *in vitro,* as MSCs and FLSs are phenotypically indistinguishable [63]. For developing healthy synovial membrane models, MSCs are better suited than CTGF-differentiated MSCs.

To mimic the geometry and cellular environment of the synovial membrane, thereby closing the gap towards the *in vivo* situation, MSCs were embedded in a synthetic hydrogel and, in contrast to a major part of previous studies, cultured under xeno-free conditions [8, 9, 38]. Both viability assay and immunofluorescence verified cell survival. During the cultivation period, the cells formed a synovial lining structure of two to four cell layers, as described for the native synovial

membrane [1]. The synovial membrane model was incubated in a trans-well system to enable future stimulation with cytokines from basal and application of immune cells from apical. We demonstrated immune cell migration through the hydrogel and the trans-well system. Short- and long-term exposure to TNF-α, IL-6, and MIF in pathophysiological concentrations showed that pro-inflammatory effects could be studied in the xeno-free synovial membrane model. In addition to the master cytokines TNF-α and IL-6 that essentially trigger inflammation in RA, they are also associated with OA pathology [64-66]. TNF-α promotes the expression and secretion of IL-6 and IL-8, which contribute to RA synovitis [8, 67-69]. Namba et al. investigated dogs' mitogen-activated protein kinase (MAPK) signaling pathway in synovial fibroblasts. They showed that TNF-α induced the IL-8 secretion and expression time-dependent [67]. In this line, MAPK pathways have been found to upregulate the expression of MMP1, MMP3, and MMP13 [70-72]. Our synovial membrane model resembles a significant induced *IL8* expression already after short-term exposure and the MMP expression after long-term exposure *in vitro*. While TNF-α induces the proliferation of synovial cells, IL-6 inhibits it in the presence of the soluble IL-6 receptor (sIL-6R) [66]. As reported by Broeren and colleagues for TNF-α, we could recreate pathogenic processes such as enhanced glycolysis and hyperproliferation of the synovial lining layer – a hallmark of RA [8, 9, 73]. This is a major advantage compared to studies using synovial biopsies or diseased cells in which hyperplasia has already occurred. In addition, we observed a substantial increase in the expression of *VEGFA* and *HIF1A*, both generally activated by hypoxia. However, recent research revealed that TNF-α and MIF could induce HIF-1a expression under normoxic conditions [74, 75].

In summary, we propose that our xeno-free synovial membrane model allows for studying disease processes in a human-centered way. MSCs have been demonstrated to be a suitable cell source as healthy synovial tissue is scarce. In future applications, to mimic the processes that occur during arthritis more closely, cell types such as macrophages and tissues such as articular cartilage will be included to study the effects on cartilage breakdown. Although the available 3D models still face major challenges, this xeno-free approach can serve as an alternative to animal experiments to (i) study basic mechanisms in RA and OA, (ii) identify targets, and (iii) test treatment strategies. This is the first human-centered xeno-free *in vitro* 3D synovial membrane model to study cytokine-driven mechanisms.

Acknowledgments

The authors would like to thank the Tissue Harvesting Core Facility of the BIH Berlin for providing bone marrow. Furthermore, A.D. was gratefully supported by the German Academic Scholarship Foundation (Studienstiftung des deutschen Volkes) and the Joachim Herz Foundation (Add-on Fellowship 2020). A.D., M.P., T.G., and F.B. are members of the Berlin-Brandenburg research platform BB3R and Charité 3R.

Authors contributions

Conceptualization, A.D., T.G., F.B.; methodology, A.D., J.B., M.K., M.P.; validation, A.D., M.K.; formal analysis, A.D., M.K.; investigation, A.D.; data curation, A.D., M.K., P.M.; writing—original draft preparation, A.D., T.G., F.B.; writing—review and editing, A.D., J.B., M.K., M.P., P.M., F.B., T.G.; visualization, A.D.; supervision, T.G., F.B.; project administration, A.D., T.G., F.B.; funding acquisition, A.D., T.G.; F.B.

All authors have read and agreed to the drafted manuscript.

Data availability statement

The data presented in this study are available on request. The data are not publicly available due to privacy and ethical restrictions.

Competing interests

The authors have declared that no competing interests exist.

References

1. Smith, M.D., *The normal synovium.* The open rheumatology journal, 2011. 5: p. 100-106.
2. Rhee, D.K., et al., *The secreted glycoprotein lubricin protects cartilage surfaces and inhibits synovial cell overgrowth.* J Clin Invest, 2005. 115(3): p. 622-31.
3. Smith, M.D., *The normal synovium.* Open Rheumatol J, 2011. 5: p. 100-6.
4. Bondeson, J., et al., *The role of synovial macrophages and macrophage-produced cytokines in driving aggrecanases, matrix metalloproteinases, and other destructive and inflammatory responses in osteoarthritis.* Arthritis Research & Therapy, 2006. 8(6): p. R187.
5. Scanzello, C.R. and S.R. Goldring, *The role of synovitis in osteoarthritis pathogenesis.* Bone, 2012. 51(2): p. 249-57.
6. Smolen, J.S., et al., *Rheumatoid arthritis.* Nat Rev Dis Primers, 2018. 4: p. 18001.
7. Firestein, G.S. and I.B. McInnes, *Immunopathogenesis of Rheumatoid Arthritis.* Immunity, 2017. 46(2): p. 183-196.
8. Broeren, M.G.A., et al., *A three-dimensional model to study human synovial pathology.* ALTEX, 2019. 36(1): p. 18-28.
9. Kiener, H.P., et al., *Synovial fibroblasts self-direct multicellular lining architecture and synthetic function in three-dimensional organ culture.* Arthritis Rheum, 2010. 62(3): p. 742-52.
10. Baymurat, A.C., et al., *Bio-engineered synovial membrane to prevent tendon adhesions in rabbit flexor tendon model.* J Biomed Mater Res A, 2015. 103(1): p. 84-90.
11. Damerau, A. and T. Gaber, *Modeling Rheumatoid Arthritis In Vitro: From Experimental Feasibility to Physiological Proximity.* International journal of molecular sciences, 2020. 21(21): p. 7916.
12. de Almeida, Danilo C., et al., *Epigenetic Classification of Human Mesenchymal Stromal Cells.* Stem Cell Reports, 2016. 6(2): p. 168-175.
13. Karonitsch, T., et al., *Targeted inhibition of Janus kinases abates interfon gamma-induced invasive behaviour of fibroblast-like synoviocytes.* Rheumatology, 2017. 57(3): p. 572-577.

14. Ge, X., et al., *Functional genomics atlas of synovial fibroblasts defining rheumatoid arthritis heritability.* Genome Biology, 2021. 22(1): p. 247.

15. Ai, R., et al., *Comprehensive epigenetic landscape of rheumatoid arthritis fibroblast-like synoviocytes.* Nature communications, 2018. 9(1): p. 1921-1921.

16. Ulukan, B., Y. Sila Ozkaya, and M. Zeybel, *Advances in the epigenetics of fibroblast biology and fibrotic diseases.* Current Opinion in Pharmacology, 2019. 49: p. 102-109.

17. Shen, J., et al., *Inflammation and epigenetic regulation in osteoarthritis.* Connective tissue research, 2017. 58(1): p. 49-63.

18. Denu, R.A., et al., *Fibroblasts and Mesenchymal Stromal/Stem Cells Are Phenotypically Indistinguishable.* Acta Haematol, 2016. 136(2): p. 85-97.

19. Blasi, A., et al., *Dermal fibroblasts display similar phenotypic and differentiation capacity to fat-derived mesenchymal stem cells, but differ in anti-inflammatory and angiogenic potential.* Vasc Cell, 2011. 3(1): p. 5.

20. Lee, C.H., et al., *CTGF directs fibroblast differentiation from human mesenchymal stem/stromal cells and defines connective tissue healing in a rodent injury model.* J Clin Invest, 2010. 120(9): p. 3340-9.

21. Tong, Z., et al., *Controlling the fibroblastic differentiation of mesenchymal stem cells via the combination of fibrous scaffolds and connective tissue growth factor.* Tissue Eng Part A, 2011. 17(21-22): p. 2773-85.

22. Lee, C.H., E.K. Moioli, and J.J. Mao, *Fibroblastic differentiation of human mesenchymal stem cells using connective tissue growth factor.* Conf Proc IEEE Eng Med Biol Soc, 2006. 2006: p. 775-8.

23. Yoon, D., et al., *Accelerated Wound Healing by Fibroblasts Differentiated from Human Embryonic Stem Cell-Derived Mesenchymal Stem Cells in a Pressure Ulcer Animal Model.* Stem Cells Int, 2018. 2018: p. 4789568.

24. Li, Y., et al., *Differentiation of Human Amniotic Mesenchymal Stem Cells into Human Anterior Cruciate Ligament Fibroblast Cells by In Vitro Coculture.* BioMed Research International, 2017. 2017: p. 7360354.

25. Han, Y., et al., *Differentiation of human umbilical cord mesenchymal stem cells into dermal fibroblasts in vitro.* Biochemical and Biophysical Research Communications, 2011. 413(4): p. 561-565.

26. Li, Y., et al., *Differentiation of Human Amniotic Mesenchymal Stem Cells into Human Anterior Cruciate Ligament Fibroblast Cells by In Vitro Coculture.* Biomed Res Int, 2017. 2017: p. 7360354.

27. Bordignon, P., et al., *Dualism of FGF and TGF-beta Signaling in Heterogeneous Cancer-Associated Fibroblast Activation with ETV1 as a Critical Determinant.* Cell Rep, 2019. 28(9): p. 2358-2372 e6.

28. Soundararajan, M. and S. Kannan, *Fibroblasts and mesenchymal stem cells: Two sides of the same coin?* J Cell Physiol, 2018. 233(12): p. 9099-9109.

29. Lv, F.J., et al., *Concise review: the surface markers and identity of human mesenchymal stem cells.* Stem Cells, 2014. 32(6): p. 1408-19.

30. Damerau, A., et al., *A Human Osteochondral Tissue Model Mimicking Cytokine-Induced Key Features of Arthritis In Vitro.* Int J Mol Sci, 2020. 22(1).

31. Damerau, A., F. Buttgereit, and T. Gaber, *Optimization of a Tricalcium Phosphate-Based Bone Model Using Cell-Sheet Technology to Simulate Bone Disorders.* 2022. 10(3): p. 550.

32. Damerau, A., et al., *Metabolic reprogramming of synovial fibroblasts in osteoarthritis by inhibition of pathologically overexpressed pyruvate dehydrogenase kinases.* Metab Eng, 2022. 72: p. 116-132.

33. Dominici, M., et al., *Minimal criteria for defining multipotent mesenchymal stromal cells. The International Society for Cellular Therapy position statement.* Cytotherapy, 2006. 8(4): p. 315-7.

34. Mizoguchi, F., et al., *Functionally distinct disease-associated fibroblast subsets in rheumatoid arthritis.* Nat Commun, 2018. 9(1): p. 789.

35. Astarita, J.L., S.E. Acton, and S.J. Turley, *Podoplanin: emerging functions in development, the immune system, and cancer.* Front Immunol, 2012. 3: p. 283.

36. Wells, R.G., *How collagen becomes 'stiff'.* Elife, 2022. 11.

37. Schroder, W.A., et al., *SerpinB2 deficiency modulates Th1Th2 responses after schistosome infection.* Parasite Immunol, 2010. 32(11-12): p. 764-8.

38. Kiener, H.P., et al., *Cadherin-11 induces rheumatoid arthritis fibroblast-like synoviocytes to form lining layers in vitro.* Am J Pathol, 2006. 168(5): p. 1486-99.

39. Orr, C., et al., *Synovial tissue research: a state-of-the-art review.* Nat Rev Rheumatol, 2017. 13(8): p. 463-475.

40. Prockop, D.J., *Marrow stromal cells as stem cells for nonhematopoietic tissues.* Science, 1997. 276(5309): p. 71-4.

41. Ichim, T.E., P. O'Heeron, and S. Kesari, *Fibroblasts as a practical alternative to mesenchymal stem cells.* Journal of Translational Medicine, 2018. 16(1): p. 212.

42. Ugurlu, B. and E. Karaoz, *Comparison of similar cells: Mesenchymal stromal cells and fibroblasts.* Acta Histochem, 2020. 122(8): p. 151634.

43. Lorenz, K., et al., *Multilineage differentiation potential of human dermal skin-derived fibroblasts.* Exp Dermatol, 2008. 17(11): p. 925-32.

44. Brohem, C.A., et al., *Comparison between fibroblasts and mesenchymal stem cells derived from dermal and adipose tissue.* Int J Cosmet Sci, 2013. 35(5): p. 448-57.

45. Brendel, C., et al., *Distinct gene expression profile of human mesenchymal stem cells in comparison to skin fibroblasts employing cDNA microarray analysis of 9600 genes.* Gene Expr, 2005. 12(4-6): p. 245-57.

46. Chen, F.G., et al., *Clonal analysis of nestin(-) vimentin(+) multipotent fibroblasts isolated from human dermis.* J Cell Sci, 2007. 120(Pt 16): p. 2875-83.

47. Sabatini, F., et al., *Human bronchial fibroblasts exhibit a mesenchymal stem cell phenotype and multilineage differentiating potentialities.* Laboratory Investigation, 2005. 85(8): p. 962-971.

48. Sabatini, F., et al., *Human bronchial fibroblasts exhibit a mesenchymal stem cell phenotype and multilineage differentiating potentialities.* Lab Invest, 2005. 85(8): p. 962-71.

49. Lin, C.-S., et al., *Commonly used mesenchymal stem cell markers and tracking labels: Limitations and challenges.* Histology and histopathology, 2013. 28(9): p. 1109-1116.

50. Lee, C.H., et al., *CTGF directs fibroblast differentiation from human mesenchymal stem/stromal cells and defines connective tissue healing in a rodent injury model.* The Journal of clinical investigation, 2010. 120(9): p. 3340-3349.

51. Xu, R., et al., *hiPS-MSCs differentiation towards fibroblasts on a 3D ECM mimicking scaffold.* Scientific Reports, 2015. 5(1): p. 8480.

52. Xu, R., et al., *Dual-delivery of FGF-2/CTGF from Silk Fibroin/PLCL-PEO Coaxial Fibers Enhances MSC Proliferation and Fibrogenesis.* Scientific Reports, 2017. 7(1): p. 8509.

53. Lee, C.H., E.K. Moioli, and J.J. Mao, *Fibroblastic differentiation of human mesenchymal stem cells using connective tissue growth factor.* Conference proceedings : ... Annual International Conference of the IEEE Engineering in Medicine and Biology Society. IEEE Engineering in Medicine and Biology Society. Annual Conference, 2006. 2006: p. 775-778.

54. Karsdal, M.A., et al., *The good and the bad collagens of fibrosis – Their role in signaling and organ function.* Advanced Drug Delivery Reviews, 2017. 121: p. 43-56.

55. Naugle, J.E., et al., *Type VI collagen induces cardiac myofibroblast differentiation: implications for postinfarction remodeling.* Am J Physiol Heart Circ Physiol, 2006. 290(1): p. H323-30.

56. Williams, L., et al., *Collagen VI as a driver and disease biomarker in human fibrosis.* FEBS J, 2021.

57. Mak, K.M. and R. Mei, *Basement Membrane Type IV Collagen and Laminin: An Overview of Their Biology and Value as Fibrosis Biomarkers of Liver Disease.* Anat Rec (Hoboken), 2017. 300(8): p. 1371-1390.

58. Evanko, S.P., et al., *Hyaluronan Controls the Deposition of Fibronectin and Collagen and Modulates TGF-beta1 Induction of Lung Myofibroblasts.* Matrix Biol, 2015. 42: p. 74-92.

59. Li, Y., et al., *Hyaluronan synthase 2 regulates fibroblast senescence in pulmonary fibrosis.* Matrix Biology, 2016. 55: p. 35-48.

60. Perryman, L. and S.G. Gray, *Fibrosis in Mesothelioma: Potential Role of Lysyl Oxidases.* Cancers, 2022. 14(4): p. 981.

61. Lee, N.-H., et al., *SERPINB2 is a novel indicator of stem cell toxicity.* Cell Death & Disease, 2018. 9(7): p. 724.

62. Rinn, J.L., et al., *Anatomic demarcation by positional variation in fibroblast gene expression programs.* PLoS Genet, 2006. 2(7): p. e119.

63. Denu, R.A., et al., *Fibroblasts and Mesenchymal Stromal/Stem Cells Are Phenotypically Indistinguishable.* Acta haematologica, 2016. 136(2): p. 85-97.

64. Yu, F.Y., et al., *TNF-α increases inflammatory factor expression in synovial fibroblasts through the toll-like receptor-3-mediated ERK/AKT signaling pathway in a mouse model of rheumatoid arthritis.* Mol Med Rep, 2018. 17(6): p. 8475-8483.

65. Akeson, G. and C.J. Malemud, *A Role for Soluble IL-6 Receptor in Osteoarthritis.* Journal of functional morphology and kinesiology, 2017. 2(3): p. 27.

66. Nishimoto, N., et al., *IL-6 inhibits the proliferation of fibroblastic synovial cells from rheumatoid arthritis patients in the presence of soluble IL-6 receptor.* Int Immunol, 2000. 12(2): p. 187-93.

67. Namba, S., et al., *ERK2 and JNK1 contribute to TNF-alpha-induced IL-8 expression in synovial fibroblasts.* PLoS One, 2017. 12(8): p. e0182923.

68. Tanabe, K., et al., *Mechanisms of tumor necrosis factor-α-induced interleukin-6 synthesis in glioma cells.* Journal of Neuroinflammation, 2010. 7(1): p. 16.

69. Mueller, L., et al., *TNF-alpha similarly induces IL-6 and MCP-1 in fibroblasts from colorectal liver metastases and normal liver fibroblasts.* Biochem Biophys Res Commun, 2010. 397(3): p. 586-91.

70. Holvoet, S., et al., *The inhibition of MAPK pathway is correlated with down-regulation of MMP-9 secretion induced by TNF-α in human keratinocytes.* Experimental Cell Research, 2003. 290(1): p. 108-119.

71. Jia, Y.-L., et al., *The expression of MAPK signaling pathways in conjunctivochalasis.* International journal of ophthalmology, 2019. 12(11): p. 1801-1806.

72. Park, S., et al., *ERK/MAPK pathways play critical roles in EGFR ligands-induced MMP1 expression.* Biochemical and Biophysical Research Communications, 2011. 407(4): p. 680-686.

73. Koedderitzsch, K., et al., *TNF induces glycolytic shift in fibroblast like synoviocytes via GLUT1 and HIF1A.* Scientific Reports, 2021. 11(1): p. 19385.

74. Zhou, J. and B. Brune, *Cytokines and hormones in the regulation of hypoxia inducible factor-1alpha (HIF-1alpha).* Cardiovasc Hematol Agents Med Chem, 2006. 4(3): p. 189-97.

75. Gaber, T., et al., *Macrophage migration inhibitory factor counterregulates dexamethasone-mediated suppression of hypoxia-inducible factor-1 alpha function and differentially influences human CD4+ T cell proliferation under hypoxia.* J Immunol, 2011. 186(2): p. 764-74.

4. CHAPTER: DISCUSSION

The aim of this thesis was to establish and characterize *in vitro* tissue equivalents of the human (1) cancellous bone (Damerau, Pfeiffenberger et al. 2020, Damerau, Buttgereit et al. 2022), (2) articular cartilage (Damerau, Pfeiffenberger et al. 2020), and (3) synovial membrane using mesenchymal stromal cells. This enables the production of a structurally complete joint model from single donor material, thereby laying the foundation for a personalized screening platform to identify novel targets and test therapeutic strategies.

To this end, (i) an *in vitro* scaffold-based 3D bone model based on human MSCs, including the bone-forming cells without osteoclasts was developed and further optimized using cell-sheet technology. Osteogenic differentiation was induced by dexamethasone, β-glycerophosphate, and ascorbic acid, verified on gene and protein level and by measuring calcification and matrix deposition. Suitability and applicability were verified by treatment with either cytokines relevant in arthritis or the hypoxia-inducible factor (HIF)-stabilizer deferoxamine (DFO), well-known to promote and support osteogenesis.

Next, (ii) scaffold-free cartilage-like constructs were developed at macro- and microscale. As a proof of principle study, these constructs were treated with disease-relevant cytokines to analyze arthritis-related changes in cell- and matrix-composition reflecting pathophysiological alterations similar to those found in RA and OA.

To better simulate the *in vivo* structure of the joint, I combined both models (iii) to generate a functional osteochondral unit. Remarkably, after stimulation with disease-relevant cytokines, the functional osteochondral unit showed a different response in a tissue-specific manner, although they were from the same donor.

Finally, (iv) a synovial membrane model was established consisting of a lining and sublining layer. As a prerequisite for the application of MSCs in this model, I demonstrated that MSCs share considerable similarities with "healthy" synovial fibroblasts in terms of e.g., morphology, surface markers, and the expression of "classical" fibroblast markers. Moreover, the synovial membrane model was validated in this work using disease-relevant cytokines as observed in RA.

Although the models still have some limitations such as missing blood vessels, nerves, and hematopoietic cells of the bone marrow, the results obtained here are very promising. The developed 3D *in vitro* joint model provides the opportunity to study bone and cartilage degrading processes and the evolving synovial pannus as a result of arthritis on cellular level within the tissue. Moreover, it allows to investigate cytokine-driven processes of arthritis and therapeutic interventions on cellular and tissue level *in vitro*.

In the case of RA, the most common immune-mediated inflammatory joint disease, the treatment goal today is to achieve sustained clinical remission or at least low disease activity. However, a strong unmet medical need remains. Strikingly, not all patients reach sustained clinical remission, and a substantial proportion of them still suffer from moderate or even high disease activity (Haugeberg, Hansen et al. 2015, Ajeganova and Huizinga 2017, Burmester and Pope 2017). The disease is characterized by systemic inflammation, persistent synovitis, expansion of synovial cells (pannus formation), and progressive cartilage and bone destruction. Progressive cartilage destruction is also the key feature of OA ─ a degenerative joint disease ─ one of the leading causes of age-related disability. So far, therapeutic approaches only address the symptomatic relief of pain (Glyn-Jones, Palmer et al. 2015). However, many details of the underlying causes and mechanisms remain elusive.

Although the development of potential new therapies was based on promising preclinical animal data, in recent years we experienced their failure in clinical trials. Despite these limitations, *in vivo* rodent models such as collagen type II induced arthritis in rats and serum transfer models in mice are still the "gold standard" in rheumatological research (Choudhary, Bhatt et al. 2018). However, their results often cannot be transferred one-to-one to humans, as arthritis does not occur spontaneously in these animal models and only depicts individual features of the disease. In the predominant animal models, arthritis has to be induced *in vivo* either chemically by a single agent or genetically by DNA manipulations (Trentham, Townes et al. 1977, Schinnerling, Rosas et al. 2019). However, chemically induced arthritis usually resolves within a few weeks without treatment, while genetically modified models of arthritis do only represent some features of human arthritis and these animals often develop additional diseases, including inflammatory bowel diseases (Trentham, Townes et al. 1977, Schinnerling, Rosas et al. 2019). Besides the fact that animals do not naturally develop RA, there are more important differences between the *in vivo* “gold standard” ─ the murine system ─ and the human system, including the balance of lymphocytes and neutrophils (Doeing, Borowicz et al. 2003), the articular cartilage thickness/structure, the loading conditions during movement (Malda, de Grauw et al. 2013), the ecological niches and the lifespan (Mestas and Hughes 2004). Although genomic comparisons of mice and humans revealed significant overlaps in transcriptional programs, they also expose noteworthy differences that may lead to challenges in clinical translation (Seok, Warren et al. 2013, Shay, Jojic et al. 2013). Additionally, rodent models are not applicable for testing biologics such as monoclonal antibodies that specifically target human proteins (Schinnerling, Rosas et al. 2019).

Thus, it is necessary to shift the traditional research approaches in biomedicine towards improved human patient-driven translation by using human-based *in vitro* models. Besides the general enhancement of the protection level for animals used in scientific experiments, the

European Union (EU) Directive 2010/63/EU includes the request that alternative methods must be developed and used if they are available in order to facilitate the replacement, reduction, and refinement of animal experiments (3R principle) (Burch 2009, European Parliament 2010). In toxicology, animal-free methods have been discussed for years. Due to the political pressure by the REACH (Registration, Evaluation, Authorization of Chemicals) guideline and the EU Cosmetic Directive 76/768/EEC, international test guidelines based on *in vitro* human skin models for skin corrosion or irritation by chemicals were successfully approved. In addition, animal experiments were banished from the cosmetics industry in Europe in 2013 (Ruet Rossignol 2005, Hartung 2008).

In biomedical research, the 3Rs are increasingly implemented although alternative methods are still scarce. Therefore, various *in vitro* model approaches have been developed and evaluated in recent years (Ringe and Sittinger 2009, Ribel-Madsen, Bartels et al. 2012, Peck, Leom et al. 2018). The variety of *in vitro* approaches ranges from simple monolayer cultures to co-culture systems and the *in vitro* cultivation of tissue explants from RA patients (Ringe and Sittinger 2009, Ribel-Madsen, Bartels et al. 2012, Peck, Leom et al. 2018). In addition, there has recently been significant progress in the development of miniaturized cell systems cultured in microfluidic devices ─ organ-on-a-chip approaches (Banh, Cheung et al. 2022, Paggi, Teixeira et al. 2022). However, until now, there is no *in vitro* joint model capable of mimicking either a healthy or inflamed joint, including most of the relevant tissue types, cells, and humoral factors, allowing the testing of a variety of specific therapeutic approaches.

Since MSCs are multipotent non-hematopoietic progenitor cells capable of differentiating into individual resident cell types of the mesenchyme, they were used in this study to develop the three main components of a donor-derived joint *in vitro*. Their advantages include ease of harvest, availability, fast expansion, potent immunosuppressive effects, and their ability to differentiate into cell types of bone, cartilage, and synovium (Kim and Park 2017). However, many fundamental biological aspects of MSCs remain elusive. This is primarily a direct consequence of the heterogeneity observed between donors, tissues, and single cells within a population (Wilson, Hodgson-Garms et al. 2019). Their heterogeneity makes them extremely attractive for tissue engineering applications since the diversity of a group of individuals can be represented (Rosenbaum, Grande et al. 2008). To precisely characterize the MSCs used in this study, I followed the minimal criteria that define MSCs proposed by the International Society for Cellular Therapy (Dominici, Le Blanc et al. 2006). This includes that MSCs must be adherent to plastic. Furthermore, they must be positive for the surface markers CD73, CD90, and CD105, while lacking CD14, CD20, CD34, CD45, and HLA-DR. Finally, MSCs must show successful differentiation into at least two different lineages (Dominici, Le Blanc et al. 2006). Only cells that fulfilled these criteria were enrolled in the study.

One of the central local destructive features of RA is focal bone loss or erosion. In the later stages of inflammation, even cancellous bone and underlying remodeling processes are affected (Karmakar, Kay et al. 2010). Bone tissue is very complex in terms of cell composition, matrix organization, vascularization, and mechanical loading. The most common approaches of bone tissue engineering focus on fabricating implants for bone regeneration (Wang, Cao et al. 2017). However, over the past years, bone tissue engineering has been extensively used to establish artificial bone models. These models have not only improved our understanding of bone-related (patho)physiological mechanisms, such as osteoporosis, but can also be used to promote bone repair and regeneration (Amini, Laurencin et al. 2012, Ehnert, Rinderknecht et al. 2020). However, depicting native bone in its complexity remains a major challenge *in vitro* due to the physical properties and the different cell types ─ osteoblasts, osteoclasts, osteocytes, and endothelial cells ─ that have to be included. In the model presented here, however, the focus was on the generation of important articular building blocks from the same donor in a simplified manner, instead of representing bone complexity.

Current *in vitro* bone modeling approaches range from scaffold-based over scaffold-free spheroids or organoids to 3D printing technologies (de Barros, Takiya et al. 2010, Dhivya, Saravanan et al. 2015, Agarwal, Kabiraj et al. 2016, Bendtsen, Quinnell et al. 2017, Duan, Haque et al. 2017). A variety of advanced scaffolds have been developed that reproduce structural properties and mechanical stiffness of bone. Biodegradable, and non-biodegradable synthetic, and natural bone graft substitutes provide cavities for nutrient supply and cell penetration (Ghassemi, Shahroodi et al. 2018). Among these, bioceramics are considered the most promising biomaterials as they generally show better tissue responses compared to polymers and metals and are well known to be osteoconductive (Liu, Zhao et al. 2007, Zimmermann and Moghaddam 2011, Bohner, Santoni et al. 2020). HA, β-tricalcium phosphate (TCP), and biphasic calcium phosphate (BCP), such as HA:β-TCP scaffolds closely resemble the native bone matrix and are therefore widely used. β-TCP is the most employed bone graft due to its biocompatibility, cell-mediated resorption, and osteotransductive and osteoinductive capacities in bone regeneration (Kondo, Ogose et al. 2005, Yuan, Fernandes et al. 2010, Le Gars Santoni, Niggli et al. 2022), which is in line with my results (Damerau, Pfeiffenberger et al. 2020, Damerau, Buttgereit et al. 2022). Osteogenic differentiation is controlled by several transcription factors such as runt-related transcription factor 2 (*RUNX2*) and osterix (*OSX*) representing early osteogenic markers (Komori 2006, Luo, Chen et al. 2008). Later osteogenic marker genes include e.g., secreted phosphoprotein 1 (*SPP1*) and osteonectin (*ON*) (Kulterer, Friedl et al. 2007, Wrobel, Leszczynska et al. 2016). Using β-TCP, mimicking the mineral bony part, we confirmed the osteogenic phenotype of MSCs based on the expression of *RUNX2*, *COL1A1*, *SPP1*, and *ON.* In addition, calcium deposition increased after 7 days, indicating the

cells' mineralization capacity within the tissue model (Damerau, Pfeiffenberger et al. 2020). The time-dependent gene expression pattern is consistent with the study of Cao et al showing the differential gene expression of *RUNX2*, *ON*, and alkaline phosphatase (*ALP*) using rat bone marrow-derived MSCs on β-TCP particles (Cao, He et al. 2019). In a study comparing the most common bone graft substitutes seeded with either MSCs or primary osteoblasts, β-TCP (Cerasorb®) was shown to be superior in terms of cell adherence, biocompatibility, cell vitality, and cell growth (Herten, Rothamel et al. 2009). In the underlying study, β-TCP facilitated the differentiation, adhesion, and homogeneous cell distribution of MSCs and closely mimicked trabecular bone's porosity (Keaveny, Morgan et al. 2001, Damerau, Pfeiffenberger et al. 2020). Furthermore, biocompatibility was confirmed by lactate dehydrogenase (LDH) assay and high cell viability after 3 weeks by LIVE/DEAD^{TM} staining, which is in agreement with the study of Mucientes et al who observed the highest cell viability when MSCs were colonized on β-TCP compared to other bone grafts (Damerau, Pfeiffenberger et al. 2020, Mucientes, Herranz et al. 2021). All the aforementioned approaches further confirm MSCs as a suitable cell source for the development of a bone model. Bioactive compounds, such as BMP-2, fibroblast growth factors (FGFs) or vascular endothelial growth factors (VEGFs), have been used in several studies to further support cell proliferation and the osteoconductive and osteoinductive properties of scaffolds for bone regeneration (Vaccaro 2002, Fernandes, Wang et al. 2016, Wang, Zhang et al. 2017, De Witte, Fratila-Apachitei et al. 2018, Yin, Qiu et al. 2018). However, the focus of my model system was foremost not on bone regeneration, where these substances are most often used. Furthermore, particularly BMP-2 causes striking side effects that should be avoided in the underlying study (James, LaChaud et al. 2016).

The mode of cell seeding and attachment of cells to a scaffold is an important step in tissue engineering. Its efficiency and distribution can influence the biological performance of *in vitro* models (Liu, Tamaddon et al. 2020). To further optimize our cancellous bone model presented here regarding cell number and cell distribution, pre-seeded β-TCP bone graft substitutes were wrapped with an osteogenically induced MSC-sheet (Damerau, Buttgereit et al. 2022). Sheet technology has been shown to result in a higher expression of osteogenic genes and showed profound matrix formation *in vitro* compared to the β-TCP without an additional cell-sheet (Lu, Zhang et al. 2019, Damerau, Buttgereit et al. 2022). The promising osteogenic potential of cell-sheets wrapped around a pre-seeded TCP was e.g., demonstrated in a femoral defect model in rats: While MSC/TCP wrapped with osteogenic cell sheets induced callus formation at week 8 post-transplantation, MSC/TCP without additional cell sheet resulted in non-union of bone (Ueha, Akahane et al. 2015). In another study, cell sheets were produced of rabbit MSCs and transplanted in subcutaneous pockets of mice demonstrating the formation of bone tissue without an additional bone graft substitute (Ma, Ren et al. 2010). These and also our studies

underline the osteogenic potential using sheet technology (Damerau, Buttgereit et al. 2022). Usually, cells seeded on artificial bone substitutes such as β-TCP do not populate the scaffold homogeneously and reproducibly, but remain trapped in suspension in the pores. In contrast, the cell-sheet provides a microenvironment that facilitates and enhances cell seeding and differentiation and is suitable to optimize production and osteogenic properties of small scale and small amounts of scaffolds (Liu, Tamaddon et al. 2020, Damerau, Buttgereit et al. 2022). To achieve the mechanical effect important for natural bone, microfluidic devices in combination with bioceramics facilitate *in vitro* osteogenesis in a defined, standardized, controlled and reproducible manner (Bouet, Cruel et al. 2015). New promising *in vitro* approaches aim to realize vascularized bone models using human umbilical vein endothelial cells (HUVECs) (Deng, Jiang et al. 2017, Marshall, Barnes et al. 2018, Yan, Chen et al. 2019, Chiesa, De Maria et al. 2020). For instance, osteogenic differentiation of MSCs was first induced on a 3D bioprinted micropore scaffold. After 2 weeks, HUVECs were applied and invaded the macropores, thereby forming a capillary-like network visualized via immunofluorescence (Chiesa, De Maria et al. 2020). To study the interaction of osteoblasts and osteoclasts, mainly *in vitro* monolayer co-cultures have been used, whereas more recent approaches focus on 3D cultivation. Novel triple cultures combine osteoblasts, osteocytes, and osteoclasts in a rat-based collagen gel to study cell-cell interactions related to bone remodeling (Bernhardt, Skottke et al. 2021, Wirsig, Kilian et al. 2022). In the bone model presented here, osteoclast-mediated bone remodeling processes, vascularization, and mechanical loading are not yet implemented. These inherent limitations need to be addressed in the future to mimic focal bone loss or erosion in late-stage RA involving osteoblasts, osteoclasts, and the vessel system.

In RA, bone remodeling processes are mainly driven by pro-inflammatory cytokines secreted by synovial fibroblasts and immune cells such as T cells and macrophages (Karmakar, Kay et al. 2010). To analyze the applicability of the bone model presented here as a tool to mimic key features of arthritis, cytokine-mediated inflammation was induced. This resulted in a higher expression of inflammatory marker (e.g., *TNFA, IL8*) and the HIF-related marker *LDHA* (Damerau, Pfeiffenberger et al. 2020). In contrast to our study, exposure to IL-6, IL-1β, and TNF-α ─ representing an OA environment ─ significantly increased catabolic activity and angiogenesis in a vascularized bone model based on a mesenchymal cell line and HUVECs (Pirosa, Tankus et al. 2021). These differences could be explained by the considerable variation in culture and stimulation duration and experimental design, which might affect the gene expression pattern. In addition, FDA-approved therapeutics, namely adalimumab and tocilizumab, were able to reduce the extent of inflammation in the model presented here (Damerau, Pfeiffenberger et al. 2020). The efficacy of drugs tackling arthritic diseases was

inter alia confirmed by a study of Zigon-Branc and colleagues (Žigon-Branc, Barlič et al. 2018). They induced inflammation via TNF-α and IL-1β on microspheroids of osteoarthritic primary chondrocytes. After treatment with adalimumab, they demonstrated significant anti-inflammatory effects (Žigon-Branc, Barlič et al. 2018). In contrast, DFO that is well-known to induce a cellular response resembling hypoxic adaptation and prevent HIF1α degradation (Guzey, Aykan et al. 2016), enhanced glycolytic, osteogenic, and angiogenic processes in my cancellous bone model (Damerau, Buttgereit et al. 2022). In summary, 3D cultivation of pre-differentiated MSCs resulted in a response to disease-associated cytokines and therapeutics, which resembled essential processes *in vivo*.

In addition to the destructive impact on bone tissue, arthritis primarily degenerates cartilage, ultimately resulting in cartilage breakdown. Similar to the bone modeling discussed above, *in vitro* 3D culturing of (pre)-chondrocytes most closely reflects the situation *in vivo* (Bhumiratana, Eton et al. 2014, Bhattacharjee, Coburn et al. 2015, Anderson, Markway et al. 2017). However, scaffolds are commonly used to provide 3D culture systems with a suitable predetermined structure. To avoid scaffold-induced cell effects, scaffold-free tissues such as cartilage are in the focus of recent developments. These engineered cartilage equivalents could serve as a promising approach for cartilage repair *in vivo*, or as an excellent *in vitro* model providing the opportunity to evaluate ECM formation and degradation without the interference of a scaffold (Murdoch, Grady et al. 2007, DuRaine, Brown et al. 2015). Since arthritis ultimately results in the non-regenerative degradation of articular cartilage driven by inflammatory processes, musculoskeletal research has mainly focused on the underlying processes in cartilage using explants or monolayer cultures as *in vitro* models (Gabriel, Innes et al. 2010, Neidlin, Chantzi et al. 2019, Mixon, Savage et al. 2021). Chondrocytes are very sensitive to the molecular and mechanical influences of their environment. Therefore, it is generally assumed that 3D tissue models with a matrix that corresponds to the natural tissue properties best mimic the situation *in vivo* (Goldring 2005). Hence, several *in vitro* tissue engineering approaches that impart a predetermined 3D structure to cells use scaffolds based on natural matrices such as porous collagen type II-based scaffolds (Zhang, Chen et al. 2013), gelatin microspheres (Peck, Leom et al. 2018), alginate beads (Andreas, Lubke et al. 2008), hyaluronic acid- and chitosan-based gels (Park, Choi et al. 2013). Peck et al. developed a 3D cartilage model based on chondrocytes isolated from porcine knee cartilage suspended in gelatin microspheres (Peck, Leom et al. 2018). Due to the use of primary chondrocytes instead of the pre-differentiated MSCs used in our approaches (Damerau, Pfeiffenberger et al. 2020, Weber, Fischer et al. 2020), the model composition was characterized by high expression of collagen type II and proteoglycans from day 1, closely resembling native cartilage (Peck, Leom et al. 2018). The stiffness and absorption properties of natural matrices cannot be adapted to the specific

requirements of the individual cartilage zones. At present, the macroSFCCs and miniSFCCs are not capable of simulating all zones of the cartilage (Damerau, Pfeiffenberger et al. 2020, Weber, Fischer et al. 2020). To overcome this limitation, Karimi et al. modeled the superficial, middle, and calcified zones using cell density gradients, mechanical strain, and growth factors to specifically reconstruct the zonal architecture of articular cartilage prospectively (Karimi, Barati et al. 2015). To date, no single scaffold has all the desired properties to mimic the complexity and restore the functionality of chondrocytes in their natural state (Chinta, Velidandi et al. 2021). In contrast to scaffold-based tissue engineering approaches, scaffold-free procedures such as those used in this study mimic the condensation and differentiation that takes place during the development of natural cartilage and thus exclude material interference (Whitney, Mera et al. 2012, Bhumiratana, Eton et al. 2014, DuRaine, Brown et al. 2015, Yasui, Ando et al. 2016, Park, Jin et al. 2018, Damerau, Pfeiffenberger et al. 2020, Weber, Fischer et al. 2020). The scaffold-free, mechanical load-induced, self-organized, macroscale chondrogenic construct presented here exhibited a cartilage-like phenotype as evidenced by *COL2A1* and *ACAN* gene expression and histological analysis (Damerau, Pfeiffenberger et al. 2020, Weber, Fischer et al. 2020). However, *COL1* was still expressed, in contrast to native human articular cartilage as observed in other studies (Furukawa, Suenaga et al. 2003, Babur, Ghanavi et al. 2013, Sato, Yamato et al. 2014, Futrega, Palmer et al. 2015, Zhang, Ba et al. 2015, Nakagawa, Muneta et al. 2016). Although macroscale scaffold-free constructs have several advantages, such as the ability to study loading effects, obtain sufficient material for a range of analyses, avoid non-human exogenous material, and serve as implants, these chondrogenic constructs require a large number of cells. In addition, diffusion of metabolites across a pellet length of approximately 2 mm is inefficient, leading to radial tissue heterogeneity (Babur, Ghanavi et al. 2013). Besides, chronic undersupply of large spheroids or organoids can lead to a necrotic center (Ryu, Lee et al. 2019). For mid- and high-throughput preclinical screening tools, the size of chondrogenic constructs must be reduced to require a smaller number of cells while maintaining uniform morphology during differentiation and avoiding necrosis in the center (Penick, Solchaga et al. 2005, Moreira Teixeira, Leijten et al. 2012). In the study presented here, macroscale SFCCs (average size: 5 mm) were therefore reduced to miniSFCCs (average size: 1.4 mm), which showed comparable expression of *COL2A1* and *ACAN* relative to *COL1A1* after less differentiation time, demonstrating enhanced chondrogenic differentiation in microscale (Babur, Ghanavi et al. 2013). In the case of arthritides such as RA, chondrocytes have been reported to be involved in the following ways: production of pro-inflammatory cytokines, increased apoptosis, suppression of matrix synthesis, and increased expression of matrix-degrading enzymes and adhesion molecules (Pap and Korb-Pap 2015). The effects of pathophysiological concentrations of cytokines seen in RA or OA synovial fluid have been shown to cause cartilage damage only after years

(Ostrowska, Maśliński et al. 2018). In contrast, the experimental settings *in vitro* last only for weeks. Therefore, using supra(patho)physiological cytokine concentrations *in vitro* is widely accepted for experimental reasons (Pratta, Di Meo et al. 1989, Schuerwegh, Dombrecht et al. 2003, Hogrefe, Joos et al. 2012, Weber, Fischer et al. 2020). Particularly in RA, pro-inflammatory stimuli such as TNF-α or IFN-γ activate catabolic and inflammatory processes in human chondrocytes and decrease their viability and proliferation while increasing matrix degradation (Schuerwegh, Dombrecht et al. 2003, Rannou, François et al. 2006, Adan, Guzman-Morales et al. 2013). In our case, TNF-α stimulation with 100 ng/mL induced the expression of pro-inflammatory cytokines such as *IL8*, increased apoptosis (e.g., Bcl-2 Associated X-protein (*BAX*) expression), decreased gene expression of matrix components such as *COL2A1* and *ACAN*, and increased catabolic processes as observed in RA (Peck, Leom et al. 2018). In agreement with the study of Wu and colleagues, MMP1 was predominant in cells of the superficial zone (Wu, Du et al. 2008), whereas MMP13 was predominant in the central region. To approximate the arthritis environment, the macroSFCCs were used in another study of our group where we evaluated their capability to respond to the combination of IL-1β and TNF-α *in vitro* (Weber, Fischer et al. 2020). The stimulation enhanced the expression of proteases and inhibited the synthesis of ECM molecules, mainly collagen type II and aggrecan (Weber, Fischer et al. 2020). These findings are in line with the results obtained by Pretzel et al. (Pretzel, Pohlers et al. 2009). They analyzed processes in bovine cartilage disc degradation after treatment with IL-1β and TNF-α. As a result, they observed an upregulation of *MMP1*, *MMP3*, and pro-inflammatory cytokines such as *IL6* and *IL8* (Pretzel, Pohlers et al. 2009).

It is well-known that the physical connection between bone and cartilage ─ the osteochondral unit ─ changes during arthritis, rendering this area critical in the disease progression of OA and RA (Sandell and Aigner 2001, Goldring and Goldring 2016, Fan, Wu et al. 2021). At least in OA, there is controversy whether the disease begins in cartilage or bone and which is the more appropriate target for the development of disease-modifying drugs (Lozito, Alexander et al. 2013). Currently, multicomponent engineering approaches are often used to mimic the main features of OA, not RA, or to develop artificial matrices for *in vivo* replacement or regeneration of damaged regions. Thus, many promising *in vitro* approaches have recently been developed using (i) heterogeneous or (ii) homogenous scaffolds for bone and cartilage, (iii) scaffold-based bone and scaffold-free cartilage, or (iv) heterogeneous (bi-layered) scaffolds (Zhao, Yan et al. 2016, Wang, Hu et al. 2018). To avoid biocompatibility issues, the use of adhesives such as fibrin which are often used to fix bilayer systems but also provide a barrier to cell-cell contact was omitted (Okada, Nakai et al. 2017). In a study using mesenchymal progenitor cells, both tissues were developed based on a homogenous poly-$_{D,L}$-lactic acid (PLA) scaffold and co-

cultured after differentiation as in our study. This bilayer osteochondral unit showed a prominent transition zone between cartilage and bone without the use of adhesives (Tuli, Nandi et al. 2004). Combining polymer-ceramic bone scaffold and scaffold-free chondrogenic constructs, I also demonstrated the formation of a well-integrated osteochondral bilayer system (Damerau, Pfeiffenberger et al. 2020). However, the long cultivation time represents a major limitation since the individual components are first prepared and then combined by co-cultivation. Lin et al. were able to overcome this limitation by using a multi-chamber bioreactor that provides a controlled environment and develops both tissue components simultaneously by feeding them with specific differentiation media streams (Lin, Lozito et al. 2014). Addressing the restriction that most artificial osteochondral units contain only cartilage and bone cells, recent approaches also attempt to integrate blood vessels in the form of a three-phase model with endothelial cells. Therein, HUVECs formed a stable capillary-like network under perfused cultivation conditions (Pirosa, Gottardi et al. 2021). To mimic the pathophysiology of RA, I repeatedly treated the osteochondral unit for three weeks with a cocktail of RA-related cytokines, TNF-α, IL-6 and MIF, at concentrations observed under pathophysiological conditions (Tetta, Camussi et al. 1990, Lettesjö, Nordström et al. 1998, Leech, Metz et al. 1999, Damerau, Pfeiffenberger et al. 2020). This treatment resulted in an increase in MMPs and proinflammatory cytokines similar to that observed in RA patients (Burrage, Mix et al. 2006, Damerau, Pfeiffenberger et al. 2020). Remarkably, bone and cartilage components derived from the same MSC donor gave different responses regarding the gene expression. In brief, *MMP1* and *MMP3* were significantly higher expressed in cartilage after stimulation, while unaffected in bone (Damerau, Pfeiffenberger et al. 2020). These findings confirmed a study of Lin and colleagues. They stimulated their osteochondral unit with the OA-related cytokine IL-1β and demonstrated that the chondral and osseous tissues are capable of responding in a disease-relevant and tissue-specific manner (Lin, Lozito et al. 2014).

The impaired bone turnover and cartilage damage in RA and OA are thought to be due to worsening synovitis, an inflammation of the third structural component of the joint, the synovial membrane or synovium (Mor, Abramson et al. 2005, Han, Fang et al. 2020). The synovial membrane can be divided into synovial intima and subintima and lines the joint cavity. FLSs of the synovial membrane maintain the structural and dynamic integrity of joints under physiological conditions but have also been identified as key drivers of synovitis and cartilage degradation in both RA and OA (Mor, Abramson et al. 2005, Mathiessen and Conaghan 2017, Han, Fang et al. 2020). Therefore, FLSs are given greater consideration in tissue engineering approaches to develop *in vitro* 3D models of the synovial membrane (Pap, Dankbar et al. 2020). The most challenging aspect of these approaches is to obtain sufficient numbers of FLSs that are not affected by inflammation. In recent years, several studies have compared

MSCs and FLSs and have shown that they express almost the same markers, exhibit multipotency potential, and immunomodulatory properties (Cappellesso-Fleury, Puissant-Lubrano et al. 2010, Denu, Nemcek et al. 2016, Ichim, O'Heeron et al. 2018, Soundararajan and Kannan 2018, Fan, Liao et al. 2022). Other scientists reported clear differences between these cell types and the need for substances such as connective tissue growth factor (CTGF) to differentiate MSCs into fibroblasts (Lee, Moioli et al. 2006, Lee, Shah et al. 2010). Therefore, in a first step, I compared MSCs with trauma-FLSs according to the minimal criteria for MSCs (Dominici, Le Blanc et al. 2006). This comparison revealed profound similarities regarding their ability to adhere to plastic, typical MSC surface marker pattern and the multipotency potential, respectively. Secondly, I compared both cell types regarding characteristic fibroblast-related features. I identified similarities in cytokine release, proliferation, and the expression of specific fibroblast-related markers on mRNA level. In contrast to Lee et al., I did not observe an increase in collagen type I after CTGF treatment (Lee, Moioli et al. 2006, Lee, Shah et al. 2010). Since treatment with CTGF did not correspond to the expression pattern of MSCs to FLSs, untreated MSCs were used to develop the *in vitro* synovial membrane model. Studying a selected gene expression pattern in FLSs exposed to an inflammatory milieu ─ OA-FLSs ─ revealed a similar fibroblast-specific gene expression profile, whereas fibronectin 1 (*FN1*) appeared to be decreased in a disease-specific manner (Damerau, Kirchner et al. 2022), in contrast to the study by Schröder et al. (Schroder, Nazet et al. 2019). So far, there are only a few reports on *in vitro* simulated synovial membranes that provide a mechanistic representation of the cellular inflammatory processes involved in synovitis. To mimic the inflamed synovial membrane, cells such as FLSs from e.g., RA patients are commonly embedded in hydrogels to map the 3D architecture (Kiener, Watts et al. 2010). The *in vitro* micromass culture of the synovial membrane was used to assess unique effects of proinflammatory cytokines on mesenchymal tissue remodeling. In this regard, IFN-γ enhanced the migrating FLSs phenotype, resulting in architectural changes, while TNF-α induced RA-FLSs aggregation (Karonitsch, Beckmann et al. 2018). To overcome the limitation of using cells already exposed to an inflammatory milieu, I used MSCs to mimic a healthy synovial membrane. Inflammation was simulated by a cytokine cocktail of TNF-α, IL-6, and MIF. Cytokine treatment significantly increased gene expression of pro-inflammatory genes such as *IL6* and *IL8*, the hypoxia-related gene *VEGFA*, cell hyperproliferation, and the tissue-degrading enzyme *MMP1*, while *MMP13* and *IL1B* tended to be more expressed compared to the control. Broeren et al stimulated their micromass synovial membrane model based on human RA-FLSs and macrophages with either TNF-a or TGF-β (Broeren, Waterborg et al. 2019). This resulted in a specific response in terms of the expression of inflammatory and fibrosis markers, respectively (Broeren, Waterborg et al. 2019). In agreement with our findings, those results emphasize the high potential of 3D *in vitro* approaches as an excellent alternative for drug

testing and mechanistic research. The synovial membrane model from Broeren and colleagues simulates the lining layer with fibroblast- and macrophage-like synoviocytes on the outer surface of the micromass culture corresponding to the natural cellular composition of the synovium (Broeren, Waterborg et al. 2019). However, the macrophage-like synoviocytes of the synovial membrane that affect and mediate inflammatory processes are not yet implemented in my MSC-based model. In the human joint, only the lining layer is oriented toward the synovial fluid, whereas immune cells primarily infiltrate the sublining layer around the vessels (Smith 2011, Mizoguchi, Slowikowski et al. 2018). This polar architecture is difficult to reproduce in a micromass culture. The synovial membrane presented here first offers the possibility to overcome this limitation: the physiological arrangement enables the simulation of the migration of immune cells in the sublining while the lining layer is in contact with the synovial fluid. Of note, all the above-mentioned studies used animal-derived Matrigel™ for micromass cultures (Kiener, Watts et al. 2010, Karonitsch, Beckmann et al. 2018, Broeren, Waterborg et al. 2019). Even though these models closely reflect the pathophysiological synovial membrane, they are all based on diseased FLSs, which are often limited in availability and affected by different stages of disease and current medications (Kasperkovitz, Timmer et al. 2005). Therefore, to mimic the healthy physiological situation that is essential for understanding pathogenic alterations of the synovium, an easy-to-handle and available cell source that shares the characteristics of FLSs would be ideal for simulating synovial tissue *in vitro*. Thus, adult MSCs sharing most of the properties with FLSs (Denu, Nemcek et al. 2016), are an ideal cell source to develop an *in vitro* 3D synovial membrane model and the other components of the joint highlighted in the study presented here.

RA is a highly complex disease involving immune cell interaction. To date, bioengineering and *in vitro* 3D approaches mostly exclude the immune component due to its great diversity and complex requirements for an appropriate microenvironment and humoral surroundings (Ramadan and Gijs 2015, Mengus, Muraro et al. 2018). Underlying mechanisms are still poorly understood and therefore the immune system needs to be considered in future 3D approaches. Microfluidic devices could be used to culture immune cell populations under a controlled microenvironment, separated e.g., by a stretchable porous membrane from a joint tissue component, to study the specific involvement of immune cells in the disease process (Paggi, Teixeira et al. 2022). In addition, to enable inter-tissue communication, the building blocks of the joint generated here need to be combined to engineer an appropriate human joint model. To date and to the best of my knowledge, there is no comprehensive *in vitro* joint model that allows for the study of inter-tissue communication and that could serve as an alternative to animal experiments in the field of rheumatic diseases. Advanced 3D models are currently combined with cutting-edge technology such as 3D printing and microfluidic devices. The

former allows the precise control of the architecture, while the latter provide e.g., fluid circulation in a controlled environment. Microfluidic devices ─ organ-on-a-chip ─ are therefore the most promising future tool to understand tissue-tissue, immune system-tissue, and drug-tissue interactions (Jorgensen and Simon 2021). The joint-on-a-chip still faces hurdles, while cartilage-on-a-chip has only been developed recently (Occhetta, Mainardi et al. 2019, Paggi, Venzac et al. 2020, Jorgensen and Simon 2021). However, novel approaches are emerging, implementing microfluidic devices that offer the opportunity to connect the tissue-specific units to an external pump or a microfluidic motherboard (Loskill, Marcus et al. 2015, Ong, Ching et al. 2019). Promotion of a xeno-free, preclinical testing tool could provide deeper insights into pathomechanisms of RA and OA. In addition, therapeutics such as biologics could be tested under controlled conditions in a high-throughput manner, and animal-free conditions could promote the transferability of results to patients.

In summary, I successfully developed tissue equivalents of an artificial joint ─ cancellous bone, articular cartilage, and synovial membrane ─ using human bone marrow-derived MSCs and demonstrated that it is possible to simulate key features of arthritis *in vitro* (Damerau, Pfeiffenberger et al. 2020, Damerau, Buttgereit et al. 2022). The combination of the bone and cartilage components created a functional osteochondral unit that responded differently to cytokine stimulation and therapeutic intervention (Damerau, Pfeiffenberger et al. 2020). In addition, the developed xeno-free synovial membrane model is scalable and can be combined with the osteochondral unit and immune cells in the future to enable the crosstalk between tissues and cells which is essential for simulating this complex rheumatic disease. Ultimately, the established 3D *in vitro* models can be used for high-throughput analyses and provide the opportunity to study cellular processes within the tissue, investigate cytokine-driven mechanisms of arthritis, and analyze therapeutic interventions at the tissue level *in vitro*. Thus, the results of this thesis provide the basis for replacing or reducing animal testing in the field of arthritis.

5. CHAPTER: OUTLOOK

Over the past decades, various protocols have been developed to individually generate *in vitro* equivalents of bone, cartilage, and synovial membrane (Schultz, Keyszer et al. 1997, Broeren, Waterborg et al. 2019, Pfeiffenberger, Damerau et al. 2021). The application of MSCs from a single donor to create an artificial joint model enables the development of personalized, tailored therapy. Furthermore, these single *in vitro* tissue equivalents are promising tools to mimic various musculoskeletal diseases such as RA or OA. When assembled, it allows the artificial creation of joint complexity to develop new diagnostics and therapeutics. In this work, cytokine-mediated cell- and matrix-related changes as they occur in inflammatory processes, were simulated in the different tissue components (Damerau, Pfeiffenberger et al. 2020, Damerau, Buttgereit et al. 2022). However, future studies by our group will implement different approaches, such as perfused cultivation, to optimize the goal of providing an artificial joint and overcome current limitations, including substrate availability and longevity.

Therefore, we developed a bioreactor platform including a specialized joint tissue chamber (Do Nguyen, Lubahn et al. 2022). This platform allows the (i) modular and scalable bioprocesses and automation of cultivation in a stand-alone device (no additional incubator required), (ii) simultaneous cultivation of all tissue components of a joint under perfusion, (iii) continuous exchange of medium via two separate circuits, (iv) adjustment of the medium pH, (v) tracking of glucose and lactate concentrations, (vi) simulation of a walking-like load by applying biomechanical stress situations such as e.g., fluid shear stress to better mimic the situation *in vivo*, and (vii) application and removal/withdrawal of e.g., pathological or therapeutic substances or cells (e.g., cytokines, immune cells, glucocorticoids, biologics) (Do Nguyen, Lubahn et al. 2022). The tissue chamber consists of two compartments in which the osteochondral unit is cultured separately from the synovial membrane model, with both tissue types in contact via the synovial fluid-filled space (simulated using Non-Animal Stabilized Hyaluronic Acid). The design of the tissue chamber allows analysis of the supernatant in the different compartments via special access points to study specific cellular, metabolic and humoral changes, such as oxygen levels, glucose and lactate concentrations, whose changes serve as measures of respiration and glycolysis, respectively (Do Nguyen, Lubahn et al. 2022). In addition, targeted cytokines, therapeutics, and immune cells can be applied through these access points. This system is also individually and standardly scalable to allow analyses in the medium to high-throughput range. The perfusion of tissue components not only enables an extension of the culture time, but also supports differentiation processes, such as chondrogenesis, and ensures the long-term cultivation of immune cells.

The immune system is a highly complex and sophisticated interactive network of many biological structures and processes that defend the body against external invaders and the development of tumors. A prerequisite for the smooth functioning of the immune system is the ability to distinguish between "friend" in the form of the body's own cells or harmless antigens and "foe", for example, potential pathogens and tumor cells. Its importance becomes clear when defense mechanisms are directed against the body itself, so to say “friend becomes foe”, as is the case in autoimmune diseases such as RA (Burmester and Pope 2017). Persistent inflammation of the joint is one of the main features of this systemic, chronic inflammatory disease. The chronic inflammatory processes in the joint ultimately lead to pannus formation and the progressive destruction of cartilage and bone (Tateiwa, Yoshikawa et al. 2019). Current *in vitro* approaches primarily exclude the immune component due to its (i) diversity, (ii) reactivity against artificial structures and non-autologous cells, (iii) complex requirements for a suitable microenvironment, (iv) distinct cellular interplay, and a defined humoral environment (Ramadan and Gijs 2015, Mengus, Muraro et al. 2018). Therefore, we aim to include specific subpopulations of immune cells such as Th1 cells, Th17 cells, plasma B cells, and M1 macrophages to investigate basic immune cell-mediated mechanisms. We will thus extend current *in vitro* models by including these cell populations: e.g., by including myeloid cells such as (i) macrophages in the synovial membrane model and (ii) osteoclasts in the cancellous subchondral bone model. To date, no bone remodeling processes have been successfully imaged in 3D over time.

In this regard, the bone models further developed in this work with cell-sheet technology could overcome the hurdle of the detachment of these highly plastic affine myeloid cells by co-culture with osteoclasts, thus enabling the crosstalk of osteoblasts and osteoclasts in 3D.

In this study, among others, the influence of DFO on the cell-sheet-based bone model was investigated but also the influence of pathogenic cytokines (TNF-α, IL-6, and MIF) and their antagonistic therapeutic antibodies on the cytokine-induced cell- and matrix-related changes of bone, cartilage, osteochondral unit and synovial membrane was analyzed (Damerau, Pfeiffenberger et al. 2020, Weber, Fischer et al. 2020, Damerau, Buttgereit et al. 2022).

All models proved to be useful to mimic both pathogenic and therapeutic effects. Due to the still high rate of non-responders in patients with RA, new promising therapeutic approaches for this patient group, with e.g., biologics and small molecules, are constantly being tested, especially in animal models (Pham 2011, Huang, Fu et al. 2021). Ultimately, the goal must be to test our model with additional clinically effective compounds to further stratify it on the way to Organization for Economic Co-operation and Development (OECD) validation. In addition, as already shown for the synovial membrane model, replacing all animal substances, including fetal calf serum (FCS) as a media additive, with a xeno-free alternative will be necessary.

Therefore, we are currently working on a comparative study of replacing FCS with, e.g., human AB serum for all our tissue equivalents. In our group, we could already successfully reproduce the development of miniSFCCs under xeno-free conditions.

To ensure that our model can be widely applied, not only in personalized medicine, we used MSCs for our models. Although research has shown that MSCs are not "immune privileged" as originally stated (Le Blanc, Tammik et al. 2003), their use should still not be a problem as recent studies have shown that allogeneic MSC therapy is safe (Hare, Fishman et al. 2012, Lalu, McIntyre et al. 2012).

Moreover, in this study, I could identify numerous similarities between bone marrow-derived MSCs and synovial fibroblasts from trauma patients, which finally allowed their practical application in the synovial membrane model. However, in-depth comparative analyses with a "healthy" fibroblast control group should be performed in further studies, as these have been lacking so far. In addition, significant differences were observed between *in vitro* tissue components from different donors, reflecting heterogeneity between donors or individual cells within a population. Breakthrough technologies such as single-cell RNA sequencing or single-cell multiplex imaging could be used to study the processed tissue components at the cellular level, significantly improving our understanding of patient heterogeneity in general and during *in vitro* 3D simulation (Hodzic 2016). This would ultimately advance personalized precision medicine.

6. CHAPTER: REFERENCES

Adan, N., J. Guzman-Morales, M. G. Ledesma-Colunga, S. I. Perales-Canales, A. Quintanar-Stephano, F. Lopez-Barrera, I. Mendez, B. Moreno-Carranza, J. Triebel, N. Binart, G. Martinez de la Escalera, S. Thebault and C. Clapp (2013). "Prolactin promotes cartilage survival and attenuates inflammation in inflammatory arthritis." J Clin Invest **123**(9): 3902-3913.

Agarwal, T., P. Kabiraj, G. H. Narayana, S. Kulanthaivel, U. Kasiviswanathan, K. Pal, S. Giri, T. K. Maiti and I. Banerjee (2016). "Alginate Bead Based Hexagonal Close Packed 3D Implant for Bone Tissue Engineering." ACS Appl Mater Interfaces **8**(47): 32132-32145.

Ajeganova, S. and T. Huizinga (2017). "Sustained remission in rheumatoid arthritis: latest evidence and clinical considerations." Ther Adv Musculoskelet Dis **9**(10): 249-262.

Amini, A. R., C. T. Laurencin and S. P. Nukavarapu (2012). "Bone tissue engineering: recent advances and challenges." Crit Rev Biomed Eng **40**(5): 363-408.

Anderson, D. E., B. D. Markway, K. J. Weekes, H. E. McCarthy and B. Johnstone (2017). "Physioxia Promotes the Articular Chondrocyte-Like Phenotype in Human Chondroprogenitor-Derived Self-Organized Tissue." Tissue Engineering Part A **24**(3-4): 264-274.

Andreas, K., C. Lubke, T. Haupl, T. Dehne, L. Morawietz, J. Ringe, C. Kaps and M. Sittinger (2008). "Key regulatory molecules of cartilage destruction in rheumatoid arthritis: an in vitro study." Arthritis Res Ther **10**(1): R9.

Asquith, D. L., A. M. Miller, I. B. McInnes and F. Y. Liew (2009). "Animal models of rheumatoid arthritis." Eur J Immunol **39**(8): 2040-2044.

Babur, B. K., P. Ghanavi, P. Levett, W. B. Lott, T. Klein, J. J. Cooper-White, R. Crawford and M. R. Doran (2013). "The interplay between chondrocyte redifferentiation pellet size and oxygen concentration." PLoS One **8**(3): e58865.

Banh, L., K. K. Cheung, M. W. Y. Chan, E. W. K. Young and S. Viswanathan (2022). "Advances in organ-on-a-chip systems for modelling joint tissue and osteoarthritic diseases." Osteoarthritis Cartilage.

Barbe, M. F., J. Driban, A. E. Barr, S. N. Popoff and F. F. Safadi (2009). Structure and Function of Joints. Bone Pathology. J. S. Khurana. Totowa, NJ, Humana Press**:** 51-60.

Barber, M. R. W., C. Drenkard, T. Falasinnu, A. Hoi, A. Mak, N. Y. Kow, E. Svenungsson, J. Peterson, A. E. Clarke and R. Ramsey-Goldman (2021). "Global epidemiology of systemic lupus erythematosus." Nature Reviews Rheumatology **17**(9): 515-532.

Bendtsen, S. T., S. P. Quinnell and M. Wei (2017). "Development of a novel alginate-polyvinyl alcohol-hydroxyapatite hydrogel for 3D bioprinting bone tissue engineered scaffolds." J Biomed Mater Res A **105**(5): 1457-1468.

Benya, P. D., S. R. Padilla and M. E. Nimni (1978). "Independent regulation of collagen types by chondrocytes during the loss of differentiated function in culture." Cell **15**(4): 1313-1321.

Bernhardt, A., J. Skottke, M. von Witzleben and M. Gelinsky (2021). "Triple Culture of Primary Human Osteoblasts, Osteoclasts and Osteocytes as an In Vitro Bone Model." **22**(14): 7316.

Bevaart, L., M. J. Vervoordeldonk and P. P. Tak (2010). "Evaluation of therapeutic targets in animal models of arthritis: how does it relate to rheumatoid arthritis?" Arthritis Rheum **62**(8): 2192-2205.

Bhat, A. and M. Janarthanan (2017). Human Joint Anatomy and Physiology. Pediatric Rheumatology: A Clinical Viewpoint. S. Sawhney and A. Aggarwal. Singapore, Springer Singapore**:** 29-35.

Bhattacharjee, M., J. Coburn, M. Centola, S. Murab, A. Barbero, D. L. Kaplan, I. Martin and S. Ghosh (2015). "Tissue engineering strategies to study cartilage development, degeneration and regeneration." Adv Drug Deliv Rev **84**: 107-122.

Bhumiratana, S., R. E. Eton, S. R. Oungoulian, L. Q. Wan, G. A. Ateshian and G. Vunjak-Novakovic (2014). "Large, stratified, and mechanically functional human cartilage grown in vitro by mesenchymal condensation." Proceedings of the National Academy of Sciences of the United States of America **111**(19): 6940-6945.

Bohner, M., B. L. G. Santoni and N. Dobelin (2020). "beta-tricalcium phosphate for bone substitution: Synthesis and properties." Acta Biomater **113**: 23-41.

Bonewald, L. F. and M. L. Johnson (2008). "Osteocytes, mechanosensing and Wnt signaling." Bone **42**(4): 606-615.

Bouet, G., M. Cruel, C. Laurent, L. Vico, L. Malaval and D. Marchat (2015). "Validation of an in vitro 3D bone culture model with perfused and mechanically stressed ceramic scaffold." Eur Cell Mater **29**: 250-266; discussion 266-257.

Brackertz, D., G. F. Mitchell and I. R. Mackay (1977). "Antigen-induced arthritis in mice. I. Induction of arthritis in various strains of mice." Arthritis Rheum **20**(3): 841-850.

Brackertz, D., G. F. Mitchell, M. A. Vadas, I. R. Mackay and J. F. Miller (1977). "Studies on antigen-induced arthritis in mice. II. Immunologic correlates of arthritis susceptibility in mice." J Immunol **118**(5): 1639-1644.

Breschi, A., T. R. Gingeras and R. Guigó (2017). "Comparative transcriptomics in human and mouse." Nat Rev Genet **18**(7): 425-440.

Broeren, M. G. A., C. E. J. Waterborg, R. Wiegertjes, R. M. Thurlings, M. I. Koenders, P. Van Lent, P. M. Van der Kraan and F. A. J. Van de Loo (2019). "A three-dimensional model to study human synovial pathology." ALTEX **36**(1): 18-28.

Buckley, C. D. (2019). "Macrophages form a protective cellular barrier in joints." Nature **572**(7771): 590-592.

Burch, W. M. S. R. a. R. L. (2009). The Principles of Humane Experimental Technique (first published 1959). Nottingham/UK, Frame.

Burmester, G. R., E. Feist and T. Dorner (2014). "Emerging cell and cytokine targets in rheumatoid arthritis." Nat Rev Rheumatol **10**(2): 77-88.

Burmester, G. R. and J. E. Pope (2017). "Novel treatment strategies in rheumatoid arthritis." Lancet **389**(10086): 2338-2348.

Burrage, P. S., K. S. Mix and C. E. Brinckerhoff (2006). "Matrix metalloproteinases: role in arthritis." Front Biosci **11**: 529-543.

Bustamante, M. F., R. Garcia-Carbonell, K. D. Whisenant and M. Guma (2017). "Fibroblast-like synoviocyte metabolism in the pathogenesis of rheumatoid arthritis." Arthritis Res Ther **19**(1): 110.

Butler, D. M., A. M. Malfait, L. J. Mason, P. J. Warden, G. Kollias, R. N. Maini, M. Feldmann and F. M. Brennan (1997). "DBA/1 mice expressing the human TNF-alpha transgene develop a severe, erosive arthritis: characterization of the cytokine cascade and cellular composition." J Immunol **159**(6): 2867-2876.

Cai, S., B. Ming, C. Ye, S. Lin, P. Hu, J. Tang, F. Zheng and L. Dong (2019). "Similar Transition Processes in Synovial Fibroblasts from Rheumatoid Arthritis and Osteoarthritis: A Single-Cell Study." J Immunol Res **2019**: 4080735.

Cao, Q., Z. He, W. Q. Sun, G. Fan, J. Zhao, N. Bao and T. Ye (2019). "Improvement of calcium phosphate scaffold osteogenesis in vitro via combination of glutamate-modified BMP-2 peptides." Materials Science and Engineering: C **96**: 412-418.

Cappellesso-Fleury, S., B. Puissant-Lubrano, P. A. Apoil, M. Titeux, P. Winterton, L. Casteilla, P. Bourin and A. Blancher (2010). "Human fibroblasts share immunosuppressive properties with bone marrow mesenchymal stem cells." J Clin Immunol **30**(4): 607-619.

Carlsen, S., A. S. Hansson, H. Olsson, D. Heinegard and R. Holmdahl (1998). "Cartilage oligomeric matrix protein (COMP)-induced arthritis in rats." Clin Exp Immunol **114**(3): 477-484.

Carlsen, S., K. S. Nandakumar, J. Backlund, J. Holmberg, M. Hultqvist, M. Vestberg and R. Holmdahl (2008). "Cartilage oligomeric matrix protein induction of chronic arthritis in mice." Arthritis Rheum **58**(7): 2000-2011.

Cascao, R., R. A. Moura, I. Perpetuo, H. Canhao, E. Vieira-Sousa, A. F. Mourao, A. M. Rodrigues, J. Polido-Pereira, M. V. Queiroz, H. S. Rosario, M. M. Souto-Carneiro, L. Graca and J. E. Fonseca (2010). "Identification of a cytokine network sustaining neutrophil and Th17 activation in untreated early rheumatoid arthritis." Arthritis Res Ther **12**(5): R196.

Cassotta, M., F. Pistollato and M. Battino (2020). "Rheumatoid arthritis research in the 21st century: Limitations of traditional models, new technologies, and opportunities for a human biology-based approach." ALTEX **37**(2): 223-242.

Causa, F., P. A. Netti and L. Ambrosio (2007). "A multi-functional scaffold for tissue regeneration: The need to engineer a tissue analogue." Biomaterials **28**(34): 5093-5099.

Chabaud, M. and P. Miossec (2001). "The combination of tumor necrosis factor alpha blockade with interleukin-1 and interleukin-17 blockade is more effective for controlling synovial inflammation and bone resorption in an ex vivo model." Arthritis Rheum **44**(6): 1293-1303.

Chatzidionysiou, K., S. Emamikia, J. Nam, S. Ramiro, J. Smolen, D. van der Heijde, M. Dougados, J. Bijlsma, G. Burmester, M. Scholte, R. van Vollenhoven and R. Landewe (2017). "Efficacy of glucocorticoids, conventional and targeted synthetic disease-modifying antirheumatic drugs: a systematic literature review informing the 2016 update of the EULAR recommendations for the management of rheumatoid arthritis." Ann Rheum Dis **76**(6): 1102-1107.

Chen, H. J., A. Y. F. Li Yim, G. R. Griffith, W. J. de Jonge, M. Mannens, E. Ferrero, P. Henneman and M. P. J. de Winther (2019). "Meta-Analysis of in vitro-Differentiated Macrophages Identifies Transcriptomic Signatures That Classify Disease Macrophages in vivo." Front Immunol **10**: 2887.

Chevrel, G., P. Garnero and P. Miossec (2002). "Addition of interleukin 1 (IL1) and IL17 soluble receptors to a tumour necrosis factor alpha soluble receptor more effectively reduces the production of IL6 and macrophage inhibitory protein-3alpha and increases that of collagen in an in vitro model of rheumatoid synoviocyte activation." Ann Rheum Dis **61**(8): 730-733.

Chiesa, I., C. De Maria, A. Lapomarda, G. M. Fortunato, F. Montemurro, R. Di Gesù, R. S. Tuan, G. Vozzi and R. Gottardi (2020). "Endothelial cells support osteogenesis in an in vitro vascularized bone model developed by 3D bioprinting." Biofabrication **12**(2): 025013.

Chinta, M. L., A. Velidandi, N. P. P. Pabbathi, S. Dahariya and S. R. Parcha (2021). "Assessment of properties, applications and limitations of scaffolds based on cellulose and its derivatives for cartilage tissue engineering: A review." Int J Biol Macromol **175**: 495-515.

Choudhary, N., L. K. Bhatt and K. S. Prabhavalkar (2018). "Experimental animal models for rheumatoid arthritis." Immunopharmacol Immunotoxicol **40**(3): 193-200.

Cieza, A., K. Causey, K. Kamenov, S. W. Hanson, S. Chatterji and T. Vos (2021). "Global estimates of the need for rehabilitation based on the Global Burden of Disease study 2019: a systematic analysis for the Global Burden of Disease Study 2019." Lancet **396**(10267): 2006-2017.

Clarke, B. (2008). "Normal bone anatomy and physiology." Clinical journal of the American Society of Nephrology : CJASN **3 Suppl 3**(Suppl 3): S131-S139.

Corrado, A., N. Maruotti and F. P. Cantatore (2017). "Osteoblast Role in Rheumatic Diseases." Int J Mol Sci **18**(6).

Courtenay, J. S., M. J. Dallman, A. D. Dayan, A. Martin and B. Mosedale (1980). "Immunisation against heterologous type II collagen induces arthritis in mice." Nature **283**(5748): 666-668.

Cova, M. and R. Toffanin (2002). "MR microscopy of hyaline cartilage: current status." Eur Radiol **12**(4): 814-823.

Croft, A. P., A. J. Naylor, J. L. Marshall, D. L. Hardie, B. Zimmermann, J. Turner, G. Desanti, H. Adams, A. I. Yemm, U. Muller-Ladner, J. M. Dayer, E. Neumann, A. Filer and C. D. Buckley (2016). "Rheumatoid synovial fibroblasts differentiate into distinct subsets in the presence of cytokines and cartilage." Arthritis Res Ther **18**(1): 270.

Damerau, A., F. Buttgereit and T. Gaber (2022). "Optimization of a Tricalcium Phosphate-Based Bone Model Using Cell-Sheet Technology to Simulate Bone Disorders." **10**(3): 550.

Damerau, A. and T. Gaber (2020). "Modeling Rheumatoid Arthritis In Vitro: From Experimental Feasibility to Physiological Proximity." Int J Mol Sci **21**(21).

Damerau, A., M. Kirchner, M. Pfeiffenberger, L. Ehlers, D. H. Do Nguyen, P. Mertins, B. Bartek, T. Maleitzke, Y. Palmowski, S. Hardt, T. Winkler, F. Buttgereit and T. Gaber (2022). "Metabolic reprogramming of synovial fibroblasts in osteoarthritis by inhibition of pathologically overexpressed pyruvate dehydrogenase kinases." Metab Eng **72**: 116-132.

Damerau, A., M. Pfeiffenberger, M. C. Weber, G. R. Burmester, F. Buttgereit, T. Gaber and A. Lang (2020). "A Human Osteochondral Tissue Model Mimicking Cytokine-Induced Key Features of Arthritis In Vitro." Int J Mol Sci **22**(1).

de Barros, A. P., C. M. Takiya, L. R. Garzoni, M. L. Leal-Ferreira, H. S. Dutra, L. B. Chiarini, M. N. Meirelles, R. Borojevic and M. I. Rossi (2010). "Osteoblasts and bone marrow mesenchymal stromal cells control hematopoietic stem cell migration and proliferation in 3D in vitro model." PLoS One **5**(2): e9093.

de Sousa, E. B., P. L. Casado, V. Moura Neto, M. E. Duarte and D. P. Aguiar (2014). "Synovial fluid and synovial membrane mesenchymal stem cells: latest discoveries and therapeutic perspectives." Stem Cell Res Ther **5**(5): 112.

De Witte, T. M., L. E. Fratila-Apachitei, A. A. Zadpoor and N. A. Peppas (2018). "Bone tissue engineering via growth factor delivery: from scaffolds to complex matrices." Regen Biomater **5**(4): 197-211.

Deane, K. D., M. K. Demoruelle, L. B. Kelmenson, K. A. Kuhn, J. M. Norris and V. M. Holers (2017). "Genetic and environmental risk factors for rheumatoid arthritis." Best Pract Res Clin Rheumatol **31**(1): 3-18.

Deng, C., Q. Zhang, P. He, B. Zhou, K. He, X. Sun, G. Lei, T. Gong and Z. Zhang (2021). "Targeted apoptosis of macrophages and osteoclasts in arthritic joints is effective against advanced inflammatory arthritis." Nature Communications **12**(1): 2174.

Deng, Y., C. Jiang, C. Li, T. Li, M. Peng, J. Wang and K. Dai (2017). "3D printed scaffolds of calcium silicate-doped beta-TCP synergize with co-cultured endothelial and stromal cells to promote vascularization and bone formation." Sci Rep **7**(1): 5588.

Dennis, G., Jr., C. T. Holweg, S. K. Kummerfeld, D. F. Choy, A. F. Setiadi, J. A. Hackney, P. M. Haverty, H. Gilbert, W. Y. Lin, L. Diehl, S. Fischer, A. Song, D. Musselman, M. Klearman, C. Gabay, A. Kavanaugh, J. Endres, D. A. Fox, F. Martin and M. J. Townsend (2014). "Synovial phenotypes in rheumatoid arthritis correlate with response to biologic therapeutics." Arthritis Res Ther **16**(2): R90.

Denu, R. A., S. Nemcek, D. D. Bloom, A. D. Goodrich, J. Kim, D. F. Mosher and P. Hematti (2016). "Fibroblasts and Mesenchymal Stromal/Stem Cells Are Phenotypically Indistinguishable." Acta Haematol **136**(2): 85-97.

Dhivya, S., S. Saravanan, T. P. Sastry and N. Selvamurugan (2015). "Nanohydroxyapatite-reinforced chitosan composite hydrogel for bone tissue repair in vitro and in vivo." J Nanobiotechnology **13**: 40.

Do Nguyen, D. H., C. Lubahn, T. Leeuw, F. Buttgereit, T. Gaber and A. Damerau (2022). "POS0225 FLUIDIC SHEAR STRESS REDUCES TNFA-MEDIATED CARTILAGE DAMAGE IN A 3D MODEL OF DEGENERATIVE JOINT DISEASE." **81**(Suppl 1): 349-349.

Doeing, D. C., J. L. Borowicz and E. T. Crockett (2003) "Gender dimorphism in differential peripheral blood leukocyte counts in mice using cardiac, tail, foot, and saphenous vein puncture methods." BMC clinical pathology **3**, 3 DOI: 10.1186/1472-6890-3-3.

Dominici, M., K. Le Blanc, I. Mueller, I. Slaper-Cortenbach, F. Marini, D. Krause, R. Deans, A. Keating, D. Prockop and E. Horwitz (2006). "Minimal criteria for defining multipotent mesenchymal stromal cells. The International Society for Cellular Therapy position statement." Cytotherapy **8**(4): 315-317.

Donlin, L. T., A. Jayatilleke, E. G. Giannopoulou, G. D. Kalliolias and L. B. Ivashkiv (2014). "Modulation of TNF-induced macrophage polarization by synovial fibroblasts." J Immunol **193**(5): 2373-2383.

Duan, W., M. Haque, M. T. Kearney and M. J. Lopez (2017). "Collagen and Hydroxyapatite Scaffolds Activate Distinct Osteogenesis Signaling Pathways in Adult Adipose-Derived Multipotent Stromal Cells." Tissue Eng Part C Methods **23**(10): 592-603.

DuRaine, G. D., W. E. Brown, J. C. Hu and K. A. Athanasiou (2015). "Emergence of scaffold-free approaches for tissue engineering musculoskeletal cartilages." Annals of biomedical engineering **43**(3): 543-554.

Ehnert, S., H. Rinderknecht, R. H. Aspera-Werz, V. Häussling and A. K. Nussler (2020). "Use of in vitro bone models to screen for altered bone metabolism, osteopathies, and fracture healing: challenges of complex models." Archives of Toxicology **94**(12): 3937-3958.

El Sayed, S. A., T. A. Nezwek and M. Varacallo (2022). Physiology, Bone. StatPearls. Treasure Island (FL).

Eschweiler, J., N. Horn, B. Rath, M. Betsch, A. Baroncini, M. Tingart and F. Migliorini (2021). "The Biomechanics of Cartilage-An Overview." Life (Basel) **11**(4).

European Parliament, C. o. t. E. U. (2010). DIRECTIVE 2010/63/EU OF THE EUROPEAN PARLIAMENT AND OF THE COUNCIL of 22 September 2010 on the protection of animals used for scientific purposes. Official Journal of the European Union

Fan, C., M. Liao, L. Xie, L. Huang, S. Lv, S. Cai, X. Su, Y. Wang, H. Wang, M. Wang, Y. Liu, Y. Wang, H. Guo, H. Yang, Y. Liu, T. Wang and L. Ma (2022). "Single-Cell Transcriptome Integration Analysis Reveals the Correlation Between Mesenchymal Stromal Cells and Fibroblasts." Front Genet **13**: 798331.

Fan, X., X. Wu, R. Crawford, Y. Xiao and I. Prasadam (2021). "Macro, Micro, and Molecular. Changes of the Osteochondral Interface in Osteoarthritis Development." Front Cell Dev Biol **9**: 659654.

Feldmann, M. (2002). "Development of anti-TNF therapy for rheumatoid arthritis." Nat Rev Immunol **2**(5): 364-371.

Fernandes, G., C. Wang, X. Yuan, Z. Liu, R. Dziak and S. Yang (2016). "Combination of Controlled Release Platelet-Rich Plasma Alginate Beads and Bone Morphogenetic Protein-2 Genetically Modified Mesenchymal Stem Cells for Bone Regeneration." J Periodontol **87**(4): 470-480.

Firestein, G. S. (2009). "Rheumatoid arthritis in a mouse?" Nat Clin Pract Rheumatol **5**(1): 1.

Firestein, G. S. and I. B. McInnes (2017). "Immunopathogenesis of Rheumatoid Arthritis." Immunity **46**(2): 183-196.

Florencio-Silva, R., G. R. d. S. Sasso, E. Sasso-Cerri, M. J. Simões and P. S. Cerri (2015). "Biology of Bone Tissue: Structure, Function, and Factors That Influence Bone Cells." BioMed Research International **2015**: 421746.

Frasnelli, M. E., D. Tarussio, V. Chobaz-Peclat, N. Busso and A. So (2005). "TLR2 modulates inflammation in zymosan-induced arthritis in mice." Arthritis Res Ther **7**(2): R370-379.

Furukawa, K. S., H. Suenaga, K. Toita, A. Numata, J. Tanaka, T. Ushida, Y. Sakai and T. Tateishi (2003). "Rapid and large-scale formation of chondrocyte aggregates by rotational culture." Cell Transplant **12**(5): 475-479.

Futrega, K., J. S. Palmer, M. Kinney, W. B. Lott, M. D. Ungrin, P. W. Zandstra and M. R. Doran (2015). "The microwell-mesh: A novel device and protocol for the high throughput manufacturing of cartilage microtissues." Biomaterials **62**: 1-12.

Gabriel, N., J. F. Innes, B. Caterson and A. Vaughan-Thomas (2010). "Development of an in vitro model of feline cartilage degradation." Journal of Feline Medicine & Surgery **12**(8): 614-620.

Gaffen, S. L., R. Jain, A. V. Garg and D. J. Cua (2014). "The IL-23-IL-17 immune axis: from mechanisms to therapeutic testing." Nat Rev Immunol **14**(9): 585-600.

Ghassemi, T., A. Shahroodi, M. H. Ebrahimzadeh, A. Mousavian, J. Movaffagh and A. Moradi (2018). "Current Concepts in Scaffolding for Bone Tissue Engineering." Arch Bone Jt Surg **6**(2): 90-99.

Gilbert, S. J., S. K. Singhrao, I. M. Khan, L. G. Gonzalez, B. M. Thomson, D. Burdon, V. C. Duance and C. W. Archer (2009). "Enhanced tissue integration during cartilage repair in vitro can be achieved by inhibiting chondrocyte death at the wound edge." Tissue Eng Part A **15**(7): 1739-1749.

Glyn-Jones, S., A. J. R. Palmer, R. Agricola, A. J. Price, T. L. Vincent, H. Weinans and A. J. Carr (2015). "Osteoarthritis." The Lancet **386**(9991): 376-387.

Goldring, M. B. (2005). "Human chondrocyte cultures as models of cartilage-specific gene regulation." Methods Mol Med **107**: 69-95.

Goldring, M. B. and F. Berenbaum (1999). "Human chondrocyte culture models for studying cyclooxygenase expression and prostaglandin regulation of collagen gene expression." Osteoarthritis Cartilage **7**(4): 386-388.

Goldring, M. B. and K. B. Marcu (2009). "Cartilage homeostasis in health and rheumatic diseases." Arthritis Research & Therapy **11**(3): 224.

Goldring, S. R. and M. B. Goldring (2016). "Changes in the osteochondral unit during osteoarthritis: structure, function and cartilage-bone crosstalk." Nat Rev Rheumatol **12**(11): 632-644.

Gotoh, H., Y. Kawaguchi, M. Harigai, M. Hara, S. Saito, T. Yamaguchi, K. Shimada, M. Kawamoto, T. Tomatsu and N. Kamatani (2004). "Increased CD40 expression on articular chondrocytes from patients with rheumatoid arthritis: contribution to production of cytokines and matrix metalloproteinases." J Rheumatol **31**(8): 1506-1512.

Guyton, A. C. (1985). Anatomy and physiology. Philadelphia, Saunders College Pub.

Guzey, S., A. Aykan, S. Ozturk, H. Avsever, Y. Karslioglu and A. Ertan (2016). "The Effects of Desferroxamine on Bone and Bone Graft Healing in Critical-Size Bone Defects." Ann Plast Surg **77**(5): 560-568.

Han, D., Y. Fang, X. Tan, H. Jiang, X. Gong, X. Wang, W. Hong, J. Tu and W. Wei (2020). "The emerging role of fibroblast-like synoviocytes-mediated synovitis in osteoarthritis: An update." J Cell Mol Med **24**(17): 9518-9532.

Hare, J. M., J. E. Fishman, G. Gerstenblith, D. L. DiFede Velazquez, J. P. Zambrano, V. Y. Suncion, M. Tracy, E. Ghersin, P. V. Johnston, J. A. Brinker, E. Breton, J. Davis-Sproul, I.

H. Schulman, J. Byrnes, A. M. Mendizabal, M. H. Lowery, D. Rouy, P. Altman, C. Wong Po Foo, P. Ruiz, A. Amador, J. Da Silva, I. K. McNiece, A. W. Heldman, R. George and A. Lardo (2012). "Comparison of allogeneic vs autologous bone marrow-derived mesenchymal stem cells delivered by transendocardial injection in patients with ischemic cardiomyopathy: the POSEIDON randomized trial." JAMA **308**(22): 2369-2379.

Hartung, T. (2008). "Food for thought ... on alternative methods for cosmetics safety testing." Altex **25**(3): 147-162.

Haugeberg, G., I. J. Hansen, D. M. Soldal and T. Sokka (2015). "Ten years of change in clinical disease status and treatment in rheumatoid arthritis: results based on standardized monitoring of patients in an ordinary outpatient clinic in southern Norway." Arthritis Res Ther **17**: 219.

Herten, M., D. Rothamel, F. Schwarz, K. Friesen, G. Koegler and J. Becker (2009). "Surface- and nonsurface-dependent in vitro effects of bone substitutes on cell viability." Clin Oral Investig **13**(2): 149-155.

Hodzic, E. (2016). "Single-cell analysis: Advances and future perspectives." Bosn J Basic Med Sci **16**(4): 313-314.

Hogrefe, C., H. Joos, V. Maheswaran, L. Durselen, A. Ignatius and R. E. Brenner (2012). "Single impact cartilage trauma and TNF-alpha: interactive effects do not increase early cell death and indicate the need for bi-/multidirectional therapeutic approaches." Int J Mol Med **30**(5): 1225-1232.

Holmdahl, R., L. Jansson, E. Larsson, K. Rubin and L. Klareskog (1986). "Homologous type II collagen induces chronic and progressive arthritis in mice." Arthritis Rheum **29**(1): 106-113.

Holmdahl, R., J. C. Lorentzen, S. Lu, P. Olofsson, L. Wester, J. Holmberg and U. Pettersson (2001). "Arthritis induced in rats with nonimmunogenic adjuvants as models for rheumatoid arthritis." Immunol Rev **184**: 184-202.

Holmdahl, R., K. Rubin, L. Klareskog, E. Larsson and H. Wigzell (1986). "Characterization of the antibody response in mice with type II collagen-induced arthritis, using monoclonal anti-type II collagen antibodies." Arthritis Rheum **29**(3): 400-410.

Hosaka, K., J. Ryu, S. Saitoh, T. Ishii, K. Kuroda and K. Shimizu (2005). "The combined effects of anti-TNFalpha antibody and IL-1 receptor antagonist in human rheumatoid arthritis synovial membrane." Cytokine **32**(6): 263-269.

Huang, J., X. Fu, X. Chen, Z. Li, Y. Huang and C. Liang (2021). "Promising Therapeutic Targets for Treatment of Rheumatoid Arthritis." Front Immunol **12**: 686155.

Hunter, D. J. and S. Bierma-Zeinstra (2019). "Osteoarthritis." The Lancet **393**(10182): 1745-1759.

Ichim, T. E., P. O'Heeron and S. Kesari (2018). "Fibroblasts as a practical alternative to mesenchymal stem cells." J Transl Med **16**(1): 212.

Ikada, Y. (2006). "Challenges in tissue engineering." J R Soc Interface **3**(10): 589-601.

James, A. W., G. LaChaud, J. Shen, G. Asatrian, V. Nguyen, X. Zhang, K. Ting and C. Soo (2016). "A Review of the Clinical Side Effects of Bone Morphogenetic Protein-2." Tissue Eng Part B Rev **22**(4): 284-297.

Joosten, L. A., S. Abdollahi-Roodsaz, M. Heuvelmans-Jacobs, M. M. Helsen, L. A. van den Bersselaar, B. Oppers-Walgreen, M. I. Koenders and W. B. van den Berg (2008). "T cell dependence of chronic destructive murine arthritis induced by repeated local activation of Toll-like receptor-driven pathways: crucial role of both interleukin-1beta and interleukin-17." Arthritis Rheum **58**(1): 98-108.

Jorgensen, C. and M. Simon (2021). "In Vitro Human Joint Models Combining Advanced 3D Cell Culture and Cutting-Edge 3D Bioprinting Technologies." **10**(3): 596.

Kaplan, M. J. (2013). "Role of neutrophils in systemic autoimmune diseases." Arthritis Res Ther **15**(5): 219.

Karimi, T., D. Barati, O. Karaman, S. Moeinzadeh and E. Jabbari (2015). "A developmentally inspired combined mechanical and biochemical signaling approach on zonal lineage commitment of mesenchymal stem cells in articular cartilage regeneration." Integr Biol (Camb) **7**(1): 112-127.

Karmakar, S., J. Kay and E. M. Gravallese (2010). "Bone damage in rheumatoid arthritis: mechanistic insights and approaches to prevention." Rheumatic diseases clinics of North America **36**(2): 385-404.

Karonitsch, T., D. Beckmann, K. Dalwigk, B. Niederreiter, P. Studenic, R. A. Byrne, J. Holinka, F. Sevelda, A. Korb-Pap, G. Steiner, J. S. Smolen, T. Pap and H. P. Kiener (2018). "Targeted inhibition of Janus kinases abates interfon gamma-induced invasive behaviour of fibroblast-like synoviocytes." Rheumatology (Oxford) **57**(3): 572-577.

Kasperkovitz, P. V., T. C. Timmer, T. J. Smeets, N. L. Verbeet, P. P. Tak, L. G. van Baarsen, B. Baltus, T. W. Huizinga, E. Pieterman, M. Fero, G. S. Firestein, T. C. van der Pouw Kraan and C. L. Verweij (2005). "Fibroblast-like synoviocytes derived from patients with rheumatoid arthritis show the imprint of synovial tissue heterogeneity: evidence of a link between an increased myofibroblast-like phenotype and high-inflammation synovitis." Arthritis Rheum **52**(2): 430-441.

Keaveny, T. M., E. F. Morgan, G. L. Niebur and O. C. Yeh (2001). "Biomechanics of trabecular bone." Annu Rev Biomed Eng **3**: 307-333.

Keffer, J., L. Probert, H. Cazlaris, S. Georgopoulos, E. Kaslaris, D. Kioussis and G. Kollias (1991). "Transgenic mice expressing human tumour necrosis factor: a predictive genetic model of arthritis." EMBO J **10**(13): 4025-4031.

Keystone, E. C., H. U. Schorlemmer, C. Pope and A. C. Allison (1977). "Zymosan-induced arthritis: a model of chronic proliferative arthritis following activation of the alternative pathway of complement." Arthritis Rheum **20**(7): 1396-1401.

Kiani, C., L. Chen, Y. J. Wu, A. J. Yee and B. B. Yang (2002). "Structure and function of aggrecan." Cell Research **12**(1): 19-32.

Kiener, H. P., B. Niederreiter, D. M. Lee, E. Jimenez-Boj, J. S. Smolen and M. B. Brenner (2009). "Cadherin 11 promotes invasive behavior of fibroblast-like synoviocytes." Arthritis Rheum **60**(5): 1305-1310.

Kiener, H. P., G. F. Watts, Y. Cui, J. Wright, T. S. Thornhill, M. Skold, S. M. Behar, B. Niederreiter, J. Lu, M. Cernadas, A. J. Coyle, G. P. Sims, J. Smolen, M. L. Warman, M. B. Brenner and D. M. Lee (2010). "Synovial fibroblasts self-direct multicellular lining architecture and synthetic function in three-dimensional organ culture." Arthritis Rheum **62**(3): 742-752.

Kim, E. Y. and K. D. Moudgil (2009). "The determinants of susceptibility/resistance to adjuvant arthritis in rats." Arthritis Res Ther **11**(4): 239.

Kim, H. A. and Y. W. Song (1999). "Apoptotic chondrocyte death in rheumatoid arthritis." Arthritis & Rheumatism **42**(7): 1528-1537.

Kim, H. J. and J. S. Park (2017). "Usage of Human Mesenchymal Stem Cells in Cell-based Therapy: Advantages and Disadvantages." Dev Reprod **21**(1): 1-10.

Kim, K., S. Bou-Ghannam, H. Thorp, D. W. Grainger and T. Okano (2019). "Human mesenchymal stem cell sheets in xeno-free media for possible allogenic applications." Sci Rep **9**(1): 14415.

Klareskog, L., D. van der Heijde, J. P. de Jager, A. Gough, J. Kalden, M. Malaise, E. Martín Mola, K. Pavelka, J. Sany, L. Settas, J. Wajdula, R. Pedersen, S. Fatenejad and M. Sanda (2004). "Therapeutic effect of the combination of etanercept and methotrexate compared with each treatment alone in patients with rheumatoid arthritis: double-blind randomised controlled trial." Lancet **363**(9410): 675-681.

Knobloch, T. J., S. Madhavan, J. Nam, S. Agarwal, Jr. and S. Agarwal (2008). "Regulation of chondrocytic gene expression by biomechanical signals." Crit Rev Eukaryot Gene Expr **18**(2): 139-150.

Koenders, M. I. and W. B. van den Berg (2016). "Secukinumab for rheumatology: development and its potential place in therapy." Drug Des Devel Ther **10**: 2069-2080.

Komori, T. (2006). "Regulation of osteoblast differentiation by transcription factors." J Cell Biochem **99**(5): 1233-1239.

Kondo, N., A. Ogose, K. Tokunaga, T. Ito, K. Arai, N. Kudo, H. Inoue, H. Irie and N. Endo (2005). "Bone formation and resorption of highly purified beta-tricalcium phosphate in the rat femoral condyle." Biomaterials **26**(28): 5600-5608.

Kotake, S., N. Udagawa, N. Takahashi, K. Matsuzaki, K. Itoh, S. Ishiyama, S. Saito, K. Inoue, N. Kamatani, M. T. Gillespie, T. J. Martin and T. Suda (1999). "IL-17 in synovial fluids from patients with rheumatoid arthritis is a potent stimulator of osteoclastogenesis." J Clin Invest **103**(9): 1345-1352.

Kouskoff, V., A. S. Korganow, V. Duchatelle, C. Degott, C. Benoist and D. Mathis (1996). "Organ-specific disease provoked by systemic autoimmunity." Cell **87**(5): 811-822.

Kulterer, B., G. Friedl, A. Jandrositz, F. Sanchez-Cabo, A. Prokesch, C. Paar, M. Scheideler, R. Windhager, K.-H. Preisegger and Z. Trajanoski (2007). "Gene expression profiling of human mesenchymal stem cells derived from bone marrow during expansion and osteoblast differentiation." BMC Genomics **8**(1): 70.

Lalu, M. M., L. McIntyre, C. Pugliese, D. Fergusson, B. W. Winston, J. C. Marshall, J. Granton and D. J. Stewart (2012). "Safety of cell therapy with mesenchymal stromal cells (SafeCell): a systematic review and meta-analysis of clinical trials." PLoS One **7**(10): e47559.

Le Blanc, K., C. Tammik, K. Rosendahl, E. Zetterberg and O. Ringdén (2003). "HLA expression and immunologic properties of differentiated and undifferentiated mesenchymal stem cells." Exp Hematol **31**(10): 890-896.

Le Gars Santoni, B., L. Niggli, S. Dolder, O. Loeffel, G. A. Sblendorio, R. Heuberger, Y. Maazouz, C. Stahli, N. Dobelin, P. Bowen, W. Hofstetter and M. Bohner (2022). "Effect of minor amounts of beta-calcium pyrophosphate and hydroxyapatite on the physico-chemical properties and osteoclastic resorption of beta-tricalcium phosphate cylinders." Bioact Mater **10**: 222-235.

Lee, C. H., E. K. Moioli and J. J. Mao (2006). "Fibroblastic differentiation of human mesenchymal stem cells using connective tissue growth factor." Conf Proc IEEE Eng Med Biol Soc **2006**: 775-778.

Lee, C. H., B. Shah, E. K. Moioli and J. J. Mao (2010). "CTGF directs fibroblast differentiation from human mesenchymal stem/stromal cells and defines connective tissue healing in a rodent injury model." J Clin Invest **120**(9): 3340-3349.

Leech, M., C. Metz, P. Hall, P. Hutchinson, K. Gianis, M. Smith, H. Weedon, S. R. Holdsworth, R. Bucala and E. F. Morand (1999). "Macrophage migration inhibitory factor in rheumatoid arthritis: Evidence of proinflammatory function and regulation by glucocorticoids." **42**(8): 1601-1608.

Leipe, J., M. Grunke, C. Dechant, C. Reindl, U. Kerzendorf, H. Schulze-Koops and A. Skapenko (2010). "Role of Th17 cells in human autoimmune arthritis." Arthritis Rheum **62**(10): 2876-2885.

Lepage, S. I. M., N. Robson, H. Gilmore, O. Davis, A. Hooper, S. St John, V. Kamesan, P. Gelis, D. Carvajal, M. Hurtig and T. G. Koch (2019). "Beyond Cartilage Repair: The Role

of the Osteochondral Unit in Joint Health and Disease." Tissue Eng Part B Rev **25**(2): 114-125.

Lettesjö, H., E. Nordström, H. Ström, B. Nilsson, B. Glinghammar, L. Dahlstedt and E. Möller (1998). "Synovial fluid cytokines in patients with rheumatoid arthritis or other arthritic lesions." Scand J Immunol **48**(3): 286-292.

Lewis, M. J., M. R. Barnes, K. Blighe, K. Goldmann, S. Rana, J. A. Hackney, N. Ramamoorthi, C. R. John, D. S. Watson, S. K. Kummerfeld, R. Hands, S. Riahi, V. Rocher-Ros, F. Rivellese, F. Humby, S. Kelly, M. Bombardieri, N. Ng, M. DiCicco, D. van der Heijde, R. Landewe, A. van der Helm-van Mil, A. Cauli, I. B. McInnes, C. D. Buckley, E. Choy, P. C. Taylor, M. J. Townsend and C. Pitzalis (2019). "Molecular Portraits of Early Rheumatoid Arthritis Identify Clinical and Treatment Response Phenotypes." Cell Rep **28**(9): 2455-2470 e2455.

Li, F., Y. Tang, B. Song, M. Yu, Q. Li, C. Zhang, J. Hou and R. Yang (2019). "Nomenclature clarification: synovial fibroblasts and synovial mesenchymal stem cells." Stem Cell Res Ther **10**(1): 260.

Lin, H., T. P. Lozito, P. G. Alexander, R. Gottardi and R. S. Tuan (2014). "Stem Cell-Based Microphysiological Osteochondral System to Model Tissue Response to Interleukin-1β." Molecular Pharmaceutics **11**(7): 2203-2212.

Lin, X., S. Patil, Y. G. Gao and A. Qian (2020). "The Bone Extracellular Matrix in Bone Formation and Regeneration." Front Pharmacol **11**: 757.

Liu, G., L. Zhao, L. Cui, W. Liu and Y. Cao (2007). "Tissue-engineered bone formation using human bone marrow stromal cells and novel beta-tricalcium phosphate." Biomed Mater **2**(2): 78-86.

Liu, S., H. Ma, H. Zhang, C. Deng and P. Xin (2021). "Recent advances on signaling pathways and their inhibitors in rheumatoid arthritis." Clin Immunol **230**: 108793.

Liu, Z., M. Tamaddon, Y. Gu, J. Yu, N. Xu, F. Gang, X. Sun and C. Liu (2020). "Cell Seeding Process Experiment and Simulation on Three-Dimensional Polyhedron and Cross-Link Design Scaffolds." Front Bioeng Biotechnol **8**: 104.

Lopes, D., C. Martins-Cruz, M. B. Oliveira and J. F. Mano (2018). "Bone physiology as inspiration for tissue regenerative therapies." Biomaterials **185**: 240-275.

Loskill, P., S. G. Marcus, A. Mathur, W. M. Reese and K. E. Healy (2015). "muOrgano: A Lego(R)-Like Plug & Play System for Modular Multi-Organ-Chips." PLoS One **10**(10): e0139587.

Lozito, T. P., P. G. Alexander, H. Lin, R. Gottardi, A. W.-M. Cheng and R. S. Tuan (2013). "Three-dimensional osteochondral microtissue to model pathogenesis of osteoarthritis." Stem Cell Research & Therapy **4**(1): S6.

Lu, Y., W. Zhang, J. Wang, G. Yang, S. Yin, T. Tang, C. Yu and X. Jiang (2019). "Recent advances in cell sheet technology for bone and cartilage regeneration: from preparation to application." International Journal of Oral Science **11**(2): 17.

Luo, X., J. Chen, W.-X. Song, N. Tang, J. Luo, Z.-L. Deng, K. A. Sharff, G. He, Y. Bi, B.-C. He, E. Bennett, J. Huang, Q. Kang, W. Jiang, Y. Su, G.-H. Zhu, H. Yin, Y. He, Y. Wang, J. S. Souris, L. Chen, G.-W. Zuo, A. G. Montag, R. R. Reid, R. C. Haydon, H. H. Luu and T.-C. He (2008). "Osteogenic BMPs promote tumor growth of human osteosarcomas that harbor differentiation defects." Laboratory Investigation **88**(12): 1264-1277.

Ma, D., L. Ren, Y. Liu, F. Chen, J. Zhang, Z. Xue and T. Mao (2010). "Engineering scaffold-free bone tissue using bone marrow stromal cell sheets." J Orthop Res **28**(5): 697-702.

Macchi, V., E. Stocco, C. Stecco, E. Belluzzi, M. Favero, A. Porzionato and R. De Caro (2018). "The infrapatellar fat pad and the synovial membrane: an anatomo-functional unit." J Anat **233**(2): 146-154.

Malda, J., J. C. de Grauw, K. E. M. Benders, M. J. L. Kik, C. H. A. van de Lest, L. B. Creemers, W. J. A. Dhert and P. R. van Weeren (2013). "Of Mice, Men and Elephants: The Relation between Articular Cartilage Thickness and Body Mass." PLOS ONE **8**(2): e57683.

Manel, N., D. Unutmaz and D. R. Littman (2008). "The differentiation of human T(H)-17 cells requires transforming growth factor-beta and induction of the nuclear receptor RORgammat." Nat Immunol **9**(6): 641-649.

Marino, S., K. A. Staines, G. Brown, R. A. Howard-Jones and M. Adamczyk (2016). "Models of ex vivo explant cultures: applications in bone research." Bonekey Rep **5**: 818.

Marshall, J., A. Barnes and P. Genever (2018). "Analysis of the Intrinsic Self-Organising Properties of Mesenchymal Stromal Cells in Three-Dimensional Co-Culture Models with Endothelial Cells." Bioengineering (Basel) **5**(4).

Mathiessen, A. and P. G. Conaghan (2017). "Synovitis in osteoarthritis: current understanding with therapeutic implications." Arthritis research & therapy **19**(1): 18-18.

Matsumoto, I., D. M. Lee, R. Goldbach-Mansky, T. Sumida, C. A. Hitchon, P. H. Schur, R. J. Anderson, J. S. Coblyn, M. E. Weinblatt, M. Brenner, B. Duclos, J. L. Pasquali, H. El-Gabalawy, D. Mathis and C. Benoist (2003). "Low prevalence of antibodies to glucose-6-phosphate isomerase in patients with rheumatoid arthritis and a spectrum of other chronic autoimmune disorders." Arthritis Rheum **48**(4): 944-954.

Mendes, L. F., H. Katagiri, W. L. Tam, Y. C. Chai, L. Geris, S. J. Roberts and F. P. Luyten (2018). "Advancing osteochondral tissue engineering: bone morphogenetic protein, transforming growth factor, and fibroblast growth factor signaling drive ordered differentiation of periosteal cells resulting in stable cartilage and bone formation in vivo." Stem Cell Research & Therapy **9**(1): 42.

Mengus, C., M. G. Muraro, V. Mele, F. Amicarella, C. Manfredonia, F. Foglietta, S. Muenst, S. D. Soysal, G. Iezzi and G. C. Spagnoli (2018). "In Vitro Modeling of Tumor–Immune System Interaction." ACS Biomaterials Science & Engineering **4**(2): 314-323.

Mestas, J. and C. C. W. Hughes (2004). "Of Mice and Not Men: Differences between Mouse and Human Immunology." The Journal of Immunology **172**(5): 2731.

Mixon, A., A. Savage, A. S. Bahar-Moni, M. Adouni and T. Faisal (2021). "An in vitro investigation to understand the synergistic role of MMPs-1 and 9 on articular cartilage biomechanical properties." Scientific Reports **11**(1): 14409.

Mizoguchi, F., K. Slowikowski, K. Wei, J. L. Marshall, D. A. Rao, S. K. Chang, H. N. Nguyen, E. H. Noss, J. D. Turner, B. E. Earp, P. E. Blazar, J. Wright, B. P. Simmons, L. T. Donlin, G. D. Kalliolias, S. M. Goodman, V. P. Bykerk, L. B. Ivashkiv, J. A. Lederer, N. Hacohen, P. A. Nigrovic, A. Filer, C. D. Buckley, S. Raychaudhuri and M. B. Brenner (2018). "Functionally distinct disease-associated fibroblast subsets in rheumatoid arthritis." Nature communications **9**(1): 789-789.

Mor, A., S. B. Abramson and M. H. Pillinger (2005). "The fibroblast-like synovial cell in rheumatoid arthritis: a key player in inflammation and joint destruction." Clinical Immunology **115**(2): 118-128.

Moreira Teixeira, L. S., J. C. Leijten, J. Sobral, R. Jin, A. A. van Apeldoorn, J. Feijen, C. van Blitterswijk, P. J. Dijkstra and M. Karperien (2012). "High throughput generated micro-aggregates of chondrocytes stimulate cartilage formation in vitro and in vivo." Eur Cell Mater **23**: 387-399.

Morrison, S. J. and D. T. Scadden (2014). "The bone marrow niche for haematopoietic stem cells." Nature **505**(7483): 327-334.

Mucientes, A., E. Herranz, E. Moro, A. González-Corchón, M. J. Peña-Soria, L. Abasolo, L. Rodriguez-Rodriguez, J. R. Lamas and B. Fernández-Gutiérrez (2021). "Influence of Mesenchymal Stem Cell Sources on Their Regenerative Capacities on Different Surfaces." Cells **10**(2).

Murdoch, A. D., L. M. Grady, M. P. Ablett, T. Katopodi, R. S. Meadows and T. E. Hardingham (2007). "Chondrogenic differentiation of human bone marrow stem cells in transwell cultures: generation of scaffold-free cartilage." Stem Cells **25**(11): 2786-2796.

Murphy, G. and M. H. Lee (2005). "What are the roles of metalloproteinases in cartilage and bone damage?" Ann Rheum Dis **64 Suppl 4**: iv44-47.

Nakagawa, Y., T. Muneta, K. Otabe, N. Ozeki, M. Mizuno, M. Udo, R. Saito, K. Yanagisawa, S. Ichinose, H. Koga, K. Tsuji and I. Sekiya (2016). "Cartilage Derived from Bone Marrow Mesenchymal Stem Cells Expresses Lubricin In Vitro and In Vivo." PLoS One **11**(2): e0148777.

Nandakumar, K. S. and R. Holmdahl (2005). "Efficient promotion of collagen antibody induced arthritis (CAIA) using four monoclonal antibodies specific for the major epitopes recognized in both collagen induced arthritis and rheumatoid arthritis." J Immunol Methods **304**(1-2): 126-136.

Neidlin, M., E. Chantzi, G. Macheras, M. G. Gustafsson and L. G. Alexopoulos (2019). "An ex vivo tissue model of cartilage degradation suggests that cartilage state can be determined from secreted key protein patterns." PLoS One **14**(10): e0224231.

Nelson, A. E. (2018). "Osteoarthritis year in review 2017: clinical." Osteoarthritis Cartilage **26**(3): 319-325.

Nozaki, T., K. Takahashi, O. Ishii, S. Endo, K. Hioki, T. Mori, T. Kikukawa, D. T. Boumpas, S. Ozaki and H. Yamada (2007). "Development of an ex vivo cellular model of rheumatoid arthritis: critical role of CD14-positive monocyte/macrophages in the development of pannus tissue." Arthritis Rheum **56**(9): 2875-2885.

O'Neil, L. J. and M. J. Kaplan (2019). "Neutrophils in Rheumatoid Arthritis: Breaking Immune Tolerance and Fueling Disease." Trends Mol Med **25**(3): 215-227.

Occhetta, P., A. Mainardi, E. Votta, Q. Vallmajo-Martin, M. Ehrbar, I. Martin, A. Barbero and M. Rasponi (2019). "Hyperphysiological compression of articular cartilage induces an osteoarthritic phenotype in a cartilage-on-a-chip model." Nat Biomed Eng **3**(7): 545-557.

Okada, M., A. Nakai, E. S. Hara, T. Taguchi, T. Nakano and T. Matsumoto (2017). "Biocompatible nanostructured solid adhesives for biological soft tissues." Acta Biomater **57**: 404-413.

Ong, L. J. Y., T. Ching, L. H. Chong, S. Arora, H. Li, M. Hashimoto, R. DasGupta, P. K. Yuen and Y. C. Toh (2019). "Self-aligning Tetris-Like (TILE) modular microfluidic platform for mimicking multi-organ interactions." Lab Chip **19**(13): 2178-2191.

Orr, C., E. Vieira-Sousa, D. L. Boyle, M. H. Buch, C. D. Buckley, J. D. Canete, A. I. Catrina, E. H. S. Choy, P. Emery, U. Fearon, A. Filer, D. Gerlag, F. Humby, J. D. Isaacs, S. A. Just, B. R. Lauwerys, B. Le Goff, A. Manzo, T. McGarry, I. B. McInnes, A. Najm, C. Pitzalis, A. Pratt, M. Smith, P. P. Tak, R. Thurlings, J. E. Fonseca, D. J. Veale and S. W. Tas (2017). "Synovial tissue research: a state-of-the-art review." Nat Rev Rheumatol **13**(8): 463-475.

Ostrowska, M., W. Maśliński, M. Prochorec-Sobieszek, M. Nieciecki and I. Sudoł-Szopińska (2018). "Cartilage and bone damage in rheumatoid arthritis." Reumatologia **56**(2): 111-120.

Pagani, S., P. Torricelli, F. Veronesi, F. Salamanna, S. Cepollaro and M. Fini (2018). "An advanced tri-culture model to evaluate the dynamic interplay among osteoblasts, osteoclasts, and endothelial cells." J Cell Physiol **233**(1): 291-301.

Paggi, C., B. Venzac, J. Leijten, L. M. Teixeira Leijten, S. Le gac and M. Karperien (2020). "Cartilage-on-chip: a multi-modal platform to study human chondrocyte's response to mechanical stimuli." Osteoarthritis and Cartilage **28**: S176-S177.

Paggi, C. A., L. M. Teixeira, S. Le Gac and M. Karperien (2022). "Joint-on-chip platforms: entering a new era of in vitro models for arthritis." Nature Reviews Rheumatology **18**(4): 217-231.

Pap, T., B. Dankbar, C. Wehmeyer, A. Korb-Pap and J. Sherwood (2020). "Synovial fibroblasts and articular tissue remodelling: Role and mechanisms." Seminars in Cell & Developmental Biology **101**: 140-145.

Pap, T. and A. Korb-Pap (2015). "Cartilage damage in osteoarthritis and rheumatoid arthritis—two unequal siblings." Nature Reviews Rheumatology **11**(10): 606-615.

Parish, L. C. (1963). "An historical approach to the nomenclature of rheumatoid arthritis." Arthritis Rheum **6**: 138-158.

Park, H., B. Choi, J. Hu and M. Lee (2013). "Injectable chitosan hyaluronic acid hydrogels for cartilage tissue engineering." Acta Biomater **9**(1): 4779-4786.

Park, I. S., R. L. Jin, H. J. Oh, M. D. Truong, B. H. Choi, S. H. Park, D. Y. Park and B. H. Min (2018). "Sizable Scaffold-Free Tissue-Engineered Articular Cartilage Construct for Cartilage Defect Repair." Artif Organs.

Peck, Y., L. T. Leom, P. F. P. Low, D. J. J. o. T. E. Wang and R. Medicine (2018). "Establishment of an in vitro three-dimensional model for cartilage damage in rheumatoid arthritis." **12**: e237 - e249.

Pene, J., S. Chevalier, L. Preisser, E. Venereau, M. H. Guilleux, S. Ghannam, J. P. Moles, Y. Danger, E. Ravon, S. Lesaux, H. Yssel and H. Gascan (2008). "Chronically inflamed human tissues are infiltrated by highly differentiated Th17 lymphocytes." J Immunol **180**(11): 7423-7430.

Penick, K. J., L. A. Solchaga and J. F. Welter (2005). "High-throughput aggregate culture system to assess the chondrogenic potential of mesenchymal stem cells." Biotechniques **39**(5): 687-691.

Pfeiffenberger, M., A. Damerau, I. Ponomarev, C. H. Bucher, Y. Chen, D. Barnewitz, C. Thöne-Reineke, P. Hoff, F. Buttgereit, T. Gaber and A. Lang (2021). "Functional Scaffold-Free Bone Equivalents Induce Osteogenic and Angiogenic Processes in a Human In Vitro Fracture Hematoma Model." J Bone Miner Res **36**(6): 1189-1201.

Pham, C. T. (2011). "Nanotherapeutic approaches for the treatment of rheumatoid arthritis." Wiley Interdiscip Rev Nanomed Nanobiotechnol **3**(6): 607-619.

Pirosa, A., R. Gottardi, P. G. Alexander, D. Puppi, F. Chiellini and R. S. Tuan (2021). "An in vitro chondro-osteo-vascular triphasic model of the osteochondral complex." Biomaterials **272**: 120773.

Pirosa, A., E. B. Tankus, A. Mainardi, P. Occhetta, L. Dönges, C. Baum, M. Rasponi, I. Martin and A. Barbero (2021). "Modeling In Vitro Osteoarthritis Phenotypes in a Vascularized Bone Model Based on a Bone-Marrow Derived Mesenchymal Cell Line and Endothelial Cells." International journal of molecular sciences **22**(17): 9581.

Pollard, K. M., D. M. Cauvi, C. B. Toomey, K. V. Morris and D. H. Kono (2013). "Interferon-gamma and systemic autoimmunity." Discov Med **16**(87): 123-131.

Poole, A. R., T. Kojima, T. Yasuda, F. Mwale, M. Kobayashi and S. Laverty (2001). "Composition and structure of articular cartilage: a template for tissue repair." Clin Orthop Relat Res(391 Suppl): S26-33.

Pratta, M. A., T. M. Di Meo, D. M. Ruhl and E. C. Arner (1989). "Effect of interleukin-1-beta and tumor necrosis factor-alpha on cartilage proteoglycan metabolism in vitro." Agents Actions **27**(3-4): 250-253.

Prein, C. and F. Beier (2019). Chapter Two - ECM signaling in cartilage development and endochondral ossification. Current Topics in Developmental Biology. B. R. Olsen, Academic Press. **133:** 25-47.

Pretzel, D., D. Pohlers, S. Weinert and R. W. Kinne (2009). "In vitro model for the analysis of synovial fibroblast-mediated degradation of intact cartilage." Arthritis Res Ther **11**(1): R25.

Purcell, P. and P. A. Trainor (2015). "The Mighty Chondrocyte: No Bones about It." J Dent Res **94**(12): 1625-1627.

Ralphs, J. R. and M. Benjamin (1994). "The joint capsule: structure, composition, ageing and disease." J Anat **184 (Pt 3)**(Pt 3): 503-509.

Ramadan, Q. and M. A. M. Gijs (2015). "In vitro micro-physiological models for translational immunology." Lab on a Chip **15**(3): 614-636.

Rannou, F., M. François, M. T. Corvol and F. Berenbaum (2006). "Cartilage breakdown in rheumatoid arthritis." Joint Bone Spine **73**(1): 29-36.

Rao, D. A., M. F. Gurish, J. L. Marshall, K. Slowikowski, C. Y. Fonseka, Y. Liu, L. T. Donlin, L. A. Henderson, K. Wei, F. Mizoguchi, N. C. Teslovich, M. E. Weinblatt, E. M. Massarotti, J. S. Coblyn, S. M. Helfgott, Y. C. Lee, D. J. Todd, V. P. Bykerk, S. M. Goodman, A. B. Pernis, L. B. Ivashkiv, E. W. Karlson, P. A. Nigrovic, A. Filer, C. D. Buckley, J. A. Lederer, S. Raychaudhuri and M. B. Brenner (2017). "Pathologically expanded peripheral T helper cell subset drives B cells in rheumatoid arthritis." Nature **542**(7639): 110-114.

Rech, J., M. Sticherling, D. Stoessel, M. H. C. Biermann, B. M. Häberle and M. Reinhardt (2020). "Psoriatic arthritis epidemiology, comorbid disease profiles and risk factors: results from a claims database analysis." Rheumatology Advances in Practice **4**(2).

Rhee, D. K., J. Marcelino, M. Baker, Y. Gong, P. Smits, V. Lefebvre, G. D. Jay, M. Stewart, H. Wang, M. L. Warman and J. D. Carpten (2005). "The secreted glycoprotein lubricin

protects cartilage surfaces and inhibits synovial cell overgrowth." J Clin Invest **115**(3): 622-631.

Ribel-Madsen, S., E. M. Bartels, A. Stockmarr, A. Borgwardt, C. Cornett, B. Danneskiold-Samsoe and H. Bliddal (2012). "A synoviocyte model for osteoarthritis and rheumatoid arthritis: response to Ibuprofen, betamethasone, and ginger extract-a cross-sectional in vitro study." Arthritis **2012**: 505842.

Ringe, J. and M. Sittinger (2009). "Tissue engineering in the rheumatic diseases." Arthritis Res Ther **11**(1): 211.

Ritchlin, C. and I. E. Adamopoulos (2021). "Axial spondyloarthritis: new advances in diagnosis and management." **372**: m4447.

Rivellese, F., D. Mauro, A. Nerviani, S. Pagani, L. Fossati-Jimack, T. Messemaker, F. A. S. Kurreeman, R. E. M. Toes, A. Ramming, S. Rauber, G. Schett, G. W. Jones, S. A. Jones, F. W. Rossi, A. de Paulis, G. Marone, M. E. M. El Shikh, F. Humby and C. Pitzalis (2018). "Mast cells in early rheumatoid arthritis associate with disease severity and support B cell autoantibody production." Ann Rheum Dis **77**(12): 1773-1781.

Roelsgaard, I. K., B. A. Esbensen, M. Østergaard, S. Rollefstad, A. G. Semb, R. Christensen and T. Thomsen (2019). "Smoking cessation intervention for reducing disease activity in chronic autoimmune inflammatory joint diseases." Cochrane Database Syst Rev **9**(9): Cd012958.

Rosenbaum, A. J., D. A. Grande and J. S. Dines (2008). "The use of mesenchymal stem cells in tissue engineering: A global assessment." Organogenesis **4**(1): 23-27.

Ruet Rossignol, M. (2005). "The 7th Amendment to the Cosmetics Directive." Altern Lab Anim **33 Suppl 1**: 19-20.

Ryu, N.-E., S.-H. Lee and H. Park (2019). "Spheroid Culture System Methods and Applications for Mesenchymal Stem Cells." Cells **8**(12): 1620.

Saadoun, D., M. Vautier and P. Cacoub (2021). "Medium- and Large-Vessel Vasculitis." Circulation **143**(3): 267-282.

Saito, S., K. Murakoshi, S. Kotake, N. Kamatani and T. Tomatsu (2008). "Granzyme B induces apoptosis of chondrocytes with natural killer cell-like cytotoxicity in rheumatoid arthritis." J Rheumatol **35**(10): 1932-1943.

Sakaguchi, N., T. Takahashi, H. Hata, T. Nomura, T. Tagami, S. Yamazaki, T. Sakihama, T. Matsutani, I. Negishi, S. Nakatsuru and S. Sakaguchi (2003). "Altered thymic T-cell selection due to a mutation of the ZAP-70 gene causes autoimmune arthritis in mice." Nature **426**(6965): 454-460.

Sanchez-Lopez, E., R. Coras, A. Torres, N. E. Lane and M. Guma (2022). "Synovial inflammation in osteoarthritis progression." Nat Rev Rheumatol **18**(5): 258-275.

Sandell, L. J. and T. Aigner (2001). "Articular cartilage and changes in Arthritis: Cell biology of osteoarthritis." Arthritis Research & Therapy **3**(2): 107.

Sato, M., M. Yamato, K. Hamahashi, T. Okano and J. Mochida (2014). "Articular cartilage regeneration using cell sheet technology." Anat Rec (Hoboken) **297**(1): 36-43.

Scanzello, C. R. and S. R. Goldring (2012). "The role of synovitis in osteoarthritis pathogenesis." Bone **51**(2): 249-257.

Scheinpflug, J., M. Pfeiffenberger, A. Damerau, F. Schwarz, M. Textor, A. Lang and F. Schulze (2018). "Journey into Bone Models: A Review." Genes (Basel) **9**(5).

Schinnerling, K., C. Rosas, L. Soto, R. Thomas and J. C. Aguillón (2019). "Humanized Mouse Models of Rheumatoid Arthritis for Studies on Immunopathogenesis and Preclinical Testing of Cell-Based Therapies." Frontiers in Immunology **10**(203).

Schroder, A., U. Nazet, D. Muschter, S. Grassel, P. Proff and C. Kirschneck (2019). "Impact of Mechanical Load on the Expression Profile of Synovial Fibroblasts from Patients with and without Osteoarthritis." Int J Mol Sci **20**(3).

Schubert, N., J. Dudeck, P. Liu, A. Karutz, S. Speier, M. Maurer, J. Tuckermann and A. Dudeck (2015). "Mast cell promotion of T cell-driven antigen-induced arthritis despite being dispensable for antibody-induced arthritis in which T cells are bypassed." Arthritis Rheumatol **67**(4): 903-913.

Schuerwegh, A. J., E. J. Dombrecht, W. J. Stevens, J. F. Van Offel, C. H. Bridts and L. S. De Clerck (2003). "Influence of pro-inflammatory (IL-1 alpha, IL-6, TNF-alpha, IFN-gamma) and anti-inflammatory (IL-4) cytokines on chondrocyte function." Osteoarthritis Cartilage **11**(9): 681-687.

Schultz, O., G. Keyszer, J. Zacher, M. Sittinger and G. R. Burmester (1997). "Development of in vitro model systems for destructive joint diseases: novel strategies for establishing inflammatory pannus." Arthritis Rheum **40**(8): 1420-1428.

Scott, D. L., F. Wolfe and T. W. Huizinga (2010). "Rheumatoid arthritis." Lancet **376**(9746): 1094-1108.

Senthelal, S., J. Li, A. Goyal, P. Bansal and M. A. Thomas (2021). Arthritis. StatPearls. Treasure Island (FL).

Seok, J., H. S. Warren, A. G. Cuenca, M. N. Mindrinos, H. V. Baker, W. Xu, D. R. Richards, G. P. McDonald-Smith, H. Gao, L. Hennessy, C. C. Finnerty, C. M. López, S. Honari, E. E. Moore, J. P. Minei, J. Cuschieri, P. E. Bankey, J. L. Johnson, J. Sperry, A. B. Nathens, T. R. Billiar, M. A. West, M. G. Jeschke, M. B. Klein, R. L. Gamelli, N. S. Gibran, B. H. Brownstein, C. Miller-Graziano, S. E. Calvano, P. H. Mason, J. P. Cobb, L. G. Rahme, S. F. Lowry, R. V. Maier, L. L. Moldawer, D. N. Herndon, R. W. Davis, W. Xiao and R. G. Tompkins (2013). "Genomic responses in mouse models poorly mimic human

inflammatory diseases." Proceedings of the National Academy of Sciences **110**(9): 3507-3512.

Shahrara, S., Q. Huang, A. M. Mandelin, 2nd and R. M. Pope (2008). "TH-17 cells in rheumatoid arthritis." Arthritis Res Ther **10**(4): R93.

Shay, T., V. Jojic, O. Zuk, K. Rothamel, D. Puyraimond-Zemmour, T. Feng, E. Wakamatsu, C. Benoist, D. Koller and A. Regev (2013). "Conservation and divergence in the transcriptional programs of the human and mouse immune systems." Proceedings of the National Academy of Sciences **110**(8): 2946-2951.

Shiozawa, Y., A. M. Havens, K. J. Pienta and R. S. Taichman (2008). "The bone marrow niche: habitat to hematopoietic and mesenchymal stem cells, and unwitting host to molecular parasites." Leukemia **22**(5): 941-950.

Smith, M. D. (2011). "The normal synovium." Open Rheumatol J **5**: 100-106.

Smolen, J. S., D. Aletaha, A. Barton, G. R. Burmester, P. Emery, G. S. Firestein, A. Kavanaugh, I. B. McInnes, D. H. Solomon, V. Strand and K. Yamamoto (2018). "Rheumatoid arthritis." Nat Rev Dis Primers **4**: 18001.

Smolen, J. S., R. Landewe, F. C. Breedveld, M. Buch, G. Burmester, M. Dougados, P. Emery, C. Gaujoux-Viala, L. Gossec, J. Nam, S. Ramiro, K. Winthrop, M. de Wit, D. Aletaha, N. Betteridge, J. W. Bijlsma, M. Boers, F. Buttgereit, B. Combe, M. Cutolo, N. Damjanov, J. M. Hazes, M. Kouloumas, T. K. Kvien, X. Mariette, K. Pavelka, P. L. van Riel, A. Rubbert-Roth, M. Scholte-Voshaar, D. L. Scott, T. Sokka-Isler, J. B. Wong and D. van der Heijde (2014). "EULAR recommendations for the management of rheumatoid arthritis with synthetic and biological disease-modifying antirheumatic drugs: 2013 update." Ann Rheum Dis **73**(3): 492-509.

Smolen, J. S., R. B. M. Landewe, J. W. J. Bijlsma, G. R. Burmester, M. Dougados, A. Kerschbaumer, I. B. McInnes, A. Sepriano, R. F. van Vollenhoven, M. de Wit, D. Aletaha, M. Aringer, J. Askling, A. Balsa, M. Boers, A. A. den Broeder, M. H. Buch, F. Buttgereit, R. Caporali, M. H. Cardiel, D. De Cock, C. Codreanu, M. Cutolo, C. J. Edwards, Y. van Eijk-Hustings, P. Emery, A. Finckh, L. Gossec, J. E. Gottenberg, M. L. Hetland, T. W. J. Huizinga, M. Koloumas, Z. Li, X. Mariette, U. Muller-Ladner, E. F. Mysler, J. A. P. da Silva, G. Poor, J. E. Pope, A. Rubbert-Roth, A. Ruyssen-Witrand, K. G. Saag, A. Strangfeld, T. Takeuchi, M. Voshaar, R. Westhovens and D. van der Heijde (2020). "EULAR recommendations for the management of rheumatoid arthritis with synthetic and biological disease-modifying antirheumatic drugs: 2019 update." Ann Rheum Dis.

Sophia Fox, A. J., A. Bedi and S. A. Rodeo (2009). "The basic science of articular cartilage: structure, composition, and function." Sports Health **1**(6): 461-468.

Soundararajan, M. and S. Kannan (2018). "Fibroblasts and mesenchymal stem cells: Two sides of the same coin?" J Cell Physiol **233**(12): 9099-9109.

Stephenson, W., L. T. Donlin, A. Butler, C. Rozo, B. Bracken, A. Rashidfarrokhi, S. M. Goodman, L. B. Ivashkiv, V. P. Bykerk, D. E. Orange, R. B. Darnell, H. P. Swerdlow and R. Satija (2018). "Single-cell RNA-seq of rheumatoid arthritis synovial tissue using low-cost microfluidic instrumentation." Nat Commun **9**(1): 791.

Stolberg-Stolberg, J., A. Boettcher, M. Sambale, S. Stuecker, J. Sherwood, M. Raschke, T. Pap and J. Bertrand (2022). "Toll-like receptor 3 activation promotes joint degeneration in osteoarthritis." Cell Death & Disease **13**(3): 224.

Tamer, T. M. (2013). "Hyaluronan and synovial joint: function, distribution and healing." Interdiscip Toxicol **6**(3): 111-125.

Tateiwa, D., H. Yoshikawa and T. Kaito (2019). "Cartilage and Bone Destruction in Arthritis: Pathogenesis and Treatment Strategy: A Literature Review." Cells **8**(8).

Tetlow, L. C. and D. E. Woolley (1998). "Comparative immunolocalization studies of collagenase 1 and collagenase 3 production in the rheumatoid lesion, and by human chondrocytes and synoviocytes in vitro." Br J Rheumatol **37**(1): 64-70.

Tetta, C., G. Camussi, V. Modena, C. Di Vittorio and C. Baglioni (1990). "Tumour necrosis factor in serum and synovial fluid of patients with active and severe rheumatoid arthritis." Ann Rheum Dis **49**(9): 665-667.

Trentham, D. E., A. S. Townes and A. H. Kang (1977). "Autoimmunity to type II collagen an experimental model of arthritis." J Exp Med **146**(3): 857-868.

Tuli, R., S. Nandi, W.-J. Li, S. Tuli, X. Huang, P. A. Manner, P. Laquerriere, U. Nöth, D. J. Hall and R. S. Tuan (2004). "Human mesenchymal progenitor cell-based tissue engineering of a single-unit osteochondral construct." Tissue engineering **10**(7-8): 1169-1179.

Turner, R., G. Counts, H. Mashburn, W. Treadway and L. DeChatelet (1980). "Drug and rheumatoid factor effects on the uptake of immunoglobulin G aggregates by neurtrophil monolayers." Inflammation **4**(1): 55-64.

Tzelepi, V., A. C. Tsamandas, V. Zolota and C. D. Scopa (2009). Bone Anatomy, Physiology and Function. Bone Metastases: A translational and clinical approach. D. Kardamakis, V. Vassiliou and E. Chow. Dordrecht, Springer Netherlands**:** 3-30.

Ueha, T., M. Akahane, T. Shimizu, Y. Uchihara, Y. Morita, N. Nitta, A. Kido, Y. Inagaki, K. Kawate and Y. Tanaka (2015). "Utility of tricalcium phosphate and osteogenic matrix cell sheet constructs for bone defect reconstruction." World J Stem Cells **7**(5): 873-882.

Vaccaro, A. R. (2002). "The role of the osteoconductive scaffold in synthetic bone graft." Orthopedics **25**(5 Suppl): s571-578.

van Gaalen, F. A., R. E. Toes, H. J. Ditzel, M. Schaller, F. C. Breedveld, C. L. Verweij and T. W. Huizinga (2004). "Association of autoantibodies to glucose-6-phosphate isomerase with extraarticular complications in rheumatoid arthritis." Arthritis Rheum **50**(2): 395-399.

van Hamburg, J. P., P. S. Asmawidjaja, N. Davelaar, A. M. Mus, E. M. Colin, J. M. Hazes, R. J. Dolhain and E. Lubberts (2011). "Th17 cells, but not Th1 cells, from patients with early rheumatoid arthritis are potent inducers of matrix metalloproteinases and proinflammatory cytokines upon synovial fibroblast interaction, including autocrine interleukin-17A production." Arthritis Rheum **63**(1): 73-83.

Vingsbo, C., P. Sahlstrand, J. G. Brun, R. Jonsson, T. Saxne and R. Holmdahl (1996). "Pristane-induced arthritis in rats: a new model for rheumatoid arthritis with a chronic disease course influenced by both major histocompatibility complex and non-major histocompatibility complex genes." Am J Pathol **149**(5): 1675-1683.

Volpe, E., N. Servant, R. Zollinger, S. I. Bogiatzi, P. Hupe, E. Barillot and V. Soumelis (2008). "A critical function for transforming growth factor-beta, interleukin 23 and proinflammatory cytokines in driving and modulating human T(H)-17 responses." Nat Immunol **9**(6): 650-657.

von der Mark, K., V. Gauss, H. von der Mark and P. Muller (1977). "Relationship between cell shape and type of collagen synthesised as chondrocytes lose their cartilage phenotype in culture." Nature **267**(5611): 531-532.

Wang, C., X. Cao and Y. Zhang (2017). "A novel bioactive osteogenesis scaffold delivers ascorbic acid, beta-glycerophosphate, and dexamethasone in vivo to promote bone regeneration." Oncotarget **8**(19): 31612-31625.

Wang, F., Y. Hu, D. He, G. Zhou and E. Ellis, 3rd (2018). "Scaffold-free cartilage cell sheet combined with bone-phase BMSCs-scaffold regenerate osteochondral construct in mini-pig model." Am J Transl Res **10**(10): 2997-3010.

Wang, Q., Y. Zhang, B. Li and L. Chen (2017). "Controlled dual delivery of low doses of BMP-2 and VEGF in a silk fibroin-nanohydroxyapatite scaffold for vascularized bone regeneration." J Mater Chem B **5**(33): 6963-6972.

Weber, M. C., L. Fischer, A. Damerau, I. Ponomarev, M. Pfeiffenberger, T. Gaber, S. Gotschel, J. Lang, S. Roblitz, F. Buttgereit, R. Ehrig and A. Lang (2020). "Macroscale mesenchymal condensation to study cytokine-driven cellular and matrix-related changes during cartilage degradation." Biofabrication **12**(4): 045016.

Wei, K., I. Korsunsky, J. L. Marshall, A. Gao, G. F. M. Watts, T. Major, A. P. Croft, J. Watts, P. E. Blazar, J. K. Lange, T. S. Thornhill, A. Filer, K. Raza, L. T. Donlin, A. Accelerating Medicines Partnership Rheumatoid, C. Systemic Lupus Erythematosus, C. W. Siebel, C. D. Buckley, S. Raychaudhuri and M. B. Brenner (2020). "Notch signalling drives synovial fibroblast identity and arthritis pathology." Nature **582**(7811): 259-264.

Whitney, G. A., H. Mera, M. Weidenbecher, A. Awadallah, J. M. Mansour and J. E. Dennis (2012). "Methods for Producing Scaffold-Free Engineered Cartilage Sheets from Auricular

and Articular Chondrocyte Cell Sources and Attachment to Porous Tantalum." BioResearch Open Access **1**(4): 157-165.

Wilder, R. L. (2001). "Streptococcal cell wall arthritis." Curr Protoc Immunol **Chapter 15**: Unit 15 10.

Wilson, A., M. Hodgson-Garms, J. E. Frith and P. Genever (2019). "Multiplicity of Mesenchymal Stromal Cells: Finding the Right Route to Therapy." Front Immunol **10**: 1112.

Winthrop, K. L., M. E. Weinblatt, J. Bathon, G. R. Burmester, P. J. Mease, L. Crofford, V. Bykerk, M. Dougados, J. T. Rosenbaum, X. Mariette, J. Sieper, F. Melchers, B. N. Cronstein, F. C. Breedveld, J. Kalden, J. S. Smolen and D. Furst (2020). "Unmet need in rheumatology: reports from the Targeted Therapies meeting 2019." Ann Rheum Dis **79**(1): 88-93.

Wirsig, K., D. Kilian, M. von Witzleben, M. Gelinsky and A. Bernhardt (2022). "Impact of Sr2+ and hypoxia on 3D triple cultures of primary human osteoblasts, osteocytes and osteoclasts." European Journal of Cell Biology **101**(3): 151256.

Wooley, P. H., J. R. Seibold, J. D. Whalen and J. M. Chapdelaine (1989). "Pristane-induced arthritis. The immunologic and genetic features of an experimental murine model of autoimmune disease." Arthritis Rheum **32**(8): 1022-1030.

Wrobel, E., J. Leszczynska and E. Brzoska (2016). "The Characteristics Of Human Bone-Derived Cells (HBDCS) during osteogenesis in vitro." Cellular & Molecular Biology Letters **21**(1): 26.

Wu, H., J. Du and Q. Zheng (2008). "Expression of MMP-1 in cartilage and synovium of experimentally induced rabbit ACLT traumatic osteoarthritis: immunohistochemical study." Rheumatol Int **29**(1): 31-36.

Wu, J., Q. Li, L. Jin, Y. Qu, B. B. Liang, X. T. Zhu, H. Y. Du, L. G. Jie and Q. H. Yu (2019). "Kirenol Inhibits the Function and Inflammation of Fibroblast-like Synoviocytes in Rheumatoid Arthritis in vitro and in vivo." Front Immunol **10**: 1304.

Yamada, H., Y. Nakashima, K. Okazaki, T. Mawatari, J. I. Fukushi, N. Kaibara, A. Hori, Y. Iwamoto and Y. Yoshikai (2008). "Th1 but not Th17 cells predominate in the joints of patients with rheumatoid arthritis." Ann Rheum Dis **67**(9): 1299-1304.

Yan, Y., H. Chen, H. Zhang, C. Guo, K. Yang, K. Chen, R. Cheng, N. Qian, N. Sandler, Y. S. Zhang, H. Shen, J. Qi, W. Cui and L. Deng (2019). "Vascularized 3D printed scaffolds for promoting bone regeneration." Biomaterials **190-191**: 97-110.

Yasui, Y., W. Ando, K. Shimomura, K. Koizumi, C. Ryota, S. Hamamoto, M. Kobayashi, H. Yoshikawa and N. Nakamura (2016). "Scaffold-free, stem cell-based cartilage repair." J Clin Orthop Trauma **7**(3): 157-163.

Yin, J., S. Qiu, B. Shi, X. Xu, Y. Zhao, J. Gao, S. Zhao and S. Min (2018). "Controlled release of FGF-2 and BMP-2 in tissue engineered periosteum promotes bone repair in rats." Biomed Mater **13**(2): 025001.

Yuan, H., H. Fernandes, P. Habibovic, J. de Boer, A. M. Barradas, A. de Ruiter, W. R. Walsh, C. A. van Blitterswijk and J. D. de Bruijn (2010). "Osteoinductive ceramics as a synthetic alternative to autologous bone grafting." Proc Natl Acad Sci U S A **107**(31): 13614-13619.

Zhang, F., K. Wei, K. Slowikowski, C. Y. Fonseka, D. A. Rao, S. Kelly, S. M. Goodman, D. Tabechian, L. B. Hughes, K. Salomon-Escoto, G. F. M. Watts, A. H. Jonsson, J. Rangel-Moreno, N. Meednu, C. Rozo, W. Apruzzese, T. M. Eisenhaure, D. J. Lieb, D. L. Boyle, A. M. Mandelin, 2nd, A. Accelerating Medicines Partnership Rheumatoid, C. Systemic Lupus Erythematosus, B. F. Boyce, E. DiCarlo, E. M. Gravallese, P. K. Gregersen, L. Moreland, G. S. Firestein, N. Hacohen, C. Nusbaum, J. A. Lederer, H. Perlman, C. Pitzalis, A. Filer, V. M. Holers, V. P. Bykerk, L. T. Donlin, J. H. Anolik, M. B. Brenner and S. Raychaudhuri (2019). "Defining inflammatory cell states in rheumatoid arthritis joint synovial tissues by integrating single-cell transcriptomics and mass cytometry." Nat Immunol **20**(7): 928-942.

Zhang, S., K. Ba, L. Wu, S. Lee, B. Peault, F. A. Petrigliano, D. R. McAllister, J. S. Adams, D. Evseenko and Y. Lin (2015). "Adventitial Cells and Perictyes Support Chondrogenesis Through Different Mechanisms in 3-Dimensional Cultures With or Without Nanoscaffolds." J Biomed Nanotechnol **11**(10): 1799-1807.

Zhang, W., J. Chen, J. Tao, Y. Jiang, C. Hu, L. Huang, J. Ji and H. W. Ouyang (2013). "The use of type 1 collagen scaffold containing stromal cell-derived factor-1 to create a matrix environment conducive to partial-thickness cartilage defects repair." Biomaterials **34**(3): 713-723.

Zhao, Y., X. Yan, X. Li, Y. Zheng, S. Li and X. Chang (2016). "PGK1, a glucose metabolism enzyme, may play an important role in rheumatoid arthritis." Inflamm Res **65**(10): 815-825.

Žigon-Branc, S., A. Barlič, M. Knežević, M. Jeras and G. Vunjak-Novakovic (2018). "Testing the potency of anti-TNF-α and anti-IL-1β drugs using spheroid cultures of human osteoarthritic chondrocytes and donor-matched chondrogenically differentiated mesenchymal stem cells." Biotechnol Prog **34**(4): 1045-1058.

Zimmermann, G. and A. Moghaddam (2011). "Allograft bone matrix versus synthetic bone graft substitutes." Injury **42 Suppl 2**: S16-21.

LIST OF PUBLICATIONS AND CONTRIBUTIONS

A. FROM THE PRESENT WORK

PEER REVIEWED PUBLICATIONS

Damerau A, Pfeiffenberger M, Weber MC, Burmester GR, Buttgereit F, Gaber T*, Lang A* (2020). A Human Osteochondral Tissue Model Mimicking Cytokine-Induced Key Features of Arthritis In Vitro. *Int J Mol Sci*. 22(1):128. doi: 10.3390/ijms22010128. PMID: 33374446. (*contributed equally)

Damerau A, Buttgereit F, Gaber T (2022). Optimization of a Tricalcium Phosphate-Based Bone Model Using Cell-Sheet Technology to Simulate Bone Disorders. *Processes*. 10(3):550. doi: 10.3390/pr10030550.

Damerau A, Gaber T (2020). Modeling Rheumatoid Arthritis In Vitro: From Experimental Feasibility to Physiological Proximity. *Int J Mol Sci*. 21(21):7916. doi: 10.3390/ijms21217916. PMID: 33113770.

SUBMITTED OR DRAFTED PUBLICATIONS

Damerau A, Do Nguyen DH, Lubahn C, Jenning M, Pfeiffenberger M, Gaber T, Buttgereit F (2022). Microscale scaffold-free *in vitro* 3D cartilage constructs replicate inflammation-mediated cartilage degeneration. *Front. Bioeng. Biotechnol.* (submitted).

Damerau A, Kirchner M, Beißel J, Pfeiffenberger M, Mertins P, Buttgereit F, Gaber T (2022). A functional xeno-free 3D synovial membrane model to study synovitis *in vitro*. (draft).

B. FROM ADDITIONAL WORK

PEER REVIEWED PUBLICATIONS

Damerau A, Kirchner M, Pfeiffenberger M, Ehlers L, Do Nguyen DH, Mertins P, Bartek B, Maleitzke T, Palmowski Y, Hardt S, Winkler T, Buttgereit F, Gaber T (2022). Metabolic reprogramming of synovial fibroblasts in osteoarthritis by inhibition of pathologically overexpressed pyruvate dehydrogenase kinases. *Metab. Eng*. 72:116-132. doi: 10.1016/j.ymben.2022.03.006. PMID: 35296430.

Weber MC*, Fischer L*, **Damerau A**, Ponomarev I, Pfeiffenberger M, Gaber T, Götschel S, Lang J, Röblitz S, Buttgereit F, Ehrig R, Lang A (2020). Macroscale mesenchymal condensation to study cytokine-driven cellular and matrix-related changes during cartilage degradation. *Biofabrication*. 12(4):045016. doi: 10.1088/1758-5090/aba08f. PMID: 32598334. (*contributed equally)

Damerau A, Gaber T, Ohrndorf S, Hoff P (2020). JAK/STAT Activation: A General Mechanism for Bone Development, Homeostasis, and Regeneration. *Int J Mol Sci*. 21(23):9004. doi: 10.3390/ijms21239004. PMID: 33256266.

Bucher CH, Berkmann JC, Burkhardt LM, Paschke C, Schlundt C, Lang A, Wolter A, **Damerau A**, Geissler S, Volk HD, Duda GN, Schmidt-Bleek K (2022). Local immune cell contributions to fracture healing in aged individuals - A novel role for interleukin 22. Exp Mol Med. 54(8):1262-1276. doi: 10.1038/s12276-022-00834-9. Epub 2022 Aug 26. PMID: 36028760.

Pfeiffenberger M, **Damerau A**, Ponomarev I, Bucher CH, Chen Y, Barnewitz D, Thöne-Reineke C, Hoff P, Buttgereit F, Gaber T, Lang A (2021). Functional Scaffold-Free Bone Equivalents Induce Osteogenic and Angiogenic Processes in a Human *In vitro* Fracture Hematoma Model. *J Bone Miner Res*. 36(6):1189-1201. doi: 10.1002/jbmr.4267. Epub 2021 Feb 25. PMID: 33534144.

Chen Y, Ye Y, Krauß PL, Löwe P, Pfeiffenberger M, **Damerau A**, Ehlers L, Buttgereit T, Hoff P, Buttgereit F, Gaber T (2022). Age-related increase of mitochondrial content in human memory CD4+ T cells contributes to ROS-mediated increased expression of proinflammatory cytokines. *Front Immunol.* 13:911050. doi: 10.3389/fimmu.2022.911050. eCollection 2022. PMID: 35935995.

Krauss PL*, Pfeiffenberger M*, **Damerau A**, Buttgereit T, Chen Y, Gaber T, Buttgereit F (2021). Production of IL-6 and Phagocytosis Are the Most Resilient Immune Functions in Metabolically Compromised Human Monocytes. *Front Immunol*. 12:730672. doi: 10.3389/fimmu.2021.730672. eCollection 2021. PMID: 34737742. (*contributed equally)

Ehlers L, Kuppe A, **Damerau A,** Wilantri S, Kirchner M, Mertins P, Strehl C, Buttgereit F, Gaber T (2021). Surface AMP deaminase 2 as a novel regulator modifying extracellular adenine nucleotide metabolism. *FASEB J*. 35(7):e21684. doi: 10.1096/fj.202002658RR. PMID: 34159634.

Pfeiffenberger M, **Damerau A**, Lang A, Buttgereit F, Hoff P, Gaber T (2021). Fracture Healing Research-Shift towards *In vitro* Modeling? *Biomedicines*. 9(7):748. doi: 10.3390/biomedicines9070748. PMID: 34203470.

Gaber T, Brinkman ACK, Pienczikowski J, Diesing K, **Damerau A**, Pfeiffenberger M, Lang A, Ohrndorf S, Burmester GR, Buttgereit F, Hoff P (2020). Impact of Janus Kinase Inhibition with Tofacitinib on Fundamental Processes of Bone Healing. *Int J Mol Sci*. 21(3):865. doi: 10.3390/ijms21030865. PMID: 32013232.

Lang A, Stefanowski J, Pfeiffenberger M, Wolter A, **Damerau A**, Hemmati-Sadeghi S, Haag R, Hauser AE, Löhning M, Duda GN, Hoff P, Schmidt-Bleek K, Gaber T*, Buttgereit F* (2022). MIF does only marginally enhance the pro-regenerative capacities of DFO in a mouse-osteotomy-model of compromised bone healing conditions. *Bone*. 154:116247. doi: 10.1016/j.bone.2021.116247. Epub 2021 Nov 4. PMID: 34743042. (*contributed equally)

Lang A, Kirchner M, Stefanowski J, Durst M, Weber MC, Pfeiffenberger M, **Damerau A**, Hauser AE, Hoff P, Duda GN, Buttgereit F, Schmidt-Bleek K, Gaber T (2019). Collagen I-based scaffolds negatively impact fracture healing in a mouse-osteotomy-model although used routinely in research and clinical application. *Acta Biomater*. 86:171-184. doi: 10.1016/j.actbio.2018.12.043. Epub 2019 Jan 5. PMID: 30616076.

Scheinpflug J*, Pfeiffenberger M*, **Damerau A**, Schwarz F, Textor M, Lang A, Schulze F (2018). Journey into Bone Models: A Review. *Genes* (Basel). 9(5):247. doi: 10.3390/genes9050247. PMID: 29748516. (*contributed equally)

ABSTRACTS & CONFERENCES PROCEEDINGS

EUSAAT 2022 – European Congress on Alternatives to Animal Testing

Julia Beißel, Christina Lubahn, Duc Ha Do Nguyen, Moritz Pfeiffenberger, Frank Buttgereit, Timo Gaber, Alexandra Damerau. A xeno-free *in vitro* 3D synovial membrane model mimicking the pathogenesis of arthritis. Poster Presentation.

EULAR 2022 – Annual European Congress of Rheumatology

Duc Ha Do Nguyen, Christina Lubahn, Thomas Leeuw, Frank Buttgereit, Timo Gaber, Alexandra Damerau. Fluidic shear stress reduces TNFα mediated cartilage damage in a 3D model of degenerative joint disease. Guided Poster Presentation.

EWRR 2022 – 41st European Workshop for Rheumatology Research

Alexandra Damerau, Marieluise Kirchner, Moritz Pfeiffenberger, Duc Ha Do Nguyen, Benjamin Bartek, Tazio Maleitzke, Sebastian Hardt, Frank Buttgereit, Timo Gaber. Synovial fibroblasts in osteoarthritis are marked by pathologically overexpressed pyruvate dehydrogenase kinases. Oral Presentation.

ACR 2021 – American College of Rheumatology

Alexandra Damerau, Marieluise Kirchner, Moritz Pfeiffenberger, Duc Ha Do Nguyen, Benjamin Bartek, Tazio Maleitzke, Sebastian Hardt, Frank Buttgereit, Timo Gaber. Metabolic reprogramming: Pyruvate dehydrogenase kinases as a potential novel target to treat osteoarthritis. Poster Presentation.

11th World Congress on Alternatives and Animal Use in the Life Sciences (WC11), 2021

Alexandra Damerau, Moritz Pfeiffenberger, Frank Buttgereit, Timo Gaber, Annemarie Lang. The human-based *in vitro* 3D arthritic joint model for preclinical drug testing. Oral Presentation.

BSMB Symposium 2021 – British Society for Matrix Biology

Alexandra Damerau, Marieluise Kirchner, Moritz Pfeiffenberger, Annemarie Lang, Frank Buttgereit, Timo Gaber. Pyruvate dehydrogenase kinases as a potential target in the treatment of osteoarthritis to unleash the metabolic flow? Oral Presentation.

University of Zurich 2020 - LTK Module 14: Current topics of Laboratory Animal Science

Alexandra Damerau. Mimicking arthritis *in vitro* – a multicomponent model. Invited Oral Presentation.

EORS 2020 – European Orthopaedic Research Society

Alexandra Damerau, Moritz Pfeiffenberger, Frank Buttgereit, Annemarie Lang, Timo Gaber. A human *in vitro* osteochondral tissue model of arthritis for preclinical drug testing. Oral Presentation.

ACR 2020 – American College of Rheumatology

Alexandra Damerau, Moritz Pfeiffenberger, Annemarie Lang, Timo Gaber, Frank Buttgereit. Mimicking cytokine-driven key features of arthritis using a human *in vitro* 3D joint model. Oral Presentation.

JRC Summer School 2019 – Joint Research Centre (JRC) of the European Commission

Alexandra Damerau, Annemarie Lang, Moritz Pfeiffenberger, Timo Gaber, Frank Buttgereit. The *in vitro* 3D multi-component 3D arthritic joint model. Oral Presentation.

EUSAAT 2019 – European Congress on Alternatives to Animal Testing

Alexandra Damerau, Moritz Pfeiffenberger, Karoline Diesing, Frank Buttgereit, Timo Gaber, Annemarie Lang. Simulating an arthritic joint *in vitro* by combining multiple tissue components. Oral Presentation.

DGRh 2019 – Deutsche Gesellschaft für Rheumatologie e.V.

Alexandra Damerau, Annemarie Lang, Moritz Pfeiffenberger, Frank Buttgereit, Timo Gaber. The 3D human-based *in vitro* arthritic joint model. Oral Presentation.

EORS 2019 – European Orthopaedic Research Society

Alexandra Damerau, Moritz Pfeiffenberger, Frank Buttgereit, Annemarie Lang, Timo Gaber. Characterizing a 3D human-based *in vitro* arthritic joint model composed of several components. Oral Presentation.

48. Seminar über Versuchstiere und Tierversuche, 2019

Alexandra Damerau. Modelling musculoskeletal disorders *in vitro* - First steps towards the *in vitro* simulation of an arthritis joint model. Invited Oral Presentation.

EULAR 2018 – Annual European Congress of Rheumatology

Alexandra Damerau, Annemarie Lang, Moritz Pfeiffenberger, Frank Buttgereit, Timo Gaber. Simulating the pathogenesis of arthritis *in vitro* by developing a human-based multicomponent 3D joint model. Guided Poster Presentation.

EUSAAT 2018 – European Congress on Alternatives to Animal Testing

Alexandra Damerau, Annemarie Lang, Moritz Pfeiffenberger, Frank Buttgereit, Timo Gaber. Development of an *in vitro* human-based multicomponent 3D joint model as basis for the simulation of an arthritic joint model. Oral Presentation.

ECI 2018 – European Congress of Immunology

Alexandra Damerau, Annemarie Lang, Moritz Pfeiffenberger, Frank Buttgereit, Timo Gaber. First steps towards a human *in vitro* 3D joint model. Poster Presentation.

3R Webinar "Alternatives to animal use in research and education – Refine, Reduce, Replace, 2018

Moritz Pfeiffenberger & Alexandra Damerau: Modelling of musculoskeletal disorders *in vitro* - with complex processes to convincing systems. Invited Oral Presentation.

BSRT Symposium 2018 – Berlin-Brandenburg School for Regenerative Therapies

Alexandra Damerau, Annemarie Lang, Moritz Pfeiffenberger, Frank Buttgereit, Timo Gaber. First steps towards the *in vitro* simulation of a human-based joint model. Oral Presentation.

Danish 3R Symposium Copenhagen 2017

Alexandra Damerau, Annemarie Lang, Moritz Pfeiffenberger, Igor Ponomarev, Timo Gaber, Frank Buttgereit. Development of an *in vitro* multi-component 3D joint model. Poser Presentation.

10th World Congress on Alternatives and Animal Use in the Life Sciences (WC10), 2017

Alexandra Damerau, Moritz Pfeiffenberger, Frank Buttgereit, Timo Gaber, Annemarie Lang. Development of an *in vitro* multi-component 3D arthritic joint model. Oral Presentation.

DRS PhD Symposium 2017 – Dahlem Research School, Freie Universität

Alexandra Damerau, Annemarie Lang, Igor Ponomarev, Moritz Pfeiffenberger, Frank Buttgereit, Timo Gaber. Development of an *in vitro* multi-component 3D arthritic joint model. Oral Presentation.

AWARDS AND SCHOLARSHIPS

- Travel Award by the Arthur-Vick Stiftung (DGRh) for the European Workshop for Rheumatology Research (EWRR) Congress 2022, Vienna, Austria.
- Ideation contest winner 2021 in the category osteoarthritis - investigating the role of synovial fibroblasts in osteoarthritis - by the German Rheumatism Foundation (Deutsche Rheuma-Liga).
- ECRT Kickbox - Young Scientist Grant 2020 by the Einstein Center for Regenerative Therapies committee, Berlin, Germany.
- SPOKES Wellcome Trust Funded Think Tank (SWTFTT) 2020 funded by the Berlin Institute of Health (BIH), Berlin, Germany.
- Add-on Fellowship 2020 funded by the Joachim Herz Foundation, Hamburg, Germany.
- Travel grant by the scientific committee of the EULAR Congress 2020 for the European Alliance of Associations for Rheumatology (EULAR) Congress, E-Congress.
- EPAA 3Rs student grants (full grant 2019) by the European Partnership for Alternative Approaches to Animal Testing (EPAA) for the 19th Annual Congress of EUSAAT & 22nd European Congress on Alternatives to Animal Testing, Linz, Austria.
- Scholarship award by the ON Foundation for the European Orthopaedic Research Society (EORS) Congress 2019, Maastricht Netherland.
- Doctorate Scholarship Grant funded by the German Academic Scholarship Foundation.
- Erasmus+ - European Commission Travel Award: staff mobility for training.
- LUSH Prize Winner 2018 supporting animal-free testing in the category Young Researcher Award – Rest of the World by LUSH Cosmetics and Ethical Consumer.
- Young scientist travel award (YSTA) by the scientific committee of the EUSAAT Congress 2018 for the 18th Annual Congress of EUSAAT & 21st European Congress on Alternatives to Animal Testing, Linz, Austria.
- BIONNALE Speed Lecture Award Winner (1st place) by Berlin Partner, Berlin, Germany.
- Travel award by the Arthur-Vick Stiftung (DGRh) for the European Alliance of Associations for Rheumatology (EULAR) Congress 2018, Amsterdam, Netherland.
- Travel award by the scientific committee of the 10th World Congress on Alternatives and Animal Use in the Life Sciences to attend this Congress, Seattle, USA.

COPYRIGHT PERMISSIONS

Damerau A, Pfeiffenberger M, Weber MC, Burmester GR, Buttgereit F, Gaber T, Lang A. A Human Osteochondral Tissue Model Mimicking Cytokine-Induced Key Features of Arthritis In Vitro. *International Journal of Molecular Sciences*. 2021; 22(1):128. https://doi.org/10.3390/ijms22010128.

Damerau A, Buttgereit F, Gaber T. Optimization of a Tricalcium Phosphate-Based Bone Model Using Cell-Sheet Technology to Simulate Bone Disorders. *Processes*. 2022; 10(3):550. https://doi.org/10.3390/pr10030550.

Damerau A, Gaber T. Modeling Rheumatoid Arthritis In Vitro: From Experimental Feasibility to Physiological Proximity. *International Journal of Molecular Sciences*. 2020; 21(21):7916. https://doi.org/10.3390/ijms21217916.

FUNDING SOURCES

The study was funded by the German Federal Ministry for Education and Research (project no. 031L0070A). Alexandra Damerau was awarded a three-year fellowship of the German Academic Scholarship Foundation (Studienstiftung des deutschen Volkes). Individual data were collected as part of the LUSH Prize supporting animal-free testing in the category Young Researcher Award – Rest of the World. Funding bodies did not have any role in designing the studies, in collecting, analyzing, and interpreting the data, in writing the manuscripts, and in deciding to submit them for publication.

CONFLICT OF INTEREST

There is no conflict of interest through financial support of the work.

ANTEILSERKLÄRUNG

Anteilserklärung von Alexandra Damerau an der vorliegenden kumulativen Arbeit gemäß § 7 Abschnitt 3 der Promotionsordnung des Fachbereichs Biologie, Chemie, Pharmazie der Freien Universität Berlin (Stand 31.05.2018).

Alexandra Damerau hat die Abbildungen/Tabellen in der Einleitung dieser kumulativen Arbeit selbst dargestellt und die Verwendung von BioRender.com und Servier Medical Art in der jeweiligen Legende kenntlich gemacht.

Ergebnisse, die in Zusammenarbeit mit anderen Wissenschaftlern entstanden und in den Manuskripten enthalten sind, werden im Folgenden detailliert aufgelistet:

(1) Damerau A, Pfeiffenberger M, Weber MC, Burmester GR, Buttgereit F, Gaber T*, Lang A*. A Human Osteochondral Tissue Model Mimicking Cytokine-Induced Key Features of Arthritis In Vitro. *Int J Mol Sci.* 2020 Dec 24;22(1):128. doi: 10.3390/ijms22010128 (*contributed equally).

Die µCT-Analyse wurde von Dr. vet. med. Annemarie Lang, PhD durchgeführt. Die Darstellung und Interpretation der Daten erfolgte selbständig von Alexandra Damerau.

(2) Damerau A, Gaber T. Modeling Rheumatoid Arthritis In Vitro: From Experimental Feasibility to Physiological Proximity. *Int J Mol Sci*. 2020 Oct 25;21(21):7916. doi: 10.3390/ijms21217916. PMID: 33113770.

Die Kapitel 1.2, 1.3 und 1.5 in der vorliegenden Arbeit sind dem Manuskript „Modeling Rheumatoid Arthritis In Vitro: From Experimental Feasibility to Physiological“ entnommen und wurden eigens von Alexandra Damerau verfasst und im Einvernehmen mit Dr. rer. nat. Timo Gaber in die Einleitung dieser kumulativen Arbeit aufgenommen. Für die Lesbarkeit wurden kleinere sprachliche Modifikationen von Alexandra Damerau vorgenommen. Die Genehmigung zur Verwendung der veröffentlichten Abschnitte in dieser kumulativen Arbeit liegt Alexandra Damerau vor und kann auf Nachfrage vorgewiesen werde.

(3) Damerau A, Kirchner M, Beißel J, Pfeiffenberger M, Mertins P, Buttgereit F, Gaber T. A functional xeno-free 3D synovial membrane model to study synovitis *in vitro*. (draft).

Die Proteomics-Analysen wurden von Dr. Marieluise Kirchner und Dr. Philipp Mertins vom Max-Delbrück-Centrum für Molekulare Medizin (MDC) und Berlin Institute of Health (BIH) Core Facility für Proteomics durchgeführt. Die Aufarbeitung und Interpretation der Daten erfolgte selbständig von Alexandra Damerau.

mbvberlin mensch und buch verlag

49,90 Euro | ISBN: 978-3-96729-202-2